
Electronic Thesis and Dissertation Repository

10-22-2020 10:00 AM

CFD Simulations of Bubble Column Equipped with Bundles of Concentric Tubes

Glen C. DSouza, *The University of Western Ontario*

Supervisor: Anand Prakash, *The University of Western Ontario*

Joint Supervisor: Chao Zhang, *The University of Western Ontario*

A thesis submitted in partial fulfillment of the requirements for the Master of Engineering Science degree in Chemical and Biochemical Engineering

© Glen C. DSouza 2020

Follow this and additional works at: <https://ir.lib.uwo.ca/etd>



Part of the [Engineering Physics Commons](#), [Fluid Dynamics Commons](#), and the [Transport Phenomena Commons](#)

Recommended Citation

DSouza, Glen C., "CFD Simulations of Bubble Column Equipped with Bundles of Concentric Tubes" (2020). *Electronic Thesis and Dissertation Repository*. 7450.
<https://ir.lib.uwo.ca/etd/7450>

This Dissertation/Thesis is brought to you for free and open access by Scholarship@Western. It has been accepted for inclusion in Electronic Thesis and Dissertation Repository by an authorized administrator of Scholarship@Western. For more information, please contact wlsadmin@uwo.ca.

Abstract

Bubble column reactors are multiphase contactors that have found several industrial applications owing to various attractive features including excellent thermal management, low maintenance cost due to simple construction and absence of moving parts. In order to attain desired performance for a given application, these reactors are usually equipped with internals such as vertical tube bundles to facilitate heat transfer. The column hydrodynamics and turbulence parameters are altered when the column is occluded with internals which adds to the complexity of the problem. The use of Computational Fluid Dynamics (CFD) tools for the study of multiphase flows has gained a lot of traction over the recent years. In the current study, CFD is applied to a 2-Dimensional Eulerian-Eulerian model coupled with Population Balance Model (PBM) to simulate bubble column reactors in the presence and absence of internals. The significance of various interfacial forces on the numerical solution has been reviewed. Based on this, a suitable model is chosen which appropriately simulates the gas-liquid flow and has been selected to perform flow transition studies which covers the bubbly, transition and churn-turbulent regime. An increase in hydrodynamic parameters like centerline liquid axial velocity and gas holdup was noticed when the bubble column was occluded with circular tube internals. Furthermore, when dense vertical internals were introduced, the hydrodynamic values varied and consequently increased. When internals were added, a significant variation was noticed in the flow pattern which contributed to superior qualities of mixing.

Keywords

Bubble column reactor, Computational Fluid Dynamics (CFD), Simulation, Hollow bubble column, Vertical internals, Hydrodynamics, Interfacial forces, Reynolds Stress Model (RSM), Population Balance Model (PBM), Gas holdup, Liquid axial velocities, Bubble size distribution

Summary for Lay Audience

Bubble column reactors are cylindrical vessels that can facilitate substantial interactions between a liquid phase and the dispersed gas phase. Bubble columns, in recent years, have found their applications in numerous industries owing to their diverse advantages like low energy input, absence of moving parts, low pressure drops, construction simplicity and superior rates of heat and mass transfer. In general, bubble columns have been used in the process, chemical, metallurgical and biological industries. Lately, these reactors have also been employed in novel areas like production of clean fuels, methanol synthesis, Fischer-Tropsch synthesis, algae cultivation, biofuel production, biomedical sector as a blood oxygenator etc. Regardless of its wide applications, the scale up of these reactors is still an open challenge. The prime hurdle in the scale up process is the presence of complex fluid dynamics. When the bubble column is obstructed with innards or internals in the form of cylindrical rods, the flow pattern and hydrodynamics vary which adds to the complexity of the problem. In the current work, a numerical tool called Computational Fluid Dynamics (CFD) has been employed to model the bubble column reactor. Information that is vital to the reactor's scale up is obtained using the tool. The use of such computational tools decreases the laborious time required to build pilot setups, thereby increasing the productivity and improving the economics.

Co-Authorship Statement

The thesis contains material that is to be submitted for publication in peer reviewed journals.

These are outlined below:

Chapter 2: Recent Advances in Numerical and Experimental Analysis of Bubble Column Reactors - A comprehensive review

The literature of numerical and experimental analysis was performed by Glen DSouza under the guidance and inputs from Dr. Anand Prakash and Dr. Chao Zhang. The analysis, comparison and drafting of manuscript was executed by Glen Dsouza while critical revision was delivered by Dr. Anand Prakash and Dr. Chao Zhang.

Chapter 3: CFD Analysis of Hydrodynamics in Hollow Bubble Column Reactors

The simulations performed for this analysis were designed and executed by Glen DSouza under the guidance and inputs from Dr. Anand Prakash and Dr. Chao Zhang. The analysis, comparison and drafting of manuscript was carried out by Glen Dsouza while critical revision was delivered by Dr. Anand Prakash and Dr. Chao Zhang.

Chapter 3: CFD Analysis of Effect of Dense Vertical Internals on the Hydrodynamic parameters in Bubble Column Reactors

The simulations performed for this analysis were designed and executed by Glen DSouza under the guidance and inputs from Dr. Anand Prakash and Dr. Chao Zhang. The analysis, comparison and drafting of manuscript was carried out by Glen Dsouza while critical revision was delivered by Dr. Anand Prakash and Dr. Chao Zhang.

Acknowledgments

I am indebted and immensely grateful to many wonderful people who extended their valuable time and efforts in helping me complete this thesis over the last two years. Foremost, I have to sincerely thank Dr. Anand Prakash and Dr. Chao Zhang who provided me with innumerable hours of guidance, academic advice, support, and motivation. Their constant inspiration and encouragement made my master's journey worthwhile, and they were crucial in helping me successfully complete this body of work.

My gratitude extends to T.K. Gaurav, who helped me determine the specifics of my thesis and research work, even before its inception, and for his guidance and counsel. I am also greatly appreciative of Dr. Anil Jhavar for his help with the initial experimentation on this work.

Dr. Charles Xu, Dr. Franco Berruti, and Dr. Ajay Ray provided me with critical academic insight from their courses for which I am filled with gratitude. A special thanks to Dr. Madhumita Ray who has mentored me over several occasions. The graduate staff from the departments of Chemical and Biochemical Engineering (CBE) and Mechanical and Materials Engineering (MME) extended tremendous support throughout my graduate journey, for which I am very thankful.

I would be remiss if I didn't convey my sincere thanks to my uncle, aunty, cousins, sisters-in-law, and their tiny tots in Mississauga, for putting up with me whenever I visit them and for bringing joy to all of my holidays here in Canada. A huge thanks to Mr. Ankush Harindranath (University at Buffalo) for standing by my side in all times.

I also want to express my heartfelt gratitude to my friends from the MME department - Raj Kumar Nayak Maloth, Dwaipayan Sarkar, Shoyon Panday, and Shivani Jariwala for not only helping me with the technical aspects of this body of work but for also being there to support me as friends during my master's journey. A special shout out to Raj Kumar for the mind-

boggling discussions that, on several occasions, went late into the night, that greatly helped tailor my research and garner a deeper understanding of the world of computational work. His help and support were invaluable, and I could not have completed this work without him. I cannot even begin to express how thankful I am to my colleagues, Carlos Muñoz, Ana Giron, Sanket Adhiya, and Shokooh Karami from the CBE department for providing me with valuable advice and emotional support. I am especially appreciative of Anantha Surya and Gayathri Aryasomayajula for always looking out for me like an older sibling would.

It would be remiss of me if I did not convey my sincerest thanks to my family in this country, my uncle, aunty, cousins, sisters-in-law and their tiny tots in Mississauga, for putting up with me whenever I visit them and for bringing joy to all my holidays here in Canada. A huge thanks to Ankush Harindranath from the University at Buffalo and Dr. Nihal Pinto for standing by my side at all times.

Most importantly, I must thank my Dad, Mom, and my little sister. To say that they were crucial to my success would be an understatement. They have been the driving force behind me for as long as I can remember, and they are the reason that I am here today. They have always supported me and have been the guiding light through all my endeavours. I cannot thank them enough for always being there for me when I needed them.

To the countless admirable people, I have met here at Western, thank for so very much for helping me in so many big and small ways, and for making this journey meaningful and purposeful.

**“THE STEADFAST LOVE OF THE LORD NEVER CEASES; HIS MERCIES NEVER COME
TO AN END; THEY ARE NEW EVERY MORNING; GREAT IS THY FAITHFULNESS.”**

LAMENTATIONS 3:22-23

Dedication

This thesis is dedicated to:

*My dad (Eric DSouza), mom (Flavia DSouza) and my little sister
(Herleen DSouza) for inspiring me the most throughout my life*

“ದೇವ್ ಬರೊ ಕರುಂ”

“Thank you”

Table of Contents

Abstract.....	ii
Summary for Lay Audience.....	iv
Co-Authorship Statement.....	v
Acknowledgments.....	vi
Dedication.....	viii
Table of Contents.....	ix
List of Tables.....	xiii
List of Figures.....	xv
List of Appendices.....	xxii
Nomenclature.....	xxiii
Chapter 1.....	1
1 Introduction.....	1
1.1 Objectives of the thesis.....	4
1.2 Structure of thesis.....	4
References.....	7
Chapter 2.....	9
2 Literature Review.....	9
2.1 Hydrodynamics of Bubble Column.....	10
2.2 Bubble Column with Internals.....	15
2.2.1 Effects of Internals on Column Hydrodynamics.....	17
2.2.1.1 Effects of Internals on Local Holdups.....	19
2.2.1.2 Effects on Liquid Flow Patterns.....	21

2.3	CFD Modeling of Bubble Column Hydrodynamics	23
2.3.1	Turbulence Models	28
2.3.1.1	Standard $k - \varepsilon$ model.....	28
2.3.1.2	RNG $k - \varepsilon$ model.....	30
2.3.1.3	Reynolds Stress Model (RSM).....	32
2.3.2	Interfacial Forces	33
2.3.2.1	Virtual Mass Force	34
2.3.2.2	Drag Force	35
2.3.2.3	Transversal Lift Force	39
2.3.2.4	Turbulence Dispersion Force	43
2.4	CFD Studies on Bubble Column with Internals	45
2.5	Concluding Remarks.....	47
	References.....	48
	Chapter 3.....	59
3	CFD Simulations of Hollow Bubble Column Reactors	59
3.1	Introduction.....	59
3.2	Numerical Model for Two-Phase Flows.....	61
3.2.1	Governing Equations	61
3.2.2	Interfacial forces	62
3.2.2.1	Virtual mass force.....	63
3.2.2.2	Drag Force	65
3.2.2.3	Lift Force	66
3.2.2.4	Turbulence Dispersion.....	68

3.2.2.5	Bubble Induced Turbulence	69
3.2.3	Population Balance Model	70
3.2.3.1	Bubble Coalescence Model	72
3.2.3.2	Bubble Breakup Model.....	73
3.2.4	Turbulence Model.....	73
3.3	Configuration of the column.....	75
3.4	Numerical Method	77
3.5	Results and Discussion	81
3.5.1	Influence of interfacial forces	81
3.5.1.1	Influence of the lift force model.....	81
3.5.1.2	Influence of bubble induced turbulence	86
3.5.1.3	Influence of turbulence dispersion force	91
3.5.1.4	Influence of the drag force model	99
3.5.2	Reactor hydrodynamics, flow patterns and turbulence parameters variation with the flow regime transition	105
3.5.3	Comparison of Bubble Breakup and Bubble Coalescence Models	121
3.5.4	Dual Bubble Size Model.....	130
3.6	Concluding Remarks.....	137
References	140
Chapter 4	150
4	CFD Simulations of Bubble Column Reactors Occluded with Circular Tube Bundle and Dense Vertical Internals	150
4.1	Objectives	152
4.2	Configuration of the Bubble Column	153

4.2.1	Computational Domain and Grid Independence Test.....	155
4.2.2	Numerical Method	158
4.2.2.1	Boundary Conditions.....	160
4.3	Results and Discussion	161
4.3.1	Influence of interfacial forces on hydrodynamics of a bubble column with internals.....	161
4.3.1.1	Influence of the lift force model.....	161
4.3.1.2	Influence of the turbulence dispersion force	165
4.3.2	Reactor hydrodynamics, flow patterns and turbulence parameters variations with the flow regime transition	168
4.4	Conclusion	189
	References.....	190
	Chapter 5.....	194
5	Conclusions and Future Scope	194
5.1	Conclusion	194
5.1.1	Hollow Bubble Column	194
5.1.2	Bubble Column with Vertical Internals	196
5.2	Future Scope	197
	Appendix – A.....	198
	Appendix – B	217
	Appendix – C	224
	Appendix – D.....	228
	Curriculum Vitae	230

List of Tables

Table 2.1 Constants for standard k- ϵ turbulence model as suggested by Launder and Spalding (1974).....	29
Table 2.2 List of lift force coefficients employed in the literature	41
Table 2.3 Lift force coefficient formulations.....	42
Table 3.1 Population Balance Equation Terms.....	71
Table 3.2 Reynolds stress model (RSM) terms	75
Table 3.3 Hollow bubble column – Mesh information.....	78
Table 3.4 An outline of numerical methods.....	79
Table 3.5 List of lift coefficients, centerline liquid velocities and global gas holdups	83
Table 3.6 Interfacial force models used for the study on the flow regime transition	106
Table 3.7 PBM details for the study on the flow regime transition.....	106
Table 3.8 Interfacial forces used in the breakup and coalescence model study	123
Table 3.9 Boundary Conditions for the breakup and coalescence model study	124
Table 3.10 Parameters of the single bubble phase PBM model	125
Table 3.11 Parameters of two bubble phase PBM model.....	125
Table 3.12 Interfacial forces used for the dual bubble size model	133
Table 3.13 Boundary conditions used for the dual bubble size model	134
Table 4.1 Summary of numerical methods.....	159
Table 4.2 Interfacial forces used in the flow regime transition studies	169

Table 4.3 Parameters used in the PBM for flow regime transition studies.....	169
Table A.1 Literature review of numerical studies performed on hollow bubble columns ...	198
Table B.1 Literature review of numerical studies performed on bubble column with internals	217

List of Figures

Figure 1.1 Parameter selections and steps involved in CFD simulations of bubble column reactors.....	3
Figure 2.1 Simplified flow regime map for multiphase systems	10
Figure 2.2 Recirculating flow pattern of liquid induced by bubbles (Adapted from Hills (1974))	13
Figure 2.3 Schematic of bubble column with vertical tube internals	16
Figure 2.4 Typical profiles in the presence of internals (Möller et al., 2018)	18
Figure 3.1 Illustration of various interfacial forces in gas-liquid flows	63
Figure 3.2 Experimental setup of the hollow bubble column reactor used in Jhawar and Prakash (2014).....	76
Figure 3.3 Medium mesh representing the hollow bubble column geometry along with axial locations of measurements.....	77
Figure 3.4 Comparison of the gas holdups along the radial direction using the medium and fine meshes.....	78
Figure 3.5 Comparison of liquid axial velocities along the radial direction from different lift fore models in the transition regime ($U_g=10$ cm/s).....	84
Figure 3.6 Comparison of gas holdup profiles along the radial direction from different lift force models in the transition regime ($U_g=10$ cm/s).....	85
Figure 3.7 Comparison of the gas holdup profiles with and without BIT along the radial direction	86
Figure 3.8 Comparison of the liquid axial velocity profiles with and without BIT along the radial direction	87

Figure 3.9 Comparison of the contours of averaged liquid axial velocity with and without the BIT	88
Figure 3.10 Comparison of the contours of averaged gas holdup with and without the BIT (a) Without the BIT and (b) With the BIT	88
Figure 3.11 Vector contours of the gas phase in the distributor region	89
Figure 3.12 Vector contours of the gas phase in the bulk region	90
Figure 3.13 Vector contours of the gaseous phase in the disengagement zone	90
Figure 3.14 Comparison of the gas holdups with and without the TDF in the transition regime ($U_G=10$ cm/s)	92
Figure 3.15 Comparison of the liquid axial velocities with and without the TDF in the transition regime ($U_G=10$ cm/s)	93
Figure 3.16 Comparison of the averaged liquid axial velocities with and without turbulent dispersion models.....	94
Figure 3.17. Influence of turbulent dispersion models on averaged radial gas holdup profiles	95
Figure 3.18. Influence of turbulent dispersion models on direction of liquid flow near the disengagement zone	97
Figure 3.19 . Influence of turbulent dispersion models on direction of liquid flow near the disengagement zone	98
Figure 3.20 Influence of turbulent dispersion models on direction of liquid flow near the disengagement zone (a) No turbulent dispersion model (b) Burns et al. ($C_{TD}=0.1$) (c) Simonin et al. ($C_{TD}=0.1$) (d) Simonin et al. ($C_{TD}=0.5$)	99
Figure 3.21 Comparison of gas holdup profiles using different drag models with the experimental data in the transition regime ($U_G=10$ cm/s)	101

Figure 3.22 Influence of drag model formulation on global gas holdup profiles in the transition regime ($U_G=10$ cm/s)	102
Figure 3.23 Comparison of the liquid axial velocity profiles using different drag models with the experimental data in the transition regime ($U_G=10$ cm/s).....	103
Figure 3.24 Contours of gas holdups using different drag models (a) Schiller-Naumann (b) Tomiyama (c) Ishii-Zuber (d) Grace et al.	104
Figure 3.25 Contours of the liquid axial velocities from different drag models (a) Schiller-Naumann (b) Tomiyama (c) Ishii-Zuber (d) Grace et al.	105
Figure 3.26 Comparison of time-averaged liquid axial velocity profiles with the experimental data in three different transition regimes	109
Figure 3.27 Comparison of numerical values of centerline liquid axial velocities at various superficial gas velocities with the experimental data	110
Figure 3.28 Comparison of time-averaged gas holdup profiles along the radial direction in various transition regimes with experimental data	112
Figure 3.29 Comparison of the overall gas holdups under various superficial gas velocities with experimental data	114
Figure 3.30 Turbulent viscosity ratio profiles along the radial direction under different superficial gas velocities	115
Figure 3.31 . Contours of averaged turbulent viscosity ratios under different superficial gas velocities	116
Figure 3.32 Bubble size fraction distribution comparison in the bubbly, transition and churn turbulent regime	117
Figure 3.33 Vector contours of the axial liquid velocity in the distributor region at different flow regimes.....	118

Figure 3.34 Vector contours of the axial liquid velocity in the bulk region at different flow regimes.....	119
Figure 3.35 Vector contours of axial liquid velocity in the disengagement region at different flow regimes.....	119
Figure 3.36 Flow mapping of hollow bubble column reactors.....	120
Figure 3.37 Radial gas holdup variation with different PBM models	127
Figure 3.38 Comparison of the variations of the mean Sauter diameter along the axial direction using different PBM models	128
Figure 3.39 Comparison of bubble fraction distributions using different PBM models	129
Figure 3.40 Division of bubble phase into small and large bubble phases (Redrawn from van Baten and Krishna (2003)	131
Figure 3.41 Contribution of small and large bubble velocities to the gas flow (Reproduced from Schumpe and Grund (1986)).....	132
Figure 3.42 Comparison of the liquid axial velocity profiles along the radial direction using the dual bubble size model with different bubble sizes	135
Figure 3.43 Comparison of the gas holdup obtained using the dual bubble size model with different bubble sizes with the experimental data.....	136
Figure 3.44 Overall gas holdup comparison for dual bubble size model	137
Figure 4.1 Recirculation patterns in the presence of vertical tube internals (Redrawn from Forret <i>et al.</i> (2003)).....	151
Figure 4.2 Experimental setup of the bubble column reactor equipped with one circular tube bundle of 15 tubes used by Jhavar and Prakash (2014)	154
Figure 4.3 Bubble column reactor equipped with dense vertical tube internals of two circular tube bundle of 38 tubes used for the purpose of the numerical analysis	154

Figure 4.4 Computational domain for the bubble column with 15 internal vertical tubes ...	156
Figure 4.5. Computational domain for bubble column with 38 internal vertical tubes	157
Figure 4.6 Grid independence test for the column with 15 internal tubes	157
Figure 4.7 Grid independence test for the column with 38 internal tubes	158
Figure 4.8 Influence of lift force models on the radial profiles of the liquid axial velocities in the transition regime ($U_G=10$ cm/s)	163
Figure 4.9 Influence of lift force models on axial liquid velocity distributions in the entire column.....	163
Figure 4.10 Influence of lift force models on the radial profiles of the gas holdups in the transition regime ($U_G=10$ cm/s).....	164
Figure 4.11 Influence of lift force models on gas holdup distributions in the entire column	165
Figure 4.12 Influence of the turbulent interaction model on the radial profiles of the liquid axial velocities	166
Figure 4.13 Influence of turbulent dispersion model on the liquid axial distribution over the entire column	166
Figure 4.14 Influence of the turbulent dispersion model on the radial profiles of the gas holdups.....	167
Figure 4.15 Influence of the turbulent dispersion model on the gas holdup distributions in the entire reactor column	168
Figure 4.16 Comparison of liquid axial velocity profiles in various transition regimes for the bubble column with 15 tubes (a single circular tube bundle)	171
Figure 4.17. Comparison of liquid axial velocity profiles in various transition regimes for the bubble column with 38 tubes (double circular tube bundles).....	172

Figure 4.18 Comparison of the centerline liquid velocities with the experimental data in different transition regimes	173
Figure 4.19 Comparison of gas holdup profiles in various transition regimes for the bubble column with 15 tubes (single circular tube bundle).....	174
Figure 4.20 Comparison of gas holdup profiles in various transition regimes for bubble column with 38 tubes (Dense tube internals).....	175
Figure 4.21 Comparison of the predicted overall gas holdups in bubbly, transition and churn-turbulent regimes with experimental data.....	177
Figure 4.22 Effect of internals on the turbulent viscosity ratio in bubbly, transition and churn-turbulent regime for the bubble column with 15 tubes (single circular tube bundle).....	178
Figure 4.23 Effect of internals on the turbulent viscosity ratio in bubbly, transition and churn-turbulent regime for the bubble column with 38 tubes (double circular tube bundles).....	179
Figure 4.24 Effect of internals on turbulent Reynolds number in bubbly, transition and churn-turbulent regime for bubble column with 15 tubes (single circular tube bundle).....	179
Figure 4.25 Effect of internals on turbulent Reynolds number in bubbly, transition and churn-turbulent regime for bubble column with 38 tubes (double circular tube bundles).....	180
Figure 4.26 Effect of the density of internals in the column on the bubble size distribution in the bubbly flow regime	181
Figure 4.27 Effect of the density of internals in the column on the bubble size distribution in the transition flow regime	181
Figure 4.28 Effect of the density of internals in the column on the bubble size distribution in the churn-turbulent flow regime	182
Figure 4.29 Flow patterns near the bottom section of the internals in the column with 15 tubes	184

Figure 4.30 Flow patterns in the bulk section of the column with 15 tubes	184
Figure 4.31 Flow patterns in the disengagement section close to the dynamic height in the column with 15 tubes	185
Figure 4.32 Flow patterns near the bottom section of the internals in the column with 38 tubes	185
Figure 4.33 Flow patterns in the bulk section of the column with 38 tubes	186
Figure 4.34 Flow patterns in the bulk section of the column with 38 tubes	186
Figure 4.35 Comparison of flow patterns and mixing patterns between the columns with 15 tubes and 38 tubes	187
Figure 4.36 Generalized flow mapping for bubble columns with less and dense vertical internals	188
Figure C.1 Two-dimensional representation of 15 tube bundle geometry	224
Figure C.2 Two-dimensional representation of 38 tube bundle geometry	226
Figure D.1 Comparison of experimental values of gas holdup values with other experimental work	229

List of Appendices

Appendix A: Literature review of numerical studies performed on hollow bubble columns	198
Appendix B: Literature review of numerical studies performed on bubble column with internals.....	217
Appendix C: Calculation of perforation fractions for 15 tube and 38 tube internal geometry	224
Appendix D: Experimental evaluation of overall gas holdup.....	228

Nomenclature

$b(v)$	bubble breakup rate, s^{-1}
$c(v, v')$	bubble coalescence kernel function, m^3s^{-1}
$C_{1,\varepsilon}$	constant in $k - \varepsilon$ turbulence modelling, dimensionless
$C_{2,\varepsilon}$	constant in $k - \varepsilon$ turbulence modelling, dimensionless
$C_{3,\varepsilon}$	constant in $k - \varepsilon$ turbulence modelling, dimensionless
C_{ke}	coefficient in Troshko-Hassan model, dimensionless
C_μ	constant in $k - \varepsilon$ turbulence modelling, dimensionless
C_D	coefficient of drag force, dimensionless
C_L	coefficient of lift force, dimensionless
C_{TD}	coefficient of turbulence dispersion force, dimensionless
C_W	coefficient of wall lubrication force, dimensionless
C_{VM}	coefficient of virtual mass force, dimensionless
C_{ij}	convection term
d_b	bubble diameter, m
d_i, d_j	bubble diameters represented by indices ' i ' and ' j ', m
D_c	column diameter, m
$D_{L,ij}$	molecular diffusion term, $kgm^{-1}s^{-3}$

$D_{T,ij}$	turbulent diffusion term
F	force per unit volume, Nm^{-3}
F_D	drag force per unit volume, Nm^{-3}
F_L	lift force per unit volume, Nm^{-3}
F_{TD}	turbulence dispersion force per unit volume, Nm^{-3}
F_{VM}	virtual mass force per unit volume, Nm^{-3}
g	gravitational acceleration, ms^{-2}
H	total height of bubble column reactor, m
k	turbulent kinetic energy per unit mass, m^2s^{-2}
\dot{m}_{lg}	mass transfer from liquid to gas phase
\dot{m}_{gl}	mass transfer from gas to liquid phase
$M_{k,i}$	interphase momentum transfer term
$n(v)$	number size distribution of bubble of size v
$N_i(t)$	number of bubbles with volumes between v_i and v_{i+1} , m^{-3}
N_p	total number of phases
N_{Re}	Reynolds number, dimensionless
N_{Eo}	Eotvos number, dimensionless
N_{Eo}'	modified Eotvos number, dimensionless
P_c	bubble coalescence probability, dimensionless

S	source term
S_q	modulus of mean strain tensor
t	flow time, s
u'_i	velocity fluctuation along the 'i' coordinate, ms^{-1}
U_L	liquid axial velocity, ms^{-1}
U_{L0}	centreline liquid axial velocity, ms^{-1}
U_G	superficial gas velocity, ms^{-1}
V_b	bubble velocity, ms^{-1}
z	variation of axial height, m

Greek Letters

ε_G	volume fraction of the gas phase, dimensionless
ε_L	volume fraction of the liquid phase, dimensionless
μ_t	turbulent viscosity, m^2/s
τ	shear stress, Pa
ν_t	turbulent kinematic viscosity, m^2/s
ρ_L	density of liquid phase, kg/m^3
ε_{ij}	turbulence dissipation term, m^2/s^3
ω	specific rate of dissipation, s^{-1}

φ_{ij}	pressure term
σ	surface tension, Nm^{-1}
σ_k	Prandtl number accounting for turbulent kinetic energy, dimensionless
σ_ε	Prandtl number accounting for turbulent energy dissipation, dimensionless
μ_k	bulk viscosity of phase 'k', $Pa \cdot s$
$\eta_{i,j}$	coefficient of transfer between bubbles arising due to bubble coalescence
$\tau_{i,j}$	time required for bubble coalescence, s
$\beta(v, v')$	daughter bubble size distribution function
$\zeta_{i,k}$	coefficient of transfer between bubbles arising due to bubble breakup
ω_c	Specific collision frequency between two bubbles, m^3/s

Subscripts

G	gas phase
L	liquid phase
loc	local
avg	average

<i>max</i>	maximum
<i>w</i>	wall
<i>t</i>	turbulent
<i>b</i>	bubble
<i>g</i>	gravity
<i>p</i>	phases
<i>P</i>	pressure
<i>D</i>	drag
<i>L</i>	lift force
<i>VM</i>	virtual mass
<i>TD</i>	turbulent dispersion
<i>G</i>	gas phase
<i>L</i>	liquid phase
<i>loc</i>	local

Abbreviations

ASMM	Algebraic Slip Mixture Model
BIT	Bubble Induced Turbulence
BSD	Bubble Size Distribution

CARPT	Computer Aided Radioactive Particle Tracking
CSA	Cross Sectional Area
CFD	Computational Fluid Dynamics
CT	Computed Tomography
E-E	Eulerian-Eulerian
E-L	Eulerian-Lagrangian
HBC	Hollow Bubble Column
LDA	Laser Doppler Anemometry
LES	Large Eddy Simulation
PBE	Population Balance Equations
PBM	Population Balance Model
PIV	Particle Image Velocimetry
QUICK	Quadratic Upwind Interpolation for Convective Kinematics
RANS	Reynolds-Averaged Navier Stokes
RNG	Re-normalization Group Method

Chapter 1

1 Introduction

Bubble column reactors are cylindrical multiphase contactors that can facilitate substantial interactions between a liquid phase and the dispersed gas phase. The gas phase is introduced into the column via a gas distributor, also called a sparger. The liquid phase can be either stationary or continuous. When solids are suspended in the liquid phase, the bubble column is called as a Slurry Bubble Column (SBC). Due to its diverse advantages like low energy input, absence of moving parts, low pressure drops, construction simplicity and superior rates of heat and mass transfer, bubble column reactors are used in process, chemical, biochemical and metallurgical industries (Youssef *et al.*, 2012; Majumder, 2019; Möller *et al.*, 2019). Other advantages of bubble columns include enhanced temperature control capability, improved mixing abilities, requirement of lesser maintenance thereby decreasing the operation cost, requirement of reduced floor area and increased interfacial areas (Li *et al.*, 2003; Kantarci *et al.*, 2005; Abdulrahman, 2015; Besagni *et al.*, 2018).

Bubble column reactors find their use in bulk processes like wastewater effluent treatment, Fischer-Tropsch synthesis, clean fuels production, methanol synthesis, biofuel production, wet air oxidation, photo-bioreactions etc. (Deckwer, 1981; Sánchez Mirón *et al.*, 2000; Krishna *et al.*, 2001; Ranjbar *et al.*, 2008). A revolutionary scale up slurry bubble column reactor with diameter 10 m was installed by SASOL at the Oryx GTL plant located at Qatar (Botes *et al.*, 2011). When bubble column reactors are employed for exothermic reactions like Fischer-Tropsch synthesis, they must be equipped with dense vertical heat exchanging tubes to facilitate effective heat exchange (Krishna and Sie, 2000). Although they are most

widely used, bubble column internals are not just limited to the heat exchanging rods. Other internals include baffles, liquid/gas distributors, perforated plates, helical springs, instrumentation probes and down-comers (Youssef *et al.*, 2013).

Over the last six decades, numerous studies have been performed to understand the mechanisms involved with scale-up of bubble column reactors. Despite several attempts and successful research, scale-up of bubble columns still imposes a major challenge (Dudukovic and Mills, 2014). Complex hydrodynamics and fluid dynamics involved in these reactors make the scale-up process really challenging. In addition, when the bubble column reactors are occluded with internals, their effect on fluid dynamics, mixing patterns, bubble behavior and other hydrodynamic parameters, will make the scale-up process more complex (Jhawar and Prakash, 2014).

Recently, a considerable progress has been achieved in the arena of Computational Fluid Dynamics (CFD), which has become an effective tool in modeling multiphase flows in bubble column reactors to study various hydrodynamic aspects, such as velocity profiles, phase holdups, mixing patterns and turbulence characteristics, in column reactors (Joshi, 2001; Ekambara *et al.*, 2008; Basha *et al.*, 2015). To date, several numerical studies have been performed on bubble column reactors. While most of the studies have focused on the hollow bubble columns, only limited studies were carried for bubble column with internals. Figure 1.1 illustrates the basic steps involved in the CFD modeling of bubble column reactors.

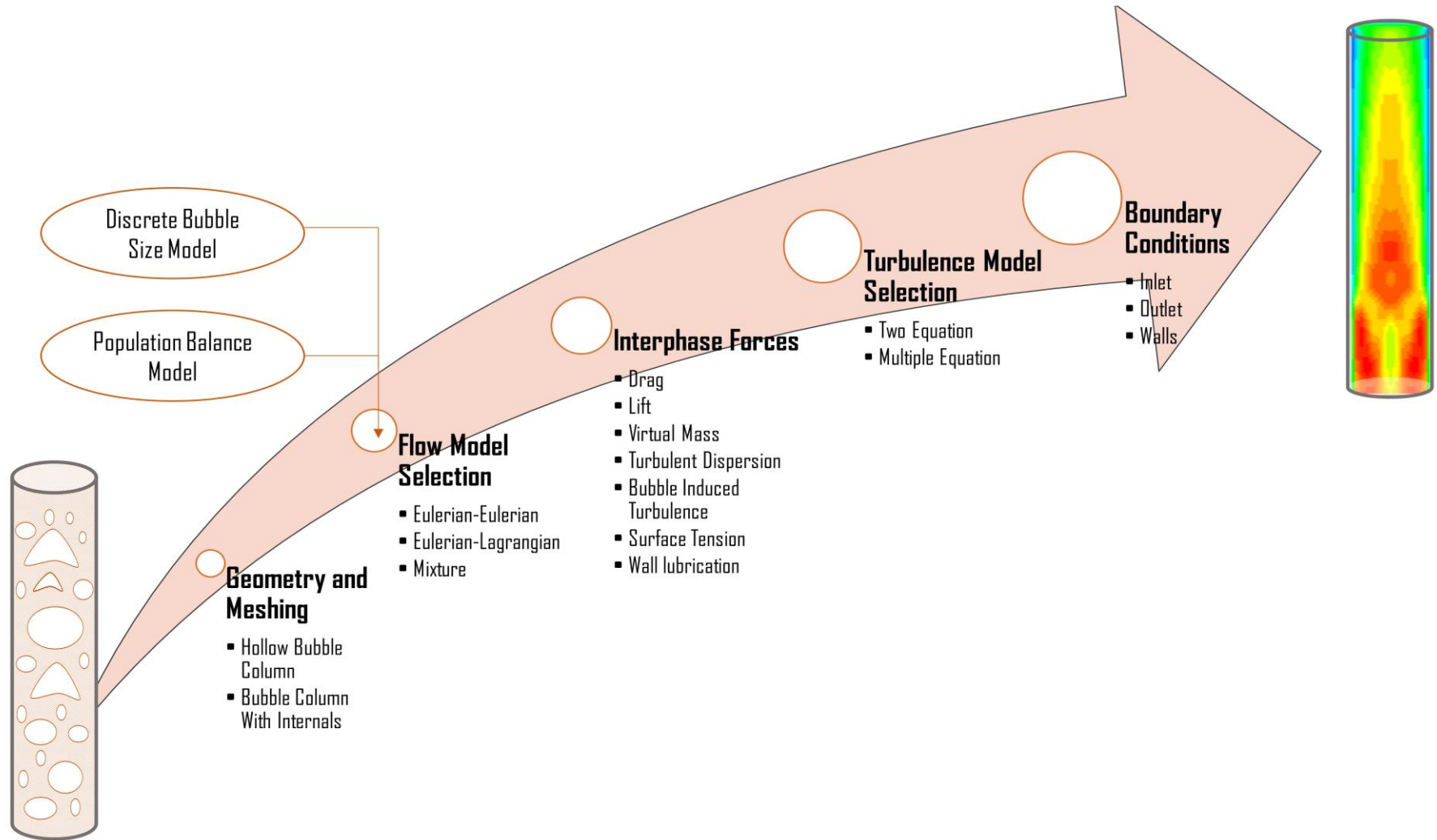


Figure 1.1 Parameter selections and steps involved in CFD simulations of bubble column reactors

1.1 Objectives of the thesis

The objectives of this study are:

- To develop a 2D CFD model based on the Eulerian-Eulerian approach for the simulation of multiphase flows in a bubble column reactor with and without internals. The interfacial forces, such as the drag and lift forces, turbulent dispersion and bubble induced turbulence will be investigated.
- To study the hydrodynamics, turbulence and dispersed phase characteristics in the bubbly, transition and churn-turbulent regime as well as the flow transition process using the proposed CFD model.
- To understand the effect of circular tube bundles and dense vertical internals on the hydrodynamics, turbulence and dispersed phase characteristics in the bubbly, transition and churn-turbulent regime, and flow transition process.

1.2 Structure of thesis

This thesis is written in an “integrated-article” format provided by the School of Graduate and Postdoctoral Studies (SGPS) at the University of Western Ontario. It consists of five chapters, the summary of which are provided below:

In Chapter 1, the introductions to the bubble column reactors in both the laboratory and industrial scales are provided. The motivation of the work is outlined, and the objectives are explicitly stated.

Chapter 2 has two main sections. In the first section, a comprehensive review of the current state in the experimental studies of bubble column reactors is presented. The effects of column diameters, design of internals, and gas distributor designs on the centerline liquid axial velocities, gas holdups and other hydrodynamic parameters are critically reviewed. In the second section, an extensive review of the numerical studies involving bubble column reactors is presented. The effects of different CFD models, including the interfacial forces and turbulence models, on the predictions of the turbulence parameters for flows in bubble column reactors with and without internals are thoroughly reviewed.

In Chapter 3, numerical models for the simulation of the multi-phase flows in the hollow bubble column are presented. First, governing equations and mathematical models are thoroughly discussed. This is followed by the experimental and numerical setups. The results have been divided into two sections. In the first section, the study of the sensitivity of interfacial forces in hollow bubble column reactors is presented. The suitable model based on the interfacial force study is selected to perform the flow transition studies in the bubbly, transition and churn-turbulent regimes. In the next section, the results of the flow transition study have been outlined.

In Chapter 4, numerical simulations involving the bubble column with internals is performed. The experimental and numerical setups are thoroughly discussed. The results are divided into two sections. In the first section, the study of the sensitivity of interfacial forces on the flows in the bubble column reactor with tube circular tube bundles is provided. The suitable model based on the interfacial forces study is selected to perform the flow transition studies in the bubbly, transition and churn-turbulent regimes. In the next section, the results of the flow transition study are given for the bubble column with circular

tube internals and bubble column with dense vertical internals. The dense internals are used to increase the available heat transfer area and induce greater levels of mixing within the column.

In Chapter 5, conclusions for hollow bubble column and bubble column with vertical internals are discussed. In addition, the future scope for the current work are presented.

References

- Abdulrahman, M. W. (2015) 'Experimental studies of direct contact heat transfer in a slurry bubble column at high gas temperature of a helium–water–alumina system', *Applied Thermal Engineering*, 91, pp. 515–524.
- Basha, O. M., Sehabiague, L., Abdel-Wahab, A. and Morsi, B. I. (2015) 'Fischer–Tropsch Synthesis in Slurry Bubble Column Reactors: Experimental Investigations and Modeling – A Review', *International Journal of Chemical Reactor Engineering*. Berlin, Boston: De Gruyter, 13(3), pp. 201–288.
- Besagni, G., Inzoli, F. and Ziegenhein, T. (2018) 'Two-phase bubble columns: A comprehensive review', *ChemEngineering*. Multidisciplinary Digital Publishing Institute, 2(2), p. 13.
- Botes, F. G., Dancuart, L. P., Nel, H. G., Steynberg, A. P., Vogel, A. P., Breman, B. B. and Font Freide, J. H. M. (2011) '11 - Middle distillate fuel production from synthesis gas via the Fischer–Tropsch process', in Khan, M. R. (ed.) *Advances in Clean Hydrocarbon Fuel Processing*. Woodhead Publishing (Woodhead Publishing Series in Energy), pp. 329–362.
- Deckwer, W.-D. (1981) 'Access of Hydrodynamic Parameters Required in the Design and Scale-Up of Bubble Column Reactors', in ACS Publications, pp. 213–241.
- Dudukovic, M. P. and Mills, P. L. (2014) 'Challenges in reaction engineering practice of heterogeneous catalytic systems', in *Advances in Chemical Engineering*. Elsevier, pp. 1–40.
- Ekambara, K., Nandakumar, K. and Joshi, J. B. (2008) 'CFD simulation of bubble column reactor using population balance', *Industrial & engineering chemistry research*. ACS Publications, 47(21), pp. 8505–8516.
- Jhawar, A. K. and Prakash, A. (2014) 'Bubble column with internals: Effects on hydrodynamics and local heat transfer', *Chemical Engineering Research and Design*. Elsevier, 92(1), pp. 25–33.
- Joshi, J. B. (2001) 'Computational flow modelling and design of bubble column reactors', *Chemical Engineering Science*. Elsevier, 56(21–22), pp. 5893–5933.
- Kantarci, N., Borak, F. and Ulgen, K. O. (2005) 'Bubble column reactors', *Process biochemistry*. Elsevier, 40(7), pp. 2263–2283.
- Krishna, R., Van Baten, J. M., Urseanu, M. I. and Ellenberger, J. (2001) 'Design and scale up of a bubble column slurry reactor for Fischer–Tropsch synthesis', *Chemical*

Engineering Science. Elsevier, 56(2), pp. 537–545.

Krishna, R. and Sie, S. T. (2000) ‘Design and scale-up of the Fischer–Tropsch bubble column slurry reactor’, *Fuel processing technology*. Elsevier, 64(1–3), pp. 73–105.

Li, H., Prakash, A., Margaritis, A. and Bergougnou, M. A. (2003) ‘Effects of micron-sized particles on hydrodynamics and local heat transfer in a slurry bubble column’, *Powder Technology*. Elsevier, 133(1–3), pp. 171–184.

Majumder, S. K. (2019) *Hydrodynamics and mass transfer in downflow slurry bubble columns*. CRC Press.

Möller, F., Kipping, R., Lavetty, C., Hampel, U. and Schubert, M. (2019) ‘Two-bubble class approach based on measured bubble size distribution for bubble columns with and without internals’, *Industrial & Engineering Chemistry Research*. ACS Publications, 58(8), pp. 2759–2769.

Ranjbar, R., Inoue, R., Shiraishi, H., Katsuda, T. and Katoh, S. (2008) ‘High efficiency production of astaxanthin by autotrophic cultivation of *Haematococcus pluvialis* in a bubble column photobioreactor’, *Biochemical Engineering Journal*. Elsevier, 39(3), pp. 575–580.

Sánchez Mirón, A., García Camacho, F., Contreras Gómez, A., Grima, E. M. and Chisti, Y. (2000) ‘Bubble-column and airlift photobioreactors for algal culture’, *AIChE Journal*. Wiley Online Library, 46(9), pp. 1872–1887.

Youssef, A. A., Al-Dahhan, M. H. and Dudukovic, M. P. (2013) ‘Bubble columns with internals: a review’, *International Journal of Chemical Reactor Engineering*. De Gruyter, 11(1), pp. 169–223.

Youssef, A. A., Hamed, M. E., Grimes, J. T., Al-Dahhan, M. H. and Duduković, M. P. (2012) ‘Hydrodynamics of pilot-scale bubble columns: effect of internals’, *Industrial & Engineering Chemistry Research*. ACS Publications, 52(1), pp. 43–55.

Chapter 2

2 Literature Review

Bubble column reactors have found applications in a wide range of industrial processes as gas-liquid and gas-liquid-solid contactors of choice for their advantages of simple construction, low maintenance, and high heat transfer and good mass transfer rates. Some of the major industrial applications include oxidation and hydrogenation reactions, Fischer-Tropsch synthesis, methanol synthesis, heavy oil upgrading, fermentation, biological waste water treatment, flue gas desulphurization, dimethyl ether production (Deckwer, 1981; Shah *et al.*, 1982; Fan, 1989; Devanathan *et al.*, 1990; Li and Prakash, 2000, 2002). Although bubble columns are relatively simple to construct, the interactions between the liquid and gaseous phases contained within are complex, intimate and difficult to predict or scale-up. For these reasons, characterization and quantification of the gaseous and liquid phase interactions is of great importance. There are two different methods that can be used to gain an understanding of bubble column systems. The first category refers to empirically-based methods in which rules and guidelines for bubble column design and scale-up are derived from trends in experimental data (Deckwer *et al.*, 1993). The second category refers to model-based methods in which theoretical models are applied to the system of interest after flow regime analysis has been carried out (Deckwer *et al.*, 1993). It is not uncommon to find a mix of both methods in an industrial setting. However, a greater dependence on model-base methods is encouraged as they provide additional insight to a reactor's performance and a basis for reactor design.

2.1 Hydrodynamics of Bubble Column

A good understanding of hydrodynamics is necessary for successful design and operation of bubble column reactors. The important hydrodynamic parameters include: Flow regimes; Phase holdups; Bubble size and bubble wake dynamics and Flow patterns and phase mixing. Bubble columns can operate in three main types of flow regimes depending on operating conditions.

1. Dispersed bubble or homogeneous flow regime
2. Coalesced bubble or heterogeneous flow regime
3. Slugging regime

Often, these flow regimes (and their boundaries) are determined visually. A simplified flow regime diagram is presented in Figure 2.1. More detailed flow regime charts are given by Fan (1989) and Schumpe et al. (2004).

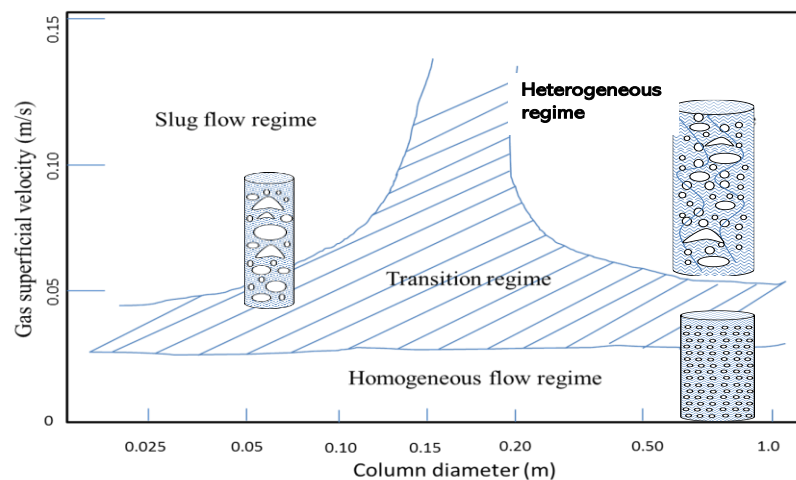


Figure 2.1 Simplified flow regime map for multiphase systems

- In the dispersed bubble regime, small bubbles are well dispersed in the bed. There is little bubble-to-bubble collision thus reducing the possibility of bubble coalescence. This regime is favored by low superficial gas velocities (< 0.05 m/s) in bubble columns and large liquid velocities and large particles (3-5mm) in three-phase fluidized beds.
- In heterogeneous or coalesced bubble regime, there is continuous bubble coalescence and break up along the column height with the dynamic mean bubble size remaining nearly constant. This regime is likely to occur with high superficial gas velocities (>0.1 m/s), low superficial liquid velocities and small particles (<2 mm).
- The slugging regime mainly occurs in small experimental columns (< 0.05 m) and is seldom encountered in industrial scale reactors.

Phase holdup which represents fraction of total volume occupied by individual phase in the system is primary design information for multiphase reactor systems. A large number of methods have been proposed in the literature for phase holdup measurements (Linneweber and Blass, 1983; Bukur et al., 1987; Maezawa *et al.*, 1995; Youssef and Al-Dahhan, 2009). Some methods measure overall average, some measure cross sectional average and some other methods measure local holdups. A simple and quick method for estimation of average gas holdup is based on static (H_s) and dispersion/expanded bed heights (H_d).

$$\varepsilon_G = \frac{H_d - H_s}{H_d} \quad (2.1)$$

Small bubbles contribute to higher gas holdups due to their low rise velocities, while large bubbles due to their fast rise velocities contribute less. Small bubbles in a dispersion provide high interfacial area for mass transfer. Therefore, their population is desirable for most applications. Bubbles are formed at the distributor and tend to grow initially due to coalescence. Large bubbles tend to split so that the ultimate bubble size distribution depends on a balance between coalescence and break-up. The processes of bubble coalescence and break-up result in wide bubble size distribution specially in coalesced bubble or heterogeneous flow regime. In multi-bubble systems, the bubble size follows a log-normal distribution (Darton, 1974; Matsuura *et al.*, 1984). The shape of the bubble depends mainly on bubble size. Under the same operating conditions, the bubble shape changes as below:

- Spherical shape (small bubbles; $d_b < 4 \text{ mm}$)
- Ellipsoidal shape (intermediate bubbles; $5\text{mm} < d_b < 1 \text{ cm}$)
- Spherical-cap (large bubbles; $d_b > 1 \text{ cm}$)

The motion of bubbles and their associated wake give rise to different flow structures and flow patterns depending upon operating flow regime (i.e. dispersed bubble flow and coalesced bubble flow). As the gas velocity exceeds 0.05 m/s, the spiral flow pattern breaks down due to intensive bubble coalescence and gradual break-up processes. Momentum is transferred from the primary bubble wakes to the surrounding liquid through the roll-up and shedding phenomena of the bubble wakes (Tsuchiya *et al.*, 1990). Large coalesced bubbles ascending in the column lead to a gross liquid flow pattern for the liquid (or slurry) with an upward flow in the core region and a downward flow near the wall (Figure 2.2).

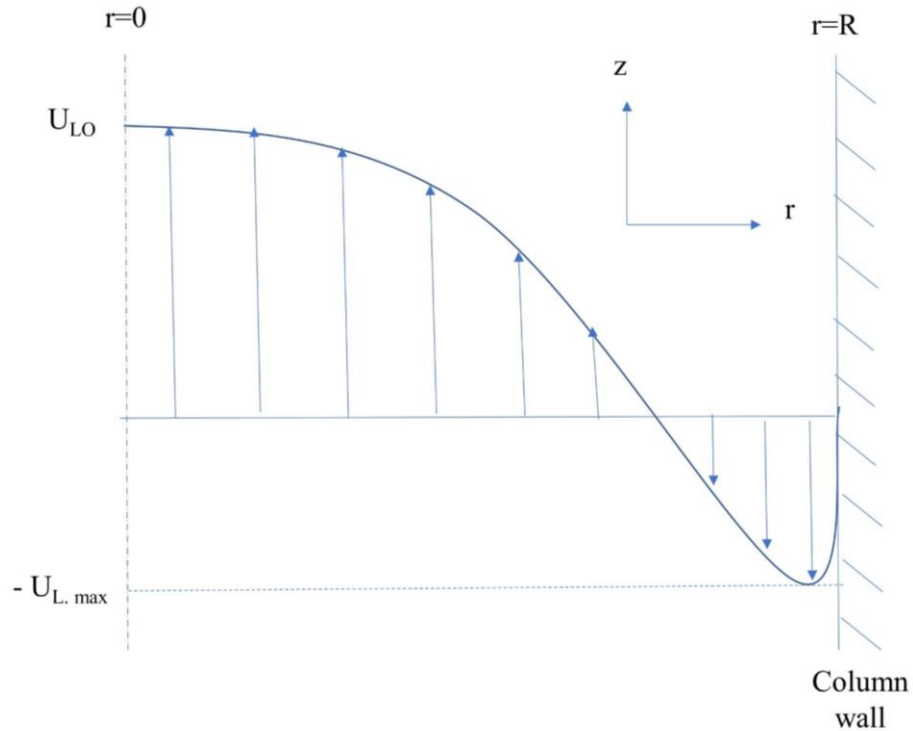


Figure 2.2 Recirculating flow pattern of liquid induced by bubbles (Adapted from Hills (1974))

The radial variation of gas holdup provides the driving force for the recirculation flow. An equation for circulating liquid flow was developed by Ueyama and Miyauchi (1979) starting with Navier-Stokes equation and following main assumptions.

- radial pressure remains constant
- molecular viscosity is negligible in turbulent core compared to turbulent viscosity

$$-\frac{1}{r} \frac{d}{dr} (r\tau_s) = \frac{dp}{dz} + (1 - \varepsilon_G(r)) \rho_L g \quad (2.2)$$

In the turbulent core, the shear stress is related to time-averaged vertical velocity of liquid through the turbulent kinematic viscosity as below:

$$\tau_s = \nu_t \rho_L \frac{dU_L}{dr} \quad (2.3)$$

Ueyama and Miyauchi (1979) developed an empirical correlation for turbulent viscosity based on literature data.

$$\nu_t = 0.0322 D_c^{1.7} \quad (2.4)$$

The radial distribution of gas holdup observed in the turbulent flow regime can be approximated as:

$$\varepsilon_{G,loc} = \varepsilon_{G,avg} \left(\frac{m+2}{m}\right) (1 - \theta^m) \quad (2.5)$$

Mean gas holdup is related to local gas holdup as follows:

$$\varepsilon_{G,avg} = \frac{1}{\pi R^2} \int_0^R 2\pi r \varepsilon_{G,loc} dr \quad (2.6)$$

Two boundary conditions are required to solve equation 2.2. One boundary condition assumes axisymmetric liquid flow in the column:

$$\frac{dU_L}{dr} = 0 \quad \text{at } r = R \quad (2.7)$$

A second boundary condition is from velocity distribution in turbulent flow. The thickness of the laminar sublayer is much smaller than the column radius R , therefore can be neglected to give the following boundary condition:

$$U = U_w \quad \text{at } r = R \quad (2.8)$$

Equation 2.2 can be integrated with above conditions to obtain local liquid velocity in column. For a value of $m = 2$ (in Eq. 2.5), Wachi et al. (1987) obtained the following equation for local liquid velocity.

$$U_L = \frac{\tau_w R}{2v_t \rho_L} (1 - \theta^2) + \frac{gR^2 \varepsilon_{G,avg}}{8v_t} (1 - \theta^2)^2 + U_{L,w} \quad (2.9)$$

Peripheral or wall liquid velocity ($U_{L,w}$) is related to wall shear stress (τ_w) by the following equation.

$$U_{L,w} = -11.63 \frac{\sqrt{|\tau_w|}}{\rho_L} \quad (2.10)$$

Wachi et al. (1987) have also developed equation for liquid velocity at wall of the column.

2.2 Bubble Column with Internals

Bubble columns often need to be equipped with internals of different types in order to obtain desired performance for a given application. These include baffles, heat transfer surfaces and gas/liquid distributors of different configurations. The internals presence and arrangement in bubble columns would affect hydrodynamics and mixing pattern, thereby affecting the reactor performance. Only a limited number of literature studies have investigated effects of internals on bubble column hydrodynamics (Jhawar and Prakash 2011; Youssef et al. 2012; Faiçal Larachi et al. 2006; J. Chen et al. 1999; Schlüter et al. 1995; Saxena et al., 1992). These studies point to alterations in flow pattern, mixing intensities and general hydrodynamics due to insertion of internals in a hollow bubble column. However, there is need to quantify the effects of internals arrangements on

important design parameters such as phase holdups, liquid backmixing and interfacial area for mass transfer.

A common type of internal is a set of vertical tubes providing heat transfer surface for temperature control as shown schematically in Figure 2.3. In-situ installation of these internals provides multiple advantages including higher heat transfer rate, better control of reactor temperature reducing the need for an external exchanger (Schlüter et al., 1995). The presence of internals, however, affect phase holdups, flow patterns and phase mixing.

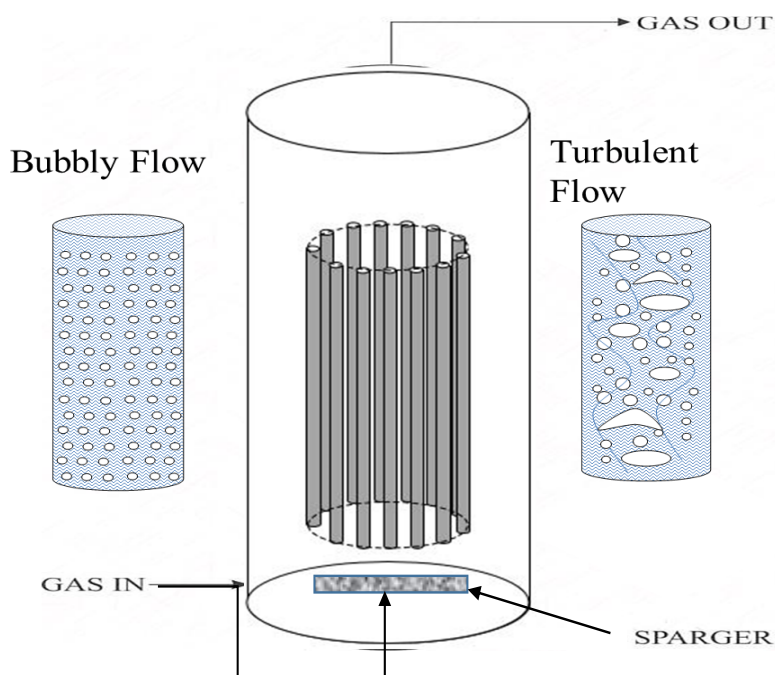


Figure 2.3 Schematic of bubble column with vertical tube internals

The selection of the number of tubes or the cross-sectional area (CSA) occluded by the tubes, and the configuration of the tubes (i.e. the diameter, pitch and arrangement) are decided by the surface area necessary for the heat transfer. This mainly depends on the exothermic nature of the reaction and the overall heat transfer coefficient. The

modifications for different CSA or tube size and configurations have significant effect on the hydrodynamics. Experimental studies on the effects of longitudinal flow tube bundle on column hydrodynamics have been reported in several literature studies (Schlüter *et al.*, 1995; Chen *et al.*, 1999; Youssef *et al.*, 2009, 2013; Jhavar *et al.*, 2014; Kagumba *et al.*, 2015; Al Mesfer *et al.*, 2016, 2017; George *et al.*, 2017; Sultan *et al.*, 2018).

2.2.1 Effects of Internals on Column Hydrodynamics

The internals design parameters mostly investigated in literature studies include, number and size of tubes, cross-sectional area (CSA) of column occupied and different arrangements of tubes. Presence of internals can further complicate, the complex hydrodynamics of bubble column. The hydrodynamic parameters affected include phase holdup profiles, flow patterns, liquid velocity profile etc. Figure 2.4 shows a representation of typical profiles as an effect of internals in the column. Further details of the effect of different internals reported in experimental literature studies have been discussed in the following sections.

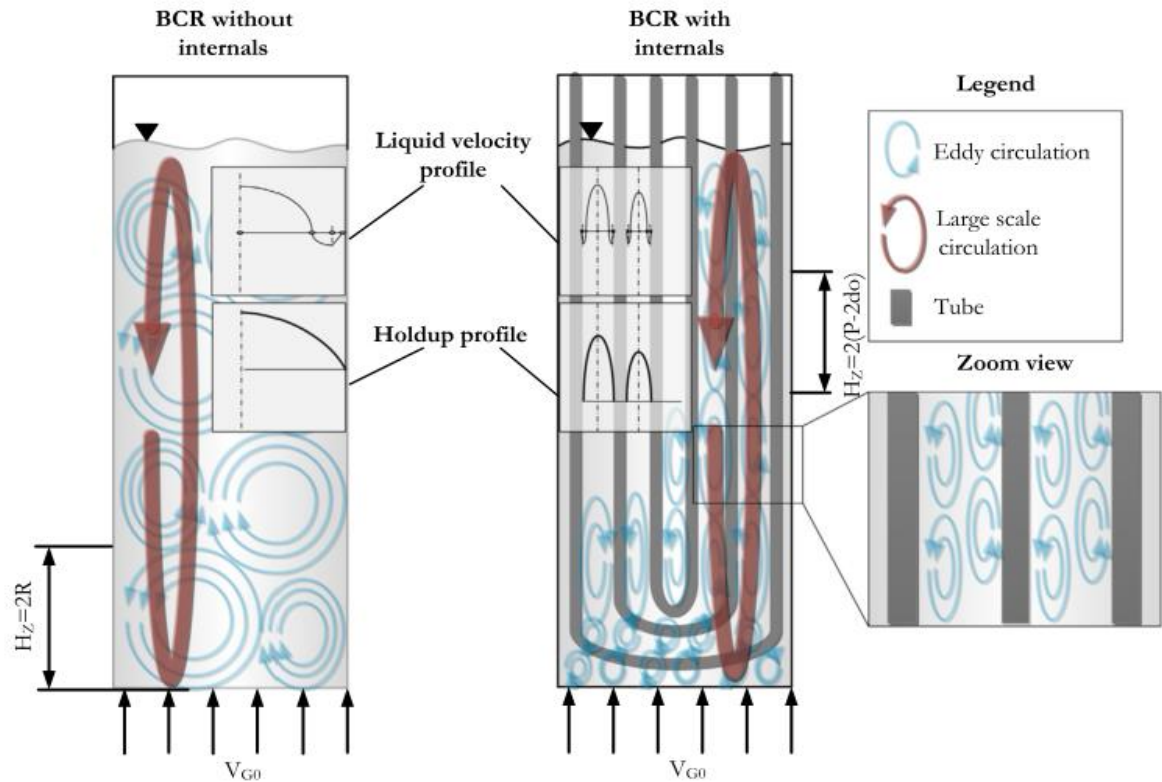


Figure 2.4 Typical profiles in the presence of internals (Möller et al., 2018)

A number of literature studies have reported increase in gas holdups in the presence of internals (Yamashita, 1987; Pradhan *et al.*, 1993; Youssef and Al-Dahhan, 2009; Al Mesfer *et al.*, 2016). The extent of increase, however, has been found to depend on the size and number of tubes and their layout. Yamashita (1987) reported an increase in gas holdup with diameter of single and multiple internals with number and size of internals while remaining same for different arrangements of the internals. The earliest explanations of these observations in various studies reasoned that the increase in gas holdup was solely due to decrease in free surface area for gas phase in the presence of internals resulting in a higher gas velocity. This was further supported by the work of Bernemann (1989). This theory was, however, contested by Al Mesfer *et al.* (2016) by plotting the gas-holdup based on

both total and free surface area. It was reported that the gas holdup at the center can be extrapolated from that of column without internals at higher inlet superficial velocities while an increase near the wall region was observed as an effect of internals. However, this phenomena is observed more with asymmetrically arranged internals than with circular tube bundles which cause bubbles to coalesce at the center region. Pradhan et al. (1993) reported higher holdup with helical coils in comparison to vertical internals. The author proposed that with the presence of internals (both helical and vertical), the area for gas phase motion is reduced, as a result the gas phase move more vigorously in radial directions. While the large tube-to-tube space of vertical internals allow large bubble to escape directly, the coils promote smaller bubbles, giving rise to higher gas holdup.

Guan *et al.* (2015) studied the hydrodynamics in a column with pin fin tube internals. They found that these internals have significant effect on local and overall gas holdup as well as liquid axial velocity. It was also reported that the presence of pin fin tube reduces the gas distributor region in the column. Further, changing the internal configuration, flow with no downward liquid flow can be realized with severe short circuiting. Further work on heat exchanging, RTD and mass transfer was suggested by the authors. Balamurugan *et al.*, (2010) studied the increase in gas holdup on inclusion of a vibrating helical coil type internal. It was reported that these internals increased the gas holdup by 135% from that without internals, due to breakup of bubbles by vibrating spring reducing their rise velocity and increasing the gas holdup.

2.2.1.1 Effects of Internals on Local Holdups

Local gas holdup measurements in presence of internals were conducted by Jasim (2016) using a four point optical probe to investigate the effect of configuration (circular and

hexagonal) and size of internals in same circular configuration (1.27 and 2.56 cm) on gas holdup and gas phase hydrodynamics with a constant CSA of 25%. A steeper increase and higher local gas holdup with both the circular arrangements was observed in the core region and a decrease at the wall regions. This implies a substantiated flow of gas to the center with circular arrangements. This may arise due to funneling effect causing gas to move at the low-pressure core region aided by bubble coalescence due to unrestricted flow at the center. For the smallest tube-to-tube space being (21.4 mm), the flow of large bubble across the bundle is restricted. While the arrangement with larger internals with a central tube and large tube-to-tube space enhanced the gas holdup and specific interfacial area near the wall regions. An asymmetrical radial profile for gas holdup and specific interfacial area were obtained for the hexagonal arrangement.

The local effects of internals configurations were investigated in more details in a recent work Möller et al. (2018) using ultrafast X-ray tomography. The study investigated the effects of different configurations and size of internals on gas holdup, bubble size distribution, bubble frequency and flow patterns. The radial gas holdup profile showed an oscillatory non uniform and flat profile in the vicinity of internals, in comparison to the parabolic profile in case of empty bubble column in both the bubbly and churn turbulent regime. They found an increasing gas holdup near the walls (kept free of internals) with decreasing pitch and subchannel area with bubbles preferentially rising in the wall zone with free wall area. Further, a distinction between the profiles for triangular and square profile was observed with considerably lower gas holdup in tube bundles for triangular pitch giving it a non-uniform holdup profile. This is attributed to smaller sub channels for triangular pitch with lower hydraulic diameters for flow in the bundle. A higher holdup

with superficial velocity was observed for square configuration (with higher hydraulic diameter) than with triangular (with lower hydraulic diameter). It was reasoned that the large bubbles formed in the triangular configuration move faster compared to the square configuration, where bubbles are trapped in subchannels having a lower velocity and increasing holdup in the column.

2.2.1.2 Effects on Liquid Flow Patterns

The gas entering a bubble column moves upwards, preferably along the center, transferring momentum to liquid flow. This upward velocity of liquid phase consequently creates a recirculation in the downward direction in the near wall region. This large-scale recirculation is the result of upward liquid velocity at the core region and a downward velocity near the walls in an empty bubble column. The presence of internals, however, affect this flow profile. While a circular bundle with no internal in the core region gives an enhanced central liquid velocity and a much more profound recirculation, the presence of a asymmetric internals decreases the magnitude of liquid velocity over the entire column, thus dampening the recirculation and large scale flow patterns. George *et al.* (2017) performed mixing experiments to examine the effects of internals on liquid recirculation and mixing in the presence of internals. The work examined a tube bundle type internal with a low CSA (approx. 10%) with an empty core region and a baffle. They reported a reduction in back-mixing effects with inclusion of baffle type internal placed below the tube bundle type internal. Further, studies revealed the effect of internals on time averaged flow patterns. It was reasoned that the presence of baffle type internal divert the large bubbles, creating a stronger vortical flow region that acts against the back-mixing, and enhancing the mixing in distributor region due to lower volume and more energetic flows.

Guan *et al.* (2014) conducted studies with different gas distributors in the presence of internals. They found that the effect of variation of distributor is global in the presence of internals as opposed to local impacts in hollow column. The type of gas distributor employed was able to modify the overall flow pattern of the column including the gas holdup and liquid velocity profiles. This was because with presence of internals, existence of well-developed region is difficult to form, and it was suggested the distributor design can be used as a source of controlling flow pattern in the column.

Forret *et al.* (2003) reported an increase in axial liquid velocity at the core while the radial profile remained the same. Also, an enhanced large scale recirculation in a large column with internals was observed, due to lower liquid velocity fluctuations with internals which is in agreement with observations of Chen *et al.* (1999). In a recent study, Möller *et al.* (2018), discovered that the presence of internals divided the column into sections of liquid ascending regions (sub channels) and descending regions (tube bridges and near the wall). Therefore, the liquid circulation eddies formed with dimensions of half the pitch, leading to a dampened liquid turbulence and energy strongly impacting the circulation pattern. It was concluded that the internals shift the gas holdup towards the wall and invert the profile compared to the empty BCR. This is most profound in configurations with highest flow resistance.

Dispersion in bubble column consists of two processes, the large-scale recirculation from upward and downward flow regions and turbulence or fluctuating velocity contributing to radial and axial mixing (Forret *et al.*, 2003). The presence of internals affects the processes responsible for dispersion and promote or dampen them. Generally, it has been reported

that the presence of internals increase large scale recirculation and decrease fluctuations (Chen *et al.*, 1999; Forret *et al.*, 2003; Youssef *et al.*, 2013; George *et al.*, 2017).

2.3 CFD Modeling of Bubble Column Hydrodynamics

Over the years, Computational Fluid Dynamic (CFD) simulations have emerged as a promising tool to investigate bubble hydrodynamics including gas holdup profiles, liquid velocity profiles, mixing time and shear stress profiles (Jakobsen, Lindborg, & Dorao, 2005; Joshi, 2001; Joshi & Nandakumar, 2015). Most of the studies have focused on hollow bubble column and only a few recent CFD simulation studies have been performed in bubble column with internals (Farıçal L

arachi *et al.*, 2006; Guan *et al.*, 2014, 2017; Guo *et al.*, 2017). The task of simulating the complex hydrodynamics of a bubble column operating in a heterogeneous regime becomes even more challenging in presence of internals. There is need to select appropriate modelling approach and modeling parameters and boundary conditions for more realistic simulation results while maintaining ensuring reasonable computational time. Two widely used modeling approaches for describing multiphase hydrodynamics in CFD simulations are Eulerian-Eulerian (E-E) and Eulerian-Lagrangian (E-L) (Buwa *et al.*, 2002; Van Wachem *et al.*, 2002; Darmana *et al.*, 2009). In the E-E model both the dispersed and continuous phases are treated as interpenetrating continuum while the volume-averaged mass and momentum equations describe the time-dependent motion of phases (Deen *et al.*, 2001; Buwa *et al.*, 2002). The number of bubbles present in a computational cell is represented by a volume fraction in the balance equations. The information of the bubble size distribution can be obtained by incorporating population balance equations to account for bubbles break-up and coalescence (Darmana *et al.*, 2009). The E-L approach tracks

motion of dispersed phase particles using Newtonian equation of motion while motion of the continuous phase is modeled using a Eulerian framework. Tracking the motion of dispersed phase particles allows direct consideration of effects related to bubble-bubble and bubble-liquid interactions. Mass transfer with and without chemical reaction, bubble coalescence and redispersion can be incorporated directly (Becker *et al.*, 1994; Delnoij *et al.*, 1997). A drawback of E-L model compared to E-E model is significant increase in computational time as number of bubbles (particles) to be simulated increase. Since for each bubble one equation of motion needs to be solved, making the method less attractive for large scale bubble column reactors (Darmana *et al.*, 2009). Since, tracking a huge number of bubbles requires a overwhelming amount of computational time, the Eulerian-Eulerian approach is more popular and used for the purposes discussed in this work. In addition, the high volume fraction of the dispersed phase renders the Lagrangian approach unsuitable for the churn turbulent regime. A two-fluid model based on the Euler-Euler approach treats both the phases as continuum and their mechanics is governed by partial differential equations. The equations are solved where variables are ensemble averaged over time and space while calculating the point phase fraction. The conservation equations are solved for each phase together with interphase exchange terms. Various interfacial forces are used to solve transport equations as closures for interactions between the phases.

Eulerian-Eulerian Model

The basic equation set consists of the continuity (conservation of mass) and momentum equations for N_p phases as detailed below (Pfleger and Becker, 2001)

Conservation of Mass

Mass variation over time + Convection term = Mass Transfer + Source Term

$$\frac{\partial}{\partial t}(\rho_l \varepsilon_l) + \frac{\partial}{\partial x_i}(\rho_l \varepsilon_l U_{l,i}) = \sum_{p=1}^{N_p-1} (\dot{m}_{lg} - \dot{m}_{gl}) + \varepsilon_l S_l \quad (2.11)$$

Here,

$$\sum_{k=1}^{N_p} \varepsilon_k = 1 \quad (2.12)$$

Momentum balance

$$\frac{\partial}{\partial t}(\rho_k \varepsilon_k U_{k,i}) + \frac{\partial}{\partial x_j}(\rho_k \varepsilon_k U_{k,i} U_{k,j}) = \varepsilon_k \frac{\partial p}{\partial x_i} + \frac{\partial}{\partial x_j} \varepsilon_k \mu_k \left(\frac{\partial U_{k,i}}{\partial x_j} + \frac{\partial U_{k,j}}{\partial x_i} \right) + \rho_k \varepsilon_k g + M_{k,i} \quad (2.13)$$

where, Pressure gradient = $\varepsilon_k \frac{\partial p}{\partial x_i}$;

Viscous stresses = $\frac{\partial}{\partial x_j} \varepsilon_k \mu_k \left(\frac{\partial U_{k,i}}{\partial x_j} + \frac{\partial U_{k,j}}{\partial x_i} \right)$;

Gravitational force = $\rho_k \varepsilon_k g$ and $M_{k,i}$ is the interphase momentum transfer term given by

$$M_{k,i} = \frac{3}{4} \frac{C_D \varepsilon_G \rho_k}{d_b} |U_G - U_L| \quad (2.14)$$

Further details of the model can be found in Pflieger and Becker (2001) and Buwa and Ranade (2002).

Eulerian-Lagrangian

This modeling approach computes the motion of each bubble from bubble mass and momentum equations. The liquid phase contributions are accounted for by the interphase mass transfer rate and the net force experienced by each bubble (Darmana *et al.*, 2009). For an incompressible bubble, the equations can be written as

Bubble mass balance:

$$\rho_b \frac{d(V_b)}{dt} = (\dot{m}_{l \rightarrow b} - \dot{m}_{b \rightarrow l}) \quad (2.15)$$

Here, V_b is bubble volume and v is bubble velocity. The term on right hand side represents mass transfer.

Bubble momentum balance:

$$\rho_b V_b \frac{dv}{dt} = \sum F - \left(\rho_b \frac{dV_b}{dt} \right) v \quad (2.16)$$

$\sum F$ represents the net force experienced by individual bubble which include gravity, pressure, drag, lift force and virtual mass.

$$\sum F = F_g + F_p + F_D + F_L + F_{VM} \quad (2.17)$$

Liquid phase balances:

The liquid phase equations consist of continuity and momentum equations represented by the volume averaged Navier-Stokes equations. The presence of bubbles is reflected by the

liquid phase volume fraction, which are outlined in Darmana *et al.* (2009) for additional details of model equations.

A summary of the literature studies based on the effect of internal geometries on hydrodynamics in the column using numerical modeling is presented in Appendix A. The first CFD study of bubble columns with vertical internals was performed by Larachi *et al.* (2006). The effect of different configurations and covered CSA were simulated. The study revealed effect of arrangements on the liquid circulation pattern, inter-tube gap on growth of flow structures (small scale recirculation) and overall effect of internals on turbulence parameters.

In a conventional bubble column reactor, the gas phase is bubbled through the stationary liquid phase. The dispersion of gas in the liquid medium imparts turbulence and alters the interphase forces such as drag, lift, virtual mass etc. Several literature studies have focused on the study of various models that are available for the turbulence and interphase forces (Joshi, 2001; Jakobsen *et al.*, 2005; Tabib *et al.*, 2008; Selma *et al.*, 2010; Besagni *et al.*, 2017). To date, different methodologies like Euler-Euler, Euler-Lagrangian and Algebraic Slip Mixture Model (ASMM) have been applied to model the gas-liquid flows.

The current review is divided into two sections. In the first section, a comprehensive review of numerical studies on hollow bubble column reactors has been made. In the next section, numerical studies on bubble columns with internals has been thoroughly reviewed and presented.

2.3.1 Turbulence Models

A wide range of viscous models have been employed to model the highly turbulent flow within bubble column reactors. These comprise of the Standard $k - \varepsilon$, $k - \varepsilon$ RNG, $k - \omega$ and the Reynolds Stress Model (RSM). Few of the recent studies have also employed the Large Eddy Simulation (LES) turbulence model to simulate the turbulence within bubble columns. The right choice of turbulence model is essential to capture the transient flows which determines the velocities and other hydrodynamic parameters within the bubble column reactor.

2.3.1.1 Standard $k - \varepsilon$ model

The equations for turbulent kinetic energy, k , and its dissipation, ε , are illustrated in the equations below

$$\frac{\partial}{\partial t}(\alpha_l \rho_l k) + \frac{\partial}{\partial x_i}(\alpha_l \rho_l k U_l) = \frac{\partial}{\partial x_j} \left[\alpha_l \left(\mu + \frac{\mu_t}{\sigma_k} \right) \frac{\partial k}{\partial x_j} \right] + \alpha_l (G_{k,l} - \rho_l \varepsilon) + \alpha_l \rho_l S_{k,l} \quad (2.18)$$

$$\frac{\partial}{\partial t}(\alpha_l \rho_l \varepsilon) + \frac{\partial}{\partial x_i}(\alpha_l \rho_l \varepsilon U_l) = \frac{\partial}{\partial x_j} \left[\alpha_l \left(\mu + \frac{\mu_t}{\sigma_\varepsilon} \right) \frac{\partial \varepsilon}{\partial x_j} \right] + \alpha_l (C_{1,\varepsilon} G_{k,l} + C_{2,\varepsilon} \rho_l \varepsilon) \frac{\varepsilon}{k} + \alpha_l \rho_l S_{\varepsilon,l} \quad (2.19)$$

Equations 2.1 and 2.2 have been modified to analyze the effect of multiphase flow (ANSYS, 2013). Turbulent viscosity is the momentum transfer by the virtue of eddies which generates internal fluid friction. This is defined as:

$$\mu_t = \rho_l C_\mu \frac{k^2}{\varepsilon} \quad (2.20)$$

$G_{k,l}$ is a source term which accounts for the turbulent kinetic energy production:

$$G_{k,l} = \mu_{l,t} S_q^2 \quad (2.21)$$

where S_q represents the modulus of the mean strain rate tensor.

$$S_q = \sqrt{S_{q,ij} S_{q,ij}} \quad (2.22)$$

$S_{k,l}$ and $S_{\varepsilon,l}$ signify the source terms that account for the consequence of turbulent two-way coupling. Here, σ_k and σ_ε represent the turbulent Prandtl numbers, and $C_{1,\varepsilon}$, $C_{2,\varepsilon}$ and C_μ are constants. The values of these constants that are suggested by Launder and Spalding (1974) have been outlined in Table 2.1.

Table 2.1 Constants for standard k- ε turbulence model as suggested by Launder and Spalding (1974)

Constants	σ_k	σ_ε	$C_{1,\varepsilon}$	$C_{2,\varepsilon}$	C_μ
Values	1.0	1.3	1.44	1.92	1.0

Simulation of cylindrical bubble columns with the standard k- ε model was tested by (Silva, d'Ávila and Mori (2012)). The study was conducted both in the bubbly regime (2 cm/s) and the heterogenous regime (8 cm/s). In the fully developed region, the radial gas holdup and axial velocities have nearly matched the experimental data. In their study, Krishna and Van Baten, (2001) have utilized the standard k- ε model to model the small and large bubble size fractions within a bubble column reactor. They have reported close conformance of axial dispersion coefficients and liquid velocities with the experimental data. A study carried out by Pflieger and Becker, (2001) have employed the standard k- ε model to simulate mono-dispersed flow within bubble column reactors. In the bubbly flow regime, the numerical

study was able to successfully predict the low scale of velocity fluctuations. Large scale instantaneous vortical flow structures were appropriately modeled by introducing the $k-\varepsilon$ turbulence model. The numerical values of liquid axial velocities closely conformed to the experimental values measured by LDA. However, the numerical values of radial gas holdup have underpredicted the local and overall gas holdups. The authors report that the addition of Bubble Induced Turbulence (BIT) term to the turbulence model improves the prediction of liquid velocities but depreciates the gas holdup estimates. In their study, Becker *et al.* (1994) have reported that the standard $k-\varepsilon$ model has overestimated the turbulent viscosities which in turn decreases the number of vortices, a behavior that contradicts to the experimental observations.

In summary, the standard $k-\varepsilon$ model is suitable in predicting the bubble column flow in the fully developed regime. This model can effectively predict hydrodynamic parameters like local and overall gas holdups and liquid velocities. Information on the suitability of the $k-\varepsilon$ model in the prediction of turbulent parameters for bubble column flows is disputed and must be further investigated.

2.3.1.2 RNG $k - \varepsilon$ model

The $k-\varepsilon$ Renormalization Group (RNG) model is superior when compared to the standard $k-\varepsilon$ model as it can effectively predict the swirling motion of flows. The principle difference between the standard and RNG $k-\varepsilon$ model is that the constants are explicitly determined by the latter compared to the determination of the constants by experimental techniques in the former. The transport equations that govern the turbulent kinetic energy and dissipation rates for the primary phase are shown in equations 2.6 and 2.7 respectively.

$$\frac{\partial}{\partial t}(\alpha_l \rho_l k) + \frac{\partial}{\partial x_i}(\alpha_l \rho_l k U_l) = \frac{\partial}{\partial x_j} \left[\alpha_l \left(\mu + \frac{\mu_t}{\sigma_k} \right) \frac{\partial k}{\partial x_j} \right] + \alpha_l (G_{k,l} - \rho_l \varepsilon) + \alpha_l \rho_l S_k^{BI} \quad (2.23)$$

$$\frac{\partial}{\partial t}(\alpha_l \rho_l \varepsilon) + \frac{\partial}{\partial x_i}(\alpha_l \rho_l \varepsilon U_l) = \frac{\partial}{\partial x_j} \left[\alpha_l \left(\mu + \frac{\mu_t}{\sigma_\varepsilon} \right) \frac{\partial \varepsilon}{\partial x_j} \right] + \alpha_l (C_{1\varepsilon} G_{k,l} - C_{2\varepsilon}^* \rho_l \varepsilon) \frac{\varepsilon}{k} + \alpha_l \rho_l S_\varepsilon^{BI} \quad (2.24)$$

$C_{2\varepsilon}^*$ and η are defined as

$$C_{2\varepsilon}^* = C_{2\varepsilon} + \frac{C_\mu \eta^3}{1 + \beta \eta^3} \left(1 - \frac{\eta}{\eta_0} \right) \quad (2.25)$$

$$\eta = \frac{Sk}{\varepsilon} \quad (2.26)$$

The source terms S_k^{BI} and S_ε^{BI} represent the effect of bubbles on the primary phase. These are modeled using the following relations

$$S_k^{BI} = F_L^{drag} (U_G - U_L) \quad (2.27)$$

$$S_\varepsilon^{BI} = \frac{C_{\varepsilon B} S_k^{BI}}{\tau} \quad (2.28)$$

where τ is the time scale and $C_{\varepsilon B}$ may depend on additional dimensionless variables corresponding to the ratio of length or velocity scales (Rzehak and Krepper, 2013).

In their study, Ekambara and Dhotre (2010) have compared the suitability of various turbulence models in bubble column simulations. In the sparger region, RNG k- ε model was unable to capture the anisotropic nature of the liquid flow. They have reported that the RNG k- ε model was able to appropriately capture the liquid axial velocities and fractional gas holdups at various axial locations. However, the RNG k- ε model overestimated the

values of turbulent kinetic energy in the distributor region. Also, the RNG k- ε model has underestimated the values of turbulence dissipation rate near the wall region at higher axial locations. In another study carried out by Liu and Hinrichsen (2014), the applicability of RNG k- ε model has been tested. This model overestimated the values of turbulence dissipation rate close to the wall region. As the bubble size distribution is affected by the turbulence dissipation rates, a large variation in the Sauter mean diameter near the wall region was observed. This resulted in the generation of bubbles with smaller diameters which contradicts to the experimental observations.

2.3.1.3 Reynolds Stress Model (RSM)

The Reynolds Stress Model (RSM) employs a different technique in modeling the Reynolds stresses. This model was first developed by (Launder, Reece and Rodi, 1975). The formulation of a separate transport equation for each tensor eliminates the assumption of proportionality between Reynolds stress tensor and mean deformation rate (Gatski and Jongen, 2000; Hamlington and Dahm, 2008). The simplified transport equations for the RSM model is illustrated in Equation 2.12.

$$\frac{\partial}{\partial t}(\rho_L \varepsilon_L u_i' u_j') + C_{ij} = \varphi_{ij} + D_{L,ij} - D_{T,ij} - P_{ij} - \varepsilon_{ij} \quad (2.29)$$

where C_{ij} is the convection term, φ_{ij} is the pressure term, $D_{L,ij}$ is the molecular diffusion term, $D_{T,ij}$ is the turbulent diffusion term, P_{ij} is the stress production term and ε_{ij} is the dissipation term. These terms are described in Table 3.1.

The Reynolds stress model is effectively superior to the standard k- ε model and RNG k- ε model in the prediction of swirling motion of flows within bubble column reactors

(Launder *et al.*, 1975; Cokljat *et al.*, 2006). In their study, Cartland Glover and Generalis (2004) have reported that the Reynolds stress model is capable of effectively capturing the unsteady flow structures present in bubble columns. The vertical velocity profile was reported to be constantly changing with each time step. This behavior was not observed on using the two model turbulence equations. Also, the hydrodynamic parameters captured by the Reynolds stress model were in close correspondence to the experimental values. In a recent study of comparison between different turbulence models carried out by Parekh and Rzehak (2018), RSM model was able to capture the pronounced wall peaks in the radial gas holdup profiles similar to the experimental trend. All the turbulence models in consideration overestimated the liquid flux in the wall region. However, RSM offered a lesser degree of overprediction compared to the other turbulence models. A close prediction of shear stress values was achieved using RSM model.

2.3.2 Interfacial Forces

Interfacial forces play a major role in the computational modelling of multiphase flows. The standard momentum balance equation is modified to include the influence of these forces. Various interfacial forces include drag, lift, added virtual mass, turbulent dispersion and turbulent interaction forces. The drag force, known as the chief force, involved in the bubble column reactor modelling, has been widely studied in various literature studies. The effect of other interfacial forces is not very pronounced in the literature and very few studies focus on the combined effect of these forces. When the numerical studies involve the combined effect of the appropriate interfacial forces, it will lead to an accurate prediction of hydrodynamic parameters.

2.3.2.1 Virtual Mass Force

In multiphase flows, the effect of virtual mass force is experienced when a dispersed phase accelerates with respect to the stationary phase. In bubble column reactors, the virtual mass force is exerted by the action of bubbles accelerating through the liquid phase. This is a result of inertial force influenced by the liquid phase when encountered by the gaseous bubbles rising through the liquid column. The influence of added mass force is prominent in the case of transient flows involved in a bubble column reactor due to the significant difference in densities between liquid and gas phase.

The added mass force is characterized by:

$$\vec{F}_{vm,L} = \varepsilon_G \rho_L C_{VM} \left(\frac{d_G}{dt} \vec{u}_G - \frac{d_L}{dt} \vec{u}_L \right) \quad (2.30)$$

The derivative associated with the above equation is termed as the phase material time form, which is defined as:

$$\frac{d_G}{dt} (f) = \frac{\partial (f)}{\partial t} + (\vec{u}_G \cdot \nabla) f \quad (2.31)$$

The value of virtual mass coefficient for spherical shaped bubbles is $C_{VM} = 0.5$. The virtual mass force plays an important role in reaching the stability at early stages of the flow formation within a bubble column reactor. When virtual mass force is enabled in the numerical study, bubbles accelerations through the liquid column are limited. Once the simulation reaches the pseudo-steady state, the influence of virtual mass force is insignificant (Smith, 1998; Dhotre *et al.*, 2009).

2.3.2.2 Drag Force

The drag force is the resistance experienced by the bubbles rising through the column of liquid. The drag force could be a combination of two types of resistances including skin friction and form drag. The influence of drag force on two-phase bubble columns is superior when compared to other interfacial forces like turbulent dispersion, lift, virtual mass and turbulent interaction forces. The axial velocities and overall holdups of gaseous phase within the bubble column are strongly governed by the drag model. It becomes an important parameter as it determines the terminal velocity and residence time of bubbles (Yang *et al.*, 2018).

Yang *et al.* (2018) have studied the influence of drag force on the bubble swarms as it is quite different from single bubbles. The bubble rise velocities of bubble swarms are non-identical to that of the single bubbles, due to which the drag coefficients and terminal velocities of the former are different from the latter. Complex bubble interactions associated with the bubble swarms is another factor which affects the variation seen in drag coefficients.

The drag force between the gas and liquid phase is described as:

$$F_{D,l} = 0.75 \varepsilon_L \rho_L \frac{C_D}{d_b} |u_G - u_L| (u_G - u_L) \quad (2.32)$$

The drag coefficient, C_D , is a function of liquid properties, hydrodynamic interaction between the bubbles and flow regimes. When the bubble size distribution within a bubble column reactor under consideration is constant, a constant drag force coefficient could be employed. A few studies by Smith (1998), Pflieger and Becker (2001) and Dhotre and Smith

(2007) have been carried out that illustrates the effect of constant drag force as the interfacial force.

Variety of drag force models such as Schiller-Naumann, Zhang-Vanderheyden, Tomiyama et al., Grace et al. and Ishii-Zuber have been widely used in numerically solving bubble column reactors.

The drag coefficient for the Schiller and Naumann drag force model is described as

$$C_d = \begin{cases} \frac{24 (1+0.15 N_{Re}^{0.687})}{N_{Re}}, & N_{Re} \leq 1000 \\ 0.24, & N_{Re} > 1000 \end{cases} \quad (2.33)$$

The Reynolds Number (Re) associated with this drag model is the bubble Reynolds number which is determined using the effective bubble diameter, slip velocity between the primary and secondary phases, liquid properties such as dynamic viscosity and density.

$$Re = \frac{\rho_L |\vec{v}_L - \vec{v}_G| d_b}{\mu_L} \quad (2.34)$$

Many literature studies have suggested that the Schiller Naumann drag force model is well suited for gas-liquid flows in the bubbly flow regime, where the superficial gas velocities are below 5 cm/s. This drag model does not account for the shape factor of the bubbles as the Eotvos number is absent in the drag force formulation. The hydrodynamics of the two-phase flows is well captured in the current drag model as it takes the Reynolds number into consideration, which in turn is a function of bubble diameter.

In a study conducted by Law *et al.* (2008), Schiller-Naumann and White and Corfield (2006) drag models were compared to simulate a bubble column in bubbly and churn-

turbulent regime. At lower and higher axial heights, the Schiller-Naumann and White and Corfield (2006) drag model exhibited close accordance of hydrodynamic parameters with experimental data. Schiller-Naumann model worked better at higher axial heights compared to the White model. In the bubbly flow regime, the authors have recommended the addition of surface tension and bubble induced turbulence models to the drag models to accurately predict the flow dynamics. In contrast to the observations made by some others, Schiller Naumann drag model has been successfully implemented by Chen *et al.* (2004) and Kumar *et al.*, (2011), to study the hydrodynamics in bubble column reactors operating in the churn turbulent regimes and the numerical results were in close conformance with those of the experimental observations.

The Tomiyama drag model is well suited for studying bubble columns in the transition and churn turbulent regimes where the bubble size distribution is wide. This drag model takes the shape factor of the gaseous bubbles into consideration as the Eotvos number (Eo) is present in the drag model formulation. The Eotvos number is a dimensionless parameter which governs the bubble shapes by comparing the gravitational and surface tension forces. In their study, Guan and Yang (2017) have reported that the use of this drag model overpredicts the values of gas phase holdups and underpredicts the circulation intensity. The study also concluded that Tomiyama drag model demonstrated least agreement with the experimental data in the absence of the effect of lateral forces like lift, turbulent dispersion and wall lubrication forces.

The bubble shape is an important parameter in the estimation of drag coefficient (Ceylan, Altunbacs and Kelbaliyev, 2001; Tran-Cong, Gay and Michaelides, 2004; Simonnet *et al.*, 2007). In their work, Grace *et al.* (1976) demonstrated that the terminal velocity of a rising

gas bubble in a stagnant liquid can be linked with the Morton and Eötvös number. Morton number is a function of the property group of the primary and secondary phases (Bhaga and Weber, 1981; Koynov *et al.*, 2005) and Eötvös number is the ratio of buoyancy to the surface tension forces (Roghair *et al.*, 2011; Aoyama *et al.*, 2016). The Grace *et al.* (1974) model has not been used extensively in the literature to simulate the bubble column flows. Silva *et al.* (2012) have studied and compared the effect of different drag models like Ishii and Zuber (1979), Zhang and Vanderheyden (2002) and Grace *et al.* (1976). They have reported that Grace drag model predicted uniform gas holdup profile in the central region while a slight deviation of 12% is noticed in the wall region as compared to the 31% by the Zhang-Vanderheyden drag model. On the other hand, the Grace drag model underpredicted the gas velocity values in comparison to the Ishii-Zuber model. The effect of Grace drag model was only studied for the homogenous regime. One such recent study that employs this drag model is carried out by Zhu *et al.* (2020). They have reported that when the lift model employed by Tomiyama *et al.* (2002) was employed, the Grace *et al.* (1976) drag model outperformed the other drag closures in the prediction of liquid axial velocity profiles. The values of axial gas velocities were in close accordance when the Grace *et al.* (1976) drag closure was combined with constant lift model. Lateral fluctuations of liquid velocity were underpredicted when this drag model was employed. In general, the combination of Grace *et al.* (1976) drag model and constant lift force outperformed rest of the combinations in determining the hydrodynamics. When this model was used in the determination of radial gas holdups, an accurate prediction has been reported.

Ishii and Zuber (1979) finds its application in modeling large bubble sizes owing to its ability to model various bubble shapes like spherical, ellipsoidal and cap. In a study carried

out by Deen *et al.* (2001), the Ishii and Zuber (1979) drag model was employed to simulate a rectangular bubble column reactor. When the drag model was enabled along with the lift force, the plume was spread across the column and the experimental trends were observed. It was noticed that this drag model outperformed when LES turbulence model was employed in comparison to the standard k- ϵ model. The numerical values of axial liquid velocities and turbulent kinetic energies were in close agreement with the experimental results using the technique of Particle Image Velocimetry (PIV). In another study carried out by Deen *et al.* (2000), the plume was seen to consistently move near the wall region resulting in asymmetric velocity profiles. In a study by Zhang *et al.* (2006), a comparison has been made between Tomiyama and Ishii-Zuber drag models. They have noticed that the Ishii-Zuber drag model closely estimates the average liquid axial velocities compared to the Tomiyama model in columns of shorter heights. However, the slip velocity was underpredicted by the Ishii-Zuber model in comparison to the Tomiyama drag model. In taller columns, a reverse trend was noticed i.e. Ishii-Zuber model underestimated the values of average liquid axial velocities in comparison to the Tomiyama drag model.

2.3.2.3 Transversal Lift Force

The component of force subjected to the dispersed phase which is perpendicular to the velocity direction is termed as the transversal or lateral or lift force. In symmetric flows, the symmetric bodies experience a zero lift force. The physical principle behind the lift forcing acting on a single spherical bubble can be divided into the Magnus and Saffman lift forces. The Magnus lift force arises from the bubble rotation which is a resultant of asymmetric pressure distribution around the bubble (Swanson, 1961). Over the last decades, numerous studies have been carried out to establish the origin of this force (Swanson, 1961; Svendsen

et al., 1992; Tzeng *et al.*, 1993). In his early study, Swanson (1961) concluded that the traversal force acts in the less chaotic region (low speed) if the bubbles tends to move with the flow or faster than the flow. On the other hand, Saffman forces move the non-rotating particle perpendicular to the flow direction when it is placed in a shear flow (Saffman, 1965). At lower Reynolds number, the Saffman force outweighs the Magnus force only if the rotating speed of the dispersed phase is not large enough (Saffman, 1965).

Thomas *et al.* (1983) have derived an expression for the traverse force experienced by a spherical gas bubble which is given as:

$$F_L = \varepsilon_G \varepsilon_L \rho_G C_L (U_G - U_L) \mathbf{x} (\nabla \mathbf{x} U_G) \quad (2.35)$$

In modeling of bubble column reactor, lift force accounts for the effect of shearing motion of the continuous phase on the movement of the dispersed bubbles. Some studies have shown that it is possibility of neglecting the lift force formulation to reduce computational time and cost (Chen *et al.*, 2005; Xu *et al.*, 2013; Pourtousi *et al.*, 2015). Nevertheless, it has been widely reported that adding the lift force formulation spreads the bubbles evenly over the bubble column cross section (Lain and Sommerfeld, 2004; Vanga *et al.*, 2004; Lucas *et al.*, 2005; Krepper *et al.*, 2007). Also, the small bubble plume generated from the gas distributor is spread across the column cross section (Vanga *et al.*, 2004).

For the most part, the two types of lift force coefficients used in bubble column modelling are constant lift coefficient and lift coefficient based on the Reynolds number and Eotvos number of the dispersed phase. Over the years, numerous studies have employed a wide range of lift force coefficients which sparks a need to delve deeper into the dynamics behind

the effective choice of this coefficient. Table 2.2 illustrates the different lift coefficients that have been employed so far in modelling bubble column reactors. Table 2.3 highlights the lift force formulations.

Table 2.2 List of lift force coefficients employed in the literature

Authors and Year	Superficial Gas Velocity, U_G (m/s)	Lift force coefficient, C_L
Drew and Lahey Jr (1987)	0.244 – 0.748	0.25 – 0.30
Grienberger and Hofmann (1992)	0.02, 0.08	-0.5
Ranade (1997)	0.02, 0.024, 0.038, 0.06, 0.08, 0.095	0.1 – 0.2
Jakobsen <i>et al.</i> (1997)	0.2-0.3	-1.5
Buwa and Ranade (2002)	0.0016	0.5
Thakre and Joshi (1999)	0.235	0.1, 0.26, 0.18, 0.19, 0.21, 0.4
Boisson and Malin (1996)	0.077, 0.08	-0.5
Dhotre <i>et al.</i> (2009)	Bubbly flow	0.1-0.5

In their study, Drew and Lahey (1987) demonstrated that the value of lift coefficient for an inviscid flow around a sphere is $C_L=0.5$. Studies by Buwa and Ranade (2002) and Zhang

et al. (2006) have confirmed this coefficient by implementing it in their model. Dhotre *et al.* (2009) have recommended a positive value of lift coefficients between 0.1 and 0.5 in the bubbly flow regime. In their work, Tabib *et al.* (2008) have demonstrated the sensitivity of lift force coefficient to reach an effective numerical solution. In the bubbly flow regime, when the lift coefficients were switched from negative to positive values, a minimal deviation was noticed in the values of radial gas holdups and liquid axial velocities. However, in the heterogenous regime, the positive values of lift force coefficient decreased the centerline liquid axial velocity and flatter gas holdup profiles were noticed. Hence, the lift coefficient based on the bubble size gave better predictions of hydrodynamic parameters.

The sign of lift force coefficient adds to the already existing misperception surrounding its choice. A number of studies involving bubble column reactors have reported a negative value of lift coefficient between -0.01 and -1.5 (Elena Díaz *et al.*, 2009). The negative values of lift force coefficient tend to push the bubbles to regions of higher liquid velocities. In their work, Sankaranarayanan and Sundaresan (2002) reported that the use of negative lift coefficients to obtain higher holdups in the central region cannot be accepted. To overcome this problem, Tomiyama (1995) and Tomiyama *et al.* (2002) have developed a lift model based on the Eotvos number which is in turn dependent on the bubble diameters.

Table 2.3 Lift force coefficient formulations

Author and Year	Lift Coefficient Formulation
Tomiyama (1995)	$C_L = -0.004Eo + 0.48$

$$N_{Eo} = \frac{gd_b^2(\rho_L - \rho_G)}{\sigma}$$

Tomiyama *et al.*
(2002)

$$C_L = \begin{cases} \min [0.288 \cdot \tanh(0.121Re_g), f(Eo')], & Eo' \leq 4 \\ f(Eo'), & 4 < Eo' \leq 10 \\ -0.27, & 10 < Eo' \end{cases}$$

where, Eo' is modified Eotvos number to estimate the deformable bubble size

$$f(Eo') = 0.00105Eo'^3 - 0.0159Eo'^2 - 0.0204Eo' + 0.474$$

$$Eo' = \frac{gd_b^2(\rho_L - \rho_G)}{\sigma} (1 + 0.163Eo'^{0.757})^{2/3}$$

$$Eo = \frac{gd_b^2(\rho_L - \rho_G)}{\sigma}$$

According to the first correlation, the value and sign of the lift force coefficient depends on the bubble diameter. For bubbles of diameter greater than 9 mm dispersed in water, the lift coefficient takes a negative value. In a modification to the initial correlation, Tomiyama *et al.* (2002) lift coefficient was developed. With this modified correlation, when the bubble diameters are less than or equal of 4 mm, the lift coefficient takes a negative value thereby pushing the small bubbles closer to the wall. Bubbles of larger diameter are pushed towards the central region.

2.3.2.4 Turbulence Dispersion Force

The turbulent dispersion force is responsible for the effect of eddies formed by the continuous phase on the bubbles. This force is a resultant of the turbulent fluctuations of liquid velocity. In bubble column reactor modeling, widely used turbulent dispersion

formulations are proposed by de Bertodano (1991) and Burns *et al.* (2004). A limited studies have employed the model proposed by Simonin *et al.* (1990). The radial gas holdup profiles are affected by the choice of turbulence dispersion force (Lucas *et al.*, 2007). The turbulent dispersion force is responsible for pushing the bubbles away from the central region of the column when negative lift force coefficient is employed.

In bubble columns, the values of coefficient of turbulent dispersion can range between 0 to 0.5 (Pourtousi *et al.*, 2014; Gaurav, 2018). In a study by Tabib *et al.* (2008), three values of turbulent dispersion coefficients, 0, 0.2 and 0.5 have been employed for homogenous and heterogenous regimes. In the bubbly flow regime, the effect of turbulent dispersion was not very pronounced. It was noticed that at higher velocities, when the value of the turbulent dispersion coefficient was increased, the gas holdups became flatter. In another study by Silva *et al.* (2012), turbulent dispersion coefficients of 0.1 and 0.2 were used for superficial gas velocities of 0.02 and 0.08 m/s. They have reported a decrease in the gas velocity profile upon implementing the turbulent dispersion force.

In summary, for bubble columns, the turbulent dispersion coefficients are between 0.1 and 0.5. For bubbly flows ($U_G < 5$ cm/s), the turbulent dispersion coefficient value could be 0.1. For transition regime ($5 < U_G < 10$ cm/s), the turbulent dispersion coefficient value could be 0.2. For churn-turbulent regimes ($U_G > 10$ cm/s), the turbulent dispersion coefficient could be set to 0.3.

2.4 CFD Studies on Bubble Column with Internals

Lately, bubble columns reactors as multiphase contactors are preferred for a wide range of industrial applications especially in the sectors of process, biochemical, metallurgical and petrochemical industries (Youssef and Al-Dahhan, 2009; Jhavar and Prakash, 2011; George *et al.*, 2017). For specific applications such as Fischer-Tropsch and methanol synthesis, bubble column reactors are provided with internals that facilitate heat transfer and improve mixing characteristics (Youssef and Al-Dahhan, 2009; Abdulmohsin and Al-Dahhan, 2012). When innards are added in a bubble column, it adds complexity to the flow dynamics. Heretofore, several laboratory and pilot scale studies have investigated the effects of internals on the hydrodynamic parameters and fluid dynamics of bubble columns. However, there is a dearth in the number of numerical studies that have been executed on bubble column reactors with internals. Some of these studies have been tabulated in Appendix B.

In one of the preliminary numerical studies on obstructed bubble columns, Larachi, F. *et al.* (2006), have investigated the effect of different circular tube internals on hydrodynamic and turbulence parameters. They have studied the effect of two bubble sizes (5 mm and 19 mm) on the flow patterns and hydrodynamics. However, the numerical results were not validated with experimental data and it was noticed that the liquid behavior was not in accordance with observations made in experiments (Guan *et al.*, 2014; Agahzamin and Pakzad, 2019). In another numerical study performed by Laborde-Boutet *et al.* (2010), U-shaped cooling tubes as internals within a bubble column reactor is simulated. Here, a suitable model that couples hydrodynamics and thermal phenomena has been investigated and the heat transfer coefficients obtained through the numerical approach has been

compared with experimental data. The authors have made use of only drag model as the interphase force and RNG k - ϵ per phase formulation as the turbulence model. The authors have reported superior heat transfer rates at higher levels of turbulence.

In their work, Guan and Yang (2017), have presented the sensitivity of interfacial forces (including drag, lift, turbulent dispersion and wall lubrication) on hydrodynamic parameters within a bubble column reactor occluded with internal rods. The right choice of lateral forces were deemed necessary to accurately predict the flow when internals are present. When lift force was considered, the liquid velocities and gas holdups steepened by a considerable amount. By adding the turbulent dispersion force, large-scale liquid recirculations were noticed. In presence of the wall lubrication effect, the gas holdups decreased in the vicinity of internal rods and increased beyond physical sense in its absence.

Bhusare *et al.* (2018) have simulated the liquid phase mixing and hydrodynamic parameters in a co-current upflow bubble column. They have employed two configurations of internal rods: (1) column with one vertical rod at the center (2) column with the same rod at the center and four vertical rods in the bulk region. The authors have reported that the turbulence induced by the internals increases the eddy diffusivity values. Also, a significant improvement in the mixing quality was noticed in the presence of internals as compared to hollow bubble columns. This was due to the increase in axial dispersion coefficients which in turn influences the mixing patterns. The numerical data was compared with experimental measurements.

In one of the recent studies presented by Agahzamin and Pakzad (2019), the impact of dense vertical internals on bubble column hydrodynamics and turbulence parameters has been investigated. The study was performed with three sets of circular rod internal configurations. They have reported a significant increase in gas holdup values, superior liquid recirculation and higher gas velocities as a general consequence of the presence of internals. By increasing the pitch of the tube layout, flatter velocity distributions and gas holdups were noticed. A narrow bubble size distribution was noticed in the presence of internals in comparison to the hollow bubble column.

2.5 Concluding Remarks

The above comprehensive review on numerical simulations of bubble column hydrodynamics shows that many studies have addressed the influence of various flow, turbulence and interfacial forces models on bubble column hydrodynamics., There is however, a lack of coherent and systematic approach to cover the applicable effects in different flow regimes for the purpose of scale and other practical implementation of simulation results.

References

- Abdulmohsin, R. S. and Al-Dahhan, M. H. (2012) 'Impact of internals on the heat-transfer coefficient in a bubble column', *Industrial & Engineering Chemistry Research*. ACS Publications, 51(7), pp. 2874–2881.
- Agahzamin, S. and Pakzad, L. (2019) 'A comprehensive CFD study on the effect of dense vertical internals on the hydrodynamics and population balance model in bubble columns', *Chemical Engineering Science*, 193, pp. 421–435.
- ANSYS (2013) 'Ansys Fluent Theory Guide', 15317, p. 513.
- Aoyama, S., Hayashi, K., Hosokawa, S. and Tomiyama, A. (2016) 'Shapes of ellipsoidal bubbles in infinite stagnant liquids', *International Journal of Multiphase Flow*. Elsevier, 79, pp. 23–30.
- Balamurugan, V., Subbarao, D. and Roy, S. (2010) 'Enhancement in gas holdup in bubble columns through use of vibrating internals', *The Canadian Journal of Chemical Engineering*. Wiley Online Library, 88(6), pp. 1010–1020.
- Becker, S., Sokolichin, A. and Eigenberger, G. (1994) 'Gas—liquid flow in bubble columns and loop reactors: Part II. Comparison of detailed experiments and flow simulations', *Chemical engineering science*. Elsevier, 49(24), pp. 5747–5762.
- Bernemann, K. (1989) *On the hydrodynamics and mixing of the liquid phase in bubble columns with longitudinal tube bundles*. Ph. D. Thesis, University of Dortmund, Germany.
- de Bertodano, M. (1991) 'Turbulent bubbly flow in a triangular duct', *New York: Rensselaer Polytechnic Institute*.
- Besagni, G., Inzoli, F., Ziegenhein, T. and Lucas, D. (2017) 'Computational Fluid-Dynamic modeling of the pseudo-homogeneous flow regime in large-scale bubble columns', *Chemical Engineering Science*. Elsevier, 160, pp. 144–160.
- Bhaga, D. and Weber, M. E. (1981) 'Bubbles in viscous liquids: shapes, wakes and velocities', *Journal of fluid Mechanics*. Citeseer, 105, pp. 61–85.
- Bhusare, V. H., Kalaga, D. V, Dhiman, M. K., Joshi, J. B. and Roy, S. (2018) 'Mixing in a co-current upflow bubble column reactors with and without internals', *The Canadian Journal of Chemical Engineering*. Wiley Online Library, 96(9), pp. 1957–1971.
- Boisson, N. and Malin, M. R. (1996) 'Numerical prediction of two-phase flow in bubble columns', *International journal for numerical methods in fluids*. Wiley Online Library, 23(12), pp. 1289–1310.

Bukur, D. B., Patel, S. A. and Matheo, R. (1987) 'Hydrodynamic studies in Fischer-Tropsch derived waxes in a bubble column', *Chemical Engineering Communications*. Taylor & Francis, 60(1–6), pp. 63–78.

Burns, A. D., Frank, T., Hamill, I., Shi, J.-M. and others (2004) 'The Favre averaged drag model for turbulent dispersion in Eulerian multi-phase flows', in *5th international conference on multiphase flow, ICMF*, pp. 1–17.

Buwa, V. V and Ranade, V. V (2002) 'Dynamics of gas–liquid flow in a rectangular bubble column: experiments and single/multi-group CFD simulations', *Chemical Engineering Science*, 57(22), pp. 4715–4736.

Cartland Glover, G. M. and Generalis, S. C. (2004) 'The modelling of buoyancy driven flow in bubble columns', *Chemical Engineering and Processing: Process Intensification*, 43(2), pp. 101–115.

Ceylan, K., Altunbaş, A. and Kelbaliyev, G. (2001) 'A new model for estimation of drag force in the flow of Newtonian fluids around rigid or deformable particles', *Powder Technology*. Elsevier, 119(2–3), pp. 250–256.

Chen, J., Kemoun, A., Al-Dahhan, M. H., Duduković, M. P., Lee, D. J. and Fan, L.-S. (1999) 'Comparative hydrodynamics study in a bubble column using computer-automated radioactive particle tracking (CARPT)/computed tomography (CT) and particle image velocimetry (PIV)', *Chemical Engineering Science*. Elsevier, 54(13–14), pp. 2199–2207.

Chen, P., Duduković, M. P. and Sanyal, J. (2005) 'Three-dimensional simulation of bubble column flows with bubble coalescence and breakup', *AIChE Journal*. Wiley Online Library, 51(3), pp. 696–712.

Chen, P., Sanyal, J. and Duduković, M. P. (2004) 'CFD modeling of bubble columns flows: implementation of population balance', *Chemical Engineering Science*, 59(22), pp. 5201–5207.

Cokljat, D., Slack, M., Vasquez, S. A., Bakker, A. and Montante, G. (2006) 'Reynolds-Stress Model for Eulerian multiphase', *Progress in Computational Fluid Dynamics, An International Journal*. Inderscience Publishers, 6(1/2/3), p. 168.

Darmana, D., Deen, N. G., Kuipers, J. A. M., Harteveld, W. K. and Mudde, R. F. (2009) 'Numerical study of homogeneous bubbly flow: Influence of the inlet conditions to the hydrodynamic behavior', *International Journal of Multiphase Flow*. Elsevier, 35(12), pp. 1077–1099.

Darton, R. (1974) 'The Rise of Single Gas Bubbles in Liquid Fluidized Beds', *Transactions*

of the Institution of Chemical Engineers, 52, pp. 301–306.

Deckwer, W.-D. (1981) ‘Access of Hydrodynamic Parameters Required in the Design and Scale-Up of Bubble Column Reactors’, in ACS Publications, pp. 213–241.

Deckwer, W.-D. and Schumpe, A. (1993) ‘Improved tools for bubble column reactor design and scale-up’, *Chemical Engineering Science*. Elsevier, 48(5), pp. 889–911.

Deen, N. G., Solberg, T. and Hjertager, B. H. (2000) ‘Numerical simulation of the gas-liquid flow in a square cross-sectioned bubble column’, in *Proceedings of 14th Int. Congress of Chemical and Process Engineering: CHISA (Praha, Czech Republic, 2000)*.

Deen, N. G., Solberg, T. and Hjertager, B. H. (2001) ‘Large eddy simulation of the Gas–Liquid flow in a square cross-sectioned bubble column’, *Chemical Engineering Science*, 56(21), pp. 6341–6349.

Delnoij, E., Kuipers, J. A. M. and van Swaaij, W. P. M. (1997) ‘Computational fluid dynamics applied to gas-liquid contactors’, *Chemical Engineering Science*. Elsevier, 52(21–22), pp. 3623–3638.

Devanathan, N., Moslemian, D. and Dudukovic, M. P. (1990) ‘Flow mapping in bubble columns using CARPT’, *Chemical Engineering Science*. Elsevier, 45(8), pp. 2285–2291.

Dhotre, M. T., Niceno, B., Smith, B. L. and Simiano, M. (2009) ‘Large-eddy simulation (LES) of the large scale bubble plume’, *Chemical Engineering Science*, 64(11), pp. 2692–2704.

Dhotre, M. T. and Smith, B. L. (2007) ‘CFD simulation of large-scale bubble plumes: Comparisons against experiments’, *Chemical Engineering Science*, 62(23), pp. 6615–6630.

Drew, D. A. and Lahey, R. T. (1987) ‘The virtual mass and lift force on a sphere in rotating and straining inviscid flow’, *International Journal of Multiphase Flow*. Elsevier, 13(1), pp. 113–121.

Elena Díaz, M., Montes, F. J. and Galán, M. A. (2009) ‘Influence of the lift force closures on the numerical simulation of bubble plumes in a rectangular bubble column’, *Chemical Engineering Science*, 64(5), pp. 930–944.

Fan, L.-S. (1989) *Gas–Liquid–Solid Fluidization Engineering*, Butterworths, Stoneham, MA. Elsevier.

Forret, A., Schweitzer, J.-M., Gauthier, T., Krishna, R. and Schweich, D. (2003) ‘Influence

of scale on the hydrodynamics of bubble column reactors: an experimental study in columns of 0.1, 0.4 and 1m diameters', *Chemical Engineering Science*. Elsevier, 58(3–6), pp. 719–724.

Gatski, T. B. and Jongen, T. (2000) 'Nonlinear eddy viscosity and algebraic stress models for solving complex turbulent flows', *Progress in Aerospace Sciences*. Elsevier, 36(8), pp. 655–682.

Gaurav, T. (2018) 'Numerical Investigations of Bubble Column Equipped with Vertical Internals in Different Arrangements', *MESc. Thesis, University of Western Ontario*.

George, K. J. H., Jhawar, A. K. and Prakash, A. (2017) 'Investigations of flow structure and liquid mixing in bubble column equipped with selected internals', *Chemical Engineering Science*. Elsevier, 170, pp. 297–305.

Grace, J. R., Th, N. and others (1976) 'Shapes and Velocities of Single Drops and Bubbles Moving Freely Through Immiscible Liquids'.

Grienberger, J. and Hofmann, H. (1992) 'Investigations and modelling of bubble columns', *Chemical Engineering Science*. Elsevier, 47(9–11), pp. 2215–2220.

Guan, X., Gao, Y., Tian, Z., Wang, L., Cheng, Y. and Li, X. (2015) 'Hydrodynamics in bubble columns with pin-fin tube internals', *Chemical Engineering Research and Design*. Elsevier, 102, pp. 196–206.

Guan, X., Li, Z., Wang, L., Cheng, Y. and Li, X. (2014) 'CFD Simulation of Bubble Dynamics in Bubble Columns with Internals', *Industrial & Engineering Chemistry Research*. ACS Publications, 53(42), pp. 16529–16538.

Guan, X. and Yang, N. (2017) 'CFD simulation of pilot-scale bubble columns with internals: Influence of interfacial forces', *Chemical Engineering Research and Design*. Elsevier, 126, pp. 109–122.

Guo, X. and Chen, C. (2017) 'Simulating the impacts of internals on gas–liquid hydrodynamics of bubble column', *Chemical Engineering Science*, 174, pp. 311–325.

Hamlington, P. E. and Dahm, W. J. A. (2008) 'Reynolds stress closure for nonequilibrium effects in turbulent flows', *Physics of Fluids*. American Institute of Physics, 20(11), p. 115101.

Hills, J. H. (1974) 'Radial Non-Uniformity Of Velocity And Voidage In A Bubble Column', *Trans Inst Chem Eng*, 52(1), pp. 1–9.

Ishii, M. and Zuber, N. (1979) 'Drag coefficient and relative velocity in bubbly, droplet or particulate flows', *AIChE Journal*. Wiley Online Library, 25(5), pp. 843–855.

Jakobsen, H. A., Grevskott, S. and Svendsen, H. F. (1997) 'Modeling of Vertical Bubble-Driven Flows', *Industrial & Engineering Chemistry Research*. ACS Publications, 36(10), pp. 4052–4074.

Jakobsen, H. A., Lindborg, H. and Dorao, C. A. (2005) 'Modeling of Bubble Column Reactors: Progress and Limitations', *Industrial & Engineering Chemistry Research*. ACS Publications, 44(14), pp. 5107–5151.

Jasim, A. (2016) 'The impact of heat exchanging internals on hydrodynamics of bubble column reactor', p. 108.

Jhawar, A. K. and Prakash, A. (2011) 'Influence of bubble column diameter on local heat transfer and related hydrodynamics', *Chemical Engineering Research and Design*. Elsevier, 89(10), pp. 1996–2002.

Jhawar, A. K. and Prakash, A. (2014) 'Bubble column with internals: Effects on hydrodynamics and local heat transfer', *Chemical Engineering Research and Design*. Elsevier, 92(1), pp. 25–33.

Joshi, J. B. (2001) 'Computational flow modelling and design of bubble column reactors', *Chemical Engineering Science*. Elsevier, 56(21–22), pp. 5893–5933.

Joshi, J. B. and Nandakumar, K. (2015) 'Computational Modeling of Multiphase Reactors.', *Annual review of chemical and biomolecular engineering*, 6, pp. 347–378.

Kagumba, M. and Al-Dahhan, M. H. (2015) 'Impact of Internals Size and Configuration on Bubble Dynamics in Bubble Columns for Alternative Clean Fuels Production', *Industrial & Engineering Chemistry Research*. ACS Publications, 54(4), pp. 1359–1372.

Koynov, A., Khinast, J. G. and Tryggvason, G. (2005) 'Mass transfer and chemical reactions in bubble swarms with dynamic interfaces', *AIChE Journal*. Wiley Online Library, 51(10), pp. 2786–2800.

Krepper, E., Reddy Vanga, B. N., Zaruba, A., Prasser, H.-M. and Lopez de Bertodano, M. A. (2007) 'Experimental and numerical studies of void fraction distribution in rectangular bubble columns', *Nuclear Engineering and Design*, 237(4), pp. 399–408.

Krishna, R. and Van Baten, J. M. (2001) 'Scaling up Bubble Column Reactors with the Aid of CFD', *Chemical Engineering Research and Design*, 79(3), pp. 283–309.

- Kumar, S., Srinivasulu, N. and Khanna, A. (2011) 'CFD simulations to validate two & three phase up-flow in bubble columns', *World Academy of Science, Engineering and Technology*, 5, pp. 11–20.
- Laborde-Boutet, C., Larachi, F., Dromard, N., Delsart, O., Béliard, P.-E. and Schweich, D. (2010) 'CFD simulations of hydrodynamic/thermal coupling phenomena in a bubble column with internals', *AIChE Journal*, 56(9), pp. 2397–2411.
- Lain, S. and Sommerfeld, M. (2004) 'LES of gas-liquid flow in a cylindrical laboratory bubble column', in *Proceedings of the 5th International Conference on Multiphase Flow (ICMF'04)*.
- Larachi, Faiçal, Desvigne, D., Donnat, L. and Schweich, D. (2006) 'Simulating the effects of liquid circulation in bubble columns with internals', *Chemical Engineering Science*, 61(13), pp. 4195–4206.
- Larachi, Faiçal, Desvigne, D., Donnat, L. and Schweich, D. (2006) 'Simulating the effects of liquid circulation in bubble columns with internals', *Chemical Engineering Science*, 61(13), pp. 4195–4206.
- Launder, B. E., Reece, G. J. and Rodi, W. (1975) 'Progress in the development of a Reynolds-stress turbulence closure', *Journal of Fluid Mechanics*. Cambridge University Press, 68(3), pp. 537–566.
- Launder, B. E. and Spalding, D. B. (1974) 'The numerical computation of turbulent flows', *Computer Methods in Applied Mechanics and Engineering*, 3(2), pp. 269–289.
- Law, D., Battaglia, F. and Heindel, T. J. (2008) 'Model validation for low and high superficial gas velocity bubble column flows', *Chemical Engineering Science*. Elsevier, 63(18), pp. 4605–4616.
- Li, H. and Prakash, A. (2000) 'Influence of slurry concentrations on bubble population and their rise velocities in a three-phase slurry bubble column', *Powder Technology*. Elsevier, 113(1–2), pp. 158–167.
- Li, H. and Prakash, A. (2002) 'Analysis of flow patterns in bubble and slurry bubble columns based on local heat transfer measurements', *Chemical Engineering Journal*. Elsevier, 86(3), pp. 269–276.
- Linneweber, K. W. and Blass, E. (1983) 'Measurement of local gas and solids holdups in three-phase bubble columns', *Ger. Chem. Eng*, 6, pp. 28–33.
- Liu, Y. and Hinrichsen, O. (2014) 'Study on CFD–PBM turbulence closures based on $k-\epsilon$

and Reynolds stress models for heterogeneous bubble column flows’, *Computers & Fluids*, 105, pp. 91–100.

Lucas, D., Krepper, E. and Prasser, H.-M. (2007) ‘Use of models for lift, wall and turbulent dispersion forces acting on bubbles for poly-disperse flows’, *Chemical Engineering Science*, 62(15), pp. 4146–4157.

Lucas, D., Prasser, H.-M. and Manera, A. (2005) ‘Influence of the lift force on the stability of a bubble column’, *Chemical Engineering Science*, 60(13), pp. 3609–3619.

Matsuura, A. and Fan, L.-S. (1984) ‘Distribution of bubble properties in a gas-liquid-solid fluidized bed’, *AIChE Journal*. Wiley Online Library, 30(6), pp. 894–903.

Al Mesfer, M. K., Sultan, A. J. and Al-Dahhan, M. H. (2016) ‘Impacts of dense heat exchanging internals on gas holdup cross-sectional distributions and profiles of bubble column using gamma ray Computed Tomography (CT) for FT synthesis’, *Chemical Engineering Journal*. Elsevier, 300, pp. 317–333.

Al Mesfer, M. K., Sultan, A. J. and Al-Dahhan, M. H. (2017) ‘Study the effect of dense internals on the liquid velocity field and turbulent parameters in bubble column for Fischer–Tropsch (FT) synthesis by using Radioactive Particle Tracking (RPT) technique’, *Chemical Engineering Science*. Elsevier, 161, pp. 228–248.

Möller, F., Lau, Y. M., Seiler, T., Hampel, U. and Schubert, M. (2018) ‘A study on the influence of the tube layout on sub-channel hydrodynamics in a bubble column with internals’, *Chemical Engineering Science*, 179, pp. 265–283.

Parekh, J. and Rzehak, R. (2018) ‘Euler–Euler multiphase CFD-simulation with full Reynolds stress model and anisotropic bubble-induced turbulence’, *International Journal of Multiphase Flow*, 99, pp. 231–245.

Pfleger, D. and Becker, S. (2001) ‘Modelling and simulation of the dynamic flow behaviour in a bubble column’, *Chemical Engineering Science*, 56(4), pp. 1737–1747.

Pourtousi, M., Sahu, J. N. and Ganesan, P. (2014) ‘Effect of interfacial forces and turbulence models on predicting flow pattern inside the bubble column’, *Chemical Engineering and Processing: Process Intensification*, 75, pp. 38–47.

Pourtousi, M., Sahu, J. N., Ganesan, P., Shamshirband, S. and Redzwan, G. (2015) ‘A combination of computational fluid dynamics (CFD) and adaptive neuro-fuzzy system (ANFIS) for prediction of the bubble column hydrodynamics’, *Powder Technology*. Elsevier, 274, pp. 466–481.

Pradhan, A. K., Parichha, R. K. and De, P. (1993) 'Gas hold-up in non-newtonian solutions in a bubble column with internals', *The Canadian Journal of Chemical Engineering*, 71(3), pp. 468–471.

Ranade, V. V (1997) 'Modelling of Turbulent Flow in a Bubble Column Reactor', *Chemical Engineering Research and Design*, 75(1), pp. 14–23.

Roghair, I., Lau, Y. M., Deen, N. G., Slagter, H. M., Baltussen, M. W., Annaland, M. V. S. and Kuipers, J. A. M. (2011) 'On the drag force of bubbles in bubble swarms at intermediate and high Reynolds numbers', *Chemical engineering science*. Elsevier, 66(14), pp. 3204–3211.

Rzehak, R. and Krepper, E. (2013) 'CFD modeling of bubble-induced turbulence', *International Journal of Multiphase Flow*, 55, pp. 138–155.

Saffman, P. G. T. (1965) 'The lift on a small sphere in a slow shear flow', *Journal of fluid mechanics*. Cambridge University Press, 22(2), pp. 385–400.

Sankaranarayanan, K. and Sundaresan, S. (2002) 'Lift force in bubbly suspensions', *Chemical Engineering Science*. Elsevier, 57(17), pp. 3521–3542.

Saxena, S. C., Rao, N. S. and Saxena, A. C. (1992) 'Heat transfer and gas holdup studies in a bubble column: Air-water-sand system', *The Canadian Journal of Chemical Engineering*. Wiley Online Library, 70(1), pp. 33–41.

Schlüter, S., Steiff, A. and Weinspach, P.-M. (1995) 'Heat transfer in two- and three-phase bubble column reactors with internals', *Chemical Engineering and Processing: Process Intensification*. Elsevier, 34(3), pp. 157–172.

Schumpe, A., Saxena, A. and Nigam, K. D. P. (2004) 'Gas/Liquid Mass Transfer in a Bubble Column With Suspended Non-Wettable Solids', *AIChE Journal*, 33, pp. 1916–1920.

Selma, B., Bannari, R. and Proulx, P. (2010) 'A full integration of a dispersion and interface closures in the standard $k-\epsilon$ model of turbulence', *Chemical engineering science*. Elsevier, 65(20), pp. 5417–5428.

Shah, Y. T., Kelkar, B. G., Godbole, S. P. and Deckwer, W.-D. (1982) 'Design parameters estimations for bubble column reactors', *AIChE Journal*. Wiley Online Library, 28(3), pp. 353–379.

Silva, M. K., d'Ávila, M. A. and Mori, M. (2012) 'Study of the interfacial forces and turbulence models in a bubble column', *Computers & Chemical Engineering*. Elsevier, 44,

pp. 34–44.

Simonin, C., Viollet, P. L. and others (1990) ‘Predictions of an oxygen droplet pulverization in a compressible subsonic coflowing hydrogen flow’, *Numerical Methods for Multiphase Flows*. American Society of Mechanical Engineers: Fluids Engineering Division New York, 91(2), pp. 65–82.

Simonnet, M., Gentric, C., Olmos, E. and Midoux, N. (2007) ‘Experimental determination of the drag coefficient in a swarm of bubbles’, *Chemical Engineering Science*. Elsevier, 62(3), pp. 858–866.

Smith, B. L. (1998) ‘On the modelling of bubble plumes in a liquid pool’, *Applied Mathematical Modelling*. Elsevier, 22(10), pp. 773–797.

Sultan, A. J., Sabri, L. S. and Al-Dahhan, M. H. (2018) ‘Impact of heat-exchanging tube configurations on the gas holdup distribution in bubble columns using gamma-ray computed tomography’, *International Journal of Multiphase Flow*. Elsevier, 106, pp. 202–219.

Svendsen, H. F., Jakobsen, H. A. and Torvik, R. (1992) ‘Local flow structures in internal loop and bubble column reactors’, *Chemical Engineering Science*. Elsevier, 47(13–14), pp. 3297–3304.

Swanson, W. M. (1961) ‘The Magnus Effect: A Summary of Investigations to Date’, *Journal of Basic Engineering*, 83(3), pp. 461–470.

Tabib, M. V, Roy, S. A. and Joshi, J. B. (2008) ‘CFD simulation of bubble column—an analysis of interphase forces and turbulence models’, *Chemical Engineering Journal*. Elsevier, 139(3), pp. 589–614.

Thakre, S. S. and Joshi, J. B. (1999) ‘CFD simulation of bubble column reactors: importance of drag force formulation’, *Chemical Engineering Science*, 54(21), pp. 5055–5060.

Thomas, N. H., Auton, T. R., Sene, K. and HUNT, J. C. R. (1983) ‘Entrapment and transport of bubbles by transient large eddies in multiphase turbulent shear flows’, in *International conference on the physical modelling of multi-phase flow*, pp. 169–184.

Tomiyama, A. (1995) ‘Effects of Eotvos number and dimensionless liquid volumetric flux on lateral motion of a bubble in a laminar duct flow’, in *2nd Int. Conf. an Multiphase Flow*.

Tomiyama, A., Tamai, H., Zun, I. and Hosokawa, S. (2002) ‘Transverse migration of single bubbles in simple shear flows’, *Chemical Engineering Science*. Elsevier, 57(11), pp. 1849–

1858.

Tran-Cong, S., Gay, M. and Michaelides, E. E. (2004) 'Drag coefficients of irregularly shaped particles', *Powder Technology*. Elsevier, 139(1), pp. 21–32.

Tsuchiya, K., Song, G.-H. and Fan, L.-S. (1990) 'Effects of particle properties on bubble rise and wake in a two-dimensional liquid—solid fluidized bed', *Chemical engineering science*. Elsevier, 45(5), pp. 1429–1434.

Tzeng, J.-W., Chen, R. C. and Fan, L.-S. (1993) 'Visualization of flow characteristics in a 2-D bubble column and three-phase fluidized bed', *AIChE journal*. Wiley Online Library, 39(5), pp. 733–744.

Ueyama, K. and Miyauchi, T. (1979) 'Properties of recirculating turbulent two phase flow in gas bubble columns', *AIChE Journal*. Wiley Online Library, 25(2), pp. 258–266.

Vanga, B. N. R., Krepper, E., Zaruba, A., Prasser, H.-M. and de Bertodano, M. L. (2004) 'On the Hydrodynamics of Bubble Columns: Comparison of Experimental Measurements with Computational Fluid Dynamics Calculations, 5th Int', in *Conf. on Multiphase Flow, ICMF-2004, Yokohama, Japan*.

Van Wachem, B. G. M. and Schouten, J. C. (2002) 'Experimental validation of 3-D Lagrangian VOF model: bubble shape and rise velocity', *AIChE journal*. Wiley Online Library, 48(12), pp. 2744–2753.

Wachi, S., Morikawa, H. and Ueyama, K. (1987) 'Gas holdup and axial dispersion in gas-liquid concurrent bubble column', *Journal of chemical engineering of Japan*. The Society of Chemical Engineers, Japan, 20(3), pp. 309–316.

Warsito, Uchida, S., Maezawa, A. and Okamura, S. (1995) 'A model for simultaneous measurement of gas and solid holdups in a bubble column using ultrasonic method', *The Canadian Journal of Chemical Engineering*. Canadian Society for Chemical Engineering, Ottawa, Canada, 73(5), pp. 734–743.

White, F. M. and Corfield, I. (2006) *Viscous fluid flow*. McGraw-Hill New York.

Xu, L., Yuan, B., Ni, H. and Chen, C. (2013) 'Numerical simulation of bubble column flows in churn-turbulent regime: comparison of bubble size models', *Industrial & Engineering Chemistry Research*. ACS Publications, 52(20), pp. 6794–6802.

Yamashita, F. (1987) 'Effects of Vertical Pipe and Rod Internals On Gas Holdup in Bubble Columns', *Journal of Chemical Engineering of Japan*, 20(2), pp. 204–206.

Yang, G., Zhang, H., Luo, J. and Wang, T. (2018) 'Drag force of bubble swarms and numerical simulations of a bubble column with a CFD-PBM coupled model', *Chemical Engineering Science*. Elsevier, 192, pp. 714–724.

Youssef, A. A. and Al-Dahhan, M. H. (2009) 'Impact of internals on the gas holdup and bubble properties of a bubble column', *Industrial & Engineering Chemistry Research*. ACS Publications, 48(17), pp. 8007–8013.

Youssef, A. A., Al-Dahhan, M. H. and Dudukovic, M. P. (2013) 'Bubble columns with internals: a review', *International Journal of Chemical Reactor Engineering*. De Gruyter, 11(1), pp. 169–223.

Youssef, A. A., Hamed, M. E., Grimes, J. T., Al-Dahhan, M. H. and Duduković, M. P. (2012) 'Hydrodynamics of pilot-scale bubble columns: effect of internals', *Industrial & Engineering Chemistry Research*. ACS Publications, 52(1), pp. 43–55.

Zhang, D., Deen, N. G. and Kuipers, J. A. M. (2006) 'Numerical simulation of the dynamic flow behavior in a bubble column: a study of closures for turbulence and interface forces', *Chemical Engineering Science*. Elsevier, 61(23), pp. 7593–7608.

Zhang, D. Z. and Vanderheyden, W. B. (2002) 'The effects of mesoscale structures on the disperse two-phase flows and their closures for dilute suspensions', *International Journal of Multiphase Flow*, 28, pp. 805–822.

Zhu, S. J., Ooi, A., Manasseh, R. and Skvortsov, A. (2020) 'Prediction of gas holdup in partially aerated bubble columns using an EE-LES coupled model', *Chemical Engineering Science*, 217, p. 115492.

Chapter 3

3 CFD Simulations of Hollow Bubble Column Reactors

3.1 Introduction

Bubble column reactors are multiphase reactors that find their use in various chemical and biochemical processes including hydrogenation, oxidation, Fischer-Tropsch synthesis, production of methanol, advanced oxidation of wastewater, chlorination, biofuels production and production of valuable protein cells and antibiotics using microorganisms. (Duduković, Larachi and Mills, 2002; Li *et al.*, 2003; Ni *et al.*, 2006; Shaikh and Al-Dahhan, 2013; Joseph, 2016; George, Jhavar and Prakash, 2017; Valero *et al.*, 2019). Bubble column reactors have many advantages that are associated with their operations and designs. Very high degree of mixing can be achieved in these reactors, which enhances the heat and mass transfer rates (Chen, Kemoun, *et al.*, 1999; Besagni, Inzoli and Ziegenhein, 2018)

Although bubble columns have distinct and various applications, their size-dependent hydrodynamic interactions make it challenging to scale up from lab and pilot scale to industrial scale reactors. The information on flow patterns within the column, local and global gas holdups, turbulence parameters, local velocities for the liquid and gaseous phases and bubble size distribution is vital to analyze bubble columns. The term hollow bubble column is used when there is no internal except a gas distributor near the column bottom.

Although simple in construction, their scale-up and sizing have proven to be really challenging due to their complex hydrodynamics and mixing effects, which vary with scale and operating flow regimes. Over the last few decades, a considerable progress has been achieved in the field of Computational Fluid Dynamics (CFD), a powerful and effective numerical tool that is used to simulate a wide range of multiphase flow systems. Although a number of studies on CFD based simulation of bubble column hydrodynamics have reported, there is a lack of systematic and coherent approach for proper selection of phase interaction parameters and turbulence models. Therefore, the objectives of this study are:

- To carry out numerical simulations of two-phase flows in a bubble column under different operating regimes.
- To investigate the effect of various phase interaction parameters on the numerical results and compare the numerical results with available experimental data from literatures to select suitable phase interaction parameters.

The simulations are carried out using ANSYS Fluent v19.2, which is one of the widely used commercial CFD packages. 2-D planar simulations are carried using the Eulerian-Eulerian multiphase model. The interfacial forces including drag, lift, turbulent dispersion, turbulent interaction and added mass are included in the multiphase CFD model. The effect of different drag force models, such as the models by Schiller and Naumann (Schiller, 1933), Grace et al. (Grace, TH and others, 1976), Tomiyama (Tomiyama, 1998) and Ishii-Zuber (Ishii and Zuber, 1979), are investigated and the numerical results are compared with the experimental data. Different lift force models, the constant lift force model with varying coefficients of positive and negative lift force coefficients, Tomiyama (Tomiyama

et al., 2002) and Saffman-Mei (Saffman, 1965), are also assessed and validated. Turbulent dispersion models, such as the model by Simonin and Viollet (Simonin, Viollet and others, 1990) with varying coefficients of turbulent dispersion coefficients and the model by Burns *et al.* (Burns *et al.*, 2004), are examined. The simulation results with and without the bubble induced turbulence model are compared. The sensitivity of the interfacial forces on the two-phase flows in the bubble column reactors are studied extensively in the current work.

After the comparison and validation, the most accurate interfacial forces are used to carry out the flow regime transition studies at superficial gas velocities of 4 cm/s, 10 cm/s and 30 cm/s, respectively. The effect of the superficial gas velocity on hydrodynamic parameters such as radial gas holdups, liquid axial velocities, global gas holdups, centerline liquid axial velocities and bubble size distributions is investigated and compared with numerous experimental data from literatures.

3.2 Numerical Model for Two-Phase Flows

3.2.1 Governing Equations

The governing equations in the Eulerian-Eulerian approach consist of the mass and momentum conservation equations for both phases, the liquid phase (*l*) and the gas phase (*g*).

Conservation of Mass

The continuity equation for the liquid phase, *l*, is

$$\frac{\partial}{\partial t}(\rho_l \varepsilon_l) + \frac{\partial}{\partial x_i}(\rho_l \varepsilon_l U_{l,i}) = (\dot{m}_{lg} - \dot{m}_{gl}) + \varepsilon_l S_l \quad (3.1)$$

The continuity equation for the gas phase, g , is

$$\frac{\partial}{\partial t}(\rho_g \varepsilon_g) + \frac{\partial}{\partial x_i}(\rho_g \varepsilon_g U_{g,i}) = (\dot{m}_{gl} - \dot{m}_{lg}) + \varepsilon_g S_g \quad (3.2)$$

Conservation of Momentum:

The momentum continuity equation for the liquid phase, L , is

$$\frac{\partial}{\partial t}(\rho_L \varepsilon_L U_{L,i}) + \frac{\partial}{\partial x_j}(\rho_L \varepsilon_L U_{L,i} U_{L,j}) = \frac{\partial}{\partial x_j} \varepsilon_L \mu_L \left(\frac{\partial U_{L,i}}{\partial x_j} + \frac{\partial U_{L,j}}{\partial x_i} \right) - \varepsilon_L \frac{\partial p}{\partial x_i} + \rho_L \varepsilon_L g + M_{L,i} \quad (3.3)$$

The momentum continuity equation for the gaseous phase, G , is

$$\frac{\partial}{\partial t}(\rho_G \varepsilon_G U_{G,i}) + \frac{\partial}{\partial x_j}(\rho_G \varepsilon_G U_{G,i} U_{G,j}) = \frac{\partial}{\partial x_j} \varepsilon_G \mu_G \left(\frac{\partial U_{G,i}}{\partial x_j} + \frac{\partial U_{G,j}}{\partial x_i} \right) - \varepsilon_G \frac{\partial p}{\partial x_i} + \rho_G \varepsilon_G g + M_{G,i} \quad (3.4)$$

$$\text{where } \varepsilon_L + \varepsilon_G = 1 \quad (3.5)$$

3.2.2 Interfacial forces

Interfacial forces play a major role in the computational modelling of multiphase flows. Various interfacial forces including drag, lift, added virtual mass, turbulent dispersion and turbulent interaction forces need to be considered for multiphase flows (Lopez et al., 2004; Nguyen *et al.*, 2013; Colombo and Fairweather, 2020). These have been illustrated in Figure 3.1. The drag force, known as the chief force, involved in the bubble column reactor modelling, has been widely studied (Kulkarni, 2008; Tabib, Roy and Joshi, 2008; Kannan *et al.*, 2019). The effect of other interfacial forces is not very pronounced in the literature

and very few studies have been done on the combined effect of these forces. Including appropriate interfacial forces will lead to a more accurate prediction of hydrodynamic parameters in multiphase flow systems.

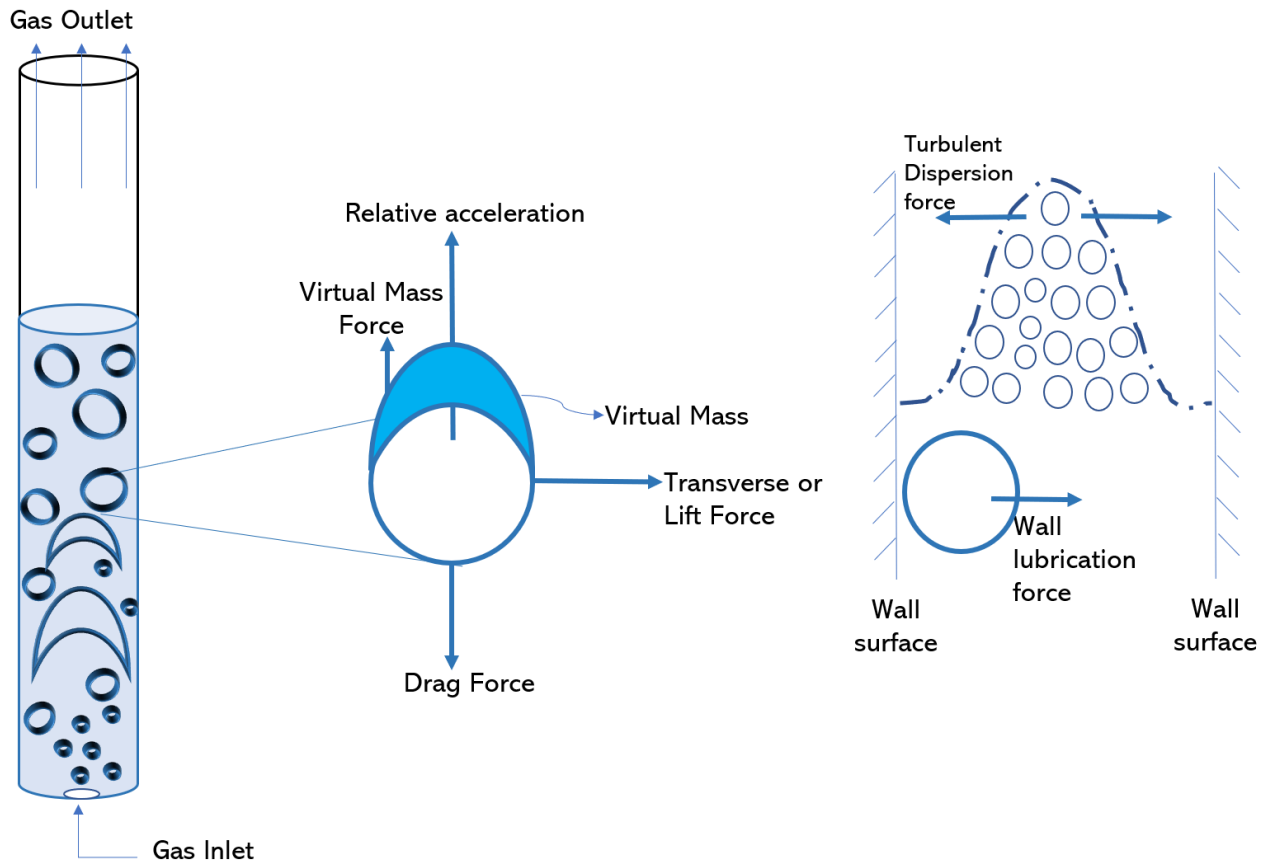


Figure 3.1 Illustration of various interfacial forces in gas-liquid flows

3.2.2.1 Virtual mass force

In multiphase flows, the effect of the virtual mass force is expected when a dispersed phase accelerates with respect to the stationary phase (ANSYS, 2013; Dhotre et al., 2008). In bubble column reactors, the virtual mass force is exerted by the action of bubbles

accelerating through the liquid phase. The influence of added mass force is prominent in the case of transient flows involved in a bubble column reactor due to the significant difference in densities between liquid and gas phases (ANSYS, 2013).

The added mass force is characterized by:

$$\vec{F}_{vm,l} = \frac{\varepsilon_g \rho_l}{2} \left(\frac{d_g}{dt} \vec{u}_g - \frac{d_l}{dt} \vec{u}_l \right) \quad (3.6)$$

$$\vec{F}_{vm,l} = \varepsilon_g \rho_l C_{VM} \left(\frac{d_g}{dt} \vec{u}_g - \frac{d_l}{dt} \vec{u}_l \right) \quad (3.7)$$

The derivatives present ($\frac{d_g}{dt}$ and $\frac{d_l}{dt}$) in the Equations 3.6 and 3.7 are in the phase material time form.

In several studies, the virtual mass effect was neglected (Chen & Fan, 2004; Tabib et al., 2008). In some other studies, the virtual mass coefficient was maintained at $C_{VM} = 0.5$, which is the prescribed value for spherical shaped bubbles. The study conducted by Gupta and Roy (2013) for rectangular bubble columns showed that the effect of virtual mass was apparent in the bulk region of the column and was negligible at the column walls. They indicated that the incorporation of virtual mass effect in the numerical study increases the time required for the convergence (Gupta and Roy, 2013).

In the current work, the value of virtual mass coefficient for spherical shaped bubbles is set at $C_{VM} = 0.5$. The virtual mass force plays an important role in reaching the stability at early stages of the flow within a bubble column reactor. When the virtual mass force is included in the numerical simulation, bubbles accelerations through the liquid column are

limited. Once the simulation reaches the pseudo-steady state, the influence of virtual mass force is insignificant as indicated by Smith (1998) and Dhotre *et al.* (2008).

3.2.2.2 Drag Force

The drag force is the resistance experienced by the bubbles rising through the column of liquid. The drag force could be a combination of two types of resistances including skin friction and form drag. The influence of the drag force on two-phase flow in bubble columns is stronger than other interfacial forces, such as turbulent dispersion, lift, virtual mass and turbulent interaction forces. The axial velocities and overall holdups of gas phase within the bubble column are strongly affected by the drag model used in the simulation. It is an important parameter as it determines the terminal velocity and residence time of bubbles (Yang *et al.*, 2018).

Yang *et al.* (2018) studied the influence of drag force on the bubble swarms as it is quite different from single bubbles. The rise velocities of bubble swarms are not the same as that of the single bubble since the drag coefficients and terminal velocities are different between bubble swarms and single bubble. Complex bubble interactions associated with the bubble swarms is another factor that affects the drag coefficients.

The drag force between the gas and liquid phase is described as:

$$F_{D,l} = 0.75 \varepsilon_l \rho_l \frac{C_D}{d_b} |u_g - u_l| (u_g - u_l) \quad (3.8)$$

The drag coefficient, C_D , is a function of liquid properties, hydrodynamic interaction between the bubbles and flow regimes. In the current study, the drag model proposed by

Schiller and Naumann (Schiller, 1933) is used. The drag coefficient in the Schiller and Naumann drag force model is described as

$$C_d = \begin{cases} \frac{24 (1+0.15 N_{Re}^{0.687})}{N_{Re}}, & N_{Re} \leq 1000 \\ 0.24, & N_{Re} > 1000 \end{cases} \quad (3.9)$$

The Reynolds Number (Re) associated with this drag coefficient is determined using the effective bubble diameter, slip velocity between the two phases, liquid properties such as dynamic viscosity and density (Law et al., 2008; Xu *et al.*, 2013).

$$Re = \frac{\rho_l |\vec{v}_l - \vec{v}_g| d_b}{\mu_l} \quad (3.10)$$

The Schiller Naumann drag force model is well suited for gas-liquid flows in the bubbly flow regime since the superficial gas velocities are below 5 cm/s (Pourtousi, Sahu and Ganesan, 2014). This drag model does not account for the shape factor of the bubbles as the Eotvos number is absent in the drag force formulation. The hydrodynamics of the two-phase flows is well captured in the current drag model as it takes the Reynolds number into consideration, which in turn is a function of bubble diameter.

3.2.2.3 Lift Force

The influence of shearing force experienced by gas bubbles in a liquid medium is modelled by the lift force (Drew and Lahey Jr, 1987; Žun, 1990). This force acts perpendicular to the flow direction. The lift force comprises of two mechanisms, namely the Magnus and Saffman forces. The first one is due to the bubble's rotation and the second one is due to the shear produced around the bubble. Drew and Lahey (1987) proposed the general form of the lift force and it depends directly on the curl of gas phase velocity and the difference between the velocity of the two phases (slip velocity).

$$\vec{F}_{lift} = -C_L \varepsilon_g \rho_l \frac{c_D}{d_b} (\vec{u}_g - \vec{u}_l) \times (\nabla \times \vec{u}_g) \quad (3.11)$$

One of the widely used lift coefficients was proposed by Tomiyama (1998), which depends on the Eotvos number. So, the lift coefficient is negative when the bubble diameters exceed 0.56 cm and positive when the bubble diameters are less than 0.56 cm (Dhotre et al., 2008).

Several researchers utilized a positive lift force coefficient (Tabib, Roy and Joshi, 2008). Tabib et al. (2008) compared the effect of the positive and negative lift force coefficients on the liquid axial velocities and the radial holdups within a bubble column. At lower superficial gas velocities, the effect of the lift coefficient sign from positive to negative was minimal while significant deviation was noticed at higher gas velocities. They explained that when the lift force coefficient is positive, the bubbles move from the center towards the column wall. This leads to the decrease in centerline liquid axial velocities and flattening of gas holdup profiles. Hence, the choice of the lift force coefficient depends on the bubble diameters which in turn depends on the flow regime. Similarly, Dhotre et al., (2009) also argued that the constant lift force coefficient with values in the range 0.1-0.5 can be used only in the bubbly flow regime.

Guan and Yang (2017) asserted that the effect of the lift force is more pronounced in the presence of internals. Their findings agreed with those made by Tabib et al. (2008). When a negative lift coefficient of -0.02 was used, the centerline liquid velocities reportedly increased by 138% in the case of internals and 20.5% in the case of hollow bubble columns (Guan and Yang, 2017). Also, an increase in the steepness of the gas holdup and liquid velocity profiles was noticed. In the current study, the numerical results using different lift force models are compared.

3.2.2.4 Turbulence Dispersion

In a transient system like bubble columns, turbulent dispersion force exists when the gas holdup fluctuates due to the continuous fluctuations in the liquid velocity. The turbulent dispersion force accounts for the influence of turbulent eddies in the continuous phase (Dhotre & Smith, 2007; Miao et al., 2013; Pourtousi et al., 2014). Smith (1998) explained that the turbulent dispersion force is responsible for the correct spreading of plume within the column.

In bubble column reactor modelling, the turbulent dispersion model proposed by Lopez de Bertodano and Burns et al. (2004) has been commonly employed (Krepper, Frank, *et al.*, 2007; Frank *et al.*, 2008; Li, Yang and Dai, 2009; Duan *et al.*, 2011; Silva, d'Ávila and Mori, 2012; Miao *et al.*, 2013). The range of coefficient of turbulent dispersion (C_{TD}) is between 0.1 and 0.5. Guan and Yang (2017) investigated the impact of the turbulence dispersion force on hydrodynamics in the presence internals. They used a $C_{TD} = 0.3$ and found that the turbulent dispersion force tends to increase and flatten the gas holdup profile. In the presence of vertical internals, enhanced liquid circulations were noticed due to the increase in gas holdups in the bulk of the cylindrical column. Li et al. (2009) reported that phase holdups and liquid axial velocity were accurately predicted using $C_{TD} = 0.2$. Tabib *et al.* (2008) used $C_{TD} = 0.2$ and found that the influence of turbulence dispersion was less pronounced in case of lower superficial gas velocities as compared to higher gas velocities.

In this work, the simulations using the turbulent dispersion models proposed by Simonin et al. (1990) and Burns et al. (2004) are carried out and the results are validated against the

experimental data. Based on the study by Mudde and Simonin (1999), the model by Simonin et al. (1990) is selected to calculate the drift velocity, as shown below.

$$\vec{v}_{drift} = -D_{TD,gl} \left(\frac{\nabla \varepsilon_g}{\varepsilon_g} - \frac{\nabla \varepsilon_l}{\varepsilon_l} \right) \quad (3.12)$$

where, $D_{TD,gl}$ is the tensor which accounts for fluid-particulate dispersion.

$$D_{TD,gl} = \frac{k_{gl} \tau_{TD,gl}}{3} \quad (3.13)$$

Here, k_{gl} is the covariance of the velocities of liquid phase and the gas phase. The turbulent dispersion for gas-liquid flows can be described as

$$\vec{F}_{TD,l} = -\vec{F}_{TD,g} = C_{TD} k_{gl} \frac{D_{TD,gl}}{\sigma_{gl}} \left(\frac{\nabla \varepsilon_l}{\varepsilon_l} - \frac{\nabla \varepsilon_g}{\varepsilon_g} \right) \quad (3.14)$$

where C_{TD} is the coefficient of turbulent dispersion and σ_{gl} is the dispersion Prandtl number between the gas and liquid phase.

3.2.2.5 Bubble Induced Turbulence

The turbulent modelling in bubble column reactors using Reynolds averaged equations is based on Boussinesq approximations (Sokolichin, Eigenberger and Lapin, 2004; Coughtrie, Borman and Sleigh, 2013; Vaidheeswaran and Hibiki, 2017; Shi, X. Yang, *et al.*, 2020). Nevertheless, the presence of bubbles adds to the complexity of the problem. In modelling bubble column reactors, the turbulence is a blend of both, the liquid turbulence (shear turbulence) and turbulence induced by bubbles (Shi *et al.*, 2019). The latter is constituted by the bubble wake generated as a result of shed vortices from the surface of

bubbles. The wake decays rapidly due to the effect of viscous dissipation. The bubble induced turbulence is anisotropic in nature and hence, the Boussinesq approximations of isotropic turbulent eddy viscosity may not be accurate to model the Reynolds stresses. Therefore, the Reynolds Stress Model (RSM) is employed in the current study.

3.2.3 Population Balance Model

The knowledge of bubble behavior within bubble columns and other applications has gained increasing importance in recent years (Mudde, Groen and Van Den Akker, 1997; Luo *et al.*, 1999; Gandhi *et al.*, 2007; Nedeltchev, Shaikh and Al-Dahhan, 2011). It is useful in identifying the transitions between the homogenous and heterogenous flow regimes due to the change in bubble sizes. The predictions of terminal rise velocities and gas holdups depend on the bubble dynamics. Industrial multiphase reactors prefer heterogenous regime due to the wide distribution of bubble sizes. The Population Balance Model (PBM) is a useful tool in the prediction of bubble size distributions (Wang, 2011). CFD has been coupled with PBM to model the bubble break-up and coalescence to determine the bubble size distribution.

The change in bubble size distribution can be determined by the Population Balance Equations (PBEs). This is an integro-differential equation which comprises of the bubble breakup and coalescence kernels. Kumar and Ramkrishna (1996) developed the discrete method to solve this equation, in which the bubble sizes were discretized into a finite number of classes or intervals. Each interval is assigned a pivot size, x_i . The integro-differential equation is integrated over each class or interval and redistributed for each pivot size.

$$\begin{aligned}
& \frac{\partial n(v, t)}{\partial t} + \nabla \cdot (U_g n(v, t)) \\
& = \int_v^\infty b(v') \beta(v, v') n(v') dv' + \frac{1}{2} \int_0^v c(v - v', v') n(v - v') n(v') dv'' \\
& \quad - b(v) n(v) - \int_0^\infty c(v, v') n(v) n(v') dv'' \quad (3.15)
\end{aligned}$$

Table 3.1 Population Balance Equation Terms

Phenomena	Governing Equation
Time variation	$\frac{\partial n(v, t)}{\partial t}$
Convection	$\nabla \cdot (U_g n(v, t))$
Bubble birth due to coalescence (Coalescence Source)	$\frac{1}{2} \int_0^s c(s - s', s') n(s - s') n(s') ds''$
Bubble birth due to breakup (Breakup Source)	$\int_v^\infty b(s') \beta(s, s') n(s') ds'$
Bubble death due to coalescence (Coalescence Sink)	$\int_0^\infty c(s, s') n(s) n(s') ds''$
Bubble death due to breakup (Breakup Sink)	$b(s) n(s)$

The discrete solution developed by Kumar and Ramkrishna (1996) is given below.

$$\begin{aligned} \frac{dN_i(t)}{dt} + \nabla \cdot (U_G N_i(t)) = & \sum_{j,k}^{j \geq k} (1 - 0.5\delta_{j,k}) \eta_{i,j,k} c_{j,k} N_j(t) N_k(t) \\ & - N_i(t) \sum_{k=1}^M c_{i,j} N_k(t) + \sum_{k=i}^M \zeta_{i,k} b_k N_k(t) - b_i N_i(t) \end{aligned} \quad (3.16)$$

where N_i is the bubble number in the i^{th} subregion and $\eta_{i,j,k}$ and $\zeta_{i,k}$ are the distribution coefficients which describe the bubble coalescence and bubble breakup, respectively. The homogenous discrete PBM assumes same phase velocities across all bins.

3.2.3.1 Bubble Coalescence Model

Bubble coalescence in gas-liquid systems has three key mechanisms – coalescence due to wake entrainment, difference in bubble rise velocities and turbulent eddies (Prince and Blanch, 1990). In a typical turbulent flow, the bubble coalescence takes place in 3 steps. Initially, the collision amid bubbles lead to liquid confinement between them. This is followed by draining of the confined liquid which allows the liquid film separating the two bubbles to reach a critical thickness. Finally, the liquid film ruptures which leads to coalescence between the two bubbles. The bubble coalescence due to turbulent eddies is the main mechanism noticed in bubble column reactors working in the bubbly and transition regimes. When the bubble columns operate in the churn turbulent regimes where the bubble size distribution is wide, the bubble coalescence is dominated by the wake entrainment effect. This effect is crucial in the formation of large bubbles in the transition and churn turbulent regime. The bubble coalescence due to the difference in bubble rise velocities is negligible as the rise velocity is directly dependent on the bubble size.

The rate of bubble coalescence between two bubbles, i and j , with diameters d_i and d_j , can be evaluated as a product of collision frequency (ω_c) and coalescence probability leading from collision (P_c):

$$c(d_i, d_j) = \overline{\omega_c}(d_i, d_j) \cdot P_c(d_i, d_j) \quad (3.17)$$

3.2.3.2 Bubble Breakup Model

Bubble breakup mechanisms include viscous shear, interfacial instability and local turbulence (Lee, Erickson and Glasgow, 1987; Kocamustafaogullari and Ishii, 1995; Liovic and Lakehal, 2007; Liao and Lucas, 2009; Chu *et al.*, 2019). The bubble breakup model proposed by Luo and Svendsen (1996) accounts for binary disintegration of bubbles due to collisions and turbulent fluctuations. This theoretical model is based on the kinetic gas theory for drop and breakup of bubbles in turbulent flows (Luo and Svendsen, 1996; Gaurav, 2018). Turbulent kinetic energy of the colliding eddy is a key factor in determining the bubble size distribution. The turbulent kinetic energy must be greater than a critical value which corresponds to the surplus in the value of surface energy before and after the process of breakup. Critical value is calculated by a model proposed by Prince and Blanch (1990). Therefore, an apt choice of turbulence model is necessary to suitably model the breakup rate.

3.2.4 Turbulence Model

In bubble column reactor modelling, the turbulence model plays an important role. In several studies carried out over several years, various turbulence models such as standard $k - \varepsilon$, RNG $k - \varepsilon$, RANS and LES, were used extensively to study the bubble columns.

Dhotre et al. (2008) compared the effect of $k - \varepsilon$ and LES turbulence models on the bubble flow characteristics. Both the turbulence models reportedly gave a good agreement for the liquid and gas axial velocities at various axial positions when compared with the experimental data. Near the gas sparger, the gas holdup, and liquid and gas velocities predicted by both models were in close agreements to the experimental data. However, the LES model overpredicted the turbulent kinetic energy near the injector. The deviations in turbulent kinetic energy predictions could be attributed to the mechanisms used to determine the energy interactions between the mean flow and the large scale, and the energy cascading from large scale to small scale (Tabib, Roy and Joshi, 2008). In conclusion, the $k - \varepsilon$ model incorporated with additional interphase force terms required less computational times and provided a good agreement with the experimental data.

A study conducted by Tabib *et al.* (2008) compared the effect of $k - \varepsilon$, RSM and LES models on bubble column hydrodynamics. The axial profiles of the liquid velocity were well predicted by the RSM and LES models in comparison to the $k - \varepsilon$ model. Turbulent kinetic energy profiles predicted by the LES and RSM models were close to the experimental values. The pressure strain mechanism engrained in the RSM modelling helps in the redistribution of turbulent kinetic energy at various components for accurate predictions. In contrast, the poor prediction of turbulent kinetic energy profiles by the $k - \varepsilon$ model is due to the isotropic assumption which leads to ineffective redistribution of energy. Their study concluded that the inherent mechanism of anisotropic energy transfer in RSM model outperformed the $k - \varepsilon$ model.

In the current study, RSM model is employed to model the turbulence within the bubble column reactor. In the RSM turbulence model, five transport equations are solved for 2-D flows to obtain the Reynolds stresses. The equations for the RSM turbulence model are illustrated as:

$$\frac{\partial}{\partial t} (\rho_L \varepsilon_L u_i' u_j') + C_{ij} = \varphi_{ij} + D_{L,ij} - D_{T,ij} - P_{ij} - \varepsilon_{ij} \quad (3.18)$$

The individual terms in Eq. (3.18) are listed in Table 3.2.

Table 3.2 Reynolds stress model (RSM) terms

Notation	Term	Equation
C_{ij}	Convection	$\frac{\partial}{\partial x_k} (\rho_L \varepsilon_L U_k \overline{u_i' u_j'})$
φ_{ij}	Pressure Strain	$\rho_L \varepsilon_L \overline{\left(\frac{\partial u_i'}{\partial x_j} + \frac{\partial u_j'}{\partial x_i} \right)}$
$D_{L,ij}$	Molecular Diffusion	$\frac{\partial}{\partial x_k} \left(\rho_L \mu_L \frac{\partial \overline{(u_i' u_j')}}{\partial x_k} \right)$
$D_{T,ij}$	Turbulent Diffusion	$\frac{\partial}{\partial x_k} [\rho_L \varepsilon_L \overline{u_i' u_j' u_k'} + \rho_L \varepsilon_L (\delta_{jk} u_i' + \delta_{ik} u_j')]$
P_{ij}	Stress Production	$\rho_L \overline{(u_i' u_k' \frac{\partial U_k}{\partial x_k} + u_j' u_k' \frac{\partial U_i}{\partial x_k})}$
ε_{ij}	Dissipation	$2 \varepsilon_L \rho_L \mu_L \overline{\left(\frac{\partial u_i'}{\partial x_k} \frac{\partial u_j'}{\partial x_k} \right)}$

3.3 Configuration of the column

The numerical modelling is based on the pilot-scale bubble column reactor (Jhavar and Prakash, 2014) as shown in Figure 3.2 . The experiments were carried out in a Plexiglas column of height 2.5 m and diameter 0.15 m. The column was equipped with a coarse

sparger, through which the secondary phase was introduced. In the experiments, tap water and compressed air were used as primary and secondary sources, respectively. The experiments were carried out at different superficial gas velocities ranging from 3 cm/s to 35 cm/s. The static height of the liquid was maintained at 1.45 m throughout the experimental run. The experimental data is used to validate the numerical results in this study.

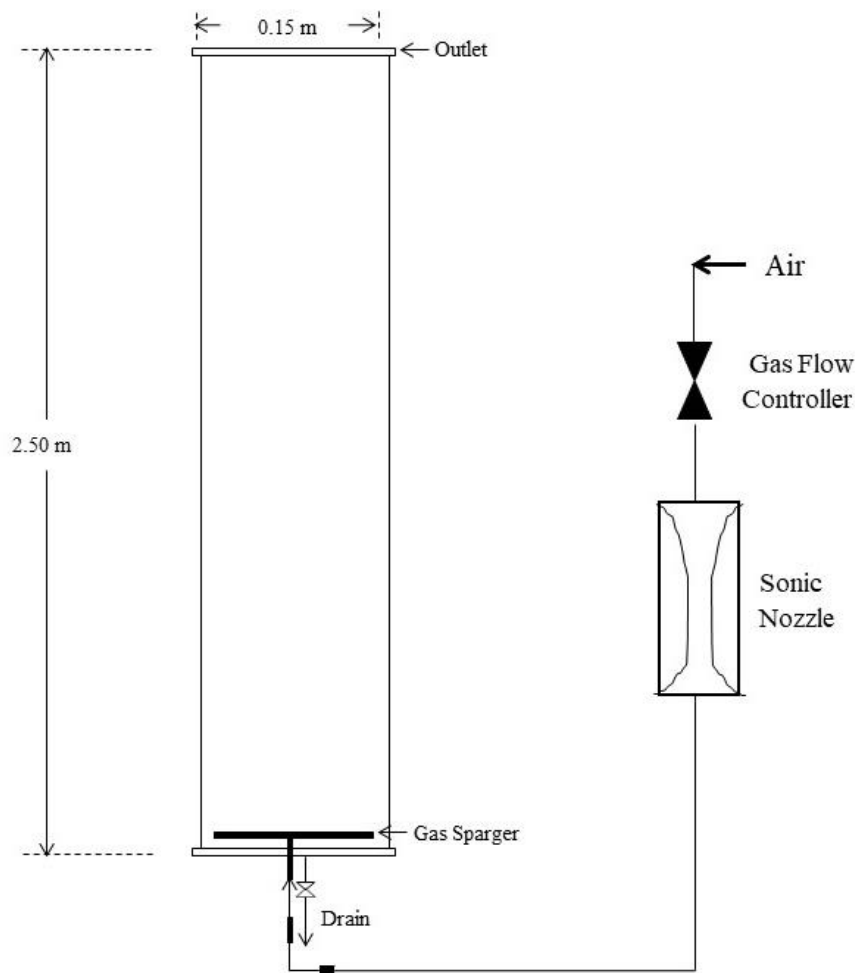


Figure 3.2 Experimental setup of the hollow bubble column reactor used in Jhawar and Prakash (2014)

3.4 Numerical Method

A 2-dimensional uniform structured mesh is developed using ICEM CFD 17.0. The grid independence tests are carried out. The node counts are outlined in Table 3.3. Medium mesh is shown in Figure 3.3. Overall gas holdups at a superficial gas velocity of 0.04 m/s obtained for the coarse and medium meshes are 0.66 and 0.075, respectively. Subsequently, centerline liquid velocities at a superficial gas velocity of 0.04 m/s obtained for the medium and fine mesh are 0.235 and 0.242, respectively. Figure 3.4 compares the radial gas holdups obtained using the medium and fine mesh, the average difference between them is 3.6%.

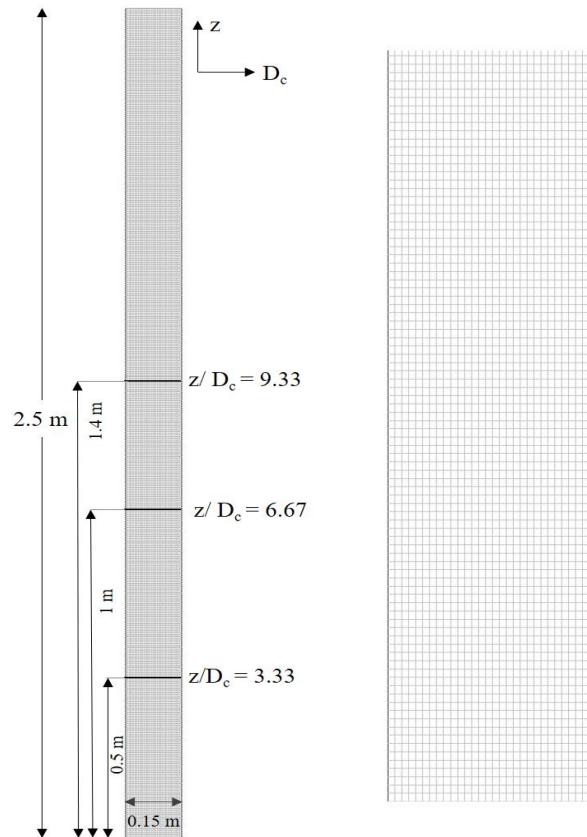
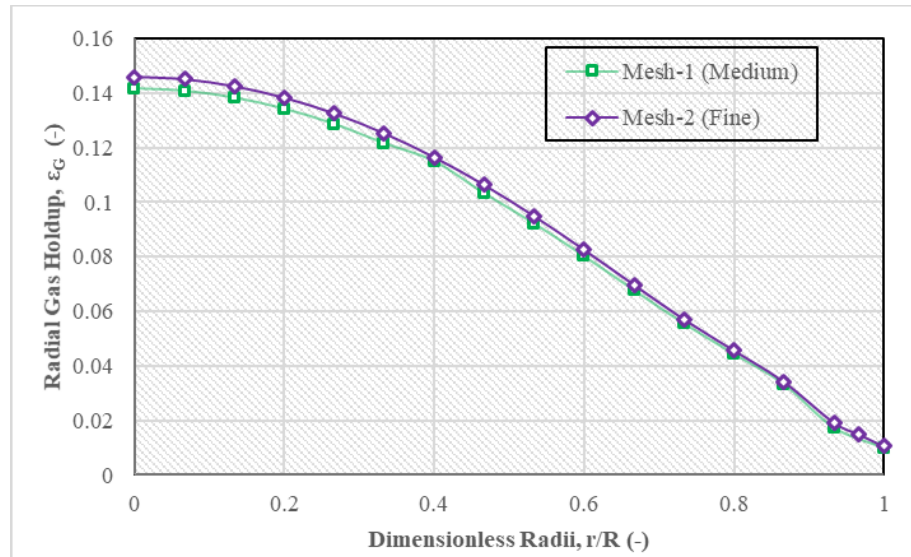


Figure 3.3 Medium mesh representing the hollow bubble column geometry along with axial locations of measurements

Table 3.3 Hollow bubble column – Mesh information

Mesh Type	Node Count
Mesh-1 (Medium)	10750
Mesh-2 (Fine)	11656

**Figure 3.4** Comparison of the gas holdups along the radial direction using the medium and fine meshes

The numerical simulations of hollow bubble column reactors are carried out using ANSYS Fluent v19.2. The geometries utilized are of the 2-Dimensional planar type. The simulations are carried out for water-air two-phase flow system and an incompressible method (pressure-based solver) is utilized to solve the governing equations. The Reynolds Stress Model (RSM) turbulence model with dispersed formulation is used in the current study since it is able to accurately predict the turbulent kinetic energy, which is a key parameter in the bubble column modelling. Water and air were selected as the primary phase and secondary phase respectively. The simulations are carried out in the bubbly regime ($U_G=4$ cm/s), transition regime ($U_G=10$ cm/s) and churn turbulent regime ($U_G=30$ cm/s). The

simulations are performed with and without the PBM and to investigate the effect of the PBM on the column hydrodynamics.

The spatial variables are discretized by Green-Gauss Cell based method. The phase-coupled SIMPLE method is used for the pressure-velocity coupling. The momentum and volume fraction equations are solved using the QUICK scheme and second order upwind scheme is used to solve the turbulence equations and gas bin fractions. The convergence criterion is set to 10^{-3} for all transport equations. The initial time step is set to 0.0001 s for the first 3 seconds of flow time and is then increased to 0.0005 s and 0.001 s after 8 seconds and 15 seconds, respectively to avert numerical divergence. The flow simulations are carried out for 200 s. The results are time averaged after a quasi-steady state has been achieved. The quasi-steady state is achieved after 30 seconds. Hence, the simulation results are averaged for about 170 s. The numerical models used in the current work is listed in Table 3.4.

Table 3.4 An outline of numerical methods

Scheme	Solution Methods
Pressure-Velocity Coupling	
Scheme	Phase-Coupled SIMPLE
Spatial Discretization	
Gradient	Green-Gauss Cell Based
Momentum	QUICK
Volume Fraction	QUICK

Turbulent Kinetic Energy	Second Order Upwind
Turbulent Dissipation Rate	Second Order Upwind
Reynolds Stresses	Second Order Upwind
Air Bins (Population Balance Model)	Second Order Upwind
Transient Formulation	
Scheme	Bounded Second Order Implicit
Under Relaxation Factors	
Pressure	0.2
Momentum	0.3
Volume Fraction	0.2
Turbulent Kinetic Energy and Turbulent Dissipation Rate	0.8
Turbulent Viscosity	1
Reynolds Stresses	0.5
Air Bin Fractions	0.5

At the inlet, the superficial gas velocity and volume fraction of the gas phase along with the initial bin fractions are specified. Very few researchers have explicitly mentioned their choice of turbulent quantities for the liquid phase at the inlet of the bubble column. This makes it a great challenge to gather the turbulence specification data for gas-liquid flows. In a recent study by Magolan *et al.* (2019), the turbulence intensity of 0.1 and turbulent

viscosity ratio of 100 were used. In another study carried out by Nygren (2014), the turbulent intensity was set at 10% and hydraulic diameter was set to 4 mm which was calculated based on the rectangular duct geometry. In this study, the turbulent intensity of 5% and hydraulic diameter of 0.15 m, which is the equivalent diameter of the bubble column reactor, are applied. The outflow is used as the outlet boundary condition as it extends the inclusion of freeboard region of discontinuous phase on top of the continuous phase.

3.5 Results and Discussion

In this section, the numerical results are categorized in two parts. First, the effects of the PBM and the interfacial forces on reactor hydrodynamics are discussed. Next the hydrodynamics and shear stress in the column with flow regime transitions are presented.

3.5.1 Influence of interfacial forces

The choice of appropriate interfacial force models is crucial in the prediction of flow patterns and reactor hydrodynamics. Therefore, the influence of various drag force models, lift models, turbulent dispersion models, turbulence interaction model and wall lubrication force models are presented in this section.

3.5.1.1 Influence of the lift force model

In this section, the effect of lift force from different models on the simulation results is investigated in the transition regime (10 cm/s). Table 3.3 presents the lift coefficients from different models and the centerline liquid velocities and global gas holdups from different lift coefficients. Figure 3.5 shows the influence of the lift force models on the liquid axial velocity profiles. If the lift force is neglected, the centerline liquid velocity is much lower

(149% lower) than that from the experimental data from Hills (1974). When a positive lift coefficient is used, an increase in U_{L0} is noticed. For the lift coefficients of 0.08 and 0.02, U_{L0} increases about 0.6% and 22%, respectively, in comparison to the case without the lift force. When the lift coefficient is positive, the gas bubbles tend to disperse from the central region and get pushed towards the reactor walls, which lowers the value of centerline liquid velocity. The use of a negative lift coefficient leads to a significant increase in the centerline liquid velocity. The negative lift force coefficient is for the bubbles of diameter greater than 5.6 mm, so the bubbles tend to rise through the central region. Out of the three negative lift coefficients tested, $C_L = -0.08$ gives the best agreement with the experimental data from Hills (1974).

The Tomiyama lift force model depends on the Eotvos number and the sign of lift coefficient will change based on bubble diameters. But, when The Tomiyama lift model is employed, the peak velocity is shifted towards the left wall, which is different from the velocity profiles predicted from other models where the peak velocity is at the center of the column. When the Saffman-Mei lift model is employed, the centerline liquid velocity is drastically reduced by about 451% compared with the experimental value (Hills, 1974). This is because the Saffman-Mei model is for spherical bubbles only, i.e. the shape factor is not included in the model. As the investigation is carried out in the transition regime, which comprises of a variety of bubble sizes and shapes, Saffman-Mei lift model cannot predict the axial velocities accurately.

Table 3.5 List of lift coefficients, centerline liquid velocities and global gas holdups

Lift force model	Coefficient, C_L	Centerline Liquid Velocity, U_{L0}	Global Gas Holdup, ϵ_G
No Lift	0	0.1830	0.182
Constant (Negative)	-0.02	0.3648	0.179
Constant (Negative)	-0.08	0.4553	0.167
Constant (Negative)	-0.1	0.4955	0.161
Constant (Positive)	0.02	0.2229	0.177
Constant (Positive)	0.08	0.1840	0.179
Tomiyama (1998)		0.0330	0.142
Saffman-Mei (Mei, 1992)		0.0810	0.169

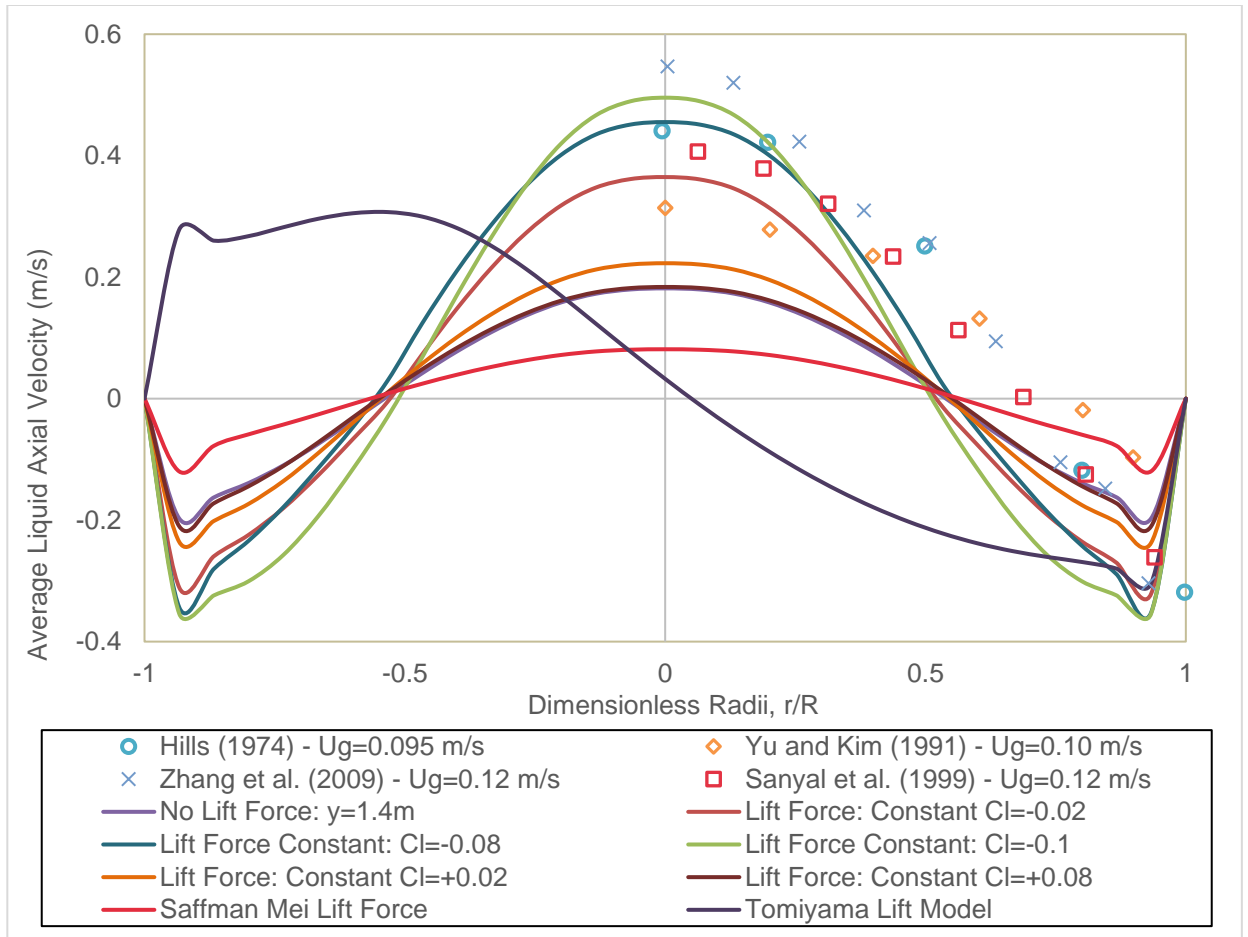


Figure 3.5 Comparison of liquid axial velocities along the radial direction from different lift fore models in the transition regime ($U_g=10$ cm/s)

The comparison of the gas holdup profiles along the radial direction using different lift force models is shown in Figure 3.6. Compared with the experimental data, it can be seen that the lift force models proposed by Tomiyama (1998) and Mei (1992) cannot predict a correct gas holdup profile along the radial direction. The gas holdup predicted by the Tomiyama model is much lower than the experimental data. On the other hand, the Saffman-Mei lift model gives a flat gas holdup profile, which is different from that observed in the experiment. It is found that the constant lift force coefficient gives a

relatively good agreement with the experimental data for the gas holdup. The gas holdup is slightly underpredicted if the lift force is neglected. The same trend is observed when a positive lift coefficient is used. The gas bubbles shift away from the bulk region when a positive lift coefficient is used, which leads to a lower gas holdup in the central region ($r/R=0$). In contrast, when a negative lift coefficient is used, the gas holdup at the central region is slightly higher. It has been pointed out in literatures that when the diameter of air bubbles exceeds 9 mm, a negative lift coefficient will result in the symmetric wake associated with the bubble deformation (Sokolichin et al., 2004). The gas holdup predicted by the negative coefficient, $C_L=-0.08$, agrees with the experimental data from Hills (1974).

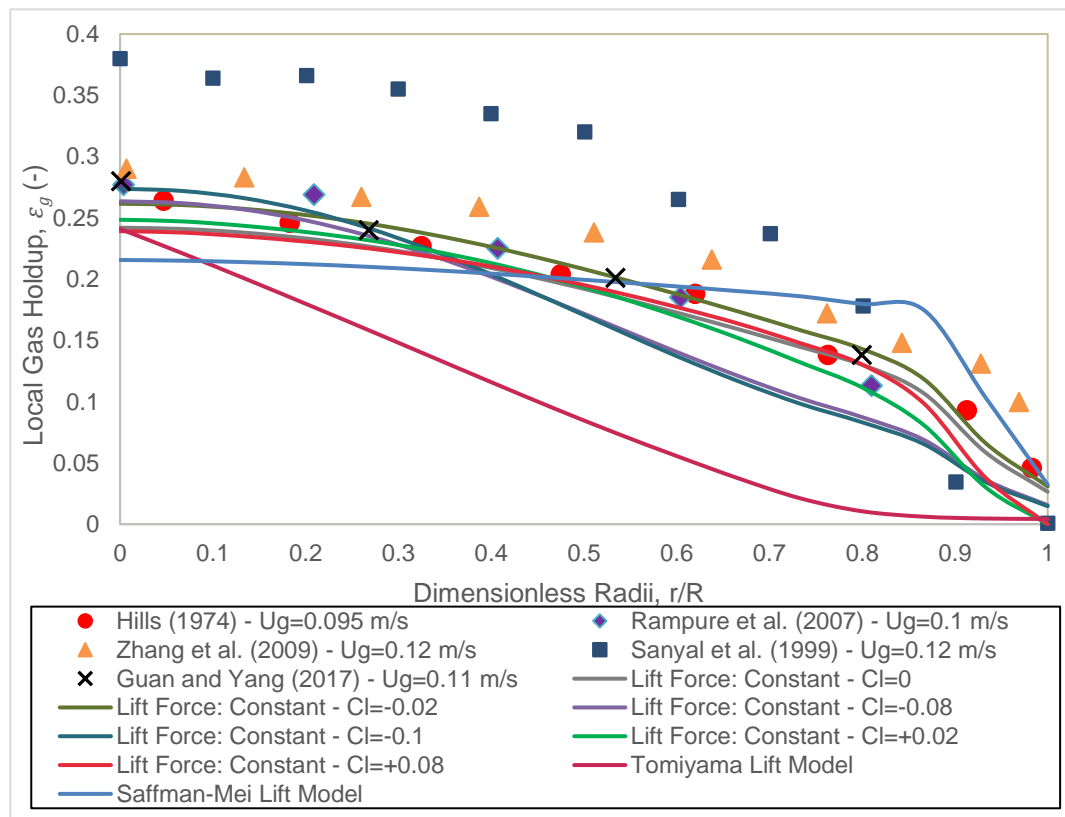


Figure 3.6 Comparison of gas holdup profiles along the radial direction from different lift force models in the transition regime ($U_g=10$ cm/s)

3.5.1.2 Influence of bubble induced turbulence

Bubble induced turbulence (BIT) is the pseudo-turbulence stimulated by the bubbles when rising through the column (Shi *et al.*, 2019), which is crucial to accurately predict the bubble size distribution within the reactor. In this study, the simulations with and without the BIT are carried to investigate the effect of the BIT on the velocity and gas holdup distributions. The BIT model proposed by Troshko and Hassan (2001) is used for simulations when the BIT is included. Figures 3.7 and 3.8 present the influence of the BIT on local gas holdups and liquid axial velocities. When the BIT is neglected, the gas holdups and liquid axial velocity profiles along the radial direction are not symmetric about the central axis, which is generally not the case in experiments. However, the central peak is observed when the BIT is included in the simulation, which is similar to that from experimental observations.

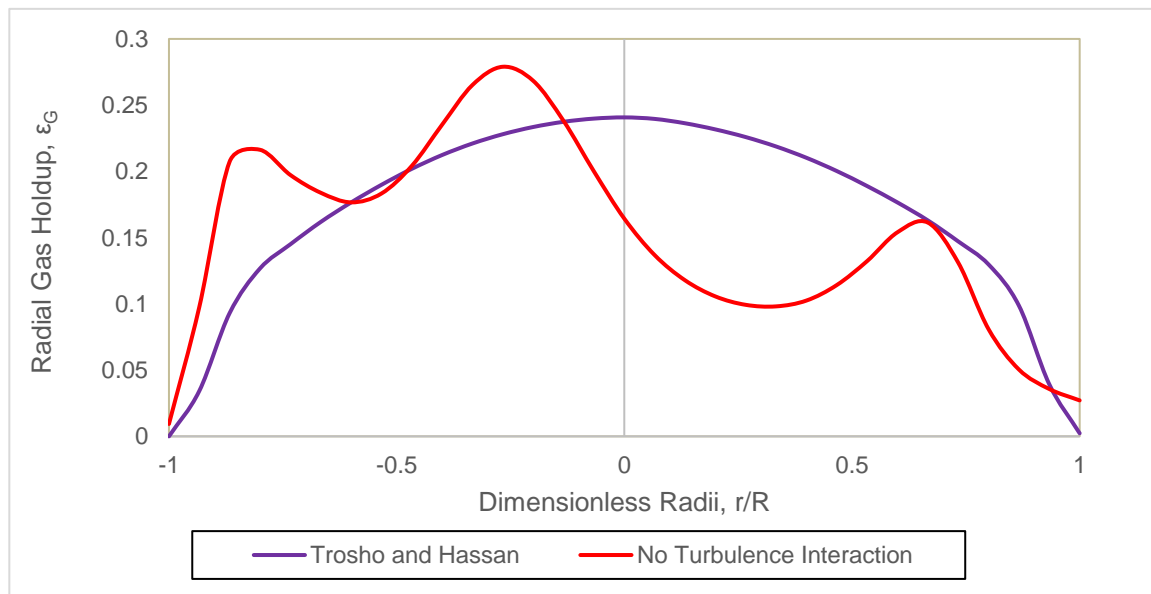


Figure 3.7 Comparison of the gas holdup profiles with and without BIT along the radial direction

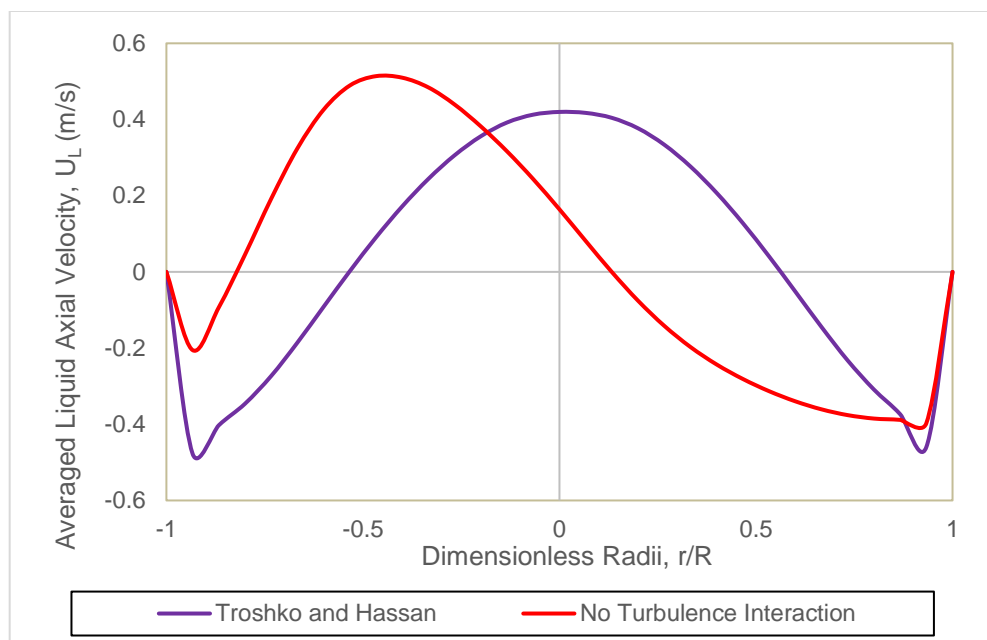


Figure 3.8 Comparison of the liquid axial velocity profiles with and without BIT along the radial direction

Contour profiles of liquid axial velocities and gas holdups are illustrated in Figures 3.9 and 3.10, respectively. When the BIT is included, a maximum axial velocity of 0.41 m/s is observed in the central region of the bubble column reactor. In contrast, without the BIT, the maximum axial velocity is not at the central region. Similar observations can be seen for gas holdup contours with and without the BIT. The gas profiles are smooth in the bulk region of the column if the BIT is included. It is noticed that the liquid level in the column is below the static height ($y=1.4$ m) if the BIT is neglected, which is signified by the increase in gas volume fraction.

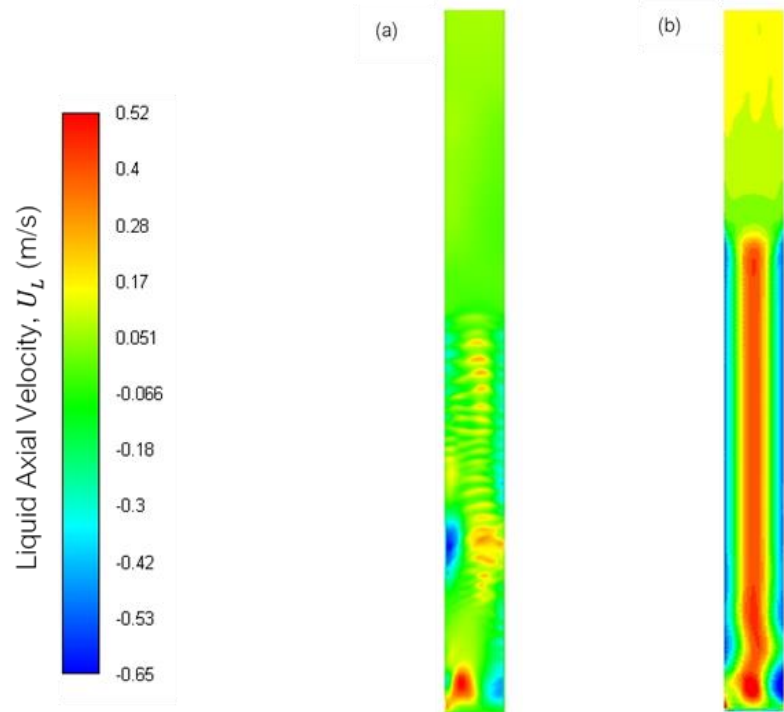


Figure 3.9 Comparison of the contours of averaged liquid axial velocity with and without the BIT

(a) Without BIT and (b) With BIT

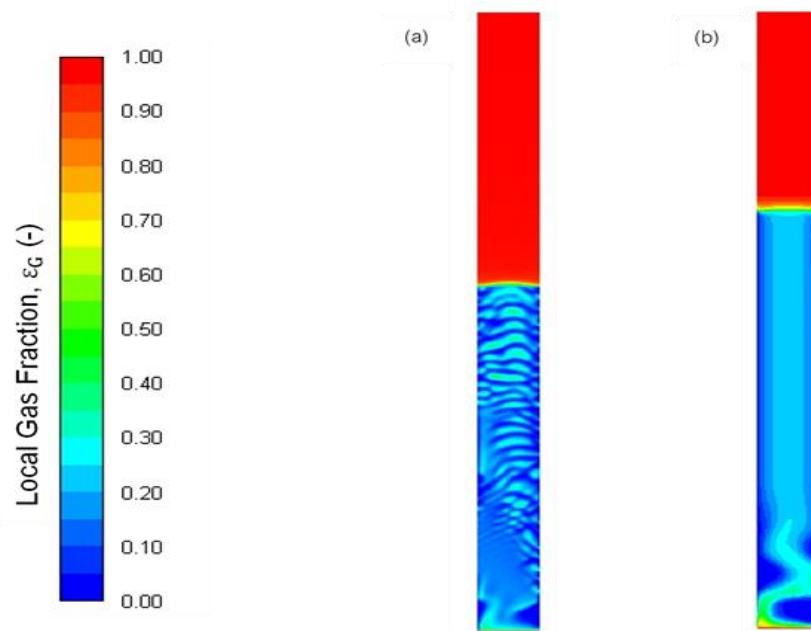


Figure 3.10 Comparison of the contours of averaged gas holdup with and without the BIT (a) Without the BIT and (b) With the BIT

The vector profiles also indicate the difference in the flow patterns with and without the BIT as shown in Figures 3.11 – 3.13. In the distributor region (Figure 3.11), similar flow patterns are noticed in both cases. However, a stronger recirculation in the central region is noticed in the case with the BIT, which is in accordance with the experimentally observed flow patterns. In the bulk region (Figure 3.12), smooth flow profiles are noticed with the BIT model. Without the BIT, the flow direction seems to be skewed to one of the sides, i.e. an asymmetric pattern, which is not usual observed in experiments. Also, in the central region, a maximum gas velocity of 1.4 m/s is observed without the BIT and 0.60 m/s with the BIT. The latter is close to the experimental data at a superficial gas velocity of 10 cm/s. In the disengagement zone (Figure 3.13), funneling pattern is clearly observed when the BIT is included in the simulation. Without BIT, the direction of fluid flow is reversed in the disengagement zone and the funneling effect disappears.

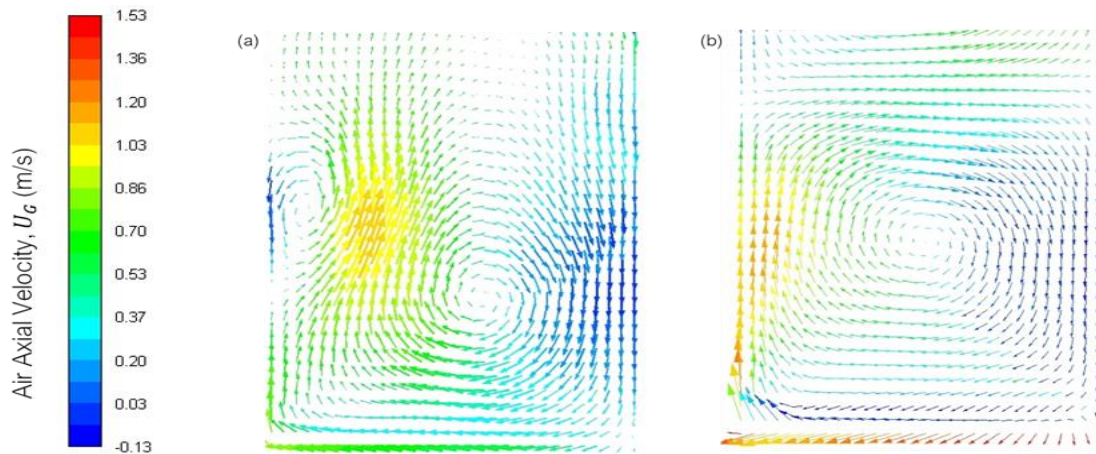


Figure 3.11 Vector contours of the gas phase in the distributor region

(a) Without the BIT and (b) With the BIT

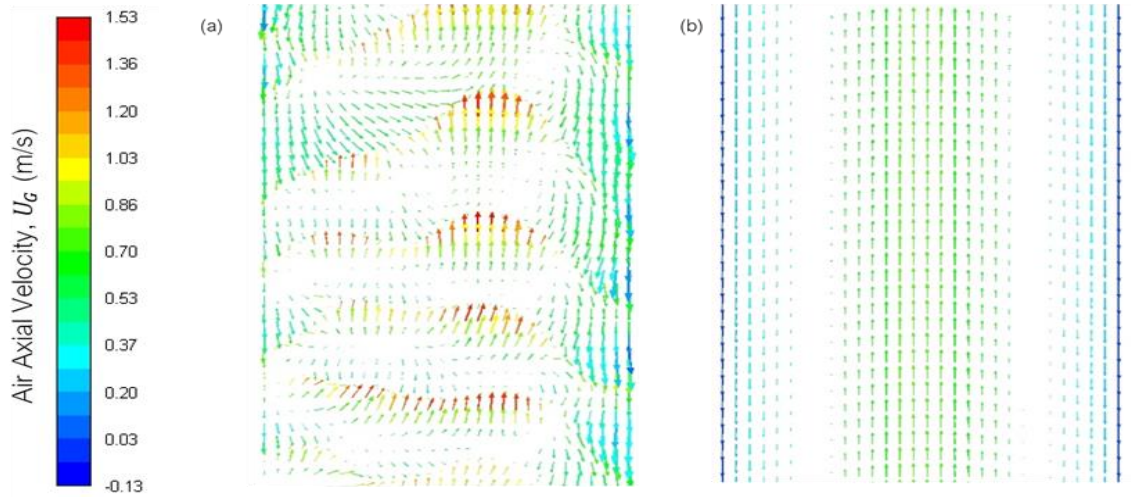


Figure 3.12 Vector contours of the gas phase in the bulk region

(a) Without BIT and (b) With BIT

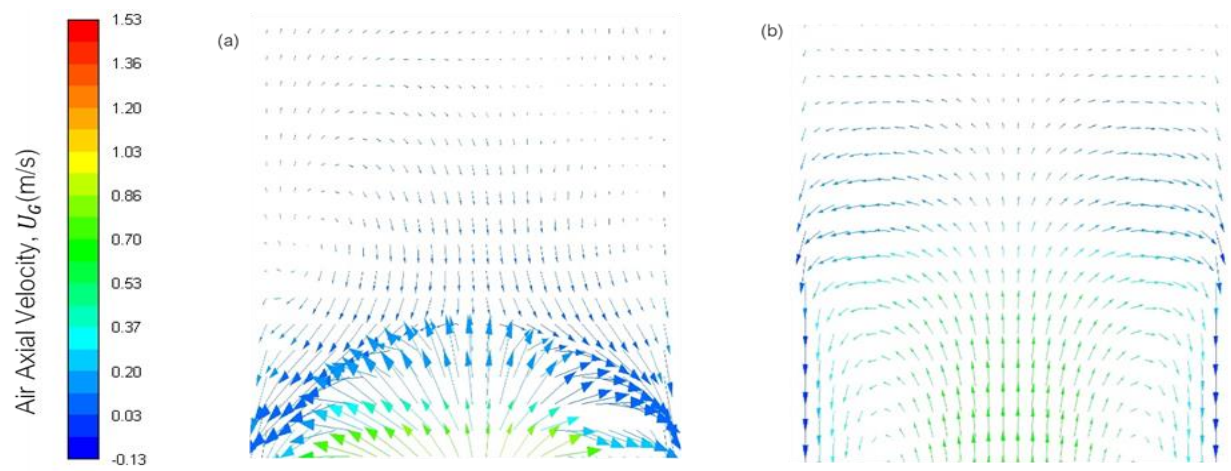


Figure 3.13 Vector contours of the gaseous phase in the disengagement zone

(a) Without BIT (b) With BIT

3.5.1.3 Influence of turbulence dispersion force

To investigate the sensitivity of the bubble column modelling to the turbulent dispersion force (TDF), two types of turbulent dispersion models, namely Simonin ($C_{TD}=0.1, 0.3$ and 0.5) (Simonin *et al.*, 1990) and Burns *et al.* ($C_{TD}= 0.3$) (Burns *et al.*, 2004)), are used. For the case without the TDF, the gas plume rises through the central region of the bubble column with a higher gas holdup peak than the cases without the TDF, as seen in Figure 3.14. Also, a rapid decline is noticed in the gas holdup away from the central region, which is not observed experimentally. The centerline liquid axial velocity as illustrated in Figure 3.15 is higher without the TDF than the cases with the TDF. This is attributed to the rapid rise of bubbles through the central region when the TDF is neglected. However, when the TDF is included, the gas plume is dispersed throughout the bulk region of the column, which leads to lower centerline liquid axial velocities due to the effective bubble dispersion in the liquid. The gas holdup profiles tend to be flattened due to the effect of bubble plume dispersion.

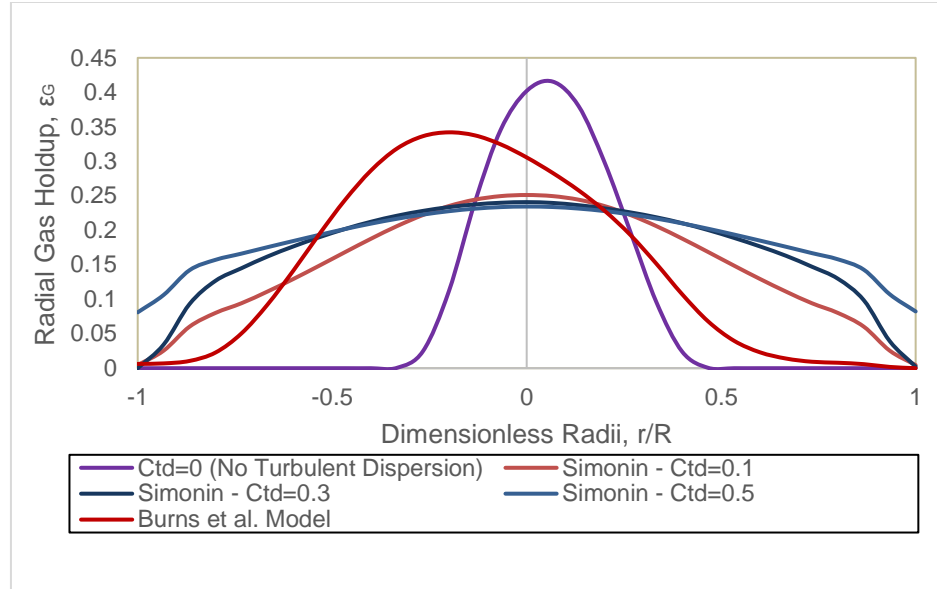


Figure 3.14 Comparison of the gas holdups with and without the TDF in the transition regime ($U_G=10$ cm/s)

The simulations carried out using the turbulent dispersion model proposed by Simonin *et al.* (1990) yield liquid axial velocities and gas holdup profiles closer to the experimental data. The influence of turbulent dispersion coefficient ($C_{TD}=0.1, 0.3$ and 0.5) on the gas-liquid flow is also examined. The centerline liquid axial velocities decrease considerably when the value of turbulent dispersion coefficient increases. The predictions made by using the coefficient, $C_{TD}=0.3$, gives the best agreement with the experimental data for the liquid axial velocity, as seen in Figure 3.15. The axial velocities and phase holdup obtained using the turbulent dispersion model by Burns *et al.* (2004) have non-symmetrical profiles, and the maximum liquid axial velocity is 0.6 m/s, which is close to the velocity in the wall region instead of the bulk region. The local gas holdup profile from the Burns model is also skewed towards the wall region due to the orientation of the gas plume.

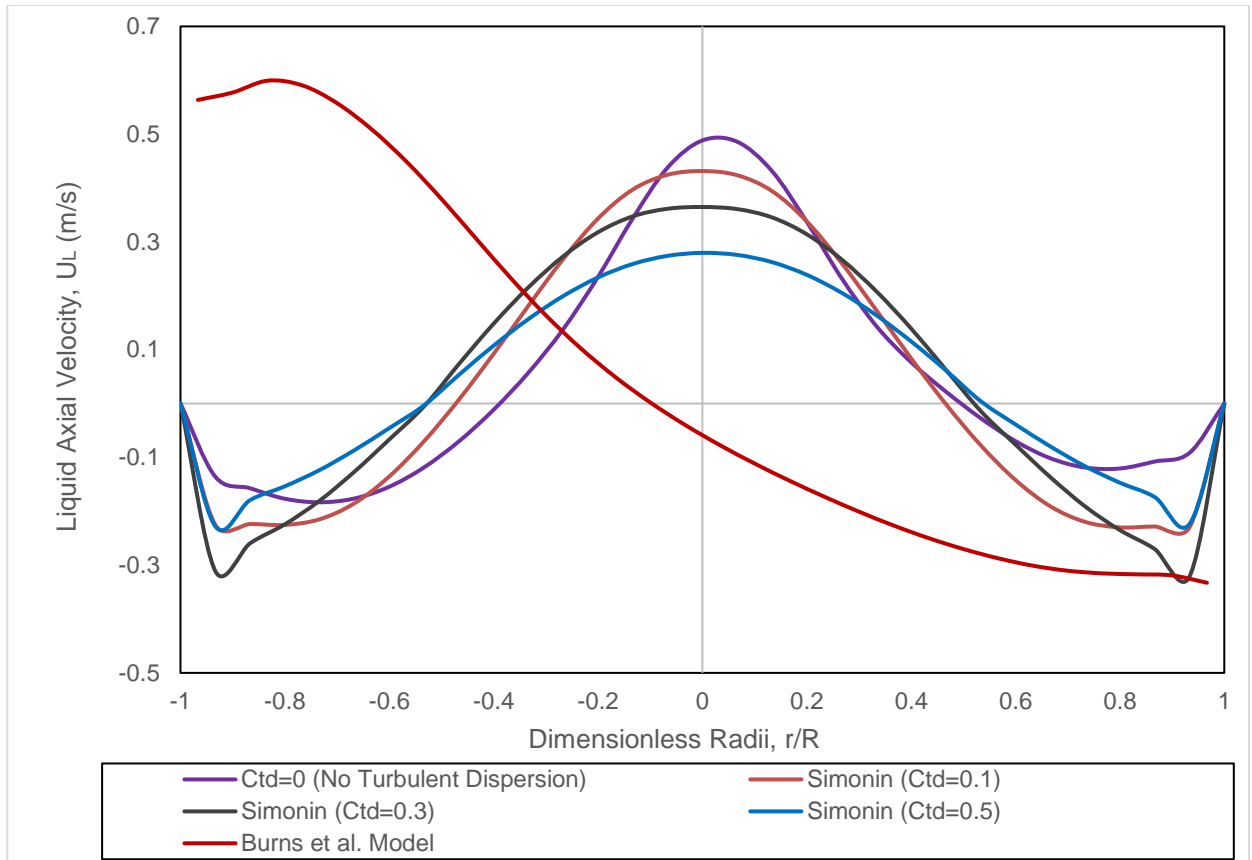


Figure 3.15 Comparison of the liquid axial velocities with and without the TDF in the transition regime ($U_G=10$ cm/s)

Based on the comparison of the liquid axial velocity contours (Figure 3.16), the influence of the TDF on the liquid and gas phases can be clearly seen. From the liquid velocity contours, the maximum liquid velocity of 0.7 m/s is in the central region in the case without the TDF. When using the TDF model from Burns *et al.* (2004), the maximum and minimum liquid velocities of 0.6 m/s (upward) and -0.3 m/s (downward) are observed close to the wall region which is not in accordance to the experimental observations. A clear distinction is noticed in the liquid velocity when the coefficients of turbulent dispersion is differed.

When C_{TD} increases from 0.1 to 0.5, the maximum centerline liquid axial velocity decreases from 0.5 to 0.3 m/s.

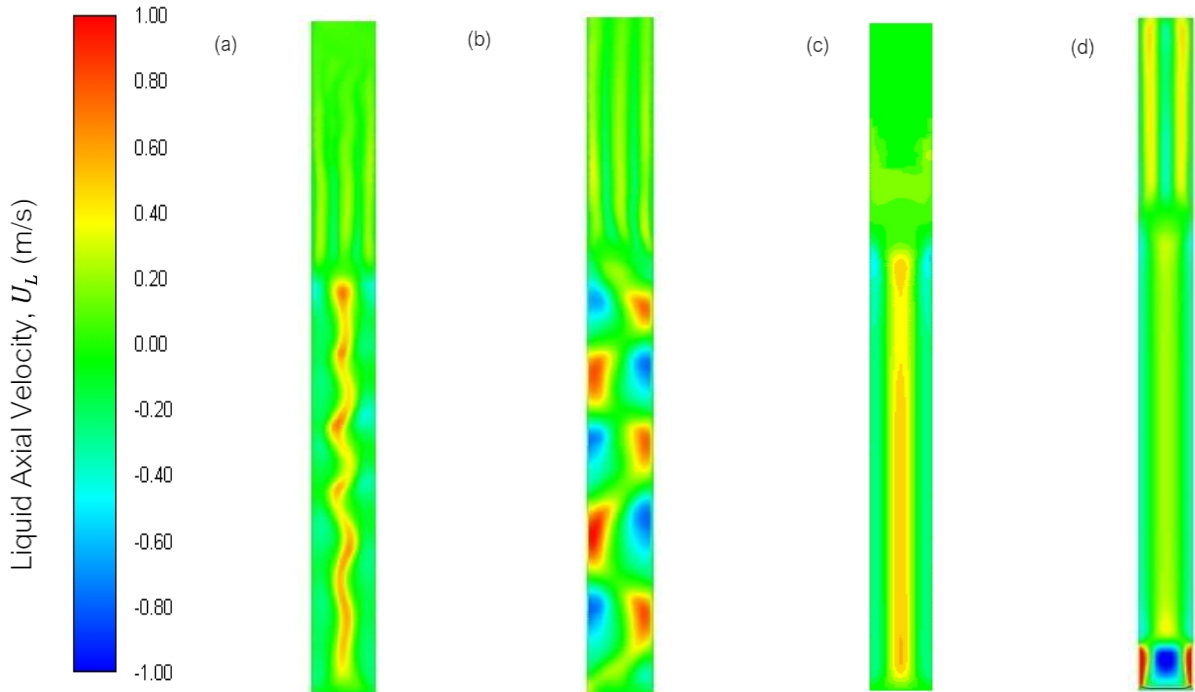


Figure 3.16 Comparison of the averaged liquid axial velocities with and without turbulent dispersion models

(a) Without the TDF (b) Burns et al. ($C_{TD}=0.1$) TDF model (c) Simonin et al. ($C_{TD}=0.1$) TDF model (d) Simonin et al. ($C_{TD}=0.5$) TDF model

From radial gas holdup contours (Figure 3.17), it can be seen that the gas dispersion in the column is very minimal in the case without the TDF. The gas plume is concentrated at the central region of the column and no dispersion is observed in the bulk region close to the column walls. On using the turbulent dispersion model proposed by (Burns *et al.*, 2004) ($C_{TD}=0.1$), the gas plume is oriented from one column wall to the other. This trend is generally not observed in experiments. However, when turbulent dispersion model

proposed by Simonin *et al.* (1990) ($C_{TD}=0.1$) was employed, the gas plume was concentrated in the central region of the column which is close to the experimental observations. When the coefficient of turbulent dispersion was varied from 0.1 to 0.5, the difference in the spread or the dispersion of the gaseous phase was very apparent. A lower value of C_{TD} ensures a high holdup in the central region leading to steep gas holdup profiles. On increasing the C_{TD} value, the spread of the gas holdup profiles become flatter which is typically observed in experiments.

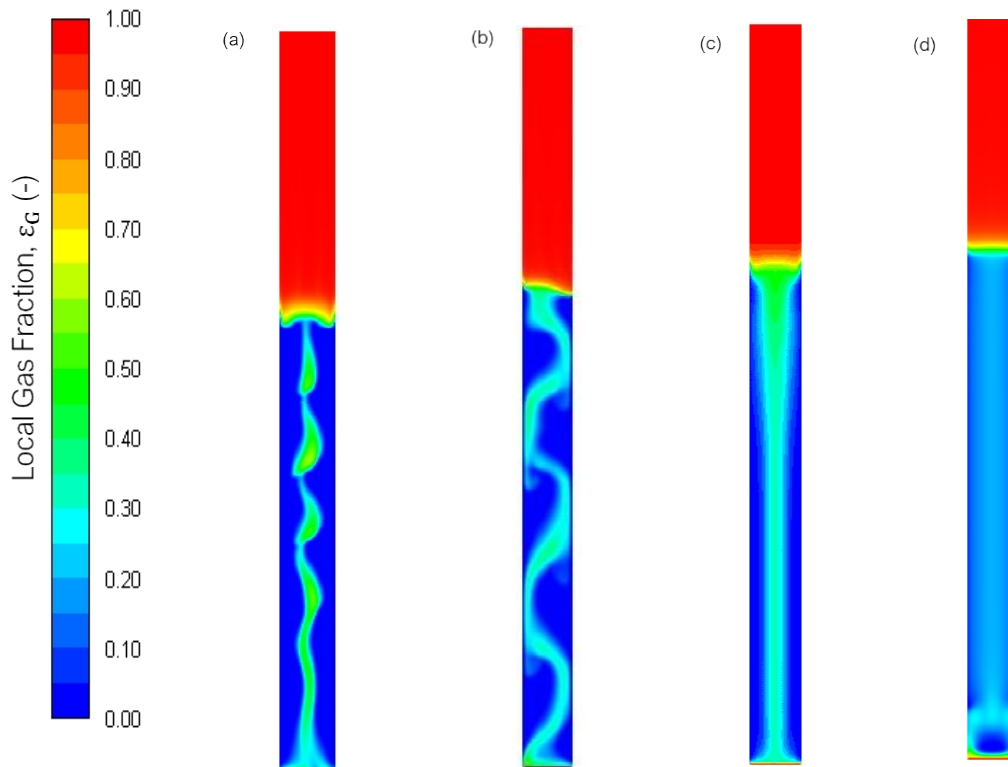


Figure 3.17. Influence of turbulent dispersion models on averaged radial gas holdup profiles

(a) Without the TDF model, (b) Burns *et al.* TDF model with $C_{TD}=0.1$, (c) Simonin *et al.* TDF model with $C_{TD}=0.1$ and (d) Simonin *et al.* TDF model with $C_{TD}=0.5$

The vector profiles shown in Figure 3.18 indicate the clear difference in the flow patterns exhibited while using various turbulent dispersion models. Without using the turbulence dispersion model, there is an upward flow in the distributor region with a maximum velocity of 0.54 m/s in the central region and 0.12 m/s close to the wall region. The liquid recirculation occurs in the bulk region of the column. When utilizing the turbulent dispersion model proposed by Burns *et al.*, (2004), the flow direction is skewed towards the wall in the distributor region. In addition, there is a presence of strong recirculation pattern in the bulk region. When employing the turbulent dispersion model by Simonin *et al.* (1990) with the turbulent dispersion coefficient of 0.1, an upward flow with a velocity of 0.5 m/s in the central region can be observed and a downward velocity of 0.2 m/s exists close to the wall region. On the other hand, when increasing the value of the turbulent dispersion coefficient to 0.5, a minimum velocity of 0.32 m/s in the downward direction can be seen in the column center. At the column walls, the maximum velocity of 0.8 m/s is observed in the upward direction. In the distributor region, when the turbulent dispersion coefficient increases, the large bubbles deflect towards the wall region, which results in an increase in the velocity.

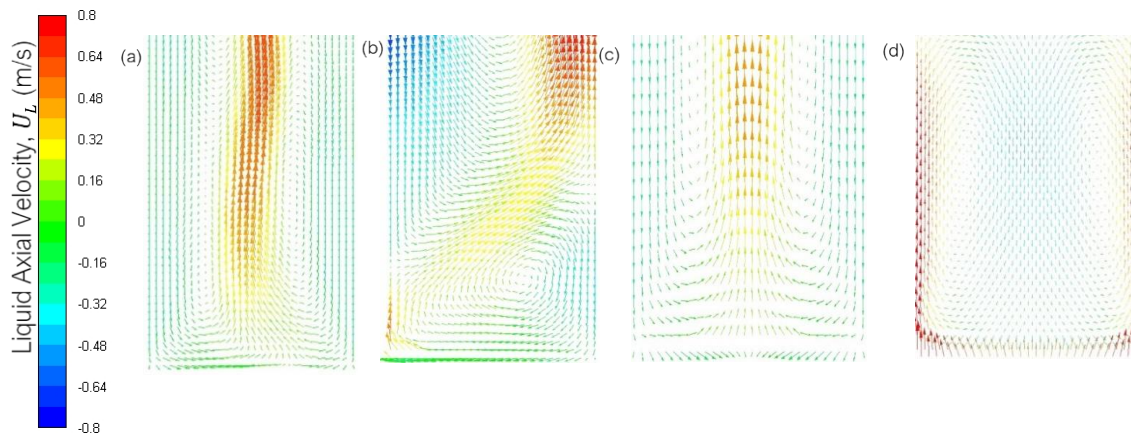


Figure 3.18. Influence of turbulent dispersion models on direction of liquid flow near the disengagement zone

(a) Without the TDF model, (b) Burns et al. TDF model with $C_{TD}=0.1$, (c) Simonin et al. TDF model with $C_{TD}=0.1$ and (d) Simonin et al. TDF model with $C_{TD}=0.5$

In the bulk region, the liquid stream rises in the central region and the profile is skewed when the turbulence dispersion model is not used, as shown in Figure 3.19. The maximum upward velocity in the central region is 0.68 m/s and the liquid recirculation occurs. The minimum velocity in the downward direction is 0.38 m/s, which is close to the wall region. When utilizing the turbulent dispersion model proposed by Burns *et al.* (2004), larger recirculation is observed in the central region. This has led to a maximum velocity of 0.6 m/s in the upward direction close to the right wall and a maximum velocity of 0.63 m/s in the downward direction close to the left wall. When employing the turbulent dispersion model by Simonin *et al.*,1(990), the flow pattern is identical to that observed in experiments. When a coefficient of turbulent dispersion of 0.1 is employed, the maximum upward velocity is 0.47 m/s in the central region and the maximum downward velocity is 0.26 m/s in the downward direction. If the coefficient of turbulent dispersion is increased

to 0.5, the maximum upward velocity in the central region decreases to 0.28 m/s and the maximum downward velocity in the wall region increases to 0.43 m/s.

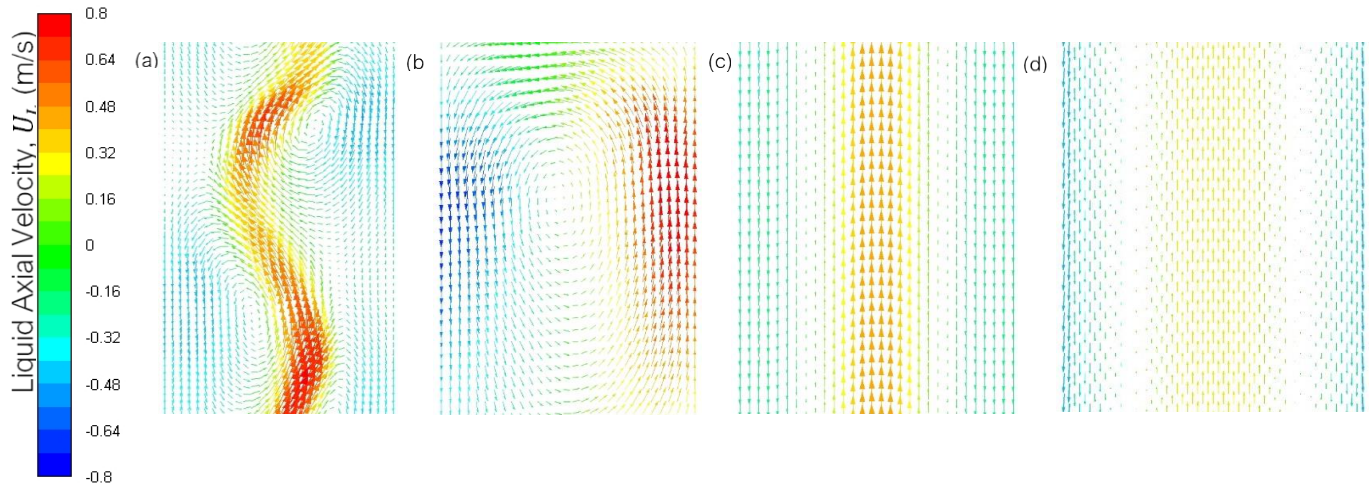


Figure 3.19 . Influence of turbulent dispersion models on direction of liquid flow near the disengagement zone

(a) Without the TDF model, (b) Burns *et al.* TDF model with $C_{TD}=0.1$, (c) Simonin *et al.* TDF model with $C_{TD}=0.1$ and (d) Simonin *et al.* TDF model with $C_{TD}=0.5$

When the TDF is neglected, the funneling flow pattern in the disengagement zone can be seen from Figure 3.20, which is quite close to the experimental observations. When the TDF is neglected, the liquid upward flow region is narrow and the maximum upward velocity is 0.7 m/s in the central region of the column. The maximum downward velocity is 0.38 m/s in the region close to the wall. Smaller liquid circulation occurs in the central region of the column. When the TDF model by Burns *et al.* (2004) is employed, the funneling flow pattern is not very prominent and the liquid is more dispersed. In this case, a maximum upward velocity of 0.38 m/s and a maximum downwards velocity of 0.36 m/s are seen in the central region and the wall region, respectively. When the TDF model

proposed by Simonin *et al.* (1990) with $C_{TD}=0.1$ is used, the liquid upward flow is concentrated in the central region and a maximum upward velocity of 0.42 m/s is noticed. Near the wall region, a maximum downward velocity is 0.40 m/s. Strong liquid recirculation occurs in the bulk of the column, which is an indication of an improvement in the liquid mixing. If the coefficient of turbulent dispersion is increased to 0.5, the maximum upward velocity in the central region decreases to 0.34 m/s and the maximum downward velocity in the wall region increases to 0.5 m/s. Strong liquid recirculation is prominent when the coefficient of turbulent dispersion is increased from 0.1 to 0.5.

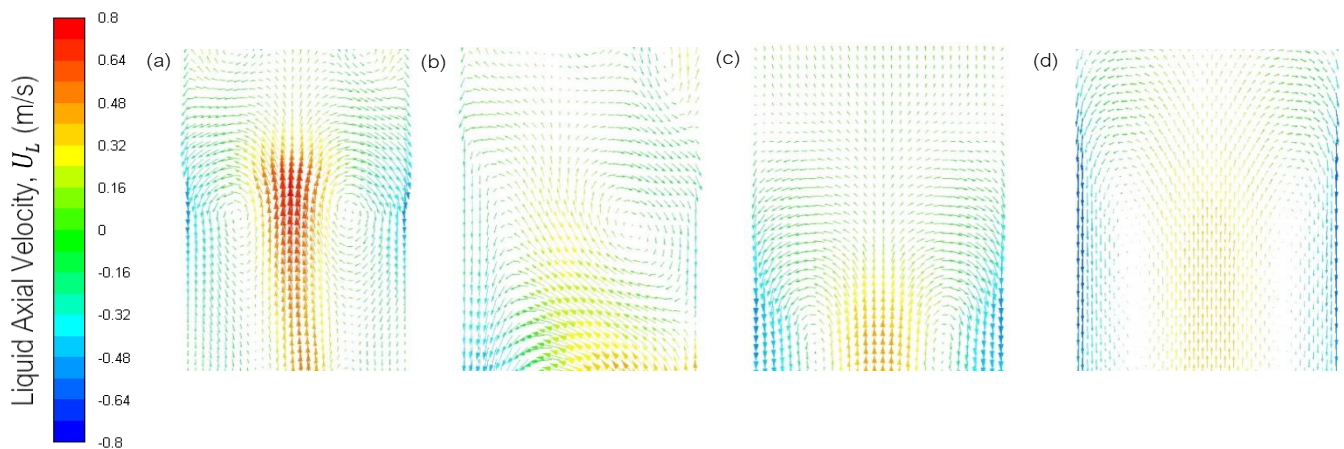


Figure 3.20 Influence of turbulent dispersion models on direction of liquid flow near the disengagement zone (a) No turbulent dispersion model (b) Burns et al. ($C_{TD}=0.1$) (c) Simonin et al. ($C_{TD}=0.1$) (d) Simonin et al. ($C_{TD}=0.5$)

3.5.1.4 Influence of the drag force model

The sensitivity of the bubble column hydrodynamic modelling on the drag models used has been carefully analyzed and compared in Figure 3.21. The suitability of four types of drag

models proposed in literatures have been tested: Schiller (1933), Tomiyama (1998), Ishii and Zuber (1979), and Grace et al. (1976). The drag models have a significant effect on the local gas holdup profiles. Out of all the drag models, the Schiller and Naumann drag model results in a good agreement for the local gas holdup with the experimental data of Hills (1974) and Rampure *et al.* (2007). Tomiyama drag model yields much higher gas holdup than the experimental results. Guan and Yang (2017) reported that the Tomiyama drag model overestimates the gas holdup and the Schiller and Naumann drag model underestimates it. The findings made by Guan and Yang (2017) about Tomiyama drag model are to the same as the findings of this study. However, the gas holdup from the Schiller and Naumann drag model agrees well with the experimental data in the bulk of the column. But, in the column center, the Schiller and Naumann drag model underpredicts the gas holdup by about 11%. Additionally, in the central region ($r/R=0$), the gas holdups using Ishii-Zuber, Grace et al. and Tomiyama drag models are overpredicted the gas holdups by 7%, 25% and 30% respectively. Near the column wall ($r/R=1$), all the drag models excluding Tomiyama model have predicted the holdups well compared with the experimental data.

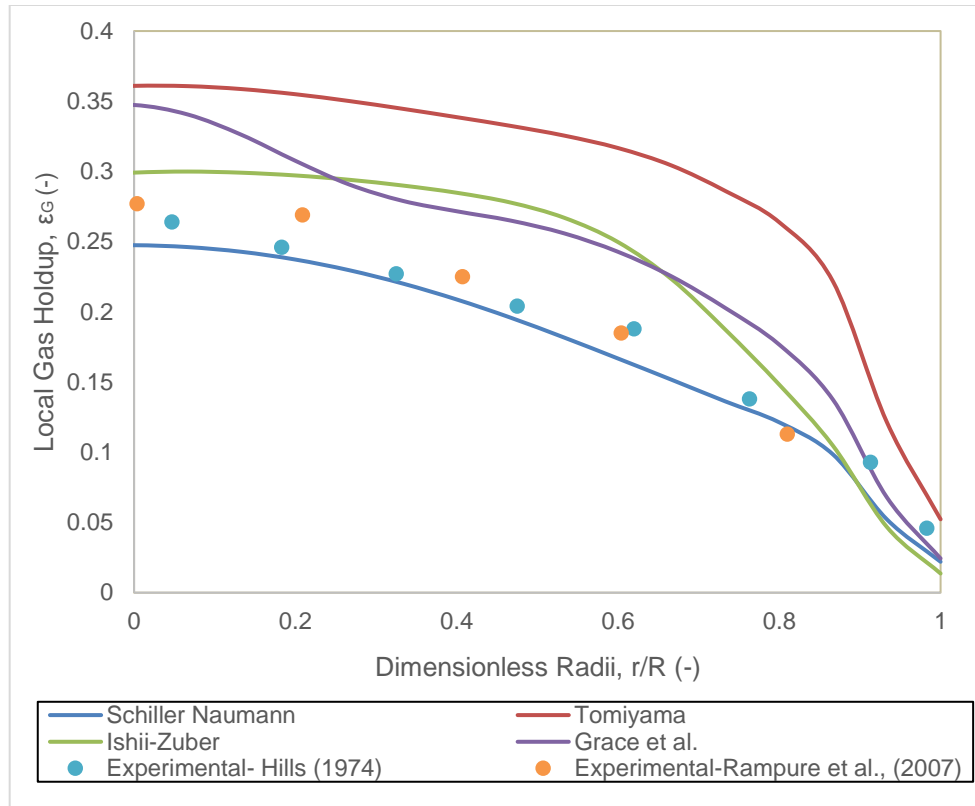


Figure 3.21 Comparison of gas holdup profiles using different drag models with the experimental data in the transition regime ($U_G=10$ cm/s)

The overall gas holdups, which is the averaged gas holdup in the column, using different drag models are shown in Figure 3.22. The overall gas holdup obtained using the Schiller and Naumann drag model is close to the experimental values reported by Li and Prakash (2000) and Jhawar and Prakash (2014). Subsequently, the overall gas holdup obtained using the Ishii and Zuber drag model is close to the experimental values reported by Forret *et al.* (2006) and Chaumat *et al.* (2006). However, the Grace *et al.* and Tomiyama models overestimate the overall gas holdups.

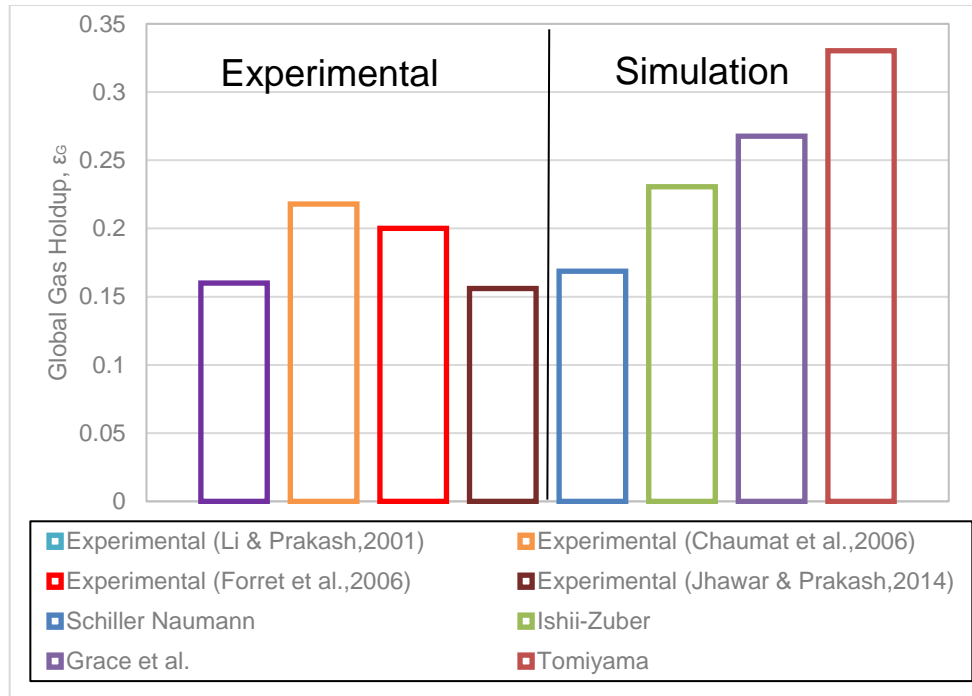


Figure 3.22 Influence of drag model formulation on global gas holdup profiles in the transition regime ($U_G=10$ cm/s)

The liquid axial velocity profiles, illustrated in Figure 3.23, predicted using all the drag models are close to each other. All the drag models are able to predict the centerline liquid velocities (at $r/R=0$) and velocities close to the central region well compared with the experimental data. However, away from the central region, the drag models have overpredicted the magnitude of the liquid axial velocity. This could be attributed to the effect of the TDF, which affects for the gas dispersion in the column.

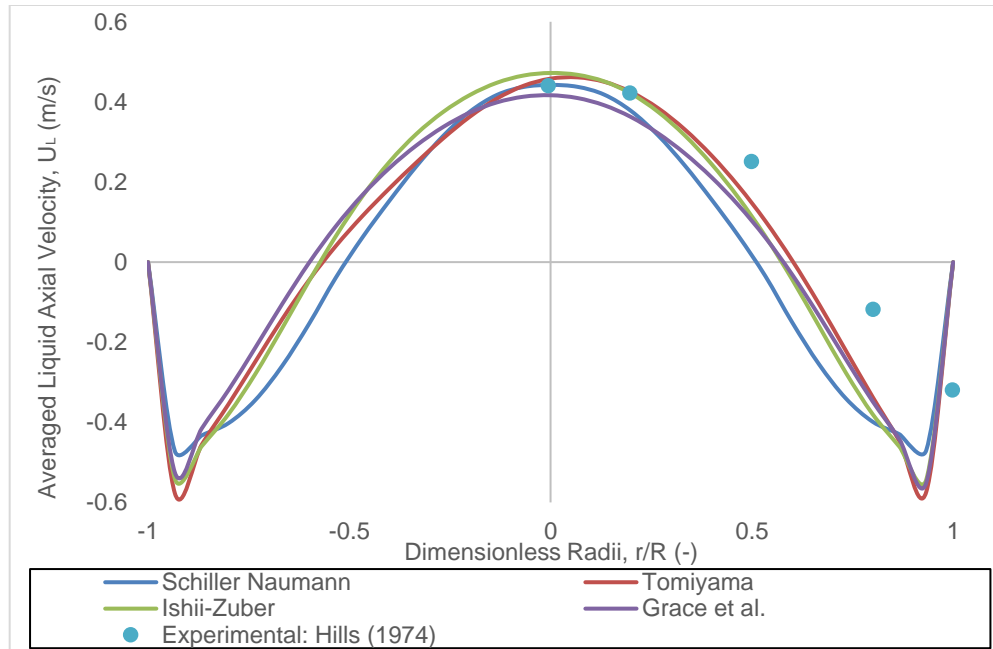


Figure 3.23 Comparison of the liquid axial velocity profiles using different drag models with the experimental data in the transition regime ($U_G=10$ cm/s)

In order to understand the effect of drag models on the prediction of the gas holdup, the gas holdup contours using different drag models are shown in Figure 3.24. The Schiller and Naumann drag model gives a maximum gas holdup of 0.25 in the central region of the column. There is a significant decrease in the gas holdup from the central region to the wall, which is in accordance to the experimental observations. With the exception of the Tomiyama drag model, the gas holdup distribution is almost uniform between the distributor region ($z/D_c=0$) and the disengagement zone ($z/D_c=9.33$). Compared to other drag models, the drag model proposed by Tomiyama gives higher gas holdup in the distributor region. It is also noticed that the Tomiyama model gives a higher dynamic height than other models, which leads to a higher overall gas holdup. The results from the drag models by Ishii-Zuber, Grace et al., and Tomiyama show that the bubble plume near

the distributor region is concentrated in the central region and the plume spreads out to the bulk of the column along the axial direction.

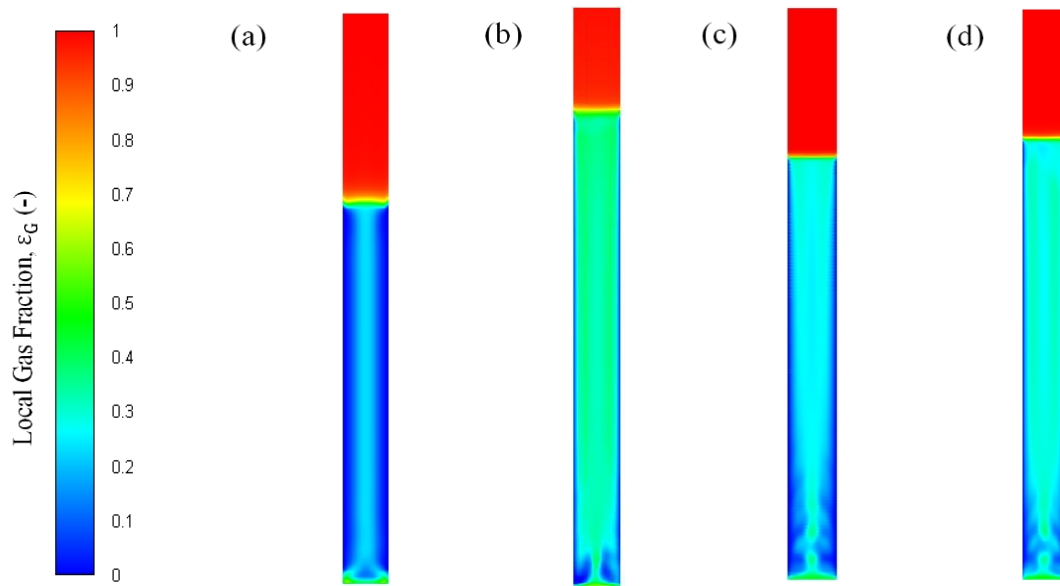


Figure 3.24 Contours of gas holdups using different drag models

(a) Schiller-Naumann (b) Tomiyama (c) Ishii-Zuber (d) Grace et al.

It can be seen from the liquid axial velocity contours using different drag models, as shown in Figure 3.25, that the maximum velocity is at the central region and minimum velocity is at the near wall region from all drag models, which is in accordance with the experimental observations. When the Schiller and Naumann drag model is used, the maximum Z-velocity (axial direction) of 0.44 m/s is in the central region at $z/D_c=9.33$. The maximum Y-velocities from the Tomiyama, Ishii-Zuber and Grace et al. models are 0.6 m/s, 0.52 m/s and 0.50 m/s at axial positions of $z/D_c=1.33$, $z/D_c=3.66$, and $z/D_c=2.33$, respectively. The liquid axial velocity by the Schiller and Naumann drag model is in a close agreement with the experimental trend. The higher liquid velocity near the distributor region of the column is due to the bubbles arising from the sparger.

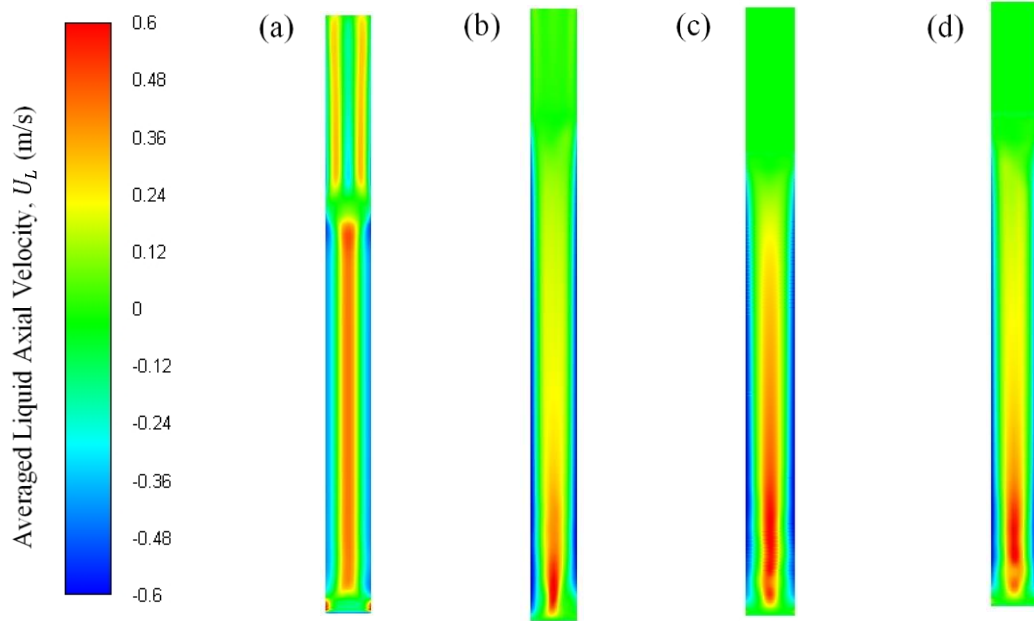


Figure 3.25 Contours of the liquid axial velocities from different drag models

(a) Schiller-Naumann (b) Tomiyama (c) Ishii-Zuber (d) Grace et al.

3.5.2 Reactor hydrodynamics, flow patterns and turbulence parameters variation with the flow regime transition

In this study, the discrete population balance model (PBM) is used to carry out the two-phase numerical simulations in a hollow bubble column reactor. The simulations are carried out in bubbly flow regime, transition regimes and churn-turbulent regimes at superficial gas velocities of 0.04 m/s, 0.10 m/s and 0.30 m/s, respectively. For the study on the flow regime transition, the interfacial force models used in this study are listed in Table 3.6. The Reynolds Stress Model (RSM) turbulence model with the dispersed formulation is used in the current study. The details about the PBM model such as number of bins, bin sizes and the choice of kernels is outlined in Table 3.7.

Table 3.6 Interfacial force models used for the study on the flow regime transition

Interfacial force type	Model	Coefficients
Added mass	Constant	$C_{VM} = 0.5$ (spherical bubbles)
Drag	Schiller-Naumann	$C_d = \begin{cases} \frac{24 (1 + 0.15 N_{Re}^{0.687})}{N_{Re}}, & N_{Re} \leq 1000 \\ 0.24, & N_{Re} > 1000 \end{cases}$
Lift	Constant	$C_L = -0.02$
Wall lubrication	None	
Turbulent dispersion	Simonin	$C_{TD} = 0.1$
Turbulence interaction	Troshko-Hassan	$C_{ke} = 0.75$ and $C_{TD} = 0.45$
Interfacial area	ia-particle	

Table 3.7 PBM details for the study on the flow regime transition

PBM Parameters	Model/Input Value
Method	Discrete
Number of bins	13
Ratio exponent	1.3
Minimum diameter	1 mm
Maximum diameter	36.75 mm
Aggregation kernel	Luo-model
Breakage kernel	Luo-model
Formulation	Ramakrishna

Bin Sizes	Bin Number	Bin Size (m)
	Bin-0	0.0367
	Bin-1	0.0272
	Bin-2	0.0202
	Bin-3	0.0149
	Bin-4	0.0111
	Bin-5	0.0082
	Bin-6	0.0061
	Bin-7	0.0045
	Bin-8	0.0033
	Bin-9	0.0024
	Bin-10	0.0018
	Bin-11	0.0013
	Bin-12	0.0010

Figure 3.26 shows the radial profiles of the liquid axial velocities under the superficial gas velocities of 0.04, 0.1, and 0.30 m/s, which represent the bubbly, transition, and churn turbulent regimes, respectively. The liquid axial velocities in the churn turbulent regime ($U_G=0.1$ m/s) agree well with experimental results from Hills (1974) and Sanyal *et al.*, (1999). Figure 3.27 provides a comparison for the centerline liquid velocities between the simulation results and experimental data. The centerline liquid velocity is a key that affects the liquid circulation within bubble columns (Wu *et al.*, 2001; Forret *et al.*, 2006; George *et al.*, 2017). At a lower superficial gas velocity of 0.04 m/s, the centerline liquid velocity is 0.25 m/s and the flow inversion takes place at $r/R=0.67$. The centerline liquid velocity attained under $U_G = 0.04$ m/s is close to the experimental value obtained by Degaleesan *et*

al. (2001) using a perforated plate with 121 holes. Other experimental values of centerline liquid velocities are in less proximity to the simulation results at the low velocity. The reason could be attributed to the sparger design and the measurement techniques employed. At lower superficial gas velocities, the number of perforations in the sparger is an important parameter that determines the bubble size distribution within the reactor. If coarse spargers are used, bubbles with large diameters could travel through the central region of the column thereby increasing the centerline liquid velocity.

In the transition regime ($U_G=0.1$ m/s), the flow inversion takes place at $r/R=0.67$ and the centerline liquid velocity is 0.44 m/s, which agrees with experimental data by Degaleesan (1998) and Jhawar and Prakash (2014) where the column diameters of 0.14 m and 0.15 m are close to the numerical setup used in this study. However, the experimental data from Menzel *et al.* (1990) could be considered as experimental outliers as their liquid velocity was extremely high. The column employed had a diameter of 0.6 m, which could be one of the reasons for higher discrepancy.

In the churn turbulent regime ($U_G=0.3$ m/s), the centerline liquid velocity is 0.69 m/s, which agrees with that from Jhawar and Prakash (2014), where the experimental value is 0.696 m/s. The flow inversion takes place at $r/R=0.6$. Since not many studies have been carried out in the churn turbulent regime, this was the only comparison that could be made.

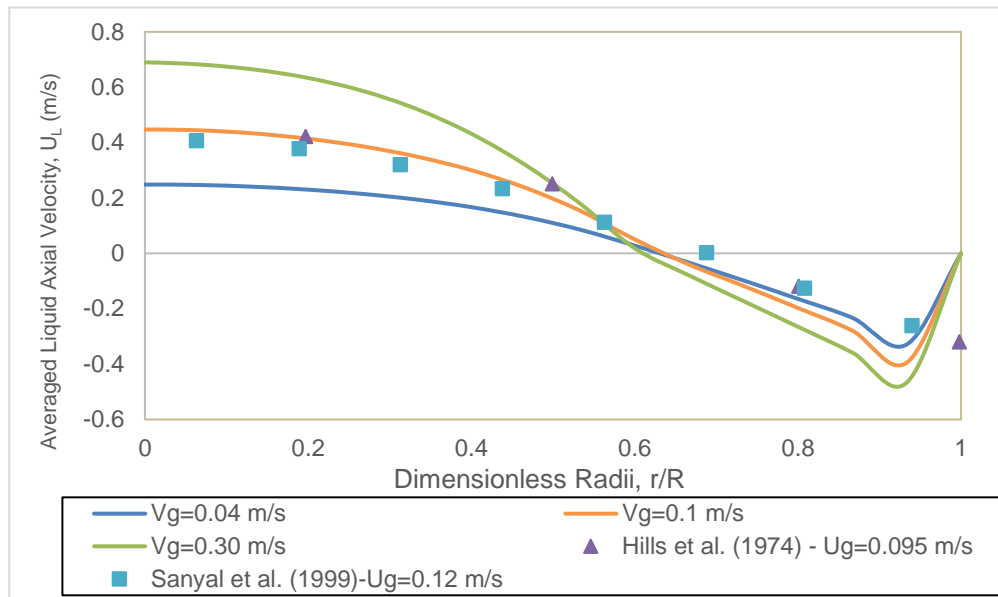


Figure 3.26 Comparison of time-averaged liquid axial velocity profiles with the experimental data in three different transition regimes

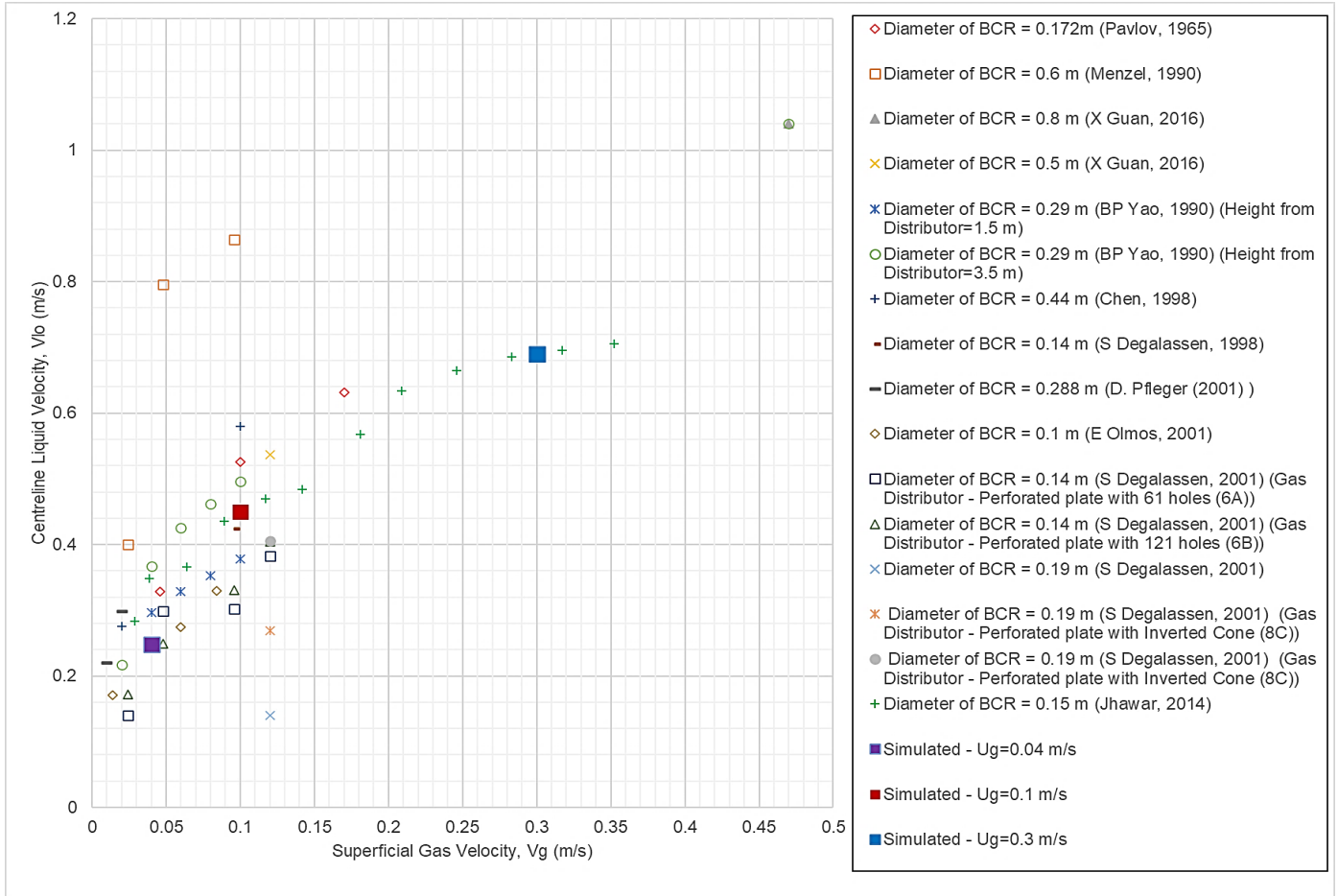


Figure 3.27. Comparison of numerical values of centerline liquid axial velocities at various superficial gas velocities with the experimental data

Figure 3.28 illustrates a comparison of the radial profiles of gas holdups under superficial gas velocities of 0.04, 0.10 and 0.30 m/s, respectively. At a superficial gas velocity of 0.04 m/s, a maximum gas holdup is 0.146 in the central region of the column and the gas holdup decreases along the radial direction from the center to the wall, which is in a close agreement with the experimental data from Hills (1974) and Rampure *et al.* (2007). Near the wall region, the gas holdup decreases more rapidly as compared to the experimental data from Hills (1974) and dual-tip probe study by Rampure *et al.* (2007). The reason could be attributed to the presence of asymmetric liquid around the gas bubbles due to which the

bubble is forced to move into the central region of the column leading to lower gas holdups in the vicinity of column walls (Tao *et al.*, 2019). This force is termed as the wall lubrication force, which is not considered in the current study due to longer simulation time and inadequate data in the literature. The predicted profile of gas holdup does not agree well with the experimental data from Chaumat *et al.* (2006) and Rampure *et al.* (2007) using a single tip probe. The study conducted by Chaumat *et al.* (2006) employed a double optic probe to measure the gas holdup along the radial locations and on the other hand, Rampure *et al.* (2007) used a single-tip conductivity probe inclined at an angle of 40°. The difference these experimental from the other experimental data could be due to various reasons like probe orientation, type of probe used, number of probes in consideration, height of measurement and averaging techniques.

At a superficial gas velocity of 0.10 m/s, a maximum holdup of 0.243 is noted in the central region of the column and the gas holdup decreases along the radial direction from the center to the wall. The gas holdup in the bulk region of the column agrees well with the experimental data from Hills (1974) and Rampure *et al.* (2007) at superficial gas velocities of 0.096 m/s and 0.10 m/s, respectively. However, near the wall region, the radial gas holdup is underpredicted due to the lack of wall lubrication effect as seen in the earlier case. In the churn-turbulent regime ($U_G=0.30$ m/s), the radial gas holdup in the central region is 0.34. The gas holdups at high velocities are not compared to any experimental data due to lack the experimental data in the existing literature.

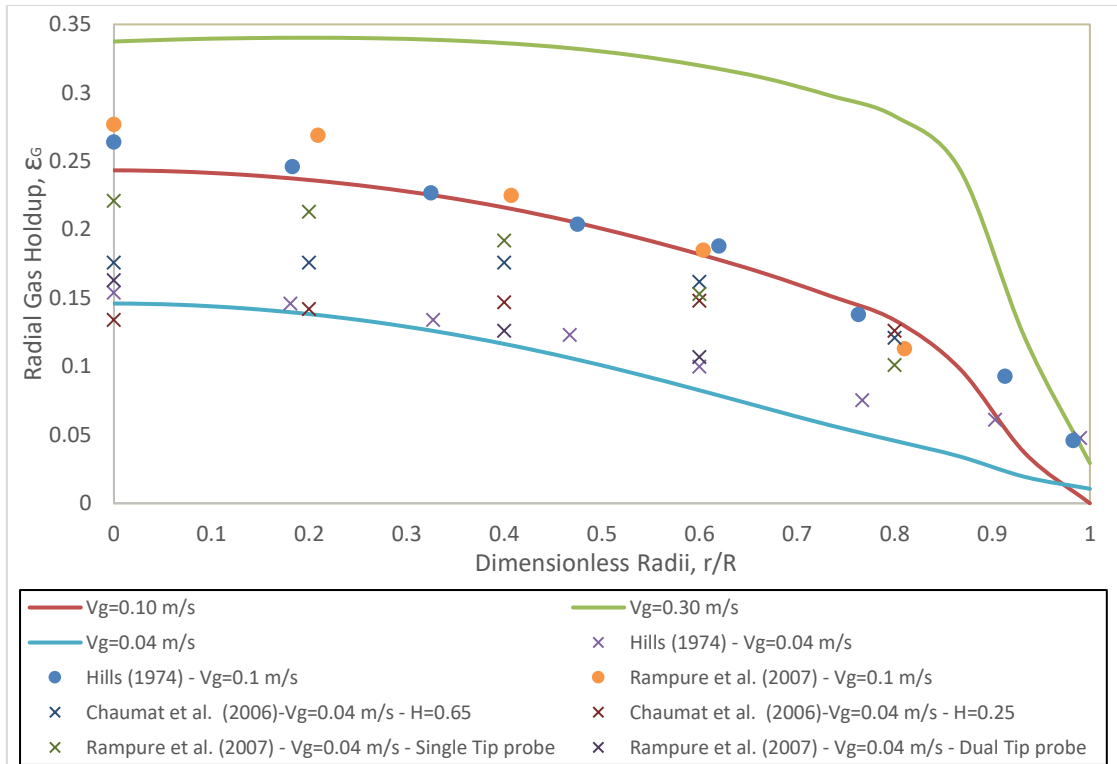


Figure 3.28 Comparison of time-averaged gas holdup profiles along the radial direction in various transition regimes with experimental data

Figure 3.29 demonstrates a comparison of the overall gas holdups between the numerical results and experimental data. As expected, the overall gas holdup increases with the increase in the superficial gas velocity. At a lower superficial gas velocity of 0.04 m/s, the overall gas holdup is close to that attained by Jhawar and Prakash (2014) and it is lower than those from Rampure *et al.* (2007), Forret *et al.* (2006), Chaumat *et al.* (2006) and Yao *et al.* (1991). At lower superficial gas velocities, the gas distributor design has strong effect on the overall gas holdup. If distributors with fine perforations of about 1 mm are employed, bubbles with smaller diameter are generated which leads to higher gas holdup (Luo *et al.*, 1999; Krishna and Sie, 2000; Forret *et al.*, 2006). Rampure *et al.* (2007), Chaumat *et al.* (2006) and Yao *et al.* (1991) used gas distributors with perforation diameters

of 1.2 mm (Rampure *et al.*, 2007), 0.5 mm (Chaumat *et al.*, 2006) and 0.2 mm (Yao *et al.*, 1991), respectively, which contributes to high values of the overall gas holdups. In the transition regime ($U_G=0.10$ m/s), the overall gas holdups agree well with those reported by Jhawar and Prakash (2014), Menzel *et al.* (1990), Hills (1974) and Forret *et al.* (2006) . However, the overall gas holdups are different from those obtained by Chaumat *et al.* (2006), Rampure *et al.* (2007) and Yu and Kim (1991). The lower overall gas holdup from Yu and Kim (1991) could be linked to the continuous mode of operation in which the gas and liquid phases flows in a concurrent fashion into the column, thereby reducing the gas holdup (Wachi *et al.*, 1987; Kantarci *et al.*, 2005). At superficial gas velocity of 0.3 m/s, a good agreement is noticed between the numerical results and all the experimental data. At higher velocities, the gas holdups become independent of column diameter and sparger configuration (Vatai and Tekić, 1989; Wilkinson *et al.*, 1992; Forret *et al.*, 2003; Kanaris *et al.*, 2018).

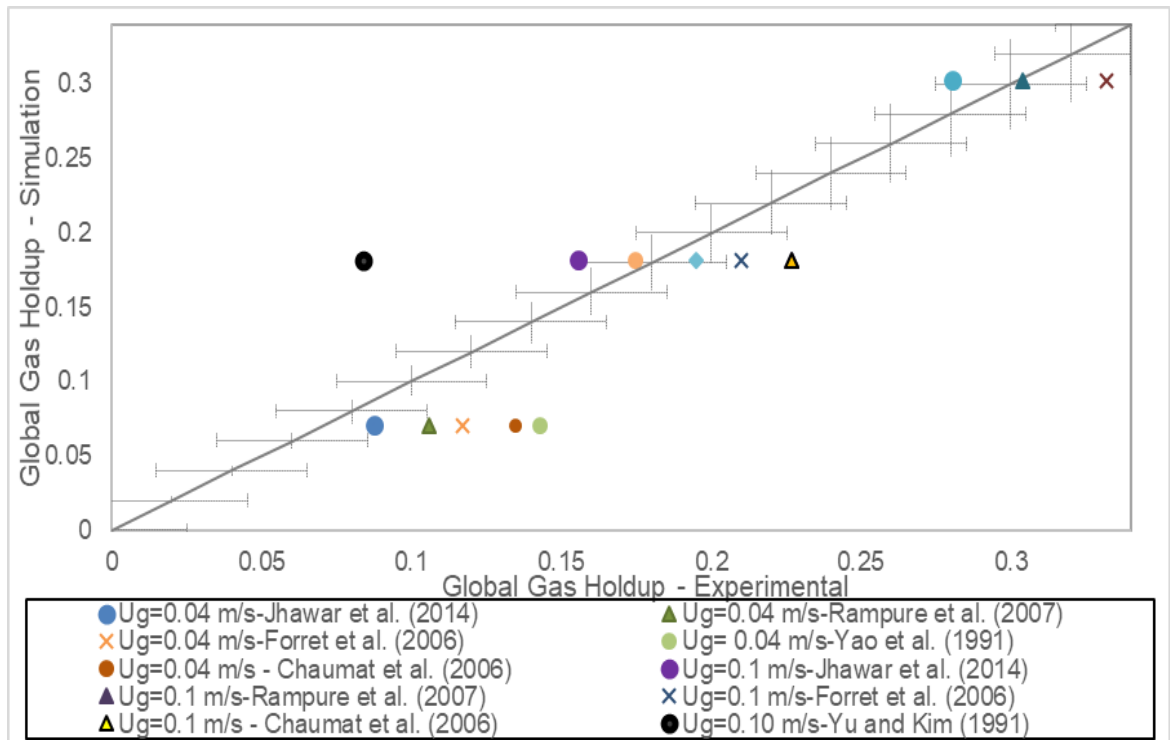


Figure 3.29 Comparison of the overall gas holdups under various superficial gas velocities with experimental data

The structure of turbulence can be measured by the strength of turbulent eddies (Besagni *et al.*, 2018). When eddies are generated as a result of initial flow, they are of large scale and comprise of high kinetic energy, which are eventually decomposed to smaller scale eddies (Okada *et al.*, 1993). Turbulent viscosity ratio is directly proportional to the Reynolds number in the turbulent regime and is defined as the ratio between turbulent viscosity and the dynamic viscosity (ANSYS, 2013). Figures 3.30 and 3.31 illustrate the effect of the superficial gas velocity on radial profile of the turbulent viscosity ratio and contour of the turbulent viscosity ratio, respectively. Clearly, the turbulent viscosity ratio increases with increase in the superficial gas velocity and it is high in the central region and decreases from the central region towards the wall region. The maximum turbulent

viscosity ratios under the superficial gas velocities of 0.04, 0.10 and 0.30 m/s are 1933, 3605 and 6600, respectively. The minimum turbulent viscosity ratios under the superficial gas velocities of 0.04, 0.10 and 0.30 m/s are 20, 32 and 50, respectively.

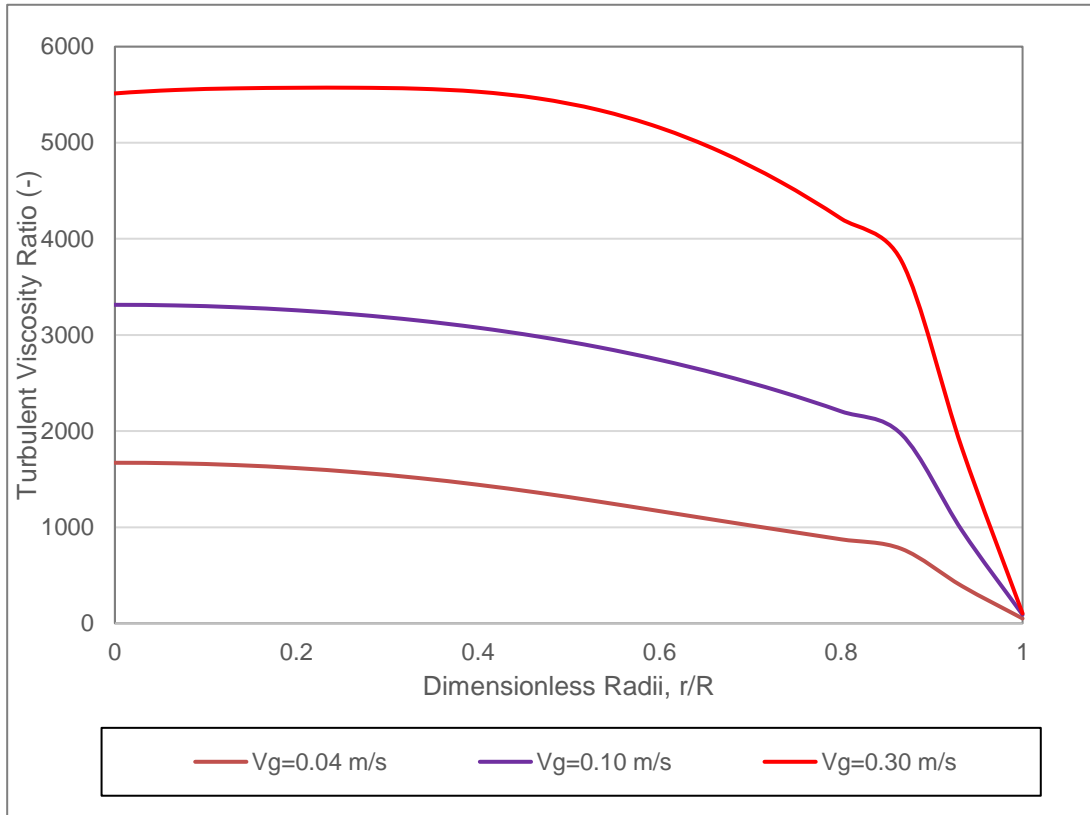


Figure 3.30 Turbulent viscosity ratio profiles along the radial direction under different superficial gas velocities

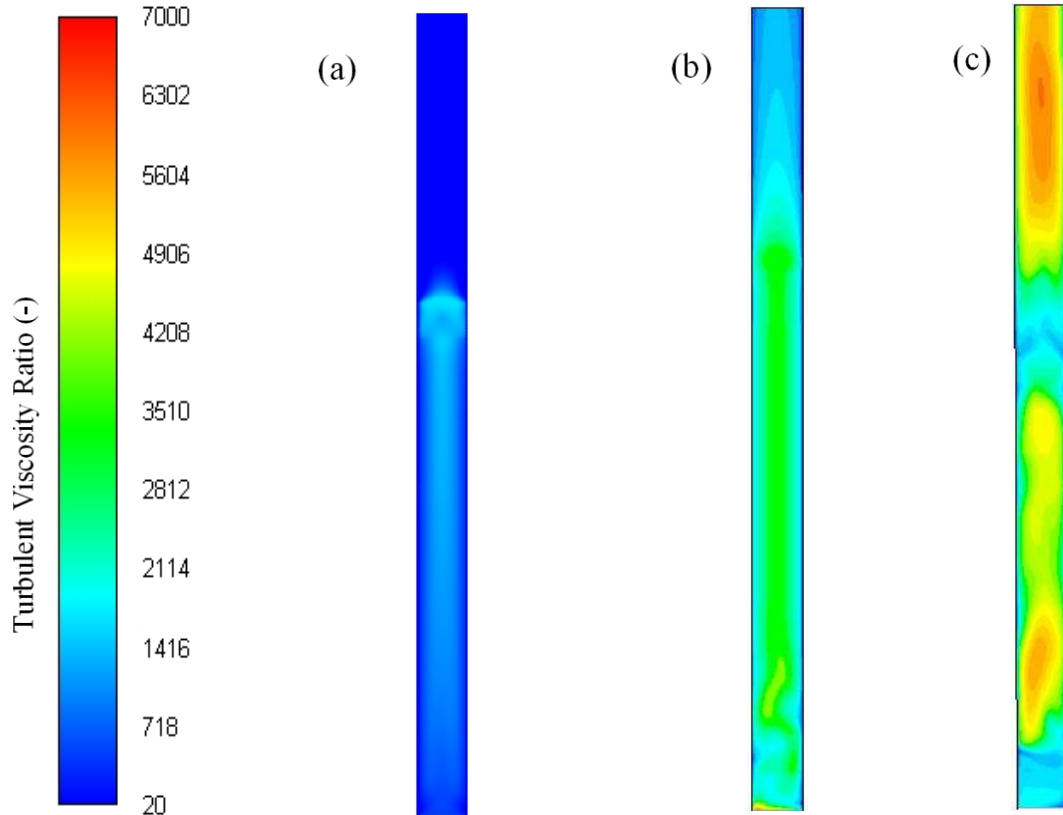


Figure 3.31 . Contours of averaged turbulent viscosity ratios under different superficial gas velocities

(a) $U_G=0.04$ m/s, (b) $U_G=0.10$ m/s and (c) $U_G=0.3$ m/s

The plots of bubble size fraction based on discrete number densities of bubbles in the bubbly, transition and churn turbulent regimes are illustrated in Figure 3.32. In the bubbly flow regime, the number density of small bubbles with chord lengths between 1 mm and 2 mm increase rapidly. The number density of 2 mm bubbles is predominantly high in the bubbly flow regime when compared to the other two regimes. This agrees with the trends noticed in experimental observations. At the superficial gas velocity of 0.04 m/s, the number density of bubbles greater than 2 mm decreases and minimal number of bubbles with chord lengths higher than 10 mm have been noticed. Consecutively, in the other

regimes, the highest peak is noticed at 2 mm bubble size followed by a decrease in the number density of larger bubbles. It is noted that, the number densities of large bubbles with chord lengths greater than 10 mm, increase with the increase in the superficial gas velocity.

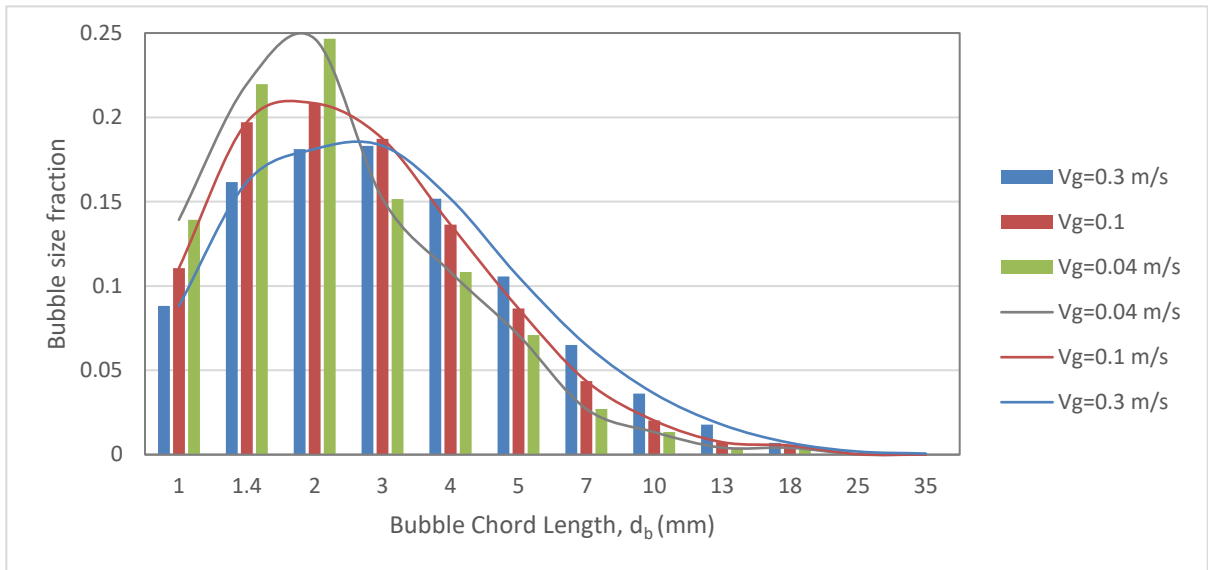


Figure 3.32 Bubble size fraction distribution comparison in the bubbly, transition and churn turbulent regime

The vector plots of the liquid axial velocity at the distribution, bulk and disengagement zones for the different flow regimes are presented in Figures 3.33, 3.34 and 3.35, respectively. In the distributor region, recirculation profiles of lower intensity are noticed in the bubbly and transition regimes. However, when increasing the superficial gas velocity, the intensity of recirculation strengthens, which is due to the higher turbulent viscosity ratio as seen earlier. In the bulk region, an upward flow in the central region and downward flow close to the walls can be seen, which conforms to the experimental observation. In the distributor region, the funneling effect is clearly noticed in the bubbly

and transition regimes. Nevertheless, such an effect is not seen in the churn-turbulent regime. Based on these vector plots, a generalized flow map for a hollow bubble column has been developed (Figure 3.36) and a comparison is made with study carried out by Devanathan et al. (1990). In their study, a maximum axial liquid velocity of 0.52 m/s was reported in the central region for a superficial gas velocity of 0.105 m/s. In this study, it is found that a maximum velocity is 0.48 m/s for a superficial gas velocity of 0.10 m/s, which is in line with the experimental observations.

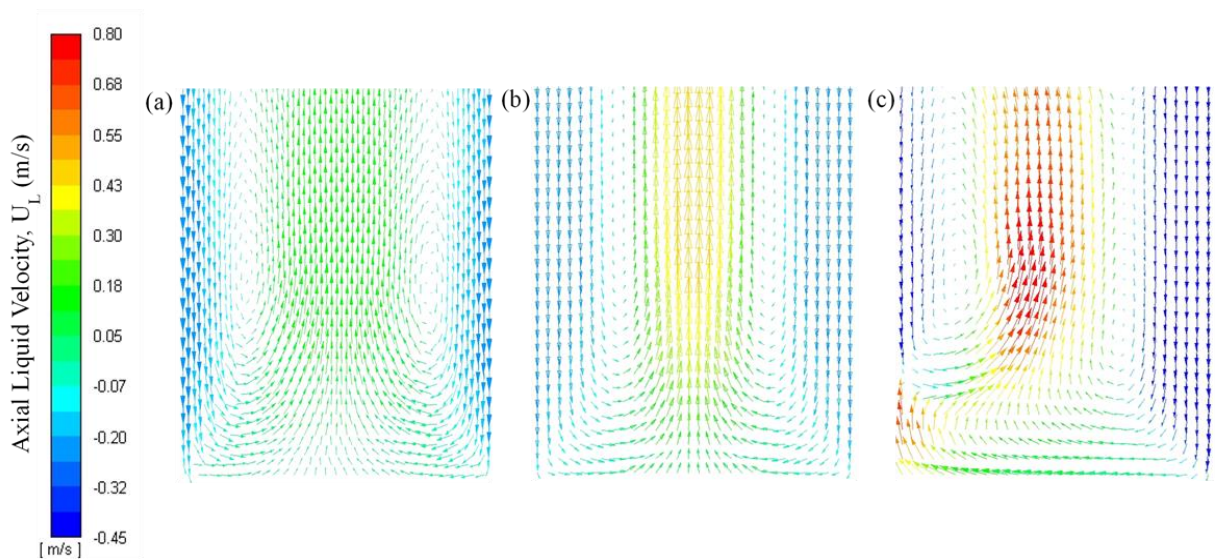


Figure 3.33 Vector contours of the axial liquid velocity in the distributor region at different flow regimes

(a) Bubbly, (b) Transition and (c) Churn-Turbulent

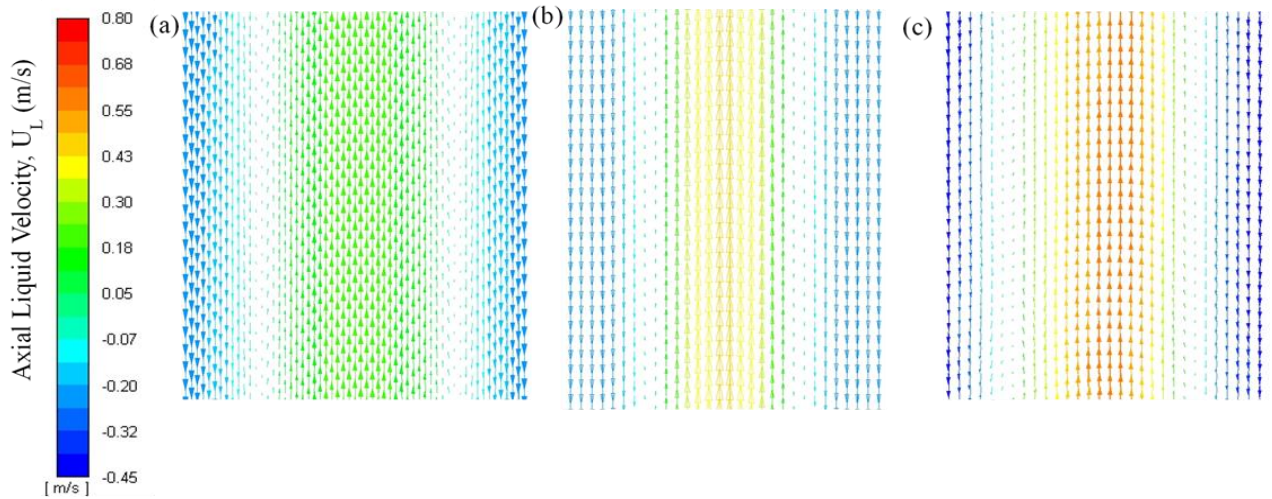


Figure 3.34 Vector contours of the axial liquid velocity in the bulk region at different flow regimes

(a) Bubbly, (b) Transition and (c) Churn-Turbulent

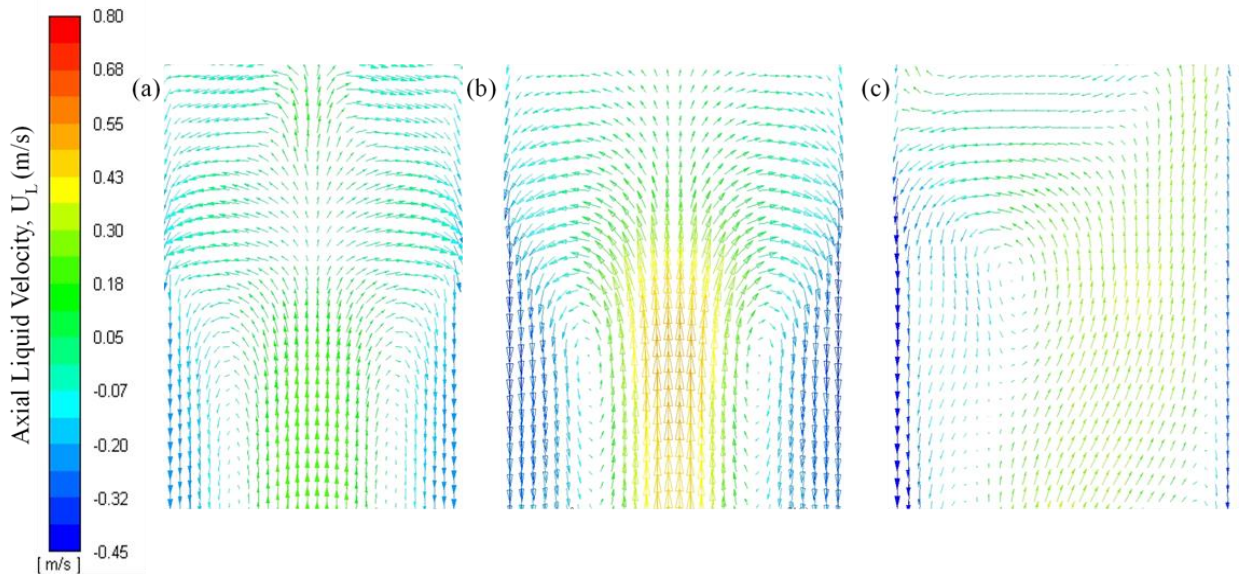


Figure 3.35 Vector contours of axial liquid velocity in the disengagement region at different flow regimes

(a) Bubbly, (b) Transition and (c) Churn-Turbulent

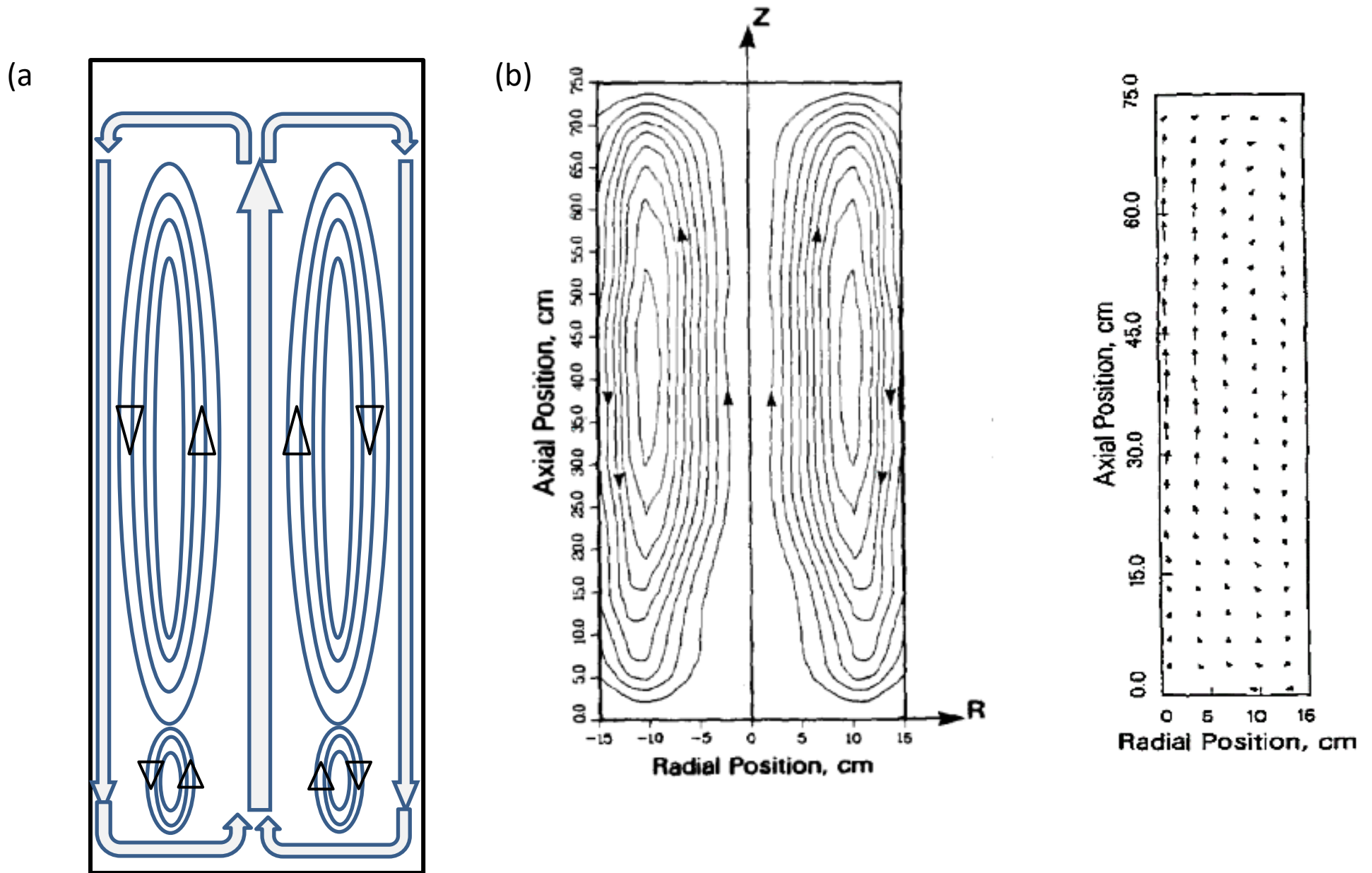


Figure 3.36 Flow mapping of hollow bubble column reactors

(a) Numerical and (b) Experimental (Devanathan et al., 1990)

3.5.3 Comparison of Bubble Breakup and Bubble Coalescence Models

Over the years, many studies have used the Population Balance Model (PBM) in the numerical simulations of bubble column reactors (Chen, Duduković and Sanyal, 2005; Bhole, Joshi and Ramkrishna, 2008; Yang, Guo and Wang, 2017; Sarhan, Naser and Brooks, 2018; Yang *et al.*, 2018; Agahzamin and Pakzad, 2019a; Shi *et al.*, 2019; Shi, J. Yang, *et al.*, 2020). The inclusion of the PBM can provide a better prediction on the bubble size distributions within the reactor. One of the key issues in using the PBM is the reasonable selection of the bubble breakup and coalescence models (Wang and Wang, 2007). In the present work, an effort has been made to understand the effect the bubble breakup and coalescence models on the numerical simulation results. The bubble coalescence model proposed by Luo (1995) is used in the current work. This model was successfully used in the past to model the bubble coalescence within the reactor (Xu *et al.*, 2014; Syed *et al.*, 2017; Zhang and Luo, 2020). Two popular breakup models proposed by Luo and Svendsen (1996) and Lehr *et al.* (2002) are compared in this study. Both the breakup models predict the daughter bubble distribution and breakup rates, the difference, however, lies in the prediction of binary bubble breakup rate. Therefore, simulations are performed using the Luo (1995) coalescence model with Luo (1996) breakup model, which is named as Luo-Luo model, and the Luo (1995) coalescence model with the Lehr (2002) breakup model, which is named as Luo-Lehr model..

In his recent work, Gaurav (2018) used indiscrete (multiple bubble phases) PBM model phase in the simulations to better predict the bubble distribution in a reactor. When the

multiple bubble phase PBM model is employed, the gas phase is divided into several groups based on the bubble sizes. This approach allows us to treat different dispersed phase groups separately, by dividing them into multiple groups based on the bubble size. Population balance equations are solved for each of these groups separately. Krepper *et al.* (2007) employed a polydisperse model based on experimental observations. Bubbles diameters between 1 and 7 mm were assigned as small bubbles and those between 7 to 35 mm were ascribed as large bubbles. Although both the models predicted the trend effectively, it was reported that the results from the multiple bubble phase model were closer to the experimental observations. In the present study, for the comparison purpose, simulations are carried out using both the single and two bubble phase models, where the gas phase is divided into two bubble groups, coupled with Luo-Luo and Luo-Lehr coalescence and breakup models.

The interfacial forces and boundary conditions employed in the current study are provided in Tables 3.8 and 3.9, respectively. The Schiller-Naumann and Tomiyama drag models have been effectively used in the past to model small and large bubbles, respectively (Gaurav, 2018). Therefore, in this study, the Tomiyama drag model is used with the single bubble phase model and the Schiller-Naumann and Tomiyama drag models are employed for small and large bubble groups respectively, when the two bubble phase model is used. For the single bubble phase model, a constant lift force model with a negative lift coefficient is employed. For the two bubble phase model, the lift force for small bubbles is neglected and the constant lift force model with a negative lift coefficient is used for large bubbles. The turbulence dispersion model proposed by Simonin *et al.* (1990) is used in the simulation. In the single bubble phase model, the coefficient of the turbulence dispersion

is assigned as 0.2. For the two bubble phase model, the coefficients of the turbulence dispersion for small and large bubbles are 0.1 and 0.2, respectively. The Sauter mean bubble diameter is assigned for each of the phases.

The parameters used in the single and two bubble phase PBM models are outlined in Tables 3.10 and 3.11, respectively. The PBM formulation proposed by Kumar and Ramkrishna (1996) is used to analyze the bubble size distributions in the column. In the single bubble phase model, the bubble sizes are distributed across 12 bins and in the two bubble phase model, small bubbles and large bubbles are distributed across 6 bins each. The minimum bubble diameter under consideration is 1 mm and maximum bubble size is 40.5 mm. The boundary conditions used in the current work are outlined in Table 3.11.

Table 3.8 Interfacial forces used in the breakup and coalescence model study

Interfacial forces	Dispersed Phase Model	Secondary Phase	Interfacial Force Model
Drag	Single bubble phase (Discrete)	Air	Tomiyama
	Two bubble phase (Indiscrete)	Air1 (Small Bubbles)	Schiller-Naumann
Air2 (Large Bubbles)		Tomiyama	
Virtual Mass	Single bubble phase (Discrete)	Air	Constant ($C_{VM}=0.5$)
	Two bubble phase (Indiscrete)	Air1 (Small Bubbles)	Constant ($C_{VM}=0.5$)
		Air2 (Large Bubbles)	Constant ($C_{VM}=0.5$)
Lift Model	Single bubble phase (Discrete)	Air	Constant ($C_L=-0.1$)

	Two bubble phase (Indiscrete)	Air1 (Small Bubbles)	No Lift force
		Air2 (Large Bubbles)	Constant ($C_L=-0.1$)
Turbulent Dispersion	Single bubble phase	Air	Simonin ($C_{TD}=0.2$)
	Two bubble phase (Indiscrete)	Air1 (Small Bubbles)	Simonin ($C_{TD}=0.1$)
		Air2 (Large Bubbles)	Simonin ($C_{TD}=0.2$)

Table 3.9 Boundary Conditions for the breakup and coalescence model study

Zone	Phase	Parameters
Inlet (Single bubble phase Model)	Water	Velocity= 0 m/s
	Air	Velocity= 0.12 m/s
		Vol Fraction=1
		Bin-3-fraction=0.5
		Bin-6-fraction=0.5
	Rest bin fractions set to zero	
Inlet (Two bubble phase Model)	Water	Velocity= 0 m/s
	Air1	Velocity= 0.12 m/s
		Vol Fraction=0.30
		Bin-1-fraction=0.5
		Bin-2-fraction=0.5
	Rest bin fractions set to zero	
	Air2	Velocity= 0.12 m/s
		Vol Fraction=0.70

	Bin-4-fraction=0.5
	Bin-5-fraction=0.5
	Rest bin fractions set to zero

Outlet	Outflow
--------	---------

Wall	No Slip
------	---------

Table 3.10 Parameters of the single bubble phase PBM model

PBM Parameters	Model/Input Value
Ratio exponent	1.45
Minimum diameter	1 mm
Maximum diameter	40.5 mm
Formulation	Ramakrishna

Bin Sizes						
Bin Number	0	1	2	3	4	5
Bubble Size (m)	0.04046	0.02890	0.02065	0.01475	0.01053	0.00753
Bin Number	6	7	8	9	10	11
Bubble Size (m)	0.00537	0.00384	0.00274	0.00196	0.00140	0.001

Table 3.11 Parameters of two bubble phase PBM model

PBM Parameters	Model/Input Value
Number of bins	12 (6 Bins for air1 (small bubbles) + 6 Bins for air2 (large bubbles))
Ratio exponent	2 (Air1); 1.2 (Air2)
Minimum diameter	1 mm

Maximum diameter	40.5 mm						
Formulation	Ramakrishna						
Bin Sizes							
Air1	Bin Number	0	1	2	3	4	5
	Bubble Size (m)	0.0101	0.00635	0.0040	0.0025	0.0016	0.001
Air2	Bin Number	0	1	2	3	4	5
	Bubble Size (m)	0.0405	0.0332	0.0252	0.0192	0.0145	0.011

A comparison of the gas holdup profiles along the radial direction using the both the single and two bubble phase models with Luo-Luo and Luo-Lehr breakup and coalescence models is provided in Figure 3.37. The result using the single bubble size model where the PBM is not employed and the bubble diameter is assumed as 6 mm is also shown in Figure 3.37 for comparison purpose. The numerical results are validated against the experimental data from Zhang *et al.* (2009) and Sanyal *et al.* (1999), as shown in Figure 3.37. The difference between the experimental data from Zhang *et al.* (2009) and Sanyal *et al.* (1999) could be attributed to different measurement techniques and averaging strategies they employed since Zhang *et al.* (2009) and Sanyal *et al.* (1999) used the conductivity probe and computed tomography (CT) techniques in the measurements of the radial gas holdups. When the PBM is used, the gas holdup profiles along the radial direction have the same trend as the experimental data. When the Luo-Luo model is used in the single and two bubble phase models, the agreement with the experimental data from Zhang *et al.* (2009) is good. However, the gas holdups using Luo-Lehr model for both the single and two bubble phase models are higher. This is attributed to the higher breakup rates noticed in the Luo-Lehr model, leading to an increase in the gas holdup. The gas holdup obtained by using the two bubble phase model with the Luo-Lehr model is close to the experimental data from Sanyal *et al.* (1999). However, when the single bubble size model is employed,

a flat gas holdup profile along the radial direction between $r/R=0$ and $r/R=0.66$ is noticed. Near the wall region, there is a sudden decrease in the gas holdup.

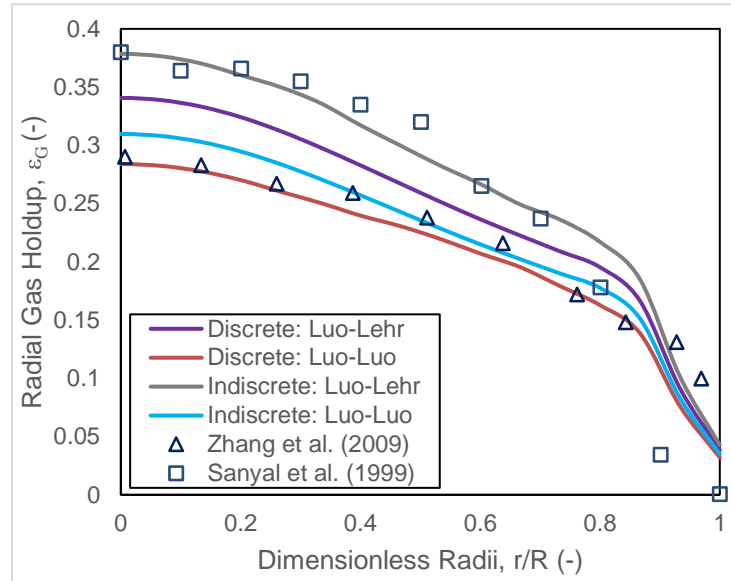


Figure 3.37 Radial gas holdup variation with different PBM models

A comparison of the axial variation of mean Sauter diameter, d_{b32} , using different break-up and coalescence models is presented in Figure 3.38. The data are at $r=0$ between the axial positions of $z=0$ and $z=1$ m. Using the single bubble phase model with the Luo-Luo and Luo-Lehr models, the mean bubble size near the inlet is 9.1 mm and 8.1 mm, respectively. The mean diameter increases slightly along the axial direction and a constant diameter of 15 mm (Luo-Luo model) and 12 mm (Luo-Lehr model) are observed in the fully developed region ($z>0.5$ m). The variations of small bubble mean diameter and large bubble mean diameter from the two bubble phase model are also illustrated in Figure 3.38. The mean bubble diameters obtained by the Luo-Luo and Luo-Lehr models with the two bubble phase model near the inlet are 5.0 mm and 5.2 mm, respectively. The result from the two bubble phase Luo-Luo model shows that there is a very small increase in the size

of small bubbles along the axial direction from the distributor and the mean bubble diameter maintains at 7 mm in the fully developed region. On the other hand, the result from the two bubble phase Luo-Luo model shows that a decrease in the small bubble mean diameter is noticed above the distributor, and a constant diameter of small bubbles is 1.8 mm in the fully developed region. The large bubble mean diameters near the inlet are 12.37 mm and 13.28 mm from Luo-Luo and Luo-Lehr models, respectively. The size of large bubbles from the two bubble phase Luo-Luo model increases steadily along the axial direction and a constant mean large bubble diameter of 19.70 mm is noted in the fully developed region. In contrast, based on the two bubble phase Luo-Lehr model, the size of large bubble increases rapidly along the axial direction above the distributor region and the mean large bubble diameter steadily increases over the entire column. At $z=1$ m, the Sauter diameter noted is 36.09 mm.

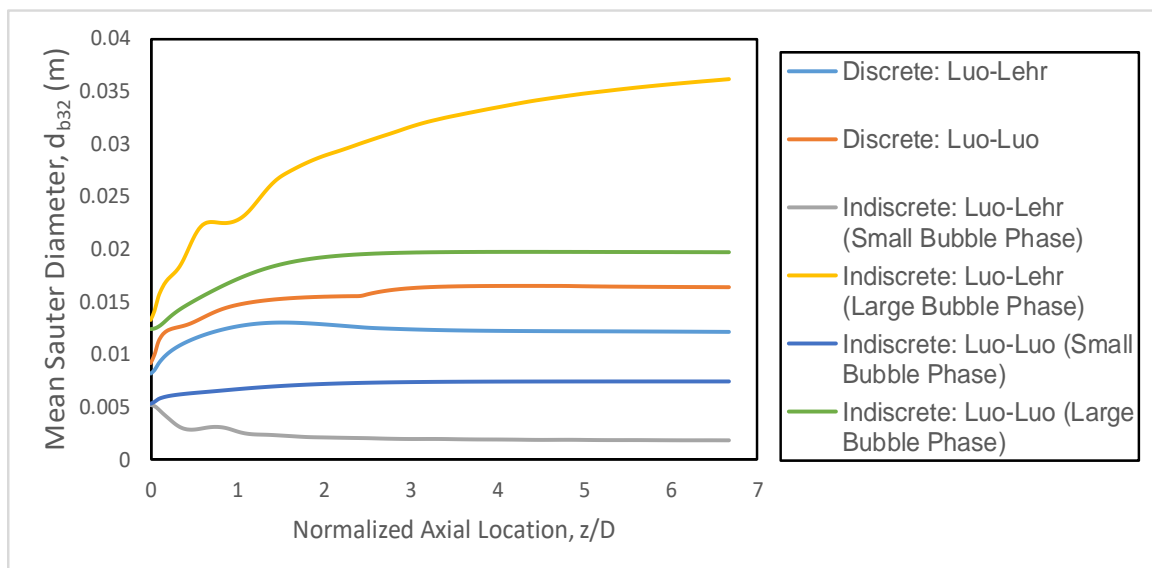


Figure 3.38 Comparison of the variations of the mean Sauter diameter along the axial direction using different PBM models

A comparison of the distribution of the small and large bubble fractions obtained from different break-up and coalescence models is presented in Figure 3.39. The fraction of small bubbles predicted by the Luo-Lehr model for both in the single and two bubble phase modes is higher than that predicted by the Luo-Luo model. This is due to the superior breakup rates imposed by the Lehr breakup model. The presence of large fraction of small bubbles increases the gas holdups, as seen earlier. On the other hand, the results from the Luo-Luo model with both the single and two bubble phase mode exhibit realistic fractional distributions since the Luo-Luo model is able to effectively account for the presence of large bubbles formed due to coalescence. It is evident that the amount of small bubbles ($d_b < 5$ mm) predicted by the two bubble phase model are higher than that predicted by the single bubble phase model. Therefore, the amount of large bubbles ($d_b > 5$ mm) predicted by the single bubble phase model are higher than that from the two bubble phase model.

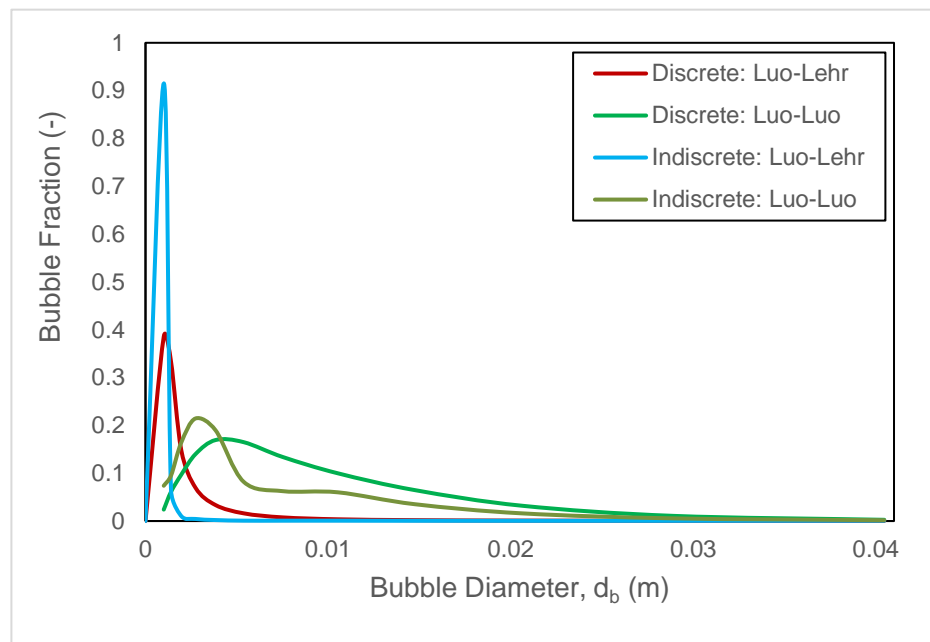


Figure 3.39 Comparison of bubble fraction distributions using different PBM models

3.5.4 Dual Bubble Size Model

The Population Balance Models (PBM) have been used for the past 5 decades, but their application was prevalent after superior computational facilities were developed (Vanni, 2000; Rigopoulos and Jones, 2003; Rigopoulos, 2010). The inclusion of the PBM adds to the overall complexity and should be used in the modelling to solve a pertinent objective (Nopens et al., 2015). Although several attempts have been made to apply Population Balance Equations (PBEs) to multiphase flows, its validation remains an open question due to the cumbersome data collection in the literature. A number of authors have endorsed the inclusion of bubble breakup and coalescence models in bubble column reactor studies. However, only certain processes, such as the mass transfer in bubble columns, strictly require the inclusion of the PBM. The main focus of the current work is to investigate the effectiveness of the two bubble population model approach proposed by Krishna and Ellenberger (1996). This work aims at applying the two bubble population model without the PBM and analyzing the resulting hydrodynamic parameters.

In the heterogenous regime, the bubbles are divided into two groups, small and large bubbles, as shown in Figure 3.40. Small bubbles ($1 \text{ mm} < d_b < 6 \text{ mm}$) are spherical and large bubble ($d_b > 20 \text{ mm}$) are ellipsoidal and spherical cap (Grace and Harrison, 1967; Wegener and Parlange, 1973; Bhaga and Weber, 1981). In the current work, the velocities of small and large bubbles are modelled using the experimental work carried out by Schumpe and Grund (1986). In their study, the contribution of small and large bubble velocities to the gas flow was studied and a correlation between the superficial gas velocity and bubble

velocities (small and large) was obtained as shown in Figure 3.41 using the experimental data of small and large bubble velocities.

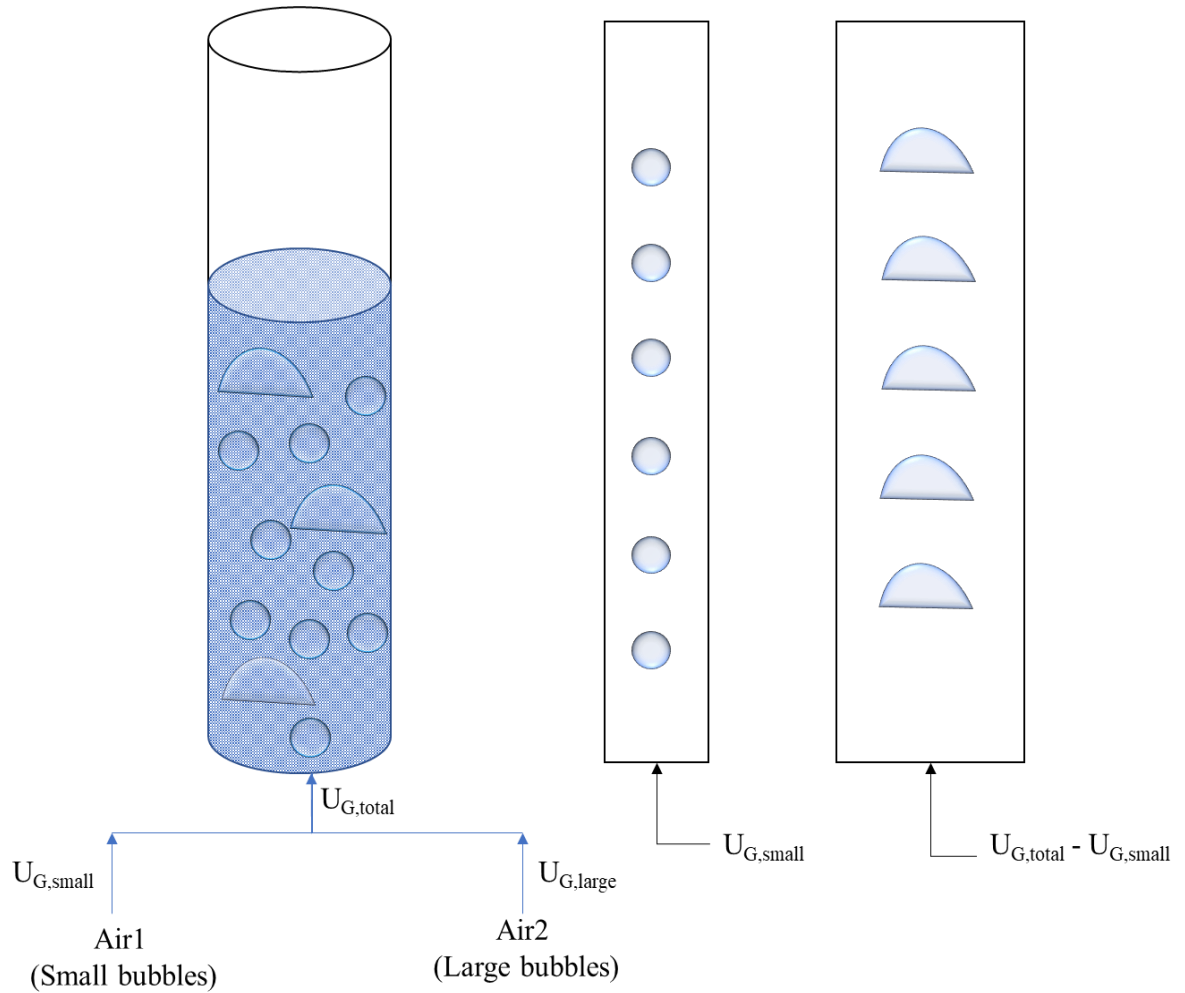


Figure 3.40 Division of bubble phase into small and large bubble phases

(Redrawn from van Baten and Krishna (2003))

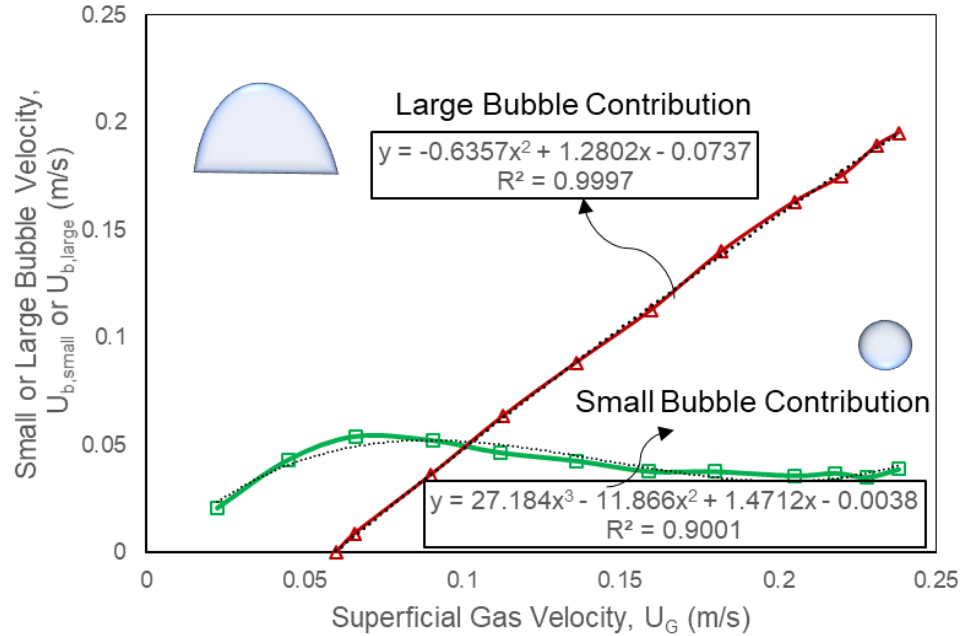


Figure 3.41 Contribution of small and large bubble velocities to the gas flow

(Reproduced from Schumpe and Grund (1986))

The total superficial gas velocity can be described as:

$$U_G = U_{G,small} + U_{G,large} \quad (3.20)$$

where $U_{G,small}$ and $U_{G,large}$ are the velocities associated with small bubbles and large bubbles, respectively. These can be described by the equations obtained based on the experimental data (Schumpe and Grund, 1986):

$$U_{G,small} = 27.184U_G^3 - 11.866U_G^2 + 1.4712U_G - 0.0038 \quad (3.19)$$

$$U_{G,large} = -0.6357U_G^2 + 1.2802U_G - 0.0737 \quad (3.20)$$

The fractions of small and large bubbles at the inlet can be obtained by:

$$\varepsilon_{b,small} = \frac{U_{G,small}}{U_G} \quad (3.21)$$

$$\varepsilon_{b,large} = \frac{U_{G,large}}{U_G} \quad (3.22)$$

The interfacial forces and boundary conditions used for the current analysis are provided in Tables 3.12 and 3.13, respectively. The Schiller-Naumann and Tomiyama drag models are used to model small and large bubble sizes, respectively. Lift force for small bubbles is neglected and a constant lift force model is used for large bubbles. The turbulence dispersion model proposed by Simonin is used in the simulation. The coefficients of the turbulence dispersion for small and large bubbles are 0.1 and 0.2, respectively. Constant bubble diameters are assigned for each bubble phase. In Case A, the diameters of small bubbles and large bubbles are 4 mm and 20 mm, respectively. In Cases B and C, the diameters of small bubbles and large bubbles are 5 mm and 15 mm, respectively. This study is carried out at a superficial gas velocity of $U_G = 12$ cm/s.

Table 3.12 Interfacial forces used for the dual bubble size model

Interfacial forces	Secondary Phase	Interfacial Force Model
Drag	Air1 (Small Bubbles)	Schiller-Naumann
	Air2 (Large Bubbles)	Tomiyama
Virtual Mass	Air1 (Small Bubbles)	Constant ($C_{VM}=0.5$)
	Air2 (Large Bubbles)	Constant ($C_{VM}=0.5$)
Lift force	Air1 (Small Bubbles)	No Lift force
	Air2 (Large Bubbles)	Constant ($C_L=-0.1$)
Turbulence Dispersion	Air1 (Small Bubbles)	Simonin ($C_{TD}=0.1$)
	Air2 (Large Bubbles)	Simonin ($C_{TD}=0.2$)

Table 3.13 Boundary conditions used for the dual bubble size model

Zone	Phase	Parameters
Inlet (Case A)	Water	Velocity= 0 m/s
Diameter of Air1=4 mm	Air1	Velocity= 0.04 m/s
Diameter of Air2=20 mm		Vol Fraction=0.33
	Air2	Velocity= 0.08 m/s
		Vol Fraction=0.67
Inlet (Case B)	Water	Velocity= 0 m/s
Diameter of Air1=5 mm	Air1	Velocity= 0.04 m/s
Diameter of Air2=15 mm		Vol Fraction=0.33
	Air2	Velocity= 0.08 m/s
		Vol Fraction=0.67
Inlet (Case C)	Water	Velocity= 0 m/s
Diameter of Air1=5 mm	Air1	Velocity= 0.05 m/s
Diameter of Air2=15 mm		Vol Fraction=0.41
	Air2	Velocity= 0.07 m/s
		Vol Fraction=0.59
Outlet	Type: Outflow	
Wall	Shear condition: No slip	

The comparison of the liquid axial velocity profiles along the radial direction using the dual bubble size modelling approach with difference bubble sizes is outlined in Figure 3.42. The highest and lowest centerline liquid velocities are in Cases B and A, respectively. The locations of the flow inversion are at $r/R=0.60$ for Cases A and C and at $r/R=0.533$ for Case B. The liquid axial velocities are also compared with the experimental data by Zhang *et al.* (2009) and Sanyal *et al.* (1999). The difference between the experimental results from Zhang *et al.* (2009) and Sanyal *et al.* (1999) could be due to the measurement techniques and averaging strategies employed in their respective studies. Zhang *et al.* (2009) used Pavlov tube technique and Sanyal *et al.* (1999), on the other hand, employed the CARPT

technique to measure the liquid axial velocities, respectively. In Case A, the liquid axial velocity is underpredicted in the central region and is close to the experimental data near the wall region. The liquid axial velocities in the central region in Cases B and C agree well with the experimental data of Zhang *et al.* (2009) and Sanyal *et al.* (1999), respectively. However, the liquid axial velocities in the region close to the wall are overpredicted in Cases B and C.

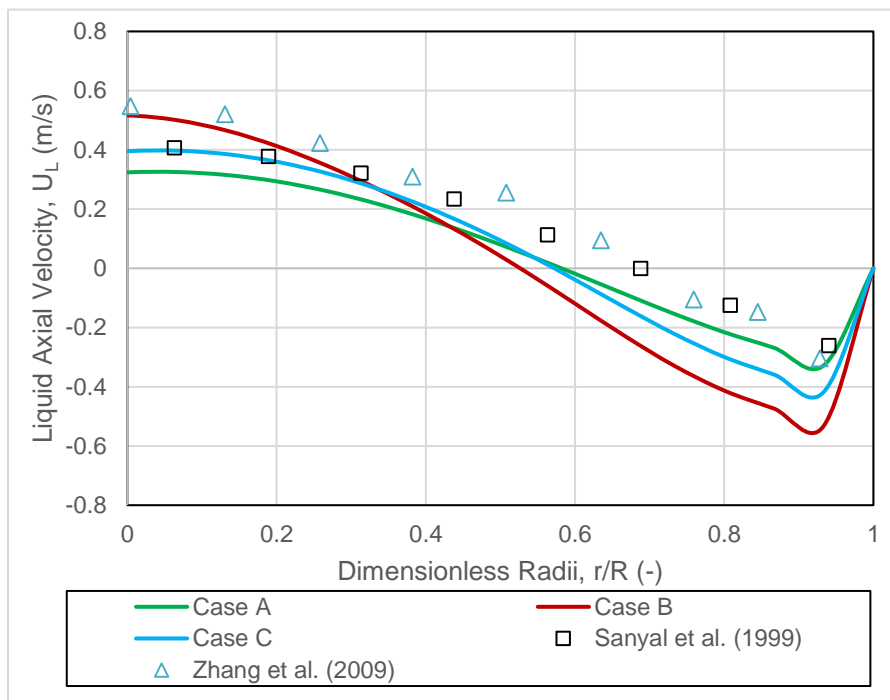


Figure 3.42 Comparison of the liquid axial velocity profiles along the radial direction using the dual bubble size model with different bubble sizes

The comparison of the gas holdup profiles along the radial direction using the dual bubble size modelling approach with different bubble sizes with the experimental data is shown in Figure 3.43. The gas holdup in Case A is underpredicted throughout the column cross section. Between $r/R = 0$ and $r/R = 0.5$, the gas holdup predicted in Case B is close to

the experimental data of Zhang *et al.* (2009). In the region, $0.5 < r/R < 0.8$, the local gas holdup is overpredicted in Case B. Close to the wall region, $r/R > 0.8$, the local gas holdup values is underpredicted in Case B. In Case C, the predicted local gas holdup is close to the experimental data near the column center and the wall region. However, the gas holdup is overestimated between $0.5 < r/R < 0.9$.

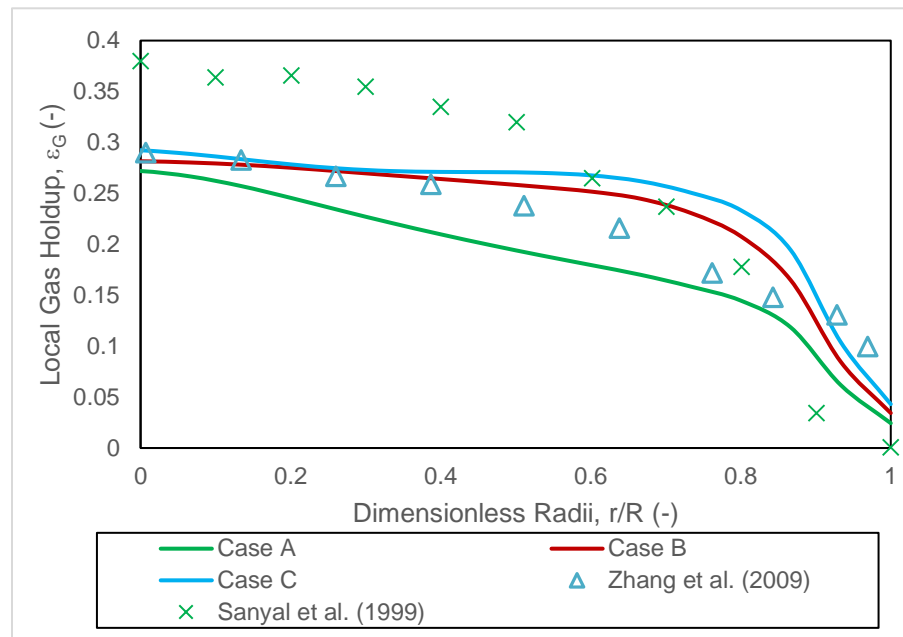


Figure 3.43 Comparison of the gas holdup obtained using the dual bubble size model with different bubble sizes with the experimental data

Figure 3.44 shows the comparison of the overall gas holdup between the numerical results using the dual bubble size modelling approach and the experimental data by Krishna and Sie (2000), Forret *et al.* (2006) and Jhawar and Prakash (2014). The difference in the experimental data from different authors could be attributed to the measurement techniques (probe location and orientation) and averaging approach employed in their respective studies since Forret *et al.* (2006) and Krishna and Sie (2000) employed used visual

techniques in the measurements of the overall gas holdups, and Jhawar and Prakash (2014) measured the gas holdup as a function of pressure difference with the help of a pressure transducer. The overall gas holdups predicted in Cases A and B are close to the experimental data attained by Jhawar and Prakash (2014). However, the overall gas holdup in Case C is overpredicted in comparison to experimental data by Jhawar and Prakash (2014). The gas holdup obtained in Case C is almost the average value of the experimental data of Jhawar and Prakash (2014), and Krishna and Sie (2000) (the data from Forret *et al.* (2006) is very close to that by Krishna and Sie (2000)).

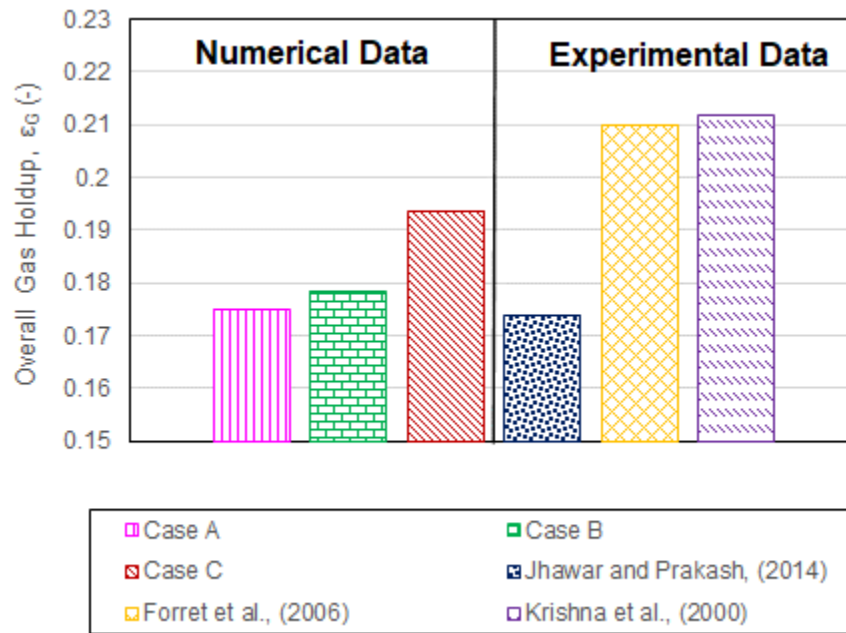


Figure 3.44 Overall gas holdup comparison for dual bubble size model

3.6 Concluding Remarks

In the current work, hollow bubble columns have been extensively analyzed using the numerical approach. The effect of interfacial forces has been thoroughly studied and an

appropriate selection of the interfacial model has been utilized to study the effect of flow regime transitions. The constant lift force model was found to give better predictions for the local gas holdups and liquid axial velocity profiles as compared to the Tomiyama and Saffman-Mei models. The addition of bubble induced turbulence led to homogeneity in the gas holdup profiles. When the turbulent dispersion model was added, the gas plume was dispersed throughout the cross section of the bubble column. The Simonin model outperformed the Burns et al. model in predicting the local gas holdup and liquid axial velocity profiles. In the drag model study, Schiller-Naumann model outperformed the other drag models in the prediction of local and overall gas holdup values.

In the flow transition studies, an increase in the liquid axial velocity was observed with an increase in the superficial gas velocity. The comparison of the centerline liquid velocity with experimental data from numerous studies was made and a good agreement was obtained. Radial gas holdups increased with an increase in the superficial gas velocity and they are closely correspond to experimental observations made by Hills (1974), Chaumat et al. (2006) and Rampure et al. (2007). Overall gas holdups obtained through numerical study have been compared with various experimental data and a good agreement has been obtained. The increase in turbulent parameters was noticed when increasing the superficial gas velocity. A comparison of normalized bubble number densities was made, and an increased number of large bubble fractions was noticed when increasing the superficial gas velocity. Liquid circulations have been studied across the distributor, bulk and the disengagement zone and a generalized flow circulation mapping has been generated for hollow bubble columns. A good agreement was observed compared with the experimental data.

When various bubble breakup and coalescence models were tested, a combination of Luo breakup model and Luo coalescence model exhibited realistic bubble fraction distributions. This model was able to effectively account for the presence of large bubbles in the dispersion. The Lehr breakup model increased the rate of breakup thereby increasing the fraction of smaller bubbles in the dispersion. Dual bubble size models was able to effectively predict the local gas holdups, liquid axial velocities and overall gas holdups. The absence of PBM in these models did not hinder the effective estimation of any of the hydrodynamic parameters.

References

Agahzamin, S. and Pakzad, L. (2019) 'A comprehensive CFD study on the effect of dense vertical internals on the hydrodynamics and population balance model in bubble columns', *Chemical Engineering Science*, 193, pp. 421–435.

ANSYS (2013) 'Ansys Fluent Theory Guide', 15317, p. 513.

van Baten, J. M. and Krishna, R. (2003) 'Scale up studies on partitioned bubble column reactors with the aid of CFD simulations', *Catalysis Today*, 79–80, pp. 219–227.

Besagni, G., Inzoli, F. and Ziegenhein, T. (2018) 'Two-phase bubble columns: A comprehensive review', *ChemEngineering*. Multidisciplinary Digital Publishing Institute, 2(2), p. 13.

Bhaga, D. and Weber, M. E. (1981) 'Bubbles in viscous liquids: shapes, wakes and velocities', *Journal of fluid Mechanics*. Citeseer, 105, pp. 61–85.

Bhole, M. R., Joshi, J. B. and Ramkrishna, D. (2008) 'CFD simulation of bubble columns incorporating population balance modeling', *Chemical Engineering Science*. Elsevier, 63(8), pp. 2267–2282.

Burns, A. D., Frank, T., Hamill, I., Shi, J.-M. and others (2004) 'The Favre averaged drag model for turbulent dispersion in Eulerian multi-phase flows', in *5th international conference on multiphase flow, ICMF*, pp. 1–17.

Chaumat, H., Billet, A.-M. and Delmas, H. (2006) 'Axial and radial investigation of hydrodynamics in a bubble column; influence of fluids flow rates and sparger type', *International Journal of Chemical Reactor Engineering*. De Gruyter, 4(1).

Chen, C. and Fan, L.-S. (2004) 'Discrete simulation of gas-liquid bubble columns and gas-liquid-solid fluidized beds', *AIChE Journal*. Wiley Online Library, 50(2), pp. 288–301.

Chen, J., Kemoun, A., Al-Dahhan, M. H., Duduković, M. P., Lee, D. J. and Fan, L.-S. (1999) 'Comparative hydrodynamics study in a bubble column using computer-automated radioactive particle tracking (CARPT)/computed tomography (CT) and particle image velocimetry (PIV)', *Chemical Engineering Science*. Elsevier, 54(13–14), pp. 2199–2207.

Chen, P., Duduković, M. P. and Sanyal, J. (2005) 'Three-dimensional simulation of bubble column flows with bubble coalescence and breakup', *AIChE Journal*. Wiley Online Library, 51(3), pp. 696–712.

Chu, P., Finch, J., Bournival, G., Ata, S., Hamlett, C. and Pugh, R. J. (2019) 'A review of

- bubble break-up', *Advances in colloid and interface science*. Elsevier, 270, pp. 108–122.
- Colombo, M. and Fairweather, M. (2020) 'Multi-Fluid Computational Fluid Dynamic Predictions of Turbulent Bubbly Flows Using an Elliptic-Blending Reynolds Stress Turbulence Closure', *Frontiers in Energy Research*, 8, p. 44.
- Coughtrie, A. R., Borman, D. J. and Sleigh, P. A. (2013) 'Effects of turbulence modelling on prediction of flow characteristics in a bench-scale anaerobic gas-lift digester', *Bioresource technology*. Elsevier, 138, pp. 297–306.
- Degaleesan, S. (1998) 'Fluid dynamic measurements and modeling of liquid mixing in bubble columns.'
- Degaleesan, S., Dudukovic, M. and Pan, Y. (2001) 'Experimental study of gas-induced liquid-flow structures in bubble columns', *AIChE journal*. Wiley Online Library, 47(9), pp. 1913–1931.
- Devanathan, N., Moslemian, D. and Dudukovic, M. P. (1990) 'Flow mapping in bubble columns using CARPT', *Chemical Engineering Science*. Elsevier, 45(8), pp. 2285–2291.
- Dhotre, M. T., Niceno, B. and Smith, B. L. (2008) 'Large eddy simulation of a bubble column using dynamic sub-grid scale model', *Chemical Engineering Journal*. Elsevier, 136(2–3), pp. 337–348.
- Dhotre, M. T. and Smith, B. L. (2007) 'CFD simulation of large-scale bubble plumes: Comparisons against experiments', *Chemical Engineering Science*, 62(23), pp. 6615–6630.
- Drew, D. A. and Lahey, R. T. (1987) 'The virtual mass and lift force on a sphere in rotating and straining inviscid flow', *International Journal of Multiphase Flow*. Elsevier, 13(1), pp. 113–121.
- Duan, X. Y., Cheung, S. C. P., Yeoh, G. H., Tu, J. Y., Krepper, E. and Lucas, D. (2011) 'Gas-liquid flows in medium and large vertical pipes', *Chemical engineering science*. Elsevier, 66(5), pp. 872–883.
- Duduković, M. P., Larachi, F. and Mills, P. L. (2002) 'Multiphase catalytic reactors: a perspective on current knowledge and future trends', *Catalysis reviews*. Taylor & Francis, 44(1), pp. 123–246.
- Forret, A., Schweitzer, J.-M., Gauthier, T., Krishna, R. and Schweich, D. (2003) 'Influence of scale on the hydrodynamics of bubble column reactors: an experimental study in columns of 0.1, 0.4 and 1m diameters', *Chemical Engineering Science*. Elsevier, 58(3–6),

pp. 719–724.

Forret, A., Schweitzer, J. M., Gauthier, T., Krishna, R. and Schweich, D. (2006) ‘Scale up of slurry bubble reactors’, *Oil & Gas Science and Technology-Revue de l’IFP*. EDP Sciences, 61(3), pp. 443–458.

Frank, T., Zwart, P. J., Krepper, E., Prasser, H.-M. and Lucas, D. (2008) ‘Validation of CFD models for mono- and polydisperse air–water two-phase flows in pipes’, *Nuclear Engineering and Design*. Elsevier, 238(3), pp. 647–659.

Gandhi, A. B., Joshi, J. B., Jayaraman, V. K. and Kulkarni, B. D. (2007) ‘Development of support vector regression (SVR)-based correlation for prediction of overall gas hold-up in bubble column reactors for various gas–liquid systems’, *Chemical Engineering Science*. Elsevier, 62(24), pp. 7078–7089.

Gaurav, T. (2018) ‘Numerical Investigations of Bubble Column Equipped with Vertical Internals in Different Arrangements’, *MESc. Thesis, University of Western Ontario*.

George, K. J. H., Jhavar, A. K. and Prakash, A. (2017) ‘Investigations of flow structure and liquid mixing in bubble column equipped with selected internals’, *Chemical Engineering Science*. Elsevier, 170, pp. 297–305.

Grace, J. R. and Harrison, D. (1967) ‘The influence of bubble shape on the rising velocities of large bubbles’, *Chemical Engineering Science*. Elsevier, 22(10), pp. 1337–1347.

Grace, J. R., TH, N. and others (1976) ‘Shapes and Velocities of Single Drops and Bubbles Moving Freely Through Immiscible Liquids’.

Guan, X. and Yang, N. (2017) ‘CFD simulation of pilot-scale bubble columns with internals: Influence of interfacial forces’, *Chemical Engineering Research and Design*. Elsevier, 126, pp. 109–122.

Gupta, A. and Roy, S. (2013) ‘Euler–Euler simulation of bubbly flow in a rectangular bubble column: Experimental validation with Radioactive Particle Tracking’, *Chemical Engineering Journal*. Elsevier, 225, pp. 818–836.

Hills, J. H. (1974) ‘Radial Non-Uniformity Of Velocity And Voidage In A Bubble Column’, *Trans Inst Chem Eng*, 52(1), pp. 1–9.

Ishii, M. and Zuber, N. (1979) ‘Drag coefficient and relative velocity in bubbly, droplet or particulate flows’, *AIChE Journal*. Wiley Online Library, 25(5), pp. 843–855.

Jhavar, A. K. and Prakash, A. (2014) ‘Bubble column with internals: Effects on

hydrodynamics and local heat transfer', *Chemical Engineering Research and Design*. Elsevier, 92(1), pp. 25–33.

Joseph, W. (2016) 'Three-phase catalytic reactors for hydrogenation and oxidation reactions', *Physical Sciences Reviews*. Berlin, Boston: De Gruyter, 1(1), p. 20150019.

Kanaris, A. G., Pavlidis, T. I., Chatzidafni, A. P. and Mouza, A. A. (2018) 'The effects of the properties of gases on the design of bubble columns equipped with a fine pore sparger', *ChemEngineering*. Multidisciplinary Digital Publishing Institute, 2(1), p. 11.

Kannan, V., Naren, P. R., Buwa, V. V and Dutta, A. (2019) 'Effect of drag correlation and bubble-induced turbulence closure on the gas hold-up in a bubble column reactor', *Journal of Chemical Technology & Biotechnology*, 94(9), pp. 2944–2954.

Kantarci, N., Borak, F. and Ulgen, K. O. (2005) 'Bubble column reactors', *Process biochemistry*. Elsevier, 40(7), pp. 2263–2283.

Kocamustafaogullari, G. and Ishii, M. (1995) 'Foundation of the interfacial area transport equation and its closure relations', *International Journal of Heat and Mass Transfer*. Elsevier, 38(3), pp. 481–493.

Krepper, E., Frank, T., Lucas, D., Prasser, H.-M. and Zwart, P. J. (2007) 'Inhomogeneous MUSIG model—a population balance approach for polydispersed bubbly flows', in *Proceedings of the 12th International Topical Meeting on Nuclear Reactor Thermal Hydraulics (NURETH-12)*, Pittsburgh, Pennsylvania, September.

Krishna, R. and Ellenberger, J. (1996) 'Gas holdup in bubble column reactors operating in the churn-turbulent flow regime', *AIChE journal*. Wiley Online Library, 42(9), pp. 2627–2634.

Krishna, R. and Sie, S. T. (2000) 'Design and scale-up of the Fischer--Tropsch bubble column slurry reactor', *Fuel processing technology*. Elsevier, 64(1–3), pp. 73–105.

Kulkarni, A. (2008) 'Lift force on bubbles in a bubble column reactor: Experimental analysis', *Chemical Engineering Science*, 63, pp. 1710–1723.

Kumar, S. and Ramkrishna, D. (1996) 'On the solution of population balance equations by discretization—I. A fixed pivot technique', *Chemical Engineering Science*. Elsevier, 51(8), pp. 1311–1332.

Law, D., Battaglia, F. and Heindel, T. J. (2008) 'Model validation for low and high superficial gas velocity bubble column flows', *Chemical Engineering Science*. Elsevier, 63(18), pp. 4605–4616.

- Lee, C.-H., Erickson, L. E. and Glasgow, L. A. (1987) 'Bubble breakup and coalescence in turbulent gas-liquid dispersions', *Chemical Engineering Communications*. Taylor & Francis, 59(1-6), pp. 65-84.
- Lehr, F., Millies, M. and Mewes, D. (2002) 'Bubble-Size distributions and flow fields in bubble columns', *AIChE Journal*, 48(11), pp. 2426-2443.
- Li, G., Yang, X. and Dai, G. (2009) 'CFD simulation of effects of the configuration of gas distributors on gas-liquid flow and mixing in a bubble column', *Chemical Engineering Science*. Elsevier, 64(24), pp. 5104-5116.
- Li, H. and Prakash, A. (2000) 'Influence of slurry concentrations on bubble population and their rise velocities in a three-phase slurry bubble column', *Powder Technology*. Elsevier, 113(1-2), pp. 158-167.
- Li, H., Prakash, A., Margaritis, A. and Bergougnou, M. A. (2003) 'Effects of micron-sized particles on hydrodynamics and local heat transfer in a slurry bubble column', *Powder Technology*. Elsevier, 133(1-3), pp. 171-184.
- Liao, Y. and Lucas, D. (2009) 'A literature review of theoretical models for drop and bubble breakup in turbulent dispersions', *Chemical Engineering Science*. Elsevier, 64(15), pp. 3389-3406.
- Liovic, P. and Lakehal, D. (2007) 'Interface-turbulence interactions in large-scale bubbling processes', *International Journal of Heat and Fluid Flow*. Elsevier, 28(1), pp. 127-144.
- Lopez De Bertodano, M., Moraga, F. J. and Drew, D A Lahey, R. T. (2004) 'The modeling of lift and dispersion forces in two-fluid model simulations of a bubbly jet', *Journal of fluids engineering*. American Society of Mechanical Engineers, 126(4), pp. 573-577.
- Luo, H. (1995) 'Coalescence, breakup and liquid circulation in bubble column reactors.'
- Luo, H. and Svendsen, H. F. (1996) 'Theoretical model for drop and bubble breakup in turbulent dispersions', *AIChE Journal*. Wiley Online Library, 42(5), pp. 1225-1233.
- Luo, X., Lee, D. J., Lau, R., Yang, G. and Fan, L.-S. (1999) 'Maximum stable bubble size and gas holdup in high-pressure slurry bubble columns', *AIChE journal*. Wiley Online Library, 45(4), pp. 665-680.
- Magolan, B., Lubchenko, N. and Baglietto, E. (2019) 'A quantitative and generalized assessment of bubble-induced turbulence models for gas-liquid systems', *Chemical Engineering Science: X*. Elsevier, 2, p. 100009.

- Mei, R. (1992) 'An approximate expression for the shear lift force on a spherical particle at finite Reynolds number', *International Journal of Multiphase Flow*. Elsevier, 18(1), pp. 145–147.
- Menzel, T., der Weide, T., Staudacher, O., Wein, O. and Onken, U. (1990) 'Reynolds shear stress for modeling of bubble column reactors', *Industrial & engineering chemistry research*. ACS Publications, 29(6), pp. 988–994.
- Miao, X., Lucas, D., Ren, Z., Eckert, S. and Gerbeth, G. (2013) 'Numerical modeling of bubble-driven liquid metal flows with external static magnetic field', *International Journal of Multiphase Flow*. Elsevier, 48, pp. 32–45.
- Mudde, R. F., Groen, J. S. and Van Den Akker, H. E. A. (1997) 'Liquid velocity field in a bubble column: LDA experiments', *Chemical Engineering Science*. Citeseer, 52(21–22), pp. 4217–4224.
- Mudde, R. F. and Saito, T. (2001) 'Hydrodynamical similarities between bubble column and bubbly pipe flow', *Journal of fluid mechanics*. Cambridge University Press, 437, pp. 203–228.
- Mudde, R. F. and Simonin, O. (1999) 'Two- and three-dimensional simulations of a bubble plume using a two-fluid model', *Chemical Engineering Science*, 54(21), pp. 5061–5069.
- Nedelchev, S., Shaikh, A. and Al-Dahhan, M. (2011) 'Flow regime identification in a bubble column via nuclear gauge densitometry and chaos analysis', *Chemical engineering & technology*. Wiley Online Library, 34(2), pp. 225–233.
- Nguyen, V. T., Song, C.-H., Bae, B.-U. and Euh, D.-J. (2013) 'The dependence of wall lubrication force on liquid velocity in turbulent bubbly two-phase flows', *Journal of Nuclear Science and Technology*. Taylor & Francis, 50(8), pp. 781–798.
- Ni, M., Leung, D. Y. C., Leung, M. K. H. and Sumathy, K. (2006) 'An overview of hydrogen production from biomass', *Fuel Processing Technology*, 87(5), pp. 461–472.
- Nopens, I., Torfs, E., Ducoste, J., Vanrolleghem, P. A. and Gernaey, K. V (2015) 'Population balance models: a useful complementary modelling framework for future WWTP modelling', *Water Science and Technology*. IWA Publishing, 71(2), pp. 159–167.
- Nygren, A. (2014) 'Simulation of bubbly flow in a flat bubble column'.
- Okada, K., Shibano, S. and Akagi, Y. (1993) 'Turbulent properties in bubble-flow region in external-loop airlift bubble column', *Journal of chemical engineering of Japan*. The Society of Chemical Engineers, Japan, 26(6), pp. 637–643.

- Pourtousi, M., Sahu, J. N. and Ganesan, P. (2014) 'Effect of interfacial forces and turbulence models on predicting flow pattern inside the bubble column', *Chemical Engineering and Processing: Process Intensification*, 75, pp. 38–47.
- Prince, M. J. and Blanch, H. W. (1990) 'Bubble coalescence and break-up in air-sparged bubble columns', *AIChE journal*. Wiley Online Library, 36(10), pp. 1485–1499.
- Rampure, M. R., Kulkarni, A. A. and Ranade, V. V (2007) 'Hydrodynamics of bubble column reactors at high gas velocity: experiments and computational fluid dynamics (CFD) simulations', *Industrial & Engineering Chemistry Research*. ACS Publications, 46(25), pp. 8431–8447.
- Rigopoulos, S. (2010) 'Population balance modelling of polydispersed particles in reactive flows', *Progress in Energy and Combustion Science*. Elsevier, 36(4), pp. 412–443.
- Rigopoulos, S. and Jones, A. G. (2003) 'Finite-element scheme for solution of the dynamic population balance equation', *AIChE Journal*, 49(5), pp. 1127–1139.
- Saffman, P. G. T. (1965) 'The lift on a small sphere in a slow shear flow', *Journal of fluid mechanics*. Cambridge University Press, 22(2), pp. 385–400.
- Sanyal, J., Vásquez, S., Roy, S. and Dudukovic, M. P. (1999) 'Numerical simulation of gas-liquid dynamics in cylindrical bubble column reactors', *Chemical Engineering Science*. Elsevier, 54(21), pp. 5071–5083.
- Sarhan, A. R., Naser, J. and Brooks, G. (2018) 'CFD modeling of bubble column: Influence of physico-chemical properties of the gas/liquid phases properties on bubble formation', *Separation and Purification Technology*, 201, pp. 130–138.
- Schiller, L. (1933) 'Über die grundlegenden Berechnungen bei der Schwerkraftaufbereitung', *Z. Vereines Deutscher Inge.*, 77, pp. 318–321.
- Schumpe, A. and Grund, G. (1986) 'The gas disengagement technique for studying gas holdup structure in bubble columns', *The Canadian Journal of Chemical Engineering*. John Wiley & Sons, Ltd, 64(6), pp. 891–896.
- Shaikh, A. and Al-Dahhan, M. (2013) 'Scale-up of bubble column reactors: a review of current state-of-the-art', *Industrial & Engineering Chemistry Research*. ACS Publications, 52(24), pp. 8091–8108.
- Shi, W., Yang, J., Li, G., Zong, Y. and Yang, X. (2020) 'Computational Fluid Dynamics–Population Balance Modeling of Gas–Liquid Two-Phase Flow in Bubble Column Reactors With an Improved Breakup Kernel Accounting for Bubble Shape Variations', *Heat*

Transfer Engineering. Taylor & Francis, 41(15–16), pp. 1414–1430.

Shi, W., Yang, X., Sommerfeld, M., Yang, J., Cai, X. and Li, G. (2020) ‘A Modified Bubble Breakage and Coalescence Model Accounting the Effect of Bubble-Induced Turbulence for CFD-PBM Modelling of Bubble Column Bubbly Flows’, *Flow Turbulence and Combustion*. Springer.

Shi, W., Yang, X., Sommerfeld, M., Yang, J., Cai, X., Li, G. and Zong, Y. (2019) ‘Modelling of mass transfer for gas-liquid two-phase flow in bubble column reactor with a bubble breakage model considering bubble-induced turbulence’, *Chemical Engineering Journal*. Elsevier, 371, pp. 470–485.

Silva, M. K., d’Ávila, M. A. and Mori, M. (2012) ‘Study of the interfacial forces and turbulence models in a bubble column’, *Computers & Chemical Engineering*. Elsevier, 44, pp. 34–44.

Simonin, C., Viollet, P. L. and others (1990) ‘Predictions of an oxygen droplet pulverization in a compressible subsonic coflowing hydrogen flow’, *Numerical Methods for Multiphase Flows*. American Society of Mechanical Engineers: Fluids Engineering Division New York, 91(2), pp. 65–82.

Smith, B. L. (1998) ‘On the modelling of bubble plumes in a liquid pool’, *Applied Mathematical Modelling*. Elsevier, 22(10), pp. 773–797.

Sokolichin, A., Eigenberger, G. and Lapin, A. (2004) ‘Simulation of buoyancy driven bubbly flow: established simplifications and open questions’, *AIChE Journal*. Wiley Online Library, 50(1), pp. 24–45.

Syed, A. H., Boulet, M., Melchiori, T. and Lavoie, J.-M. (2017) ‘CFD simulations of an air-water bubble column: Effect of Luo coalescence parameter and breakup kernels’, *Frontiers in Chemistry*. Frontiers, 5, p. 68.

Tabib, M. V, Roy, S. A. and Joshi, J. B. (2008) ‘CFD simulation of bubble column—an analysis of interphase forces and turbulence models’, *Chemical Engineering Journal*. Elsevier, 139(3), pp. 589–614.

Tao, F., Ning, S., Zhang, B., Jin, H. and He, G. (2019) ‘Simulation Study on Gas Holdup of Large and Small Bubbles in a High Pressure Gas-Liquid Bubble Column’, *Processes*. Multidisciplinary Digital Publishing Institute, 7(9), p. 594.

Tomiya, A. (1998) ‘Struggle with computational bubble dynamics’, *Multiphase Science and Technology*, 10(4), pp. 369–405.

- Tomiyama, A., Tamai, H., Zun, I. and Hosokawa, S. (2002) 'Transverse migration of single bubbles in simple shear flows', *Chemical Engineering Science*. Elsevier, 57(11), pp. 1849–1858.
- Vaidheeswaran, A. and Hibiki, T. (2017) 'Bubble-induced turbulence modeling for vertical bubbly flows', *International Journal of Heat and Mass Transfer*. Elsevier, 115, pp. 741–752.
- Valero, M. M., Martinez, M., Pozo, F. and Planas, E. (2019) 'A successful experience with the flipped classroom in the Transport Phenomena course', *Education for Chemical Engineers*. Elsevier, 26, pp. 67–79.
- Vanni, M. (2000) 'Approximate Population Balance Equations for Aggregation–Breakage Processes', *Journal of Colloid and Interface Science*, 221(2), pp. 143–160.
- Vatai, G. Y. and Tekić, M. N. (1989) 'Gas hold-up and mass transfer in bubble columns with pseudoplastic liquids', *Chemical Engineering Science*, 44(10), pp. 2402–2407.
- Wachi, S., Morikawa, H. and Ueyama, K. (1987) 'Gas holdup and axial dispersion in gas-liquid concurrent bubble column', *Journal of chemical engineering of Japan*. The Society of Chemical Engineers, Japan, 20(3), pp. 309–316.
- Wang, T. (2011) 'Simulation of bubble column reactors using CFD coupled with a population balance model', *Frontiers of Chemical Science and Engineering*. Springer, 5(2), pp. 162–172.
- Wang, T. and Wang, J. (2007) 'Numerical simulations of gas–liquid mass transfer in bubble columns with a CFD–PBM coupled model', *Chemical Engineering Science*, 62(24), pp. 7107–7118.
- Wegener, P. P. and Parlange, J.-Y. (1973) 'Spherical-cap bubbles', *Annual Review of Fluid Mechanics*. Annual Reviews 4139 El Camino Way, PO Box 10139, Palo Alto, CA 94303-0139, USA, 5(1), pp. 79–100.
- Wilkinson, P. M., Spek, A. P. and van Dierendonck, L. L. (1992) 'Design parameters estimation for scale-up of high-pressure bubble columns', *AIChE Journal*. Wiley Online Library, 38(4), pp. 544–554.
- Wu, Y., Ong, B. C. and Al-Dahhan, M. H. (2001) 'Predictions of radial gas holdup profiles in bubble column reactors', *Chemical engineering science*. Elsevier, 56(3), pp. 1207–1210.
- Xu, L., Xia, Z., Guo, X. and Chen, C. (2014) 'Application of population balance model in the simulation of slurry bubble column', *Industrial & Engineering Chemistry Research*.

ACS Publications, 53(12), pp. 4922–4930.

Xu, L., Yuan, B., Ni, H. and Chen, C. (2013) ‘Numerical simulation of bubble column flows in churn-turbulent regime: comparison of bubble size models’, *Industrial & Engineering Chemistry Research*. ACS Publications, 52(20), pp. 6794–6802.

Xue, J., Al-Dahhan, M., Dudukovic, M. P. and Mudde, R. F. (2008) ‘Bubble velocity, size, and interfacial area measurements in a bubble column by four-point optical probe’, *AIChE journal*. Wiley Online Library, 54(2), pp. 350–363.

Yang, G., Guo, K. and Wang, T. (2017) ‘Numerical simulation of the bubble column at elevated pressure with a CFD-PBM coupled model’, *Chemical Engineering Science*, 170, pp. 251–262.

Yang, G., Zhang, H., Luo, J. and Wang, T. (2018) ‘Drag force of bubble swarms and numerical simulations of a bubble column with a CFD-PBM coupled model’, *Chemical Engineering Science*. Elsevier, 192, pp. 714–724.

Yao, B. P., Zheng, C., Gasche, H. E. and Hofmann, H. (1991) ‘Bubble behaviour and flow structure of bubble columns’, *Chemical Engineering and Processing: Process Intensification*. Elsevier, 29(2), pp. 65–75.

Yu, Y. H. and Kim, S. D. (1991) ‘Bubble properties and local liquid velocity in the radial direction of cocurrent gas—liquid flow’, *chemical Engineering science*. Elsevier, 46(1), pp. 313–320.

Zhang, X.-B. and Luo, Z.-H. (2020) ‘Effects of Bubble Coalescence and Breakup Models on the Simulation of Bubble Columns’, *Chemical Engineering Science*. Elsevier, p. 115850.

Zhang, Y., Li, H., Li, Z., Wang, L. and Li, X. (2011) ‘Hydrodynamics of turbulent slurry bubble column (IV) Modeling and simulation of bubble column with vertical pipe bundles [J]’, *CIESC Journal*, 12.

Zhang, Y., Lu, J., Wang, L. and Li, X. (2009) ‘Studies on hydrodynamics of turbulent slurry bubble column (III) Effect of vertical pipe bundles [J]’, *Journal of the Chemical Industry and Engineering Society of China*, 5.

Žun, I. (1990) ‘The mechanism of bubble non-homogeneous distribution in two-phase shear flow’, *Nuclear engineering and design*. Elsevier, 118(2), pp. 155–162.

Chapter 4

4 CFD Simulations of Bubble Column Reactors Occluded with Circular Tube Bundle and Dense Vertical Internals

Bubble column reactors have found their applications in various processes in chemical and biochemical industries owing to their multitude advantages like high heat and mass transfer rates, lack of moving parts, simple construction and low maintenance costs (Duduković, Larachi and Mills, 2002; Li *et al.*, 2003; Ni *et al.*, 2006; Shaikh and Al-Dahhan, 2013; Joseph, 2016; George, Jhavar and Prakash, 2017; Valero *et al.*, 2019). The main factor that differentiates these reactors from the typical continuous stirred tank reactors and fixed bed reactors is their ability to establish superior levels of heat and mass transfer rates at low energy inputs. As of late, these reactors are preferred to carry out Fischer-Tropsch, methanol synthesis and CO₂ methanation which are highly exothermic reactions (Ledakowicz *et al.*, 1992; van der Laan *et al.*, 1999; Rados, Al-Dahhan and Dudukovic, 2003; Rahimpour *et al.*, 2012; Zhang *et al.*, 2014; Lefebvre *et al.*, 2015; Ali *et al.*, 2020).

Vertical heat exchanging rods are a popular choice of internals within the reactor that facilitate the heat removal and heat circulation using high pressure steam (Desvigne *et al.*, 2006; Abdulmohsin and Al-Dahhan, 2012; Besagni and Inzoli, 2016; Möller *et al.*, 2019). Therefore, the costs associated with the installation of circulation pumps and addition of new heat exchanger assemblies can be reduced. The rate of heat exchange depends on the cross-sectional area (CSA) occluded by the internals. Until now, bubble columns with a CSA occlusion between 20% and 60% have been commonly studied. When the available CSA is covered with internals, the hydrodynamics parameters vary, and their analysis is a

difficult process owing to the complexity of equipment needed and their associated expenses.

Many studies suggested that the phase holdups could be drastically altered in the presence of internals. An increase in the gas velocity caused by the decrease in the cross sectional area in the presence of internals was found to be the main reason for the increase of gas holdups. The decrease in the bubble size leads to increases in the interfacial area and gas holdup (Saxena *et al.*, 1992; Hulet *et al.*, 2009; Youssef *et al.*, 2012). Even though vertical tube internals are advantageous, superior degree of backmixing has been noticed as compared to hollow bubble columns (Shaykhutdinov, Bakirov and Usmanov, 1971; Knickle *et al.*, 1983). Forret *et al.* (2003) noticed an increase in the magnitude of large scale liquid recirculation and a decrease in the fluctuating liquid velocities when bubble columns are occluded with internals as shown in Figure 4.1.

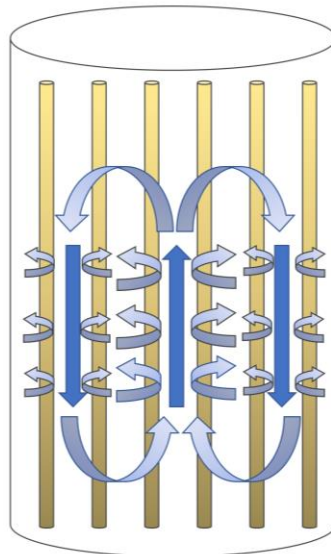


Figure 4.1 Recirculation patterns in the presence of vertical tube internals (Redrawn from Forret *et al.* (2003))

Full-fledged scale up of bubble column reactors are expensive and the scale up has proven to be really challenging due to the underlying fluid dynamic aspects. When a bubble column reactor must be occluded with internals, the choice of various innards and the associated operation variables make it even more challenging for an effective scale up. A considerable progress has been made in the field of computational fluid dynamics (CFD) over the last few decades. CFD is a powerful and effective tool that is used to simulate a wide range of industrial processes. Multiphase flow CFD simulations are bound to provide numerous challenges as compared to singular phase flows. In the current study, CFD simulations have been performed to study the hydrodynamics and turbulence parameters for a bubble column reactor with internals in the form of circular vertical-tube bundles.

4.1 Objectives

The numerical simulations of bubble column reactors with a single circular tube bundle comprising of 15 rods and denser vertical internals comprising of 38 rods are carried out using ANSYS Fluent v19.2, which is one of the widely used commercial CFD packages. 2-D planar simulations are carried out to study the hydrodynamic and turbulence parameters.

The simulations are carried out in bubbly flow regime, transition regime and churn-turbulent regime at superficial gas velocities of 0.04 m/s, 0.10 m/s and 0.30 m/s, respectively. The effect of the superficial gas velocity on hydrodynamic parameters such as radial profiles of gas holdups, liquid axial velocities, overall gas holdups, centerline liquid axial velocities and bubble size distributions have been investigated and compared with numerous experimental data. The effect of flow regimes on turbulence parameters, such as turbulence viscosity ratio and turbulence Reynolds number, has been investigated.

4.2 Configuration of the Bubble Column

The numerical modelling of a single circular tube bundle is based on the pilot-scale bubble column of Jhavar and Prakash (2014) shown in Figure 4.2. In their experimental study, Jhavar and Prakash (2014) used a circular tube bundle consisting of 15 tubes with the length and diameter of 1.5 m and 9.5 mm, respectively. On the other hand, the dense vertical tube model shown in Figure 4.3 has been designed for the sole purpose of the numerical study. The focus of the current study is to investigate the hydrodynamics of bubble column reactor when it is obstructed with vertical internals. Jhavar and Prakash (2014) carried out their experiments in a Plexiglas column of 2.5 m in height and 0.15 m in diameter. The column was equipped with a coarse sparger, through which the secondary phase was introduced. In their study, tap water and compressed air were used as primary and secondary sources, respectively. The study was carried out at various superficial gas velocities ranging from 3 cm/s to 35 cm/s. The static height of the liquid was maintained at 1.45 m throughout their experimental runs.

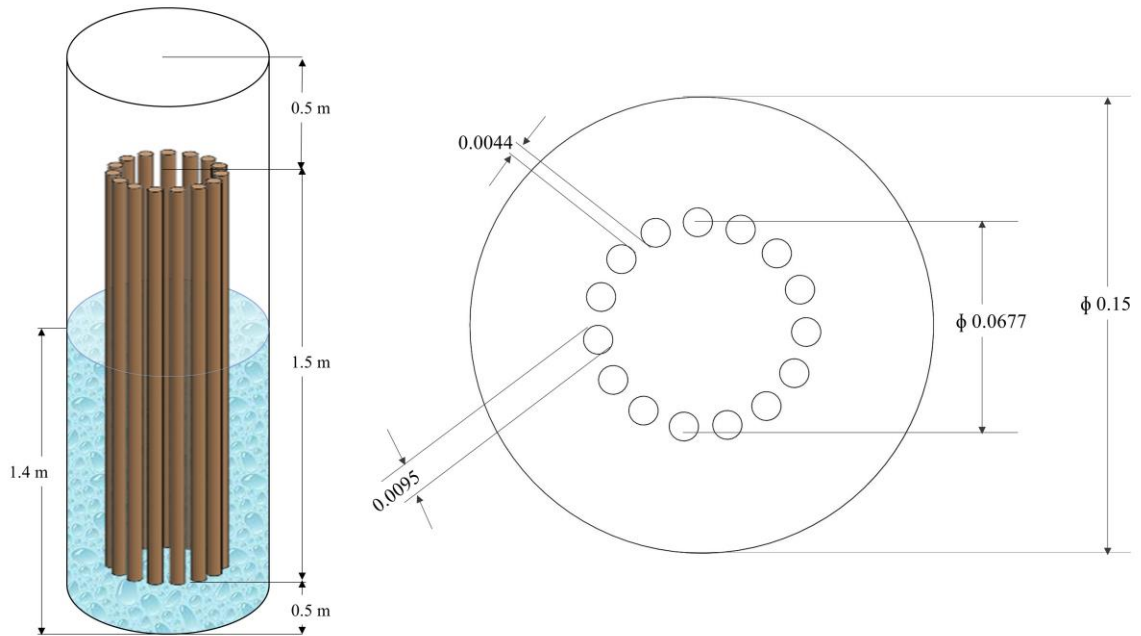


Figure 4.2 Experimental setup of the bubble column reactor equipped with one circular tube bundle of 15 tubes used by Jhawar and Prakash (2014)

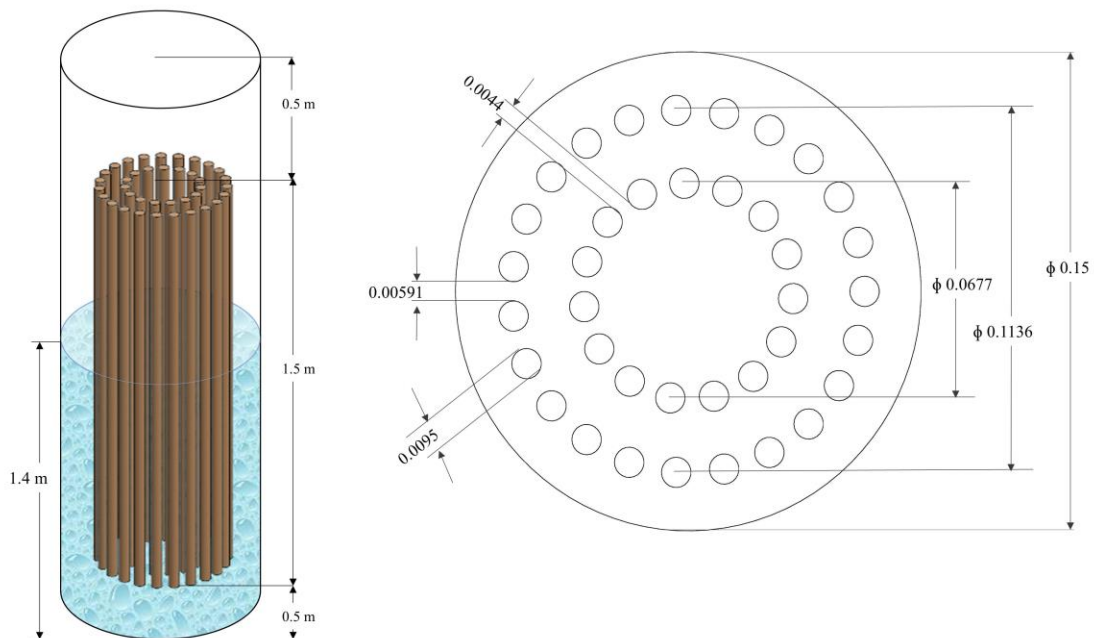


Figure 4.3 Bubble column reactor equipped with dense vertical tube internals of two circular tube bundle of 38 tubes used for the purpose of the numerical analysis

4.2.1 Computational Domain and Grid Independence Test

Two-dimensional simulations of the bubble column are carried out in this study. The structured mesh for the two-dimensional computational domain is generated using ICEM CFD 17.0. In the two-dimensional computational domain for the column with a single circular bundle of 15 tubes, the internals on the central plane of the three-dimensional column are replaced by 2 vertical perforated rods and the size of each perforation is equal to the pitch of tubes (4.4 mm). For the column with two circular bundles of 38 tubes, the internals are represented by 4 vertical perforated rods. The size of the perforation for the inner circular tube bundle is equal to 4.4 mm and that for the outer tube bundle is 5.9 mm. In addition, the fraction of spaces in the internal rod is made equal to the available total free surface area of the 3D circular tube bundle. The space fraction for the 15 tube internals is 31% and for the outer tube consisting of 23 tubes is 38%. The total height of the internals is kept equal to 1.5 m (Jhawar and Prakash, 2014). The internals are placed at a height of 0.5 m from the distributor. Details of the internal geometry and the calculations are provided in Appendix C.

The grid independence tests are carried out using three meshes and the effect of mesh density on radial gas holdups is investigated for the columns with 15 tubes and 38 tubes. The medium mesh is chosen after taking the accuracy of the solution and the convergence time into the consideration. The difference between the results from the medium and fine mesh is within the acceptable tolerance levels of 4%. The comparison of the radial profiles of gas holdups from the medium and fine meshes is illustrated in Figures 4.6 and 4.7 for columns with 15 tubes and 38 tubes, respectively. Smaller grid sizes are used close to the column and internal walls to capture the effective physics. The first grid point from the

wall is maintained in a way such that the Y^+ value lied in the viscous sub layer since the enhanced wall functions are used. Four nodes between the tubes are ascribed to capture the liquid recirculation patterns effectively.

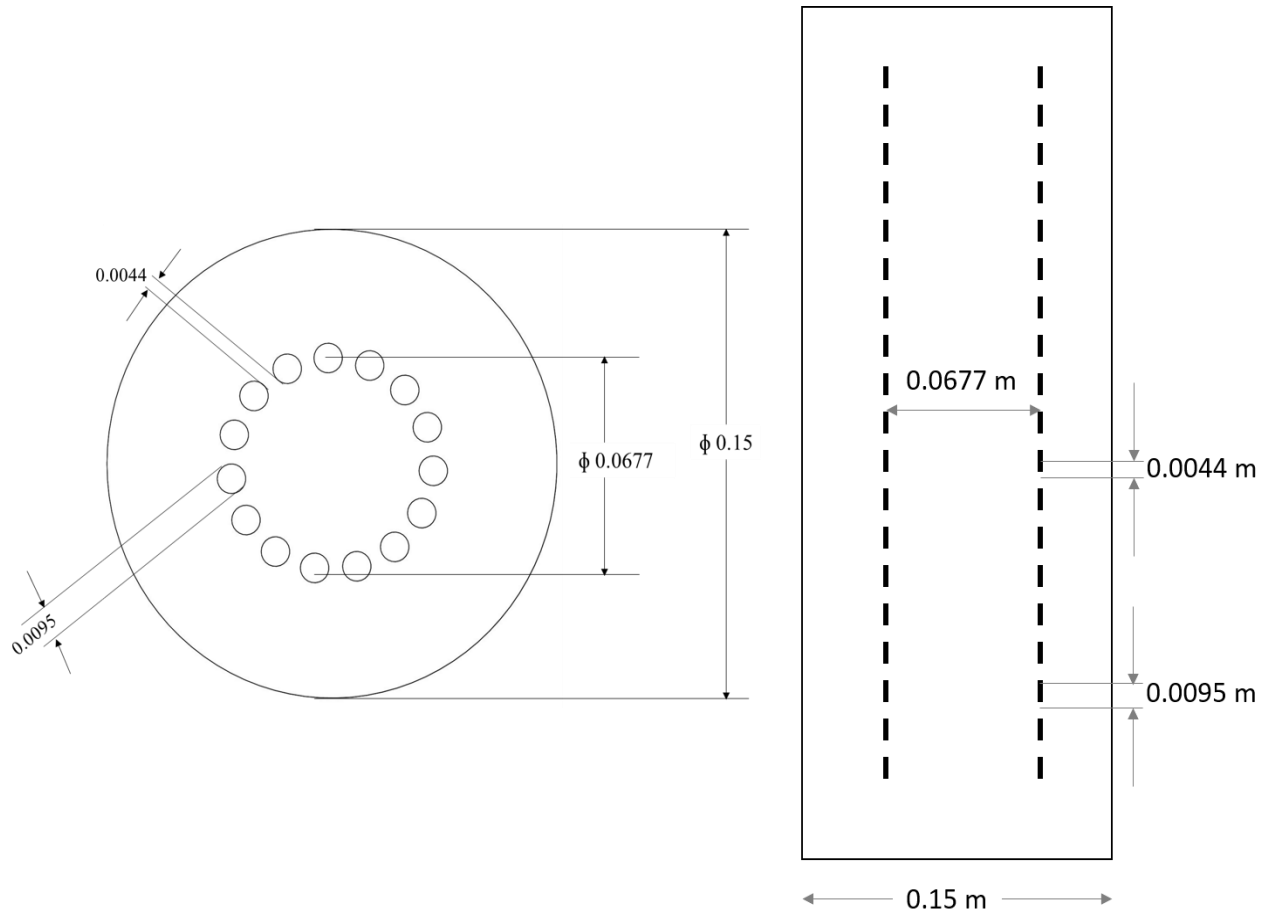


Figure 4.4 Computational domain for the bubble column with 15 internal vertical tubes

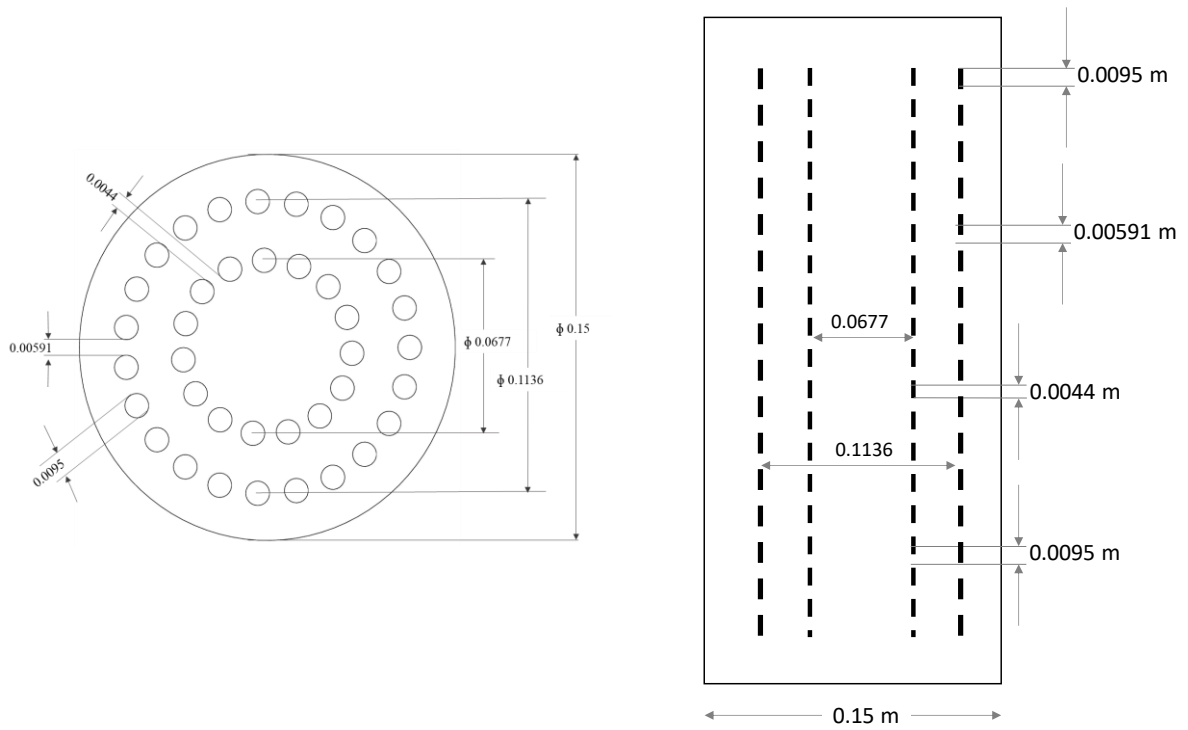


Figure 4.5. Computational domain for bubble column with 38 internal vertical tubes

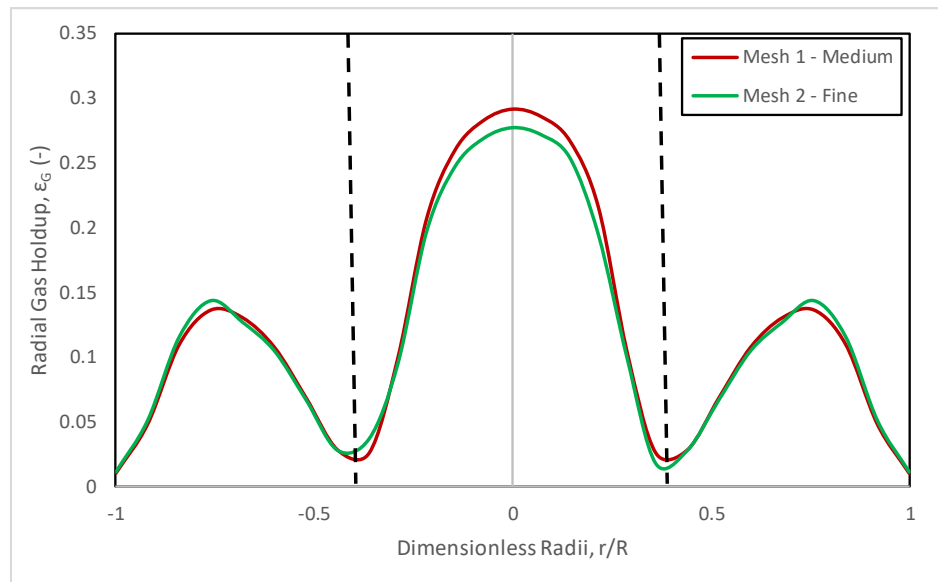


Figure 4.6 Grid independence test for the column with 15 internal tubes

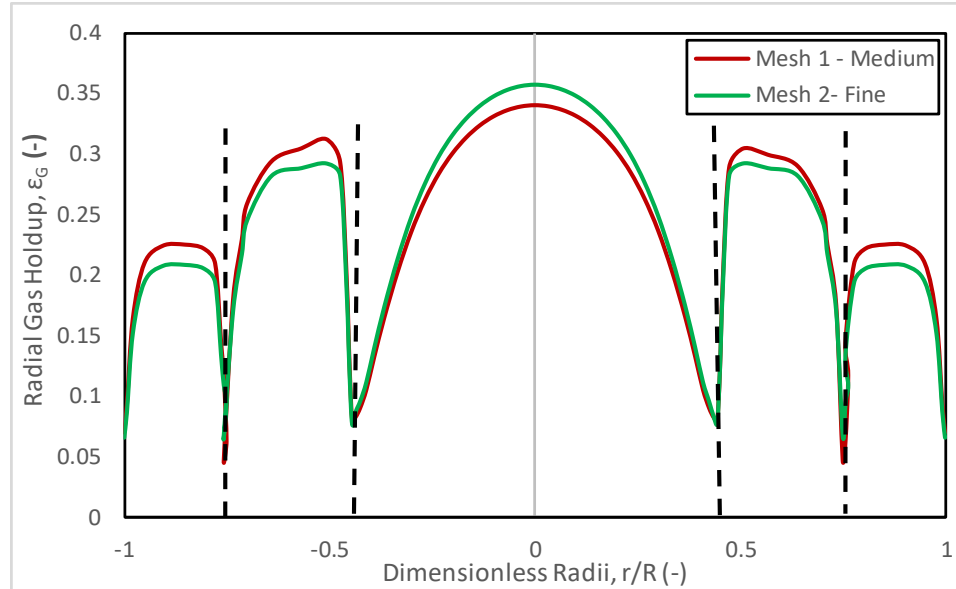


Figure 4.7 Grid independence test for the column with 38 internal tubes

4.2.2 Numerical Method

The numerical simulations of the bubble column reactor are carried out using ANSYS Fluent v19.2. The simulations are carried out for a water-air system and an incompressible method (Pressure-based solver) is utilized. The Reynolds Stress Model (RSM) with dispersed formulation is used in the current study as it can accurately capture the anisotropic nature of the turbulent kinetic energy, a key parameter in the bubble column modelling. For the flow transition study, simulations of the bubble column with a single circular tube bundle of 15 tubes and two circular tube bundles of 38 tubes are carried out using low ($U_G=0.04$ m/s), medium ($U_G=0.10$ m/s) and high ($U_G=0.30$ m/s) gas flow rates.

Water and air are selected as the primary phase and secondary phase, respectively. The discrete phase PBM is employed in the current analysis. The spatial variables are discretized by Green-Gauss Cell based method. The phase-coupled SIMPLE method is used for the pressure-velocity coupling. In the current study, the QUICK scheme is used for the momentum and volume fraction equations and the second order upwind scheme is used for the governing equations for the turbulence parameters and gas bin fractions as suggested by Gaurav (2018) and Gupta and Roy (2013). The convergence criterion is set to as 10^{-3} for the absolute residuals of all transport equations. The initial time step is set as 0.0001 s for the first 3 seconds of flow time and is then increased in succession to 0.0005 s and 0.001 s after 8 seconds and 15 seconds, respectively to avert numerical divergence. The flow simulation is carried out for 200 seconds and time averaging of flow properties, such as radial gas holdups, axial liquid velocities, turbulence parameters and Sauter diameter, are commenced after a quasi-steady state is achieved in the simulation, which is about 30 seconds of the flow time. Hence, the simulation results are averaged for about 170 s. The numerical models used in the current work are summarized in Table 4.1.

Table 4.1 Summary of numerical methods

Scheme	Solution Methods
Pressure-Velocity Coupling	
Scheme	Phase-Coupled SIMPLE
Spatial Discretization	
Gradient	Green-Gauss Cell Based
Momentum	QUICK
Volume Fraction	QUICK
Turbulent Kinetic Energy	Second Order Upwind
Turbulent Dissipation Rate	Second Order Upwind

Reynolds Stresses	Second Order Upwind
Air Bins (Population Balance Model)	Second Order Upwind
Transient Formulation	
Scheme	Bounded Second Order Implicit
Under Relaxation Factors	
Pressure	0.2
Momentum	0.3
Volume Fraction	0.2
Turbulent Kinetic Energy and Turbulent Dissipation Rate	0.8
Turbulent Viscosity	1
Reynolds Stresses	0.5
Air Bin Fractions	0.5

4.2.2.1 Boundary Conditions

At the inlet, the superficial gas velocity, the volume fraction of the gas phase, and the initial bin fractions are specified. Very few researchers have explicitly mentioned their choice of turbulent quantities for the liquid phase at the inlet, which makes it a great challenge to specify the turbulence parameters at the inlet for gas-liquid flows. In a recent study by Magolan et al. (2019), turbulence intensity of 0.1 and turbulent viscosity ratio of 100 were used. In another study carried out by Nygren (2014), the turbulent intensity was set at 10% at the inlet. In the current study, the turbulent intensity of 5% and hydraulic diameter of 0.15 m (equivalent to the diameter of the bubble column reactor) are applied. The outflow boundary condition is applied at the outlet. No slip boundary condition is applied at the column walls and the internal walls.

4.3 Results and Discussion

The current section is divided into two segments. In the first segment, the influence of interfacial forces (lift and turbulent dispersion forces) is studied on bubble column with 15 internals. The second segment highlights the effect of flow regime transition on hydrodynamic parameters for bubble column with 15 and 38 tube vertical internals. All the results presented in this section are time averaged.

4.3.1 Influence of interfacial forces on hydrodynamics of a bubble column with internals

The choice of appropriate interfacial forces is crucial in the prediction of flow patterns and reactor hydrodynamics. So far, very little work has been done to help understand the sensitivity of interfacial forces flow patterns and reactor hydrodynamics when bubble columns are equipped with internals. The current section discusses the influence of lift models and turbulent dispersion models on the flow pattern in the bubble column with a single circular tube bundle of 15 tubes.

4.3.1.1 Influence of the lift force model

The effect of lift force coefficient is investigated in the transition regime (10 cm/s) and the radial variation of liquid axial velocities are illustrated in Figure 4.8. The centerline liquid axial velocity from the positive lift force coefficient of $C_L=+0.1$ is underpredicted as compared to the zero lift force ($C_L=0$) and negative lift coefficients. When a positive lift coefficient is used, the bubbles migrate from regions of higher velocities to the lower velocity regions. However, when a positive lift coefficient is employed, a higher simulation stability (fewer divergence issues) is noticed, which is in accordance to the observations

made by Lucas et al., (2005). The liquid velocities predicted by using a zero lift force ($C_L=0$) and small magnitude of a negative lift coefficient ($C_L=-0.05$) are closer to the experimental data (shown in Figure 4.18) obtained by Jhawar and Prakash (2014). When simulations are performed with a higher magnitude of a negative lift coefficient ($C_L=-0.1$), the liquid axial velocity is overpredicted by 36%. Tomiyama lift model results in an asymmetrical axial liquid velocity profile as shown in Figure 4.8. The trends of the liquid velocity variation can be well comprehended from the contours illustrated in Figure 4.9. It is noticed that the higher axial liquid velocity occurs between the two internals from the bottom of the internals to the dispersion height ($z=1.4$ m) using $C_L=0$, $C_L=-0.1$ and Tomiyama lift models. However, the magnitude of the negative liquid velocity between the internal and column wall is overestimated by the negative lift force coefficient. Tomiyama model dispersed the plume from one internal wall to the other leading to uneven liquid velocity profiles.

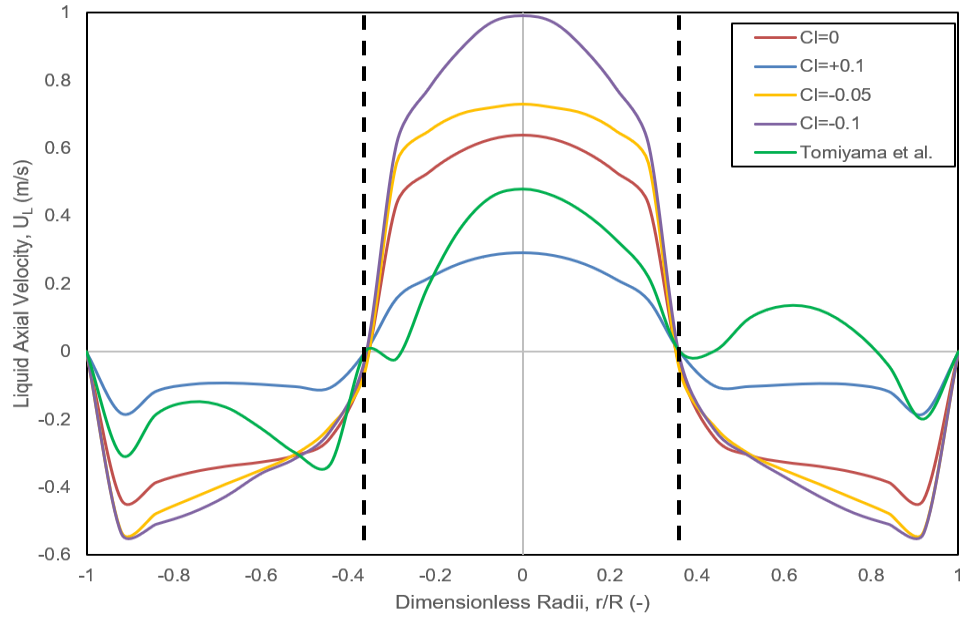


Figure 4.8 Influence of lift force models on the radial profiles of the liquid axial velocities in the transition regime ($U_G=10$ cm/s)

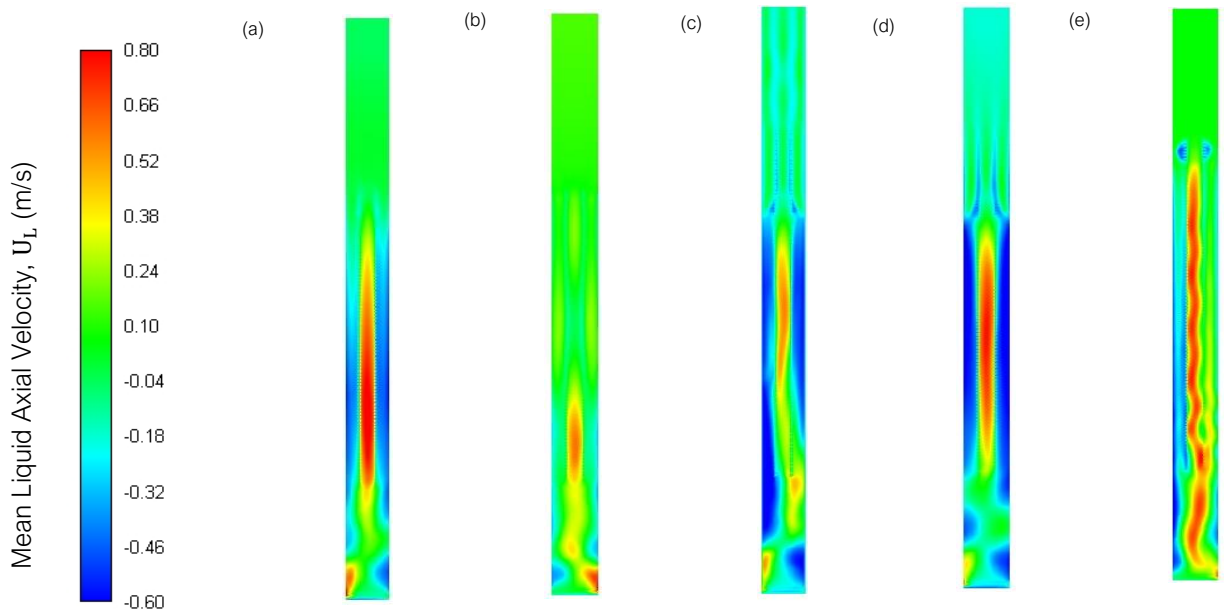


Figure 4.9 Influence of lift force models on axial liquid velocity distributions in the entire column

(a) No Lift Force, (b) Positive ($C_L=0.1$), (c) Negative ($C_L=-0.05$), (d) Negative ($C_L=-0.1$) and (e) Tomiyama model

The influence of lift force model on the gas holdup profiles is depicted in Figure 4.10 and Figure 4.11. In the case of a zero lift force, the radial profiles of the gas holdups between the internals, and between the internal and the column wall are close to the experimental trends in the literature. The same trend is noticed for $C_L = -0.05$. However, when the magnitude of negative lift force increases ($C_L = -0.1$), the bubbles tend to move to the central region, which is of high liquid velocity. This leads to a steep increase in the gas holdup at $r/R=0$ followed by a decrease in the gas holdup between the internal and column wall. Using a positive lift coefficient leads to a slight underprediction of the gas holdup at $r/R=0$ and overestimation of gas holdup between the internal and column wall as compared to the zero and negative lift coefficients. Out of all the lift coefficients, Tomiyama model overpredicted the gas holdups in the central region as well as the region between the internal and column wall.

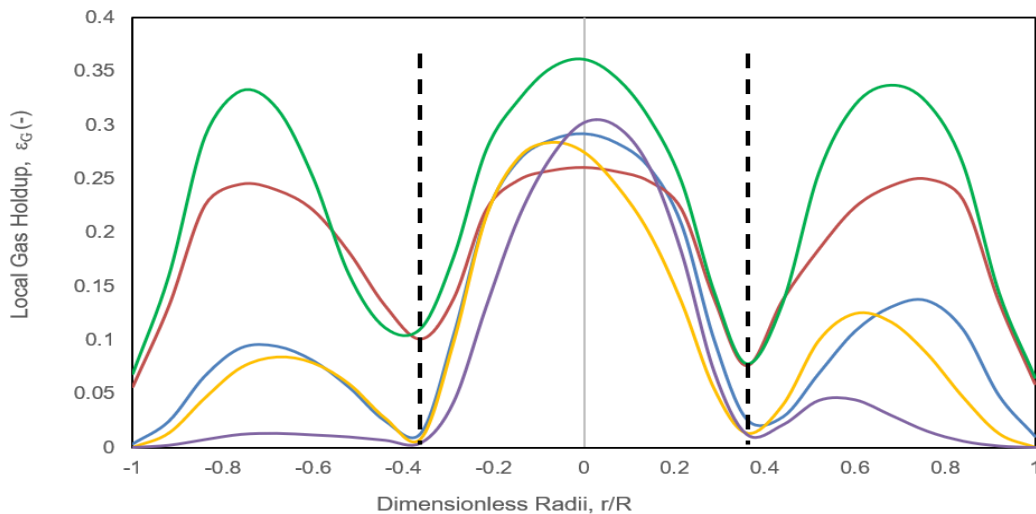


Figure 4.10 Influence of lift force models on the radial profiles of the gas holdups in the transition regime ($U_G=10$ cm/s)

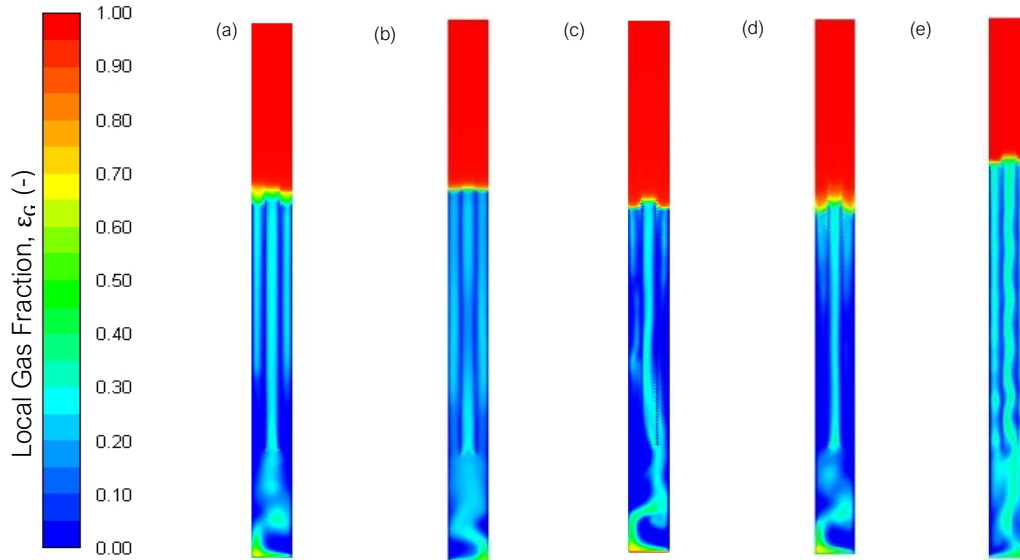


Figure 4.11 Influence of lift force models on gas holdup distributions in the entire column

(a) No Lift Force, (b) Positive ($C_L=0.1$), (c) Negative ($C_L=-0.05$),
(d) Negative ($C_L=-0.1$) and (e) Tomiyama model

4.3.1.2 Influence of the turbulence dispersion force

The effect of turbulent dispersion model on the flow patterns in the reactor column is investigated in the transition regime (10 cm/s) and the radial profiles and contours of the liquid axial velocities using different turbulent dispersion models are shown in Figure 4.12 and Figure 4.13, respectively. When the turbulent dispersion force is neglected ($C_{TD}=0$), the liquid velocity distribution in the radial direction is asymmetric as shown in Figure 4.12. This can be attributed to the improper spreading of the plume within the column when the turbulent dispersion force is neglected. Positive axial velocity is noticed between $r/R=0$ and $r/R = -0.361$ (between column wall and internal) which is contradictory to the experimental observations. When turbulent dispersion model proposed by Simonin et al. (1990) is used, the predicted radial profile for the liquid axial velocity is symmetric. With $C_{TD}=0.3$, a good match of centerline liquid velocity with experimental observation (shown

in Figure 4.18) is achieved. However, lowering the value of C_{TD} leads to overestimation of the liquid axial velocity.

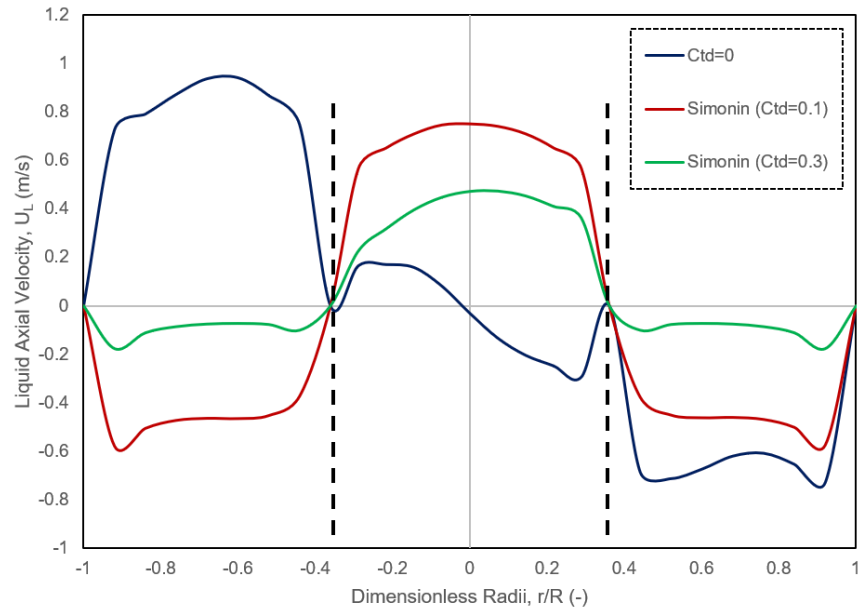


Figure 4.12 Influence of the turbulent interaction model on the radial profiles of the liquid axial velocities

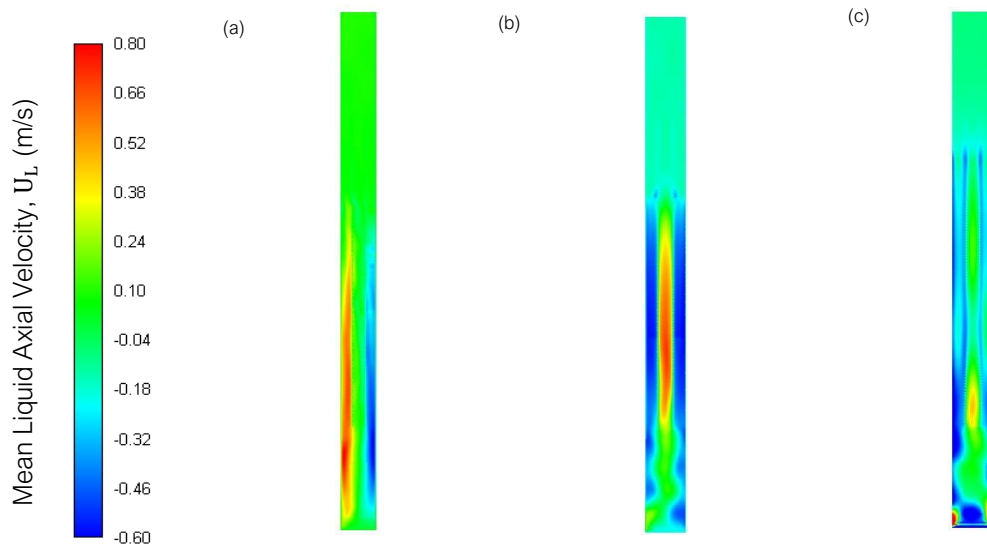


Figure 4.13 Influence of turbulent dispersion model on the liquid axial distribution over the entire column

(a) No turbulent dispersion ($C_{TD}=0$) (b) Simonin et al. model ($C_{TD}=0.1$) (c) Simonin et al. model ($C_{TD}=0.3$)

The influence of the turbulent dispersion force model on the gas holdup distributions can be seen in Figure 4.14. When $C_{TD}=0$, the plume travels through the central region between the internals and between the internal and the column wall, which limits the dispersion and leads to an asymmetric radial profile for the gas holdup in the central region as shown in Figure 4.14. This also leads to overestimation of radial gas holdup peak by 42.3% in the central region and about 17% in the region between the internal and the column wall as compared to when $C_{TD}=0.1$ is employed. When employing the turbulent dispersion model proposed by Simonin et al., the gas plume seems to disperse, which lowers the gas holdup peak. When increasing the turbulent dispersion coefficient from 0.1 to 0.3, the gas holdup at the wall increases. In comparison, the gas holdups obtained with $C_{TD}=0.1$ are close to the experimental data. The radial gas distribution within the column is depicted in Figure 4.15.

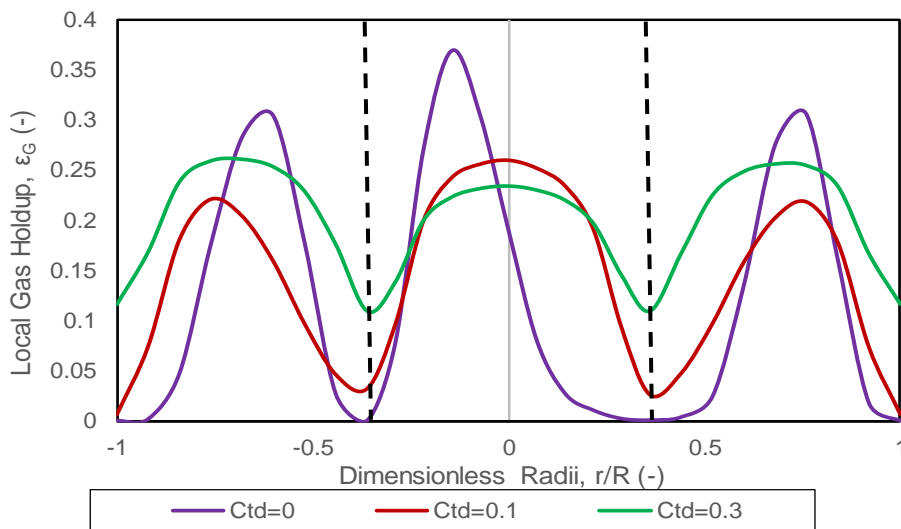


Figure 4.14 Influence of the turbulent dispersion model on the radial profiles of the gas holdups

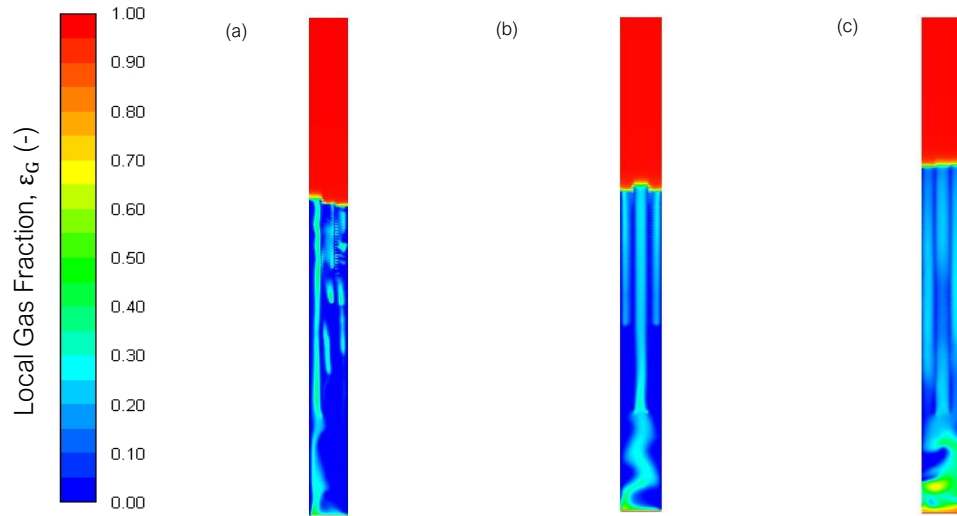


Figure 4.15 Influence of the turbulent dispersion model on the gas holdup distributions in the entire reactor column

(a) No turbulent dispersion ($C_{TD}=0$), (b) Simonin et al. model ($C_{TD}=0.1$), (c) Simonin et al. model ($C_{TD}=0.3$) and (d) Negative ($C_L = -0.1$) (e) Tomiyama model

4.3.2 Reactor hydrodynamics, flow patterns and turbulence parameters variations with the flow regime transition

In this study, the discrete PBM is used to carry out the two-phase numerical simulations in a hollow bubble column reactor. The simulations are carried out in bubbly flow, transition and churn-turbulent regimes at superficial gas velocities of 0.04 m/s, 0.10 m/s and 0.30 m/s, respectively. For the flow regime transition studies, the interfacial forces are kept the same for all flow regimes and they are listed in Table 4.2. The Reynolds Stress Model (RSM) with the dispersed formulation is used as the turbulence model in the current study. The parameters used in the PBM model, such as number of bins, bin sizes and the choice of kernels, are outlined in Table 4.3. The centerline liquid velocities obtained from the simulation in all the flow regimes are validated against experimental data of Chen *et al.* (1999), Jhawar and Prakash (2014) and Al Mesfer *et al.* (2017). The predicted overall gas

holdups in all the flow regimes are validated against a wide range of experimental data (Hamed, 2010) Kagumba, 2013, Jhavar and Prakash, 2014 , Guan *et al.*,2015, and Al Mesfer *et al.*, 2016). Further, the predicted overall gas holdups are also compared with our experimental values using visual photography technique (Appendix – D).

Table 4.2 Interfacial forces used in the flow regime transition studies

Interfacial force type	Model	Coefficients
Added mass	Constant	$C_{VM} = 0.5$ (spherical bubbles)
Drag	Schiller-Naumann	$C_d = \begin{cases} \frac{24 (1 + 0.15 N_{Re}^{0.687})}{N_{Re}}, & N_{Re} \leq 1000 \\ 0.24, & N_{Re} > 1000 \end{cases}$
Lift	Constant	$C_L = -0.05$
Wall lubrication	None	
Turbulent dispersion	Simonin	$C_{TD} = 0.1$
Turbulence interaction	Troshko-Hassan	$C_{ke} = 0.75$ and $C_{TD} = 0.45$
Interfacial area	ia-particle	

Table 4.3 Parameters used in the PBM for flow regime transition studies

PBM Parameters	Model/Input Value
Method	Discrete
Number of bins	13
Ratio exponent	1.3

Minimum diameter	1 mm	
Maximum diameter	36.75 mm	
Aggregation kernel	Luo-model	
Breakage kernel	Luo-model	
Formulation	Ramakrishna	
Bin Sizes	Bin Number	Bin Size (m)
	Bin-0	0.0367
	Bin-1	0.0272
	Bin-2	0.0202
	Bin-3	0.0149
	Bin-4	0.0111
	Bin-5	0.0082
	Bin-6	0.0061
	Bin-7	0.0045
	Bin-8	0.0033
	Bin-9	0.0024
	Bin-10	0.0018
	Bin-11	0.0013
	Bin-12	0.0010

Variations of axial liquid velocities in the radial direction for the bubble column with 15 vertical internals are shown in Figure 4.16. The trend in the radial distribution of axial liquid velocities is similar to that seen in experimental observations. An upward flow of the liquid between the internals is noticed and a reverse flow between the internal and column wall is noted. The flow inversion takes place at the internal wall. When the superficial gas velocity increases from 0.04 to 0.1 m/s, the centerline liquid velocity increases from 0.377 m/s to 0.567 m/s, respectively. At a superficial gas velocity of 0.3 m/s, the centerline liquid velocity is 0.856 m/s. It should also be pointed out here that the center line liquid velocities with the concentric tube internals are about 30% higher than

those in the hollow bubble column (Figure 3.26). This is due to tunneling effect of the internals, which directs the large bubbles and their associated wake to pass through the central region. Variations of axial liquid velocities in the radial direction for the bubble column with 38 vertical internals are shown in Figure 4.17. It can be observed that radial profiles are flatter at the center than those in the single tube bundle column and the second tube bundle is clearly affecting the profile of the inverted flow. It is observed that the radial profiles between the second internal and the column wall are relatively flat.

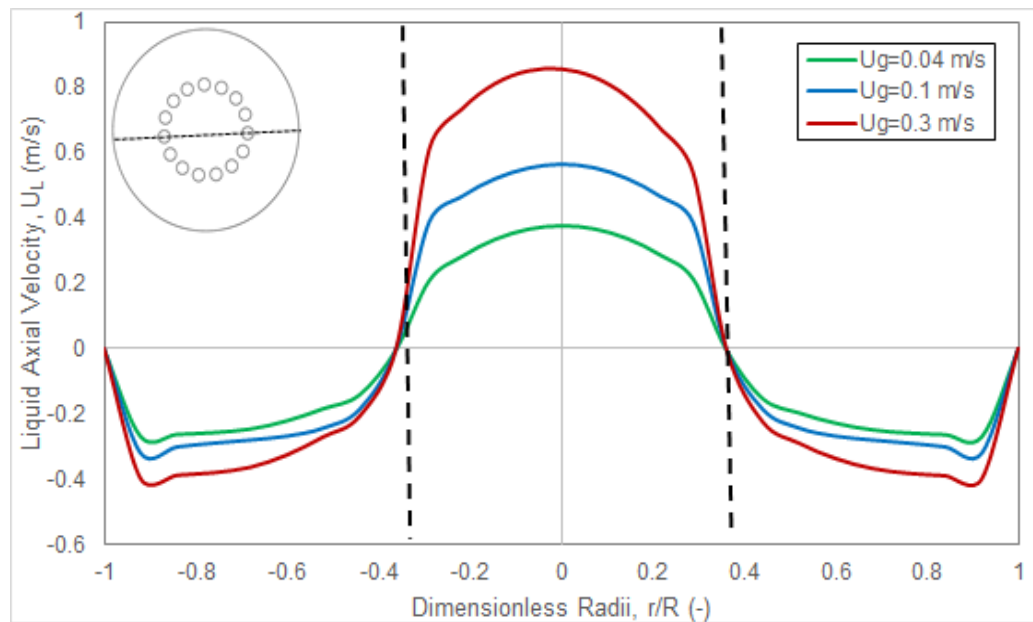


Figure 4.16 Comparison of liquid axial velocity profiles in various transition regimes for the bubble column with 15 tubes (a single circular tube bundle)

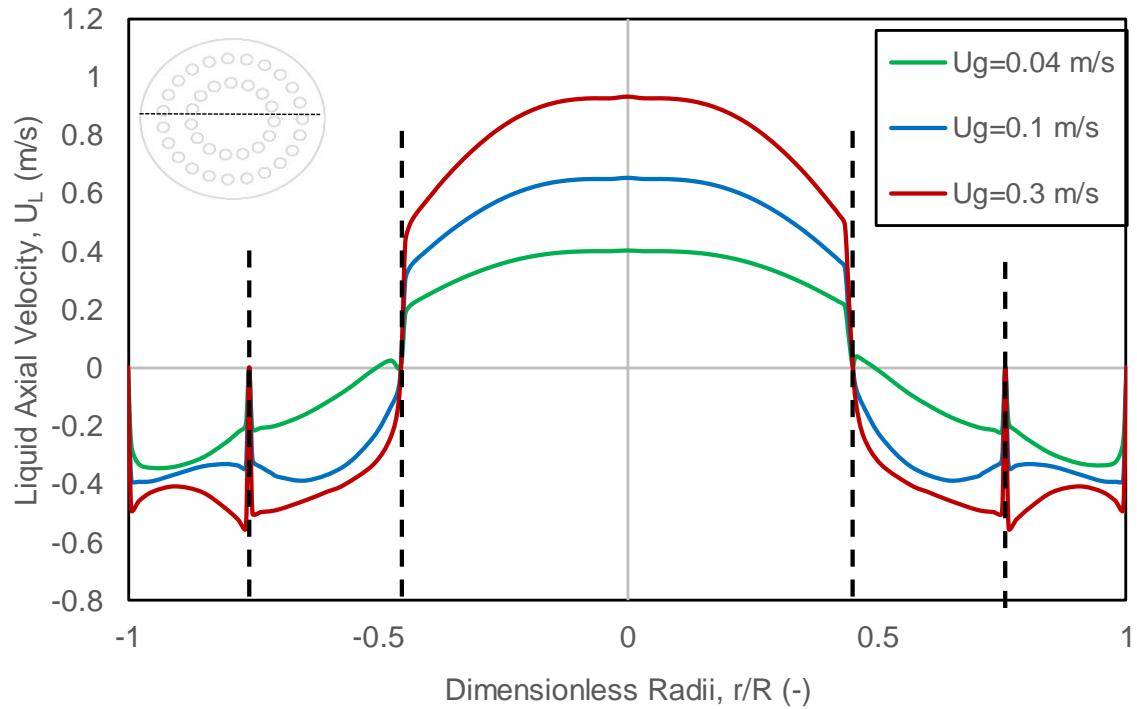


Figure 4.17. Comparison of liquid axial velocity profiles in various transition regimes for the bubble column with 38 tubes (double circular tube bundles)

A comparison of centerline liquid axial velocities with the experimental data from Jhawar and Prakash (2014), Al Mesfer et al. (2017) and Chen et al. (1999) is shown in Figure 4.18. A good agreement between the experimental and numerical results can be seen. In the bubbly regime, the centerline liquid velocity in the bubble column with 15-tube internals is close to that in the bubble column with 38-tube internals. However, for higher superficial gas velocities, the centerline liquid velocities in the bubble column with 38-tube internals are higher than those in the bubble column with 15-tube internals. This is due to the decrease in the flow area if there are more tubes in the column, which results in a higher velocity.

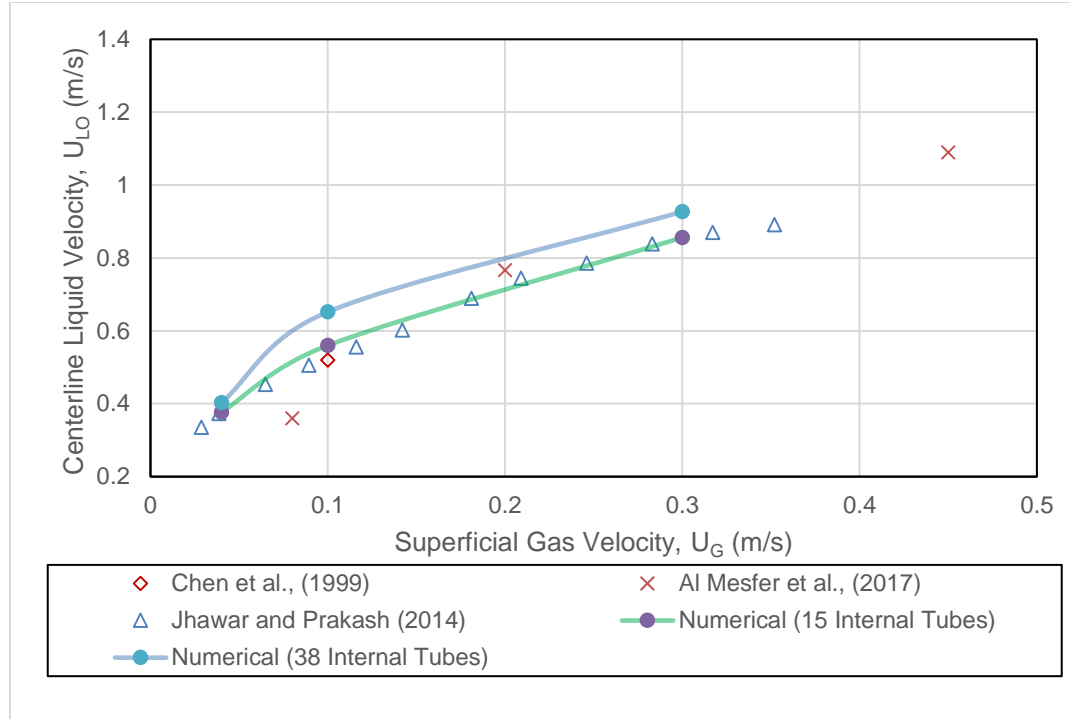


Figure 4.18 Comparison of the centerline liquid velocities with the experimental data in different transition regimes

The variations of gas holdups in the radial direction for the bubble column with 15 tubes are shown in Figure 4.19. Such trends in the radial distribution of gas holdups between internals were described by Sultan et al. (2018b). In the core region, the gas holdups are higher than those between the internal and column wall. In the proximity of the wall, the radial gas holdups are low due to the increased shear stress. The downward liquid flow in the annular region entrains smaller bubbles (2 to 4 mm) due to their low rise velocities. This leads to increased residence time of the small bubbles in the region, which leads to higher gas holdups. It is noticed that the local gas holdups increase when transitioning from the bubbly regime to the churn-turbulent regime, which is consistent with the experimental observations of Sultan et al. (2018b).

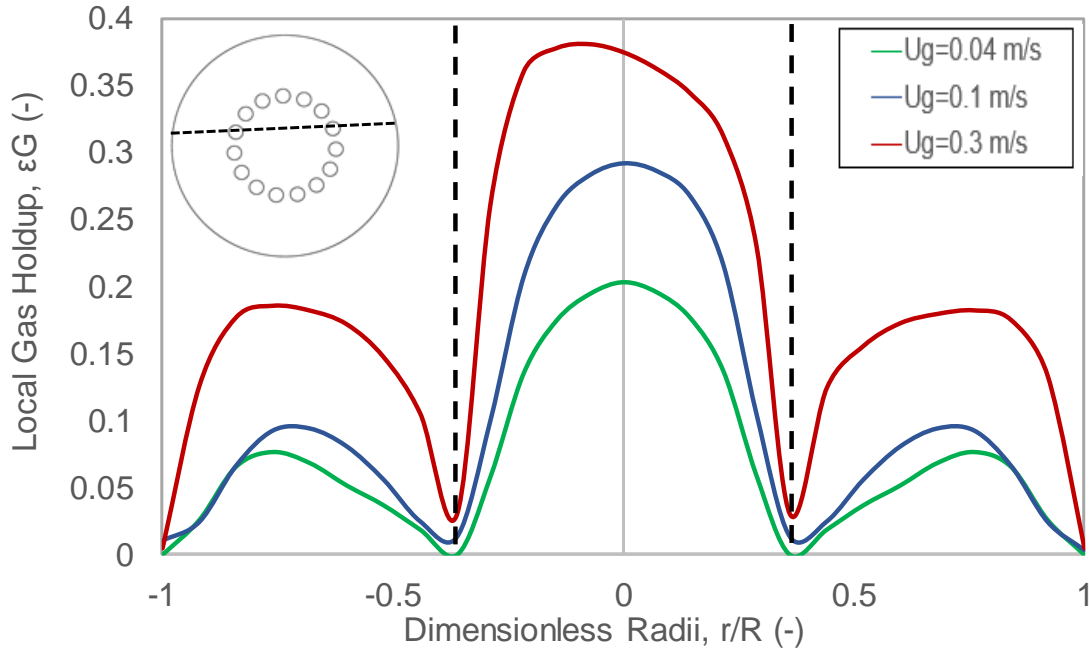


Figure 4.19 Comparison of gas holdup profiles in various transition regimes for the bubble column with 15 tubes (single circular tube bundle)

The radial profiles of the gas holdups in different transition regimes for the bubble column with 38 tube internals are illustrated in Figure 4.20. Similar to the case for the 15-tube column, the gas holdups are significantly increased with the increase in the superficial gas velocity. In the transition and churn turbulent regimes, higher gas holdup values are noticed between the internals, and between the internal and column wall compared to those in the 15-tube column. The trend of the predicted radial profiles of the gas holdup is in line with the experimental observations by Bhusare *et al.* (2018) and Sultan *et al.* (2018b). The bulk circulation patterns in a bubble column are developed by the fast rising of larger bubbles and their wakes in the core region. The entrained liquid moves towards the top of the bed, then flows down in the annular region, which entrains smaller bubbles into this region. Part of this down flow liquid can be pulled into the core region. However, this effect can be reduced due to the reduced flow area caused in the presence of tube bundles. This can lead to

greater accumulation of smaller bubbles in the annular region, which results in a higher gas holdup.

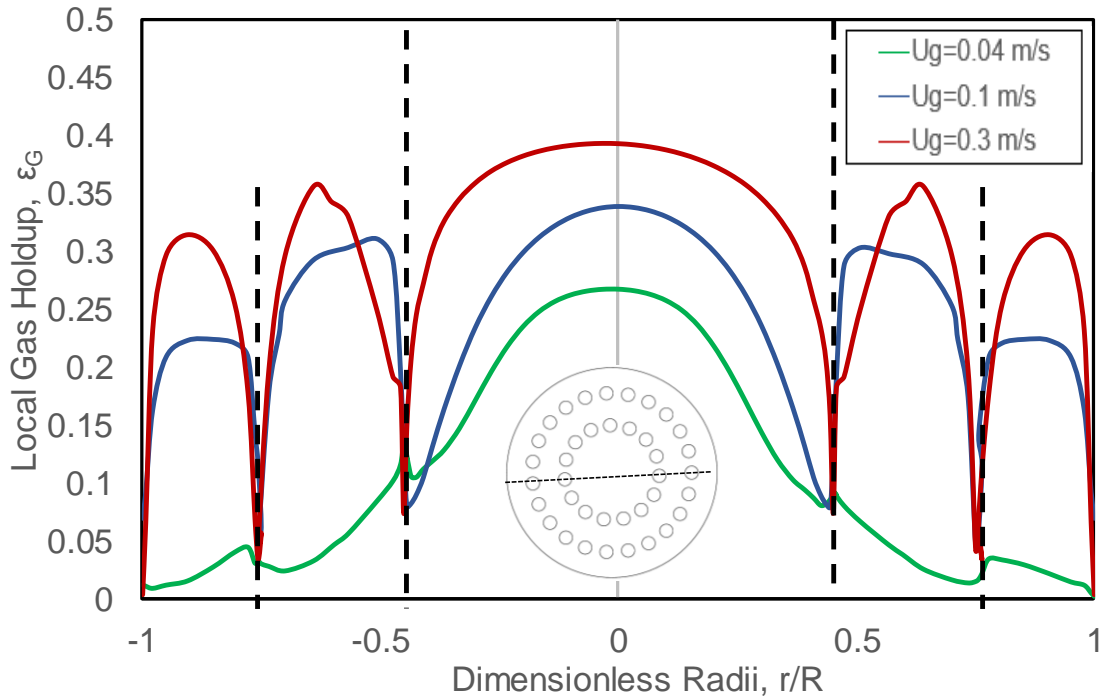


Figure 4.20 Comparison of gas holdup profiles in various transition regimes for bubble column with 38 tubes (Dense tube internals)

Figure 4.21 shows the comparison between the predicted overall gas holdups and the experimental data from Jhawar and Prakash (2014); Kagumba (2013); Guan *et al.* (2015) and Hamed (2012). It can be seen that an increase in the overall gas holdups with the increase in the superficial gas velocity. For 15 tube internal column, at superficial gas velocities of 0.04 and 0.1 m/s, the overall gas holdups are close to the experimental values reported by Hamed (2010), Kagumba (2013), Jhawar and Prakash (2014), Guan *et al.* (2015), and Al Mesfer *et al.* (2016). In the churn-turbulent regime, the gas holdup obtained by Jhawar and Prakash (2014) is lower than those attained in other studies. This could be attributed to various factors like difference in measurement technique, percentage of area

occluded by internals and averaging techniques. However, the numerical model has slightly overpredicted the overall gas holdup at $U_G=0.3$ m/s, but it is close to that obtained by Guan *et al.* (2015). For the 38 tube internal column, in the transition regime ($U_G=10$ cm/s), there is a slight increase in the overall gas holdup when compared to the 15 tube column. At a lower superficial gas velocity, the increase is 22.45% followed by 16.31% and 15.94% at superficial gas velocities of 0.1 and 0.3 m/s, respectively. When the column is occluded with internals increases, the larger bubbles break into smaller bubbles. Small bubbles tend to increase the overall gas holdup in the column. In our experimentation, visual photographic method was employed to determine the overall gas holdups. At lower gas superficial velocities, the overall gas holdups are close to the experimental data. At higher gas superficial velocities ($U_G>0.1$ m/s), our experiments give a higher gas holdup. In the transition and churn turbulent regimes, more bubbles are produced near the disengagement region as a result of gas-liquid dispersion. In our visual technique, the foam generated was accounted for which results in higher values of overall gas holdup. The values have been presented after subtracting the height of foam layer.

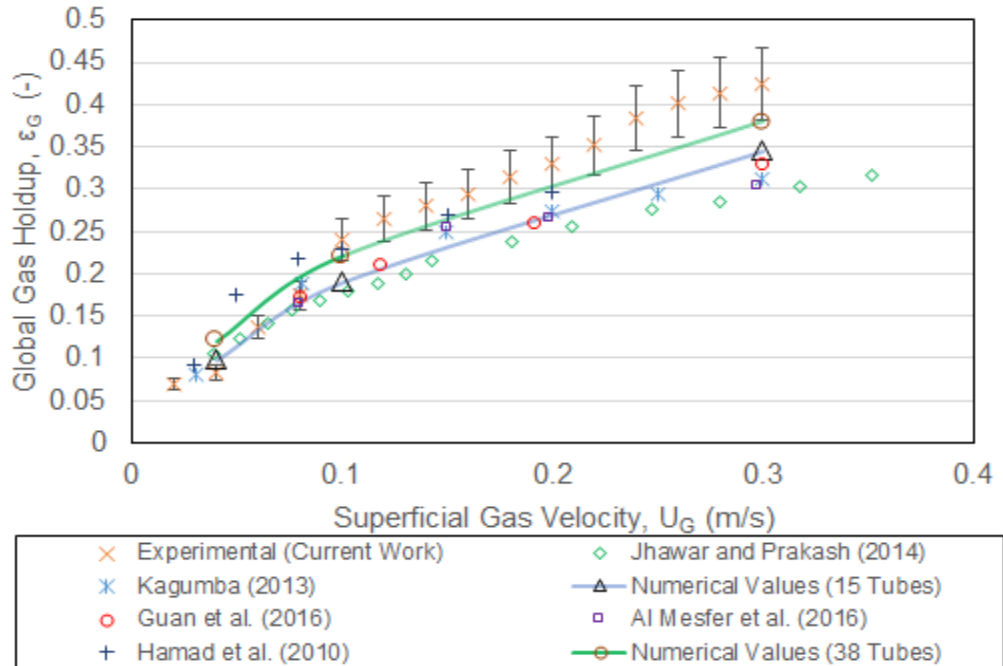


Figure 4.21 Comparison of the predicted overall gas holdups in bubbly, transition and churn-turbulent regimes with experimental data

The variations of turbulence parameters, of the turbulent viscosity ratio and turbulent Reynolds number, in the bubble columns with 15 and 38 tube internals are shown in Figures 4.22 and 4.23, and Figures 4.24 and 4.25, respectively. All RANS model accounts for the effect of turbulent eddies by determining the turbulent viscosity (ANSYS, 2013). Hence, finding turbulent viscosity ratio accurately accounts for the presence of eddies in the simulation. The turbulent Reynolds number is defined at the defined at the energy containing scale ($Re_T = k^{3/2}/\varepsilon$) (ANSYS, 2013). A decrease in the turbulent Reynolds number and turbulent viscosity ratio is noticed in the region occluded by internals as compared to the axial locations below the internals, which agree with the findings made in several literature studies (Chen, Li, *et al.*, 1999); (Ann Forret *et al.*, 2003); (Hamed, 2012)

and (Al Mesfer, et al., 2017). The presence of vertical internals dampens the energy of turbulent eddies of bubble-induced turbulence.

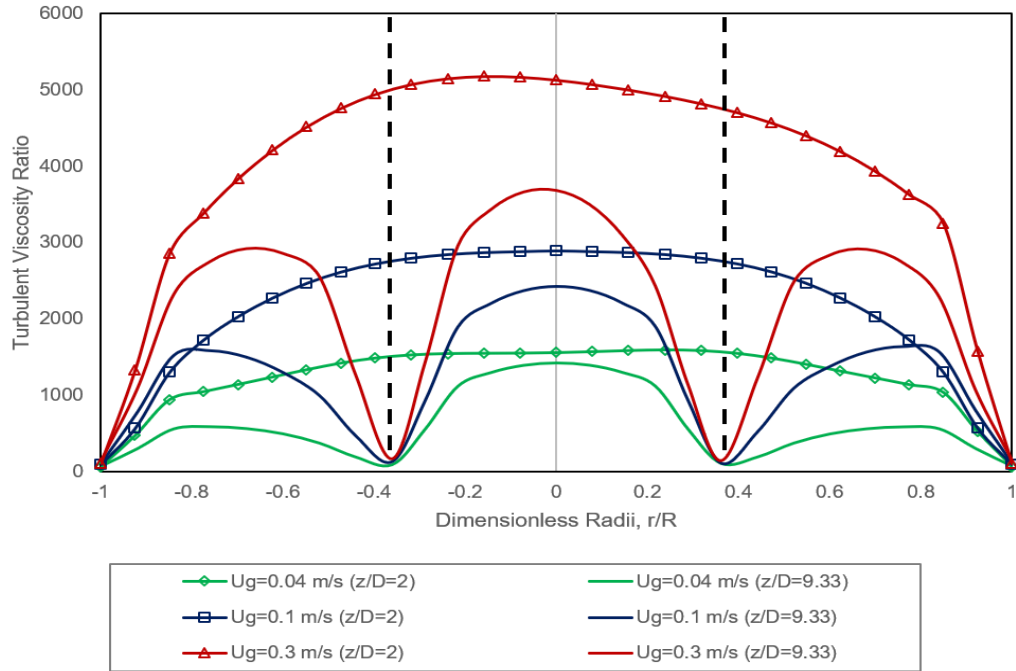


Figure 4.22 Effect of internals on the turbulent viscosity ratio in bubbly, transition and churn-turbulent regime for the bubble column with 15 tubes (single circular tube bundle)

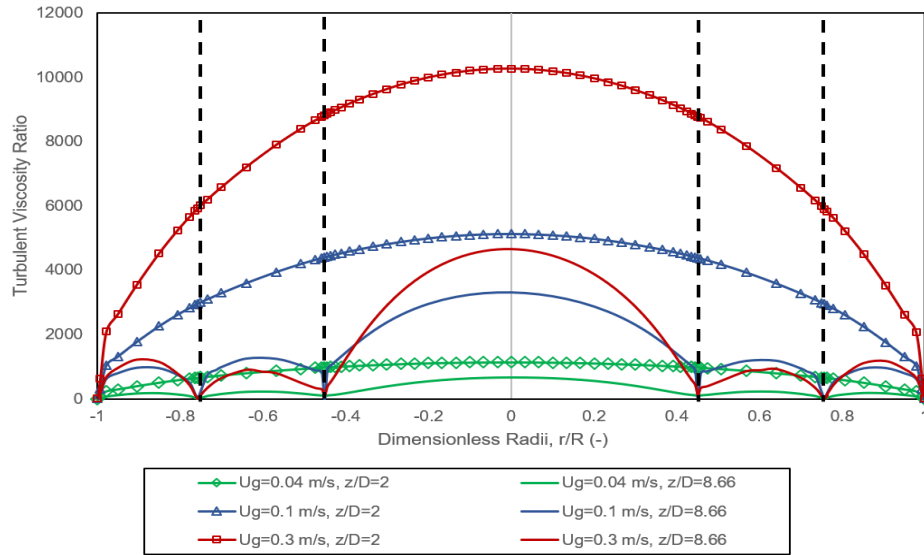


Figure 4.23 Effect of internals on the turbulent viscosity ratio in bubbly, transition and churn-turbulent regime for the bubble column with 38 tubes (double circular tube bundles)

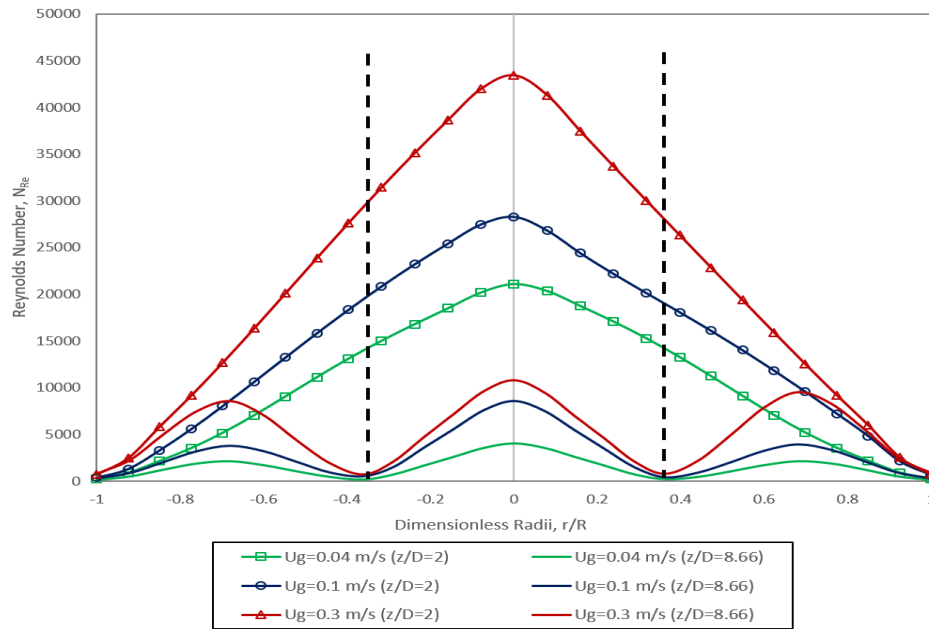


Figure 4.24 Effect of internals on turbulent Reynolds number in bubbly, transition and churn-turbulent regime for bubble column with 15 tubes (single circular tube bundle)

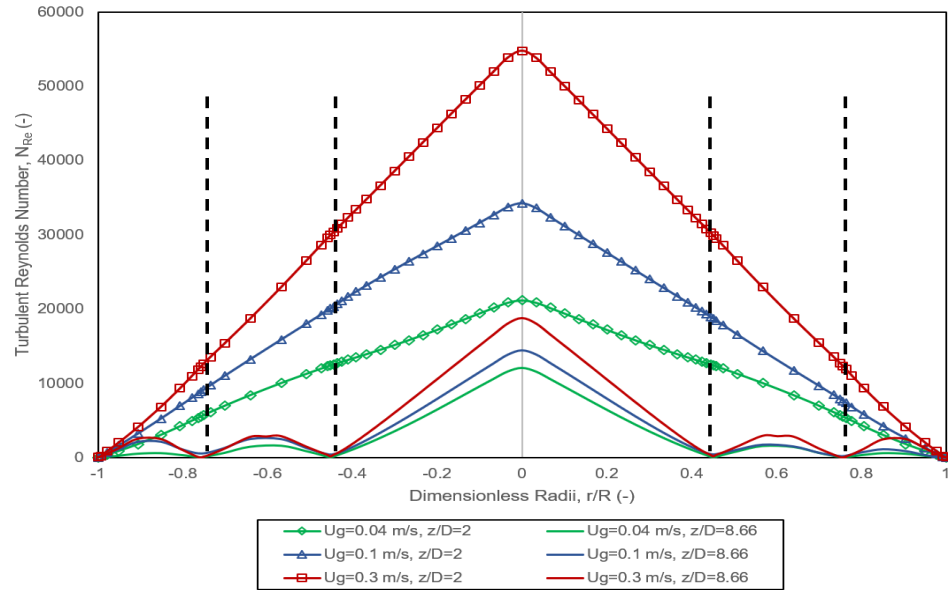


Figure 4.25 Effect of internals on turbulent Reynolds number in bubbly, transition and churn-turbulent regime for bubble column with 38 tubes (double circular tube bundles)

A comparison of bubble fraction distributions between the two bubble columns with different internal configurations is made for each flow regime and is illustrated in Figures 4.26, 4.27 and 4.28, respectively. In all the flow regimes, it is noticed that fraction of small bubbles is high for the column with 38 internals. Also, the fraction of large bubbles is low for the column with 38 internals as compared to the column with 15 internals. A higher break-up rate is apparent with the increase in the density of internals within the bubble column. These trends are similar to the experimental observations made by Thimmapuram *et al.* (1993) and Youssef *et al.* (2012). In a recent experimental study, Möller *et al.* (2018) observed that increasing the density of the internals in the column gives a distinct difference in the peak of small bubbles at lower superficial gas velocities and the peak reduces with the increase in superficial gas velocities. It is worth noting that the difference in the peaks of small bubble fraction between the columns with 15 internals and 38 internals decreases when transitioning from the bubbly regime to the churn-turbulent regime.

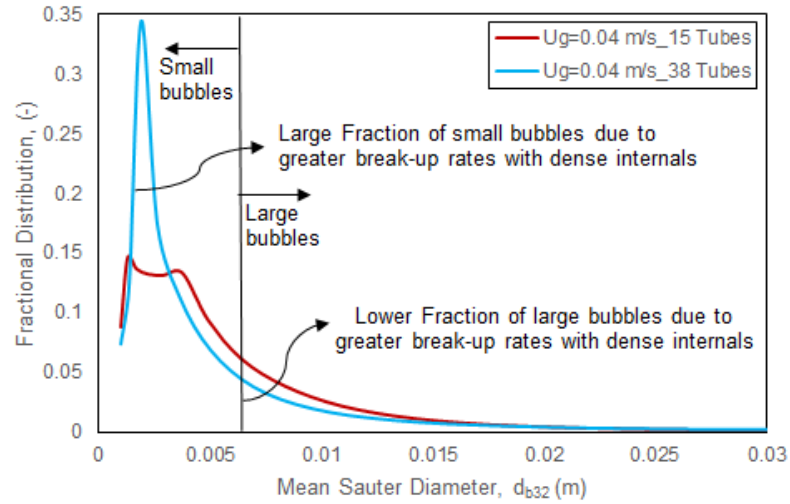


Figure 4.26 Effect of the density of internals in the column on the bubble size distribution in the bubbly flow regime

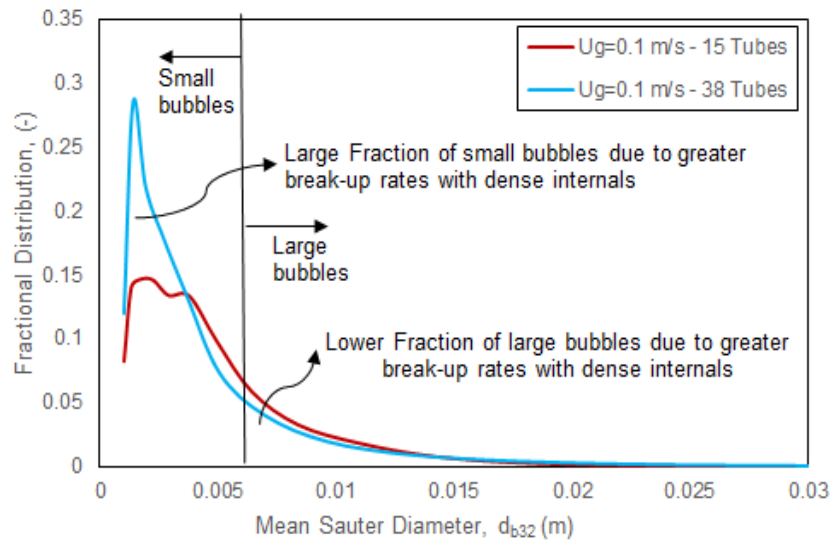


Figure 4.27 Effect of the density of internals in the column on the bubble size distribution in the transition flow regime

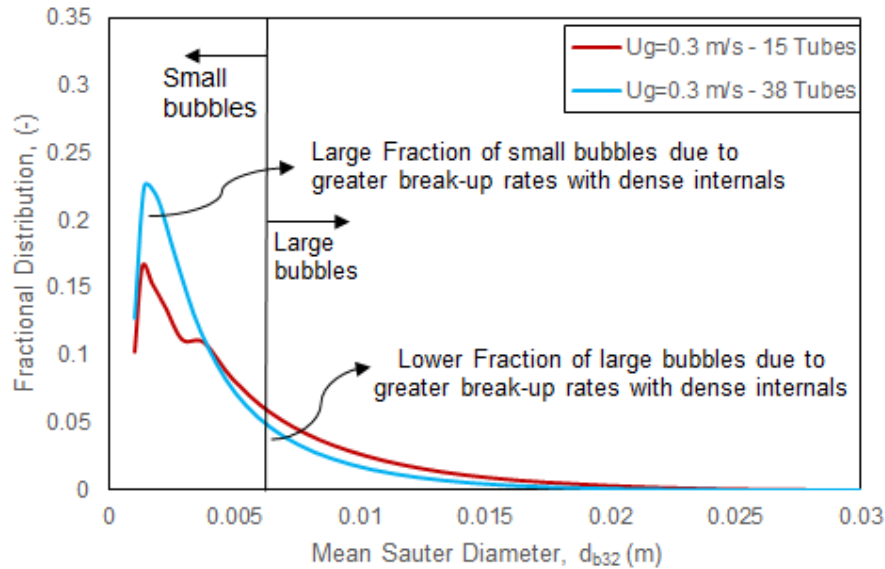


Figure 4.28 Effect of the density of internals in the column on the bubble size distribution in the churn-turbulent flow regime

The flow patterns near the bottom of the internals, bulk section and top region close to the disengagement zone in the column with 15 internals are illustrated in Figures 4.29, 4.30 and 4.31, respectively. In addition, Figures 4.32, 4.33 and 4.34 show the flow patterns near the bottom of the internals, bulk section and top region close to the disengagement zone in the column with 38 internals, respectively. A downward flow is noticed close to the wall region and an upward flow occurs in the core region between the internals. Near the bottom section of the internals in the column with 15 tubes, the liquid flowing downward near the wall region flows to the core region via the gaps between the tubes and through the circular tube bundle opening. Near the bulk section of the internals in the column with 15 tubes, the liquid flows from the core region to the region close to the wall via the gaps between the tubes and the liquid then flows in a downward direction. Close to the dynamic height in the column with 15 tubes, funneling patterns are noticed in which some of the liquid follows upward and the rest flows in between the tube gaps where the liquid flows in a downward

direction. When the density of internals in the column increases, the flow patterns within the bubble column are close to those noticed in the column with less internals. However, a higher degree of mixing is noticed when the internal density increases as shown in Figure 4.35. When an extra tube bundle is added parallel to the existing tube bundle, the liquid flows between the tube gaps of the outer bundle to the tube gaps in the inner bundle and vice versa which increases the liquid circulations within the column. A generalized flow mapping for bubble columns with 15 tube and 38 tube internals is depicted in Figure 4.36. The mixing patterns with a single tube bundle close to the experimental observations made by George et al. (2017).

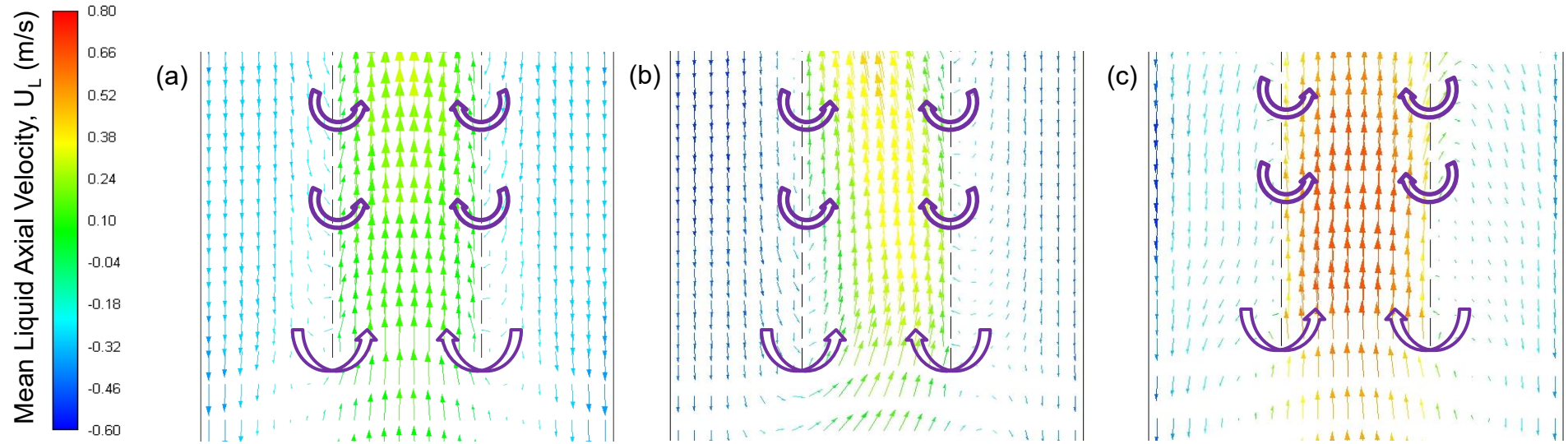


Figure 4.29 Flow patterns near the bottom section of the internals in the column with 15 tubes

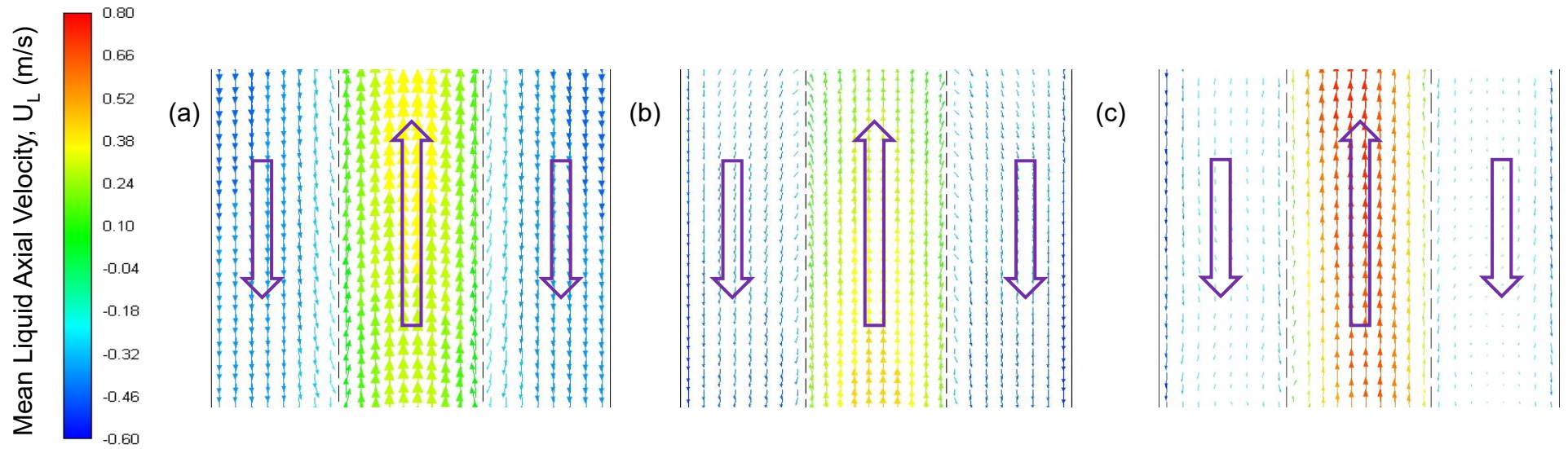


Figure 4.30 Flow patterns in the bulk section of the column with 15 tubes

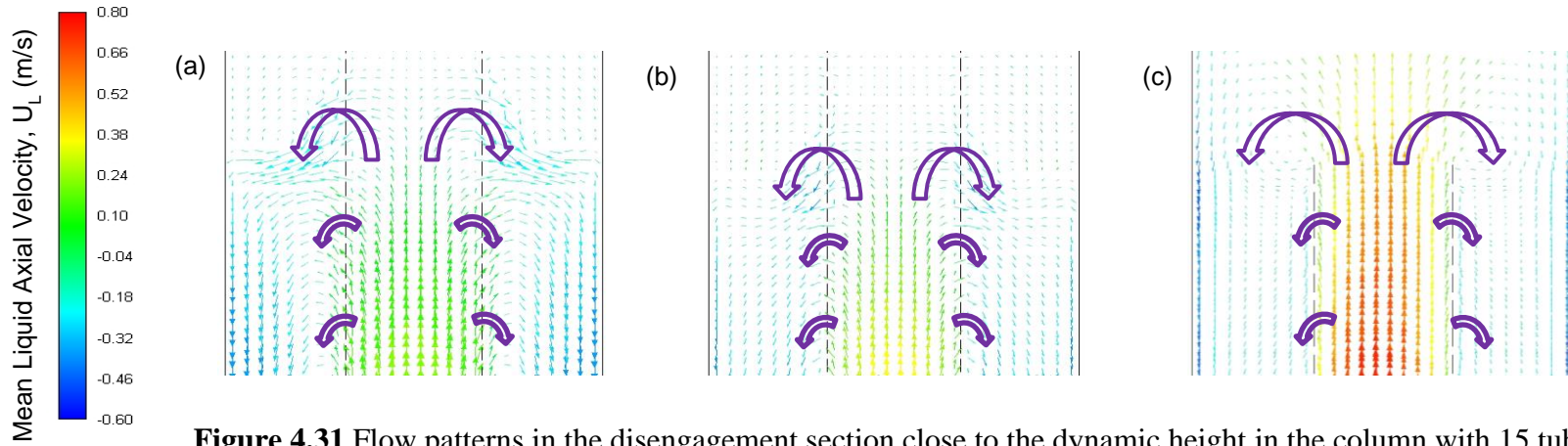


Figure 4.31 Flow patterns in the disengagement section close to the dynamic height in the column with 15 tubes

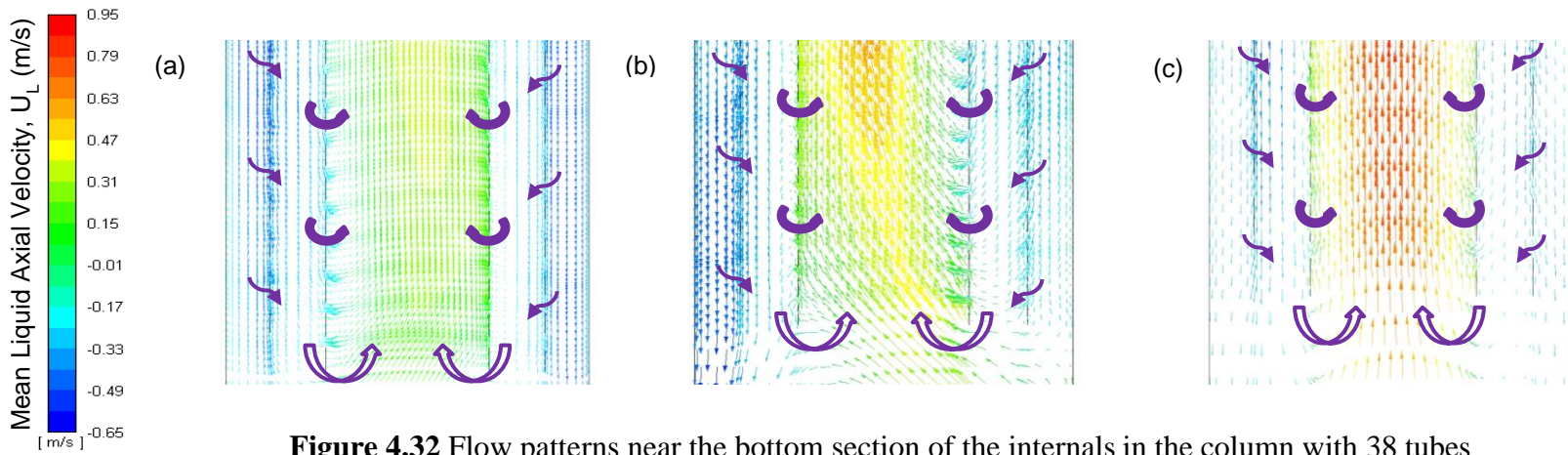


Figure 4.32 Flow patterns near the bottom section of the internals in the column with 38 tubes

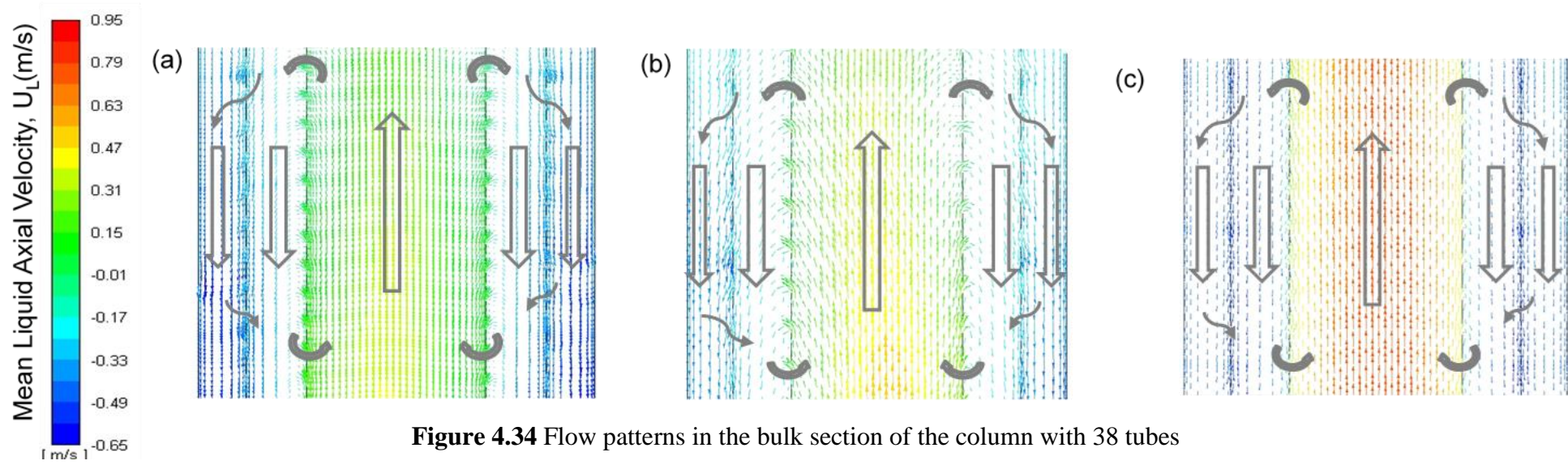


Figure 4.34 Flow patterns in the bulk section of the column with 38 tubes

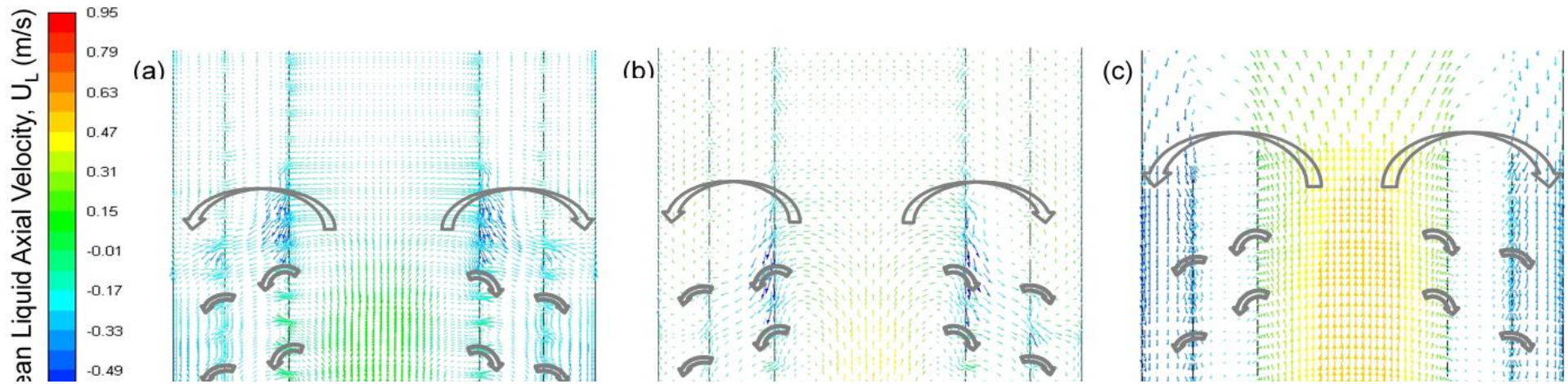


Figure 4.33 Flow patterns in the bulk section of the column with 38 tubes

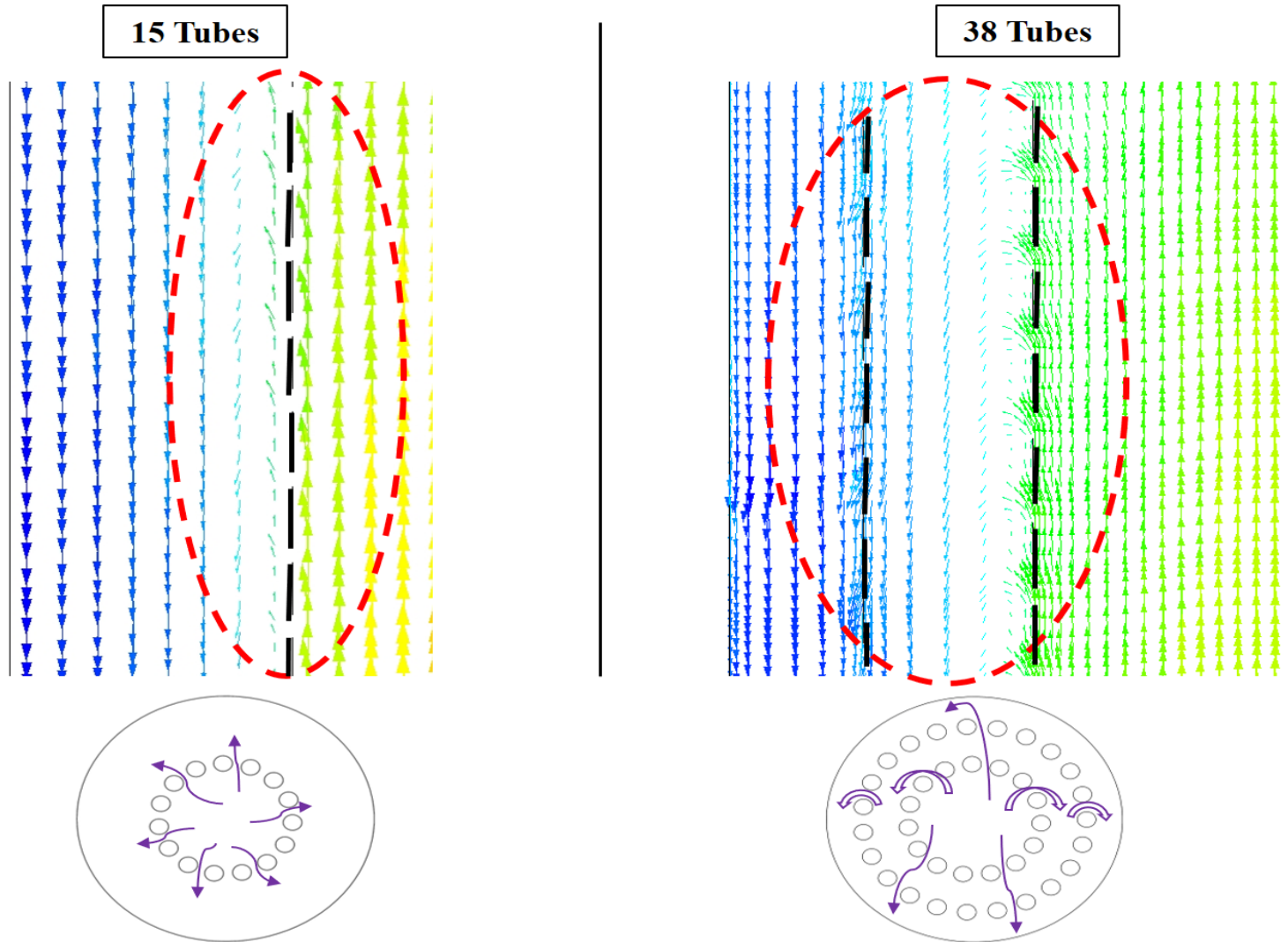


Figure 4.35 Comparison of flow patterns and mixing patterns between the columns with 15 tubes and 38 tubes

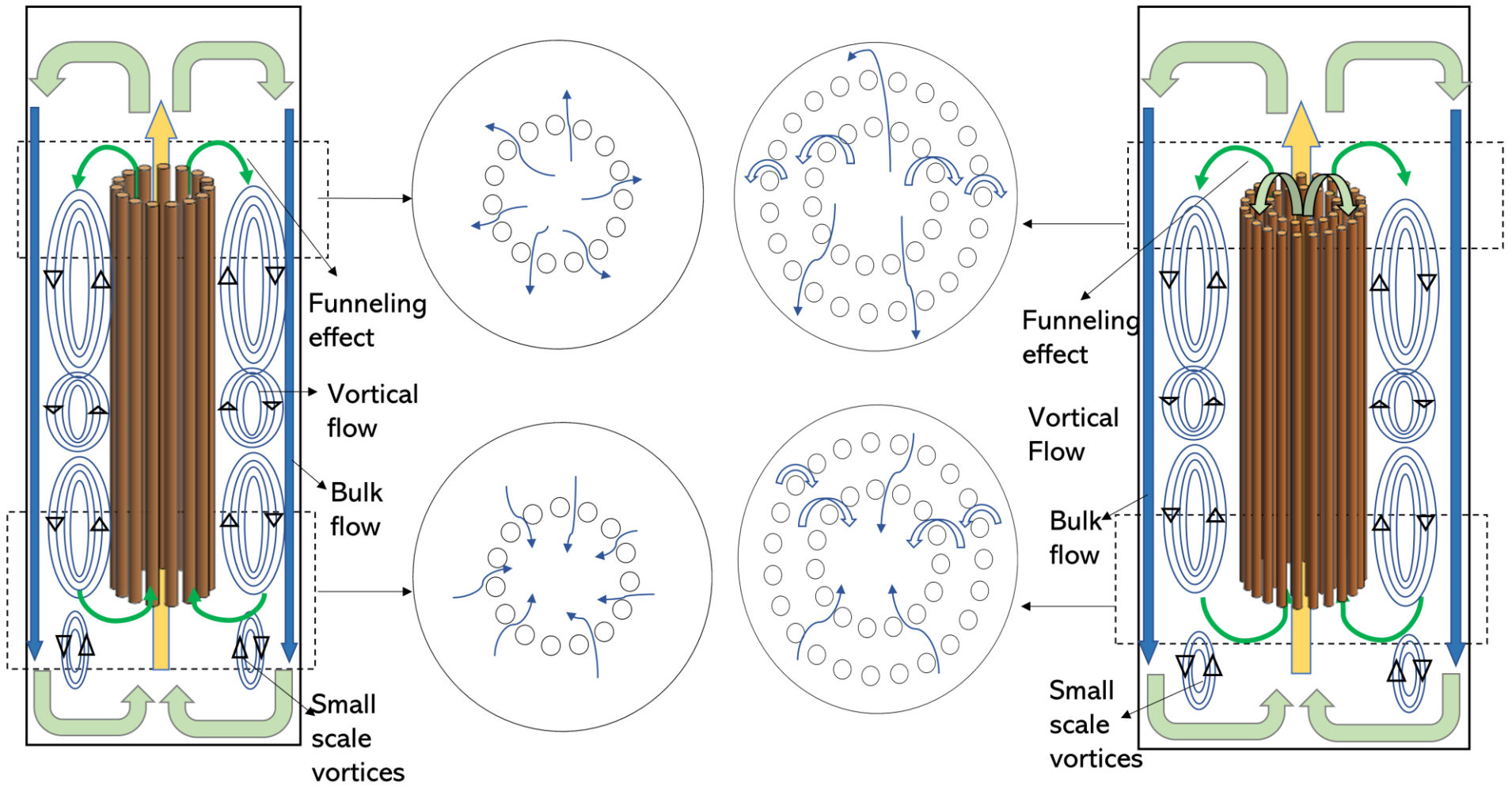


Figure 4.36 Generalized flow mapping for bubble columns with less and dense vertical internals

4.4 Conclusion

In the present work, the effect of internals on the flow hydrodynamics has been thoroughly investigated. The influence of the lift force and turbulence dispersion on the numerical solution has been studied. The zero lift force model can predict the gas holdup and liquid axial velocity distributions reasonably well. Simonin turbulence dispersion model is able to effectively predict the dispersion of the gas phase and give good gas holdup and liquid axial velocity distributions. The presence of an additional bundle results in flatter liquid velocity profiles in the column center. Higher axial liquid velocity and gas holdup are noticed with the addition of a second internal tube. This leads to greater accumulation of small bubbles, which adds to the gas holdup. Lower turbulence parameters in the bulk region are attributed to the dissipation of turbulent eddies in the presence of internals. A higher fraction of small bubbles is noticed in the presence of more internals, which indicates an increased rate of bubble break-up in the column.

References

- Abdulmohsin, R. S. and Al-Dahhan, M. H. (2012) 'Impact of internals on the heat-transfer coefficient in a bubble column', *Industrial & Engineering Chemistry Research*. ACS Publications, 51(7), pp. 2874–2881.
- Ali, N., Bilal, M., Nazir, M. S., Khan, A., Ali, F. and Iqbal, H. M. N. (2020) 'Thermochemical and electrochemical aspects of carbon dioxide methanation: A sustainable approach to generate fuel via waste to energy theme', *Science of The Total Environment*, 712, p. 136482.
- Besagni, G. and Inzoli, F. (2016) 'Influence of internals on counter-current bubble column hydrodynamics: Holdup, flow regime transition and local flow properties', *Chemical Engineering Science*. Elsevier, 145, pp. 162–180.
- Bhusare, V. H., Kalaga, D. V, Dhiman, M. K., Joshi, J. B. and Roy, S. (2018) 'Mixing in a co-current upflow bubble column reactors with and without internals', *The Canadian Journal of Chemical Engineering*. Wiley Online Library, 96(9), pp. 1957–1971.
- Chen, J., Li, F., Degaleesan, S., Gupta, P., Al-Dahhan, M. H., Dudukovic, M. P. and Toseland, B. A. (1999) 'Fluid dynamic parameters in bubble columns with internals', *Chemical Engineering Science*. Elsevier, 54(13–14), pp. 2187–2197.
- Desvigne, D., Donnat, L., Schweich, D. and others (2006) 'Simulating the effects of liquid circulation in bubble columns with internals', *Chemical engineering science*. Elsevier, 61(13), pp. 4195–4206.
- Duduković, M. P., Larachi, F. and Mills, P. L. (2002) 'Multiphase catalytic reactors: a perspective on current knowledge and future trends', *Catalysis reviews*. Taylor & Francis, 44(1), pp. 123–246.
- Forret, A, Schweitzer, J.-M., Gauthier, T., Krishna, R. and Schweich, D. (2003) 'Influence of scale on the hydrodynamics of bubble column reactors: an experimental study in columns of 0.1, 0.4 and 1m diameters', *Chemical Engineering Science*. Elsevier, 58(3–6), pp. 719–724.
- Forret, Ann, Schweitzer, J.-M., Gauthier, T., Krishna, R. and Schweich, D. (2003) 'Liquid Dispersion in Large Diameter Bubble Columns, with and without Internals', *The Canadian Journal of Chemical Engineering*, 81(3–4), pp. 360–366.
- George, K. J. H., Jhavar, A. K. and Prakash, A. (2017) 'Investigations of flow structure and liquid mixing in bubble column equipped with selected internals', *Chemical Engineering Science*. Elsevier, 170, pp. 297–305.

- Guan, X., Gao, Y., Tian, Z., Wang, L., Cheng, Y. and Li, X. (2015) 'Hydrodynamics in bubble columns with pin-fin tube internals', *Chemical Engineering Research and Design*. Elsevier, 102, pp. 196–206.
- Guan, X. and Yang, N. (2017) 'CFD simulation of pilot-scale bubble columns with internals: Influence of interfacial forces', *Chemical Engineering Research and Design*. Elsevier, 126, pp. 109–122.
- Hamed, M. (2012) 'Hydrodynamics, mixing, and mass transfer in bubble columns with internals'.
- Hulet, C., Clement, P., Tochon, P., Schweich, D., Dromard, N. and Anfray, J. (2009) 'Literature Review on Heat Transfer in Two- and Three-Phase Bubble Columns', *International Journal of Chemical Reactor Engineering*. Berlin, Boston: De Gruyter, 7(1).
- Jhawar, A. K. and Prakash, A. (2014) 'Bubble column with internals: Effects on hydrodynamics and local heat transfer', *Chemical Engineering Research and Design*. Elsevier, 92(1), pp. 25–33.
- Joseph, W. (2016) 'Three-phase catalytic reactors for hydrogenation and oxidation reactions', *Physical Sciences Reviews*. Berlin, Boston: De Gruyter, 1(1), p. 20150019.
- Kagumba, M. O. O. (2013) 'Heat transfer and bubble dynamics in bubble and slurry bubble columns with internals for Fischer-Tropsch synthesis of clean alternative fuels and chemicals'. Missouri University of Science and Technology.
- Knickle, H. N., Holcombe, N. T., O'Dowd, W. and Smith, D. N. (1983) 'Backmixing and heat transfer coefficients in bubble columns using aqueous glycerol solutions', in *AICHE Symp. Ser.:(United States)*.
- van der Laan, G. P., Beenackers, A. A. C. M. and Krishna, R. (1999) 'Multicomponent reaction engineering model for Fe-catalyzed Fischer-Tropsch synthesis in commercial scale slurry bubble column reactors', *Chemical Engineering Science*. Elsevier, 54(21), pp. 5013–5019.
- Ledakowicz, S., Stelmachowski, M., Chacuk, A. and Deckwer, W.-D. (1992) 'Methanol synthesis in bubble column slurry reactors', *Chemical Engineering and Processing: Process Intensification*. Elsevier, 31(4), pp. 213–219.
- Lefebvre, J., Götz, M., Bajohr, S., Reimert, R. and Kolb, T. (2015) 'Improvement of three-phase methanation reactor performance for steady-state and transient operation', *Fuel processing technology*. Elsevier, 132, pp. 83–90.

Li, H., Prakash, A., Margaritis, A. and Bergougnou, M. A. (2003) 'Effects of micron-sized particles on hydrodynamics and local heat transfer in a slurry bubble column', *Powder Technology*. Elsevier, 133(1–3), pp. 171–184.

Lucas, D., Prasser, H.-M. and Manera, A. (2005) 'Influence of the lift force on the stability of a bubble column', *Chemical Engineering Science*, 60(13), pp. 3609–3619.

Magolan, B., Lubchenko, N. and Baglietto, E. (2019) 'A quantitative and generalized assessment of bubble-induced turbulence models for gas-liquid systems', *Chemical Engineering Science: X*. Elsevier, 2, p. 100009.

Al Mesfer, M. K., Sultan, A. J. and Al-Dahhan, M. H. (2017) 'Study the effect of dense internals on the liquid velocity field and turbulent parameters in bubble column for Fischer–Tropsch (FT) synthesis by using Radioactive Particle Tracking (RPT) technique', *Chemical Engineering Science*. Elsevier, 161, pp. 228–248.

Möller, F., Lau, Y. M., Seiler, T., Hampel, U. and Schubert, M. (2018) 'A study on the influence of the tube layout on sub-channel hydrodynamics in a bubble column with internals', *Chemical Engineering Science*, 179, pp. 265–283.

Möller, F., Lavetty, C., Schleicher, E., Löschau, M., Hampel, U. and Schubert, M. (2019) 'Hydrodynamics, mixing and mass transfer in a pilot-scale bubble column with dense internals', *Chemical Engineering Science*. Elsevier, 202, pp. 491–507.

Ni, M., Leung, D. Y. C., Leung, M. K. H. and Sumathy, K. (2006) 'An overview of hydrogen production from biomass', *Fuel Processing Technology*, 87(5), pp. 461–472.

Nygren, A. (2014) 'Simulation of bubbly flow in a flat bubble column'.

Rados, N., Al-Dahhan, M. H. and Dudukovic, M. P. (2003) 'Modeling of the Fischer–Tropsch synthesis in slurry bubble column reactors', *Catalysis Today*. Elsevier, 79, pp. 211–218.

Rahimpour, M. R., Jokar, S. M. and Jamshidnejad, Z. (2012) 'A novel slurry bubble column membrane reactor concept for Fischer–Tropsch synthesis in GTL technology', *Chemical engineering research and design*. Elsevier, 90(3), pp. 383–396.

Saxena, S. C., Rao, N. S. and Thimmapuram, P. R. (1992) 'Gas phase holdup in slurry bubble columns for two-and three-phase systems', *The Chemical Engineering Journal*. Elsevier, 49(3), pp. 151–159.

Shaikh, A. and Al-Dahhan, M. (2013) 'Scale-up of bubble column reactors: a review of current state-of-the-art', *Industrial & Engineering Chemistry Research*. ACS Publications,

52(24), pp. 8091–8108.

Shaykhutdinov, A. G., Bakirov, N. U. and Usmanov, A. G. (1971) ‘Determination and mathematical correlation of heat transfer coefficient under conditions of bubble flow, cellular and turbulent foam’, *Int. Chem. Eng. J.*, 11, pp. 641–645.

Simonin, C., Viollet, P. L. and others (1990) ‘Predictions of an oxygen droplet pulverization in a compressible subsonic coflowing hydrogen flow’, *Numerical Methods for Multiphase Flows*. American Society of Mechanical Engineers: Fluids Engineering Division New York, 91(2), pp. 65–82.

Sultan, A. J., Sabri, L. S. and Al-Dahhan, M. H. (2018) ‘Influence of the size of heat exchanging internals on the gas holdup distribution in a bubble column using gamma-ray computed tomography’, *Chemical Engineering Science*. Elsevier, 186, pp. 1–25.

Thimmapuram, P. R., Rao, N. S. and Saxena, S. C. (1993) ‘Heat Transfer From Immersed Tubes in a Baffled Slurry Bubble Column’, *Chemical Engineering Communications*. Taylor & Francis, 120(1), pp. 27–43.

Valero, M. M., Martinez, M., Pozo, F. and Planas, E. (2019) ‘A successful experience with the flipped classroom in the Transport Phenomena course’, *Education for Chemical Engineers*. Elsevier, 26, pp. 67–79.

Youssef, A. A., Hamed, M. E., Grimes, J. T., Al-Dahhan, M. H. and Duduković, M. P. (2012) ‘Hydrodynamics of pilot-scale bubble columns: effect of internals’, *Industrial & Engineering Chemistry Research*. ACS Publications, 52(1), pp. 43–55.

Zhang, J., Bai, Y., Zhang, Q., Wang, X., Zhang, T., Tan, Y. and Han, Y. (2014) ‘Low-temperature methanation of syngas in slurry phase over Zr-doped Ni/ γ -Al₂O₃ catalysts prepared using different methods’, *Fuel*. Elsevier, 132, pp. 211–218.

Chapter 5

5 Conclusions and Future Scope

The conclusions obtained from the CFD study of hollow bubble column and bubble column with internals have been presented. Subsequently, the future scope of the current study has been discussed.

5.1 Conclusion

5.1.1 Hollow Bubble Column

- The effect of interfacial forces has been thoroughly studied and an appropriate selection of the interfacial model has been utilized to study the effect of flow regime transitions in hollow bubble columns. Constant lift force model with negative lift force coefficient was found to closely predict local gas holdups and liquid axial velocity plots as compared to the Tomiyama and Saffman-Mei models. The addition of Troshko-Hassan bubble induced turbulence model led to homogeneity in the gas holdup profiles. When turbulent dispersion model was added, gas plume was dispersed throughout the cross section of the bubble column. Simonin model, with $C_{TD}=0.1$, outperformed the Burns et al. model in predicting the local gas holdup and liquid axial velocity profiles. In the drag model study, Schiller-Naumann model outperformed the other drag models in the prediction of local and overall gas holdup values.
- In the flow transition studies, an increase in liquid axial velocities and centerline liquid velocities was observed with an increase in superficial gas velocity. These have closely conformed to the experimental values. Radial and overall gas holdups

increased with an increase in superficial gas velocity and the values closely correspond to experimental observations made in selected studies. Also, an increase in turbulent viscosity ratios was noticed with increasing superficial gas velocity.

- A comparison of normalized bubble number densities was made, and an increase in large bubble fractions was noticed with increasing superficial gas velocity. Liquid circulations have been studied across the distributor, bulk and the disengagement zone and a generalized flow circulation mapping profile has been generated for hollow bubble columns. A close fit was observed when this was compared with experimental studies carried out by (Devanathan, Moslemian and Dudukovic, 1990).
- When various bubble breakup and coalescence models were tested, a combination of Luo breakup model and Luo coalescence model exhibited realistic fractional bubble distributions. At higher velocities, this combination was able to effectively account for the presence of large bubbles in the dispersion which conforms to the experimental observations. When Lehr breakup model was employed, an increase in the breakup rate was observed which is evident from the increased fraction of smaller bubbles in the dispersion. Dual bubble size models based on the work of Krishna and Ellenberger, 1996 was able to effectively predict the local gas holdups, liquid axial velocities and overall gas holdups. The absence of PBM in the Dual bubble size model did not hinder the effective estimation of any of the hydrodynamic parameters.

5.1.2 Bubble Column with Vertical Internals

- The influence of lift force and turbulence dispersion on the hydrodynamic parameters has been studied. When negative lift force coefficients were used, higher centerline liquid velocities were obtained, and positive lift force coefficients underestimated the centerline liquid velocities values. In comparison, the absence of lift force ($C_L=0$) in the formulation estimated reasonable values of local gas holdups and liquid axial velocities. Simonin turbulence dispersion model with coefficient of turbulence dispersion, $C_{TD}=0.1$, was able to effectively disperse the gas phase and predicted sensible values of local gas holdups and liquid axial velocities.
- As seen in hollow bubble columns, in the presence of internals too, the centerline liquid velocities increased with increase in superficial gas velocities. For similar superficial gas velocities, the centerline liquid velocity increased with the increase in internal tube density. Due to the presence of an additional tube bundle, a flatter liquid velocity profile was observed in the column center.
- Higher radial and overall gas holdups were noticed with the addition of a second internal tube which is attributed to the decrease in flow area on the gas dispersion offered by the tube bundles. This leads to greater accumulation of small bubbles which adds to the holdup.
- Lower values of turbulence parameters in the bulk region was attributed to the dissipation of turbulent eddies in the presence of internals.
- A higher fraction of small bubbles was noticed in the presence of denser internals which indicates an increased rate of bubble break-up in the column.

5.2 Future Scope

- Future studies could investigate effects of internals on heat and mass transfer effects in bubble columns as well determine limiting internals density. Mixing and mass transfer could be coupled and the effect of interfacial forces like drag force, lift, turbulence dispersion and turbulence interaction model on the mixing time can be further investigated
- Since, the process of heat transfer and hydrodynamics are closely related, it would be interesting to study them simultaneously with increasing density of internals in bubble column. This could include investigating the effect of temperature on the bubble size distributions, local heat flux and other hydrodynamic parameters.
- The modelling approach employed for bubble column with internals can be extended to test the effect of other internals such as helical coils, circular plates, circular baffles and vibrating internals. The results obtained could be verified with a number of experimental studies that have tested the effect of these internals on the reactor hydrodynamics
- The suitability of Method of Moments (MOM) which includes Quadrature Method of Moments (QMOM) and (DQMOM) on bubble properties could be tested
- The application of Dual Bubble Size modelling approach for the churn turbulent regime could be extensively investigated and validated with literature studies
- The effect of high pressure on bubble properties such as Sauter mean diameter, bubble size distributions and bubble velocities could be an addition to the current study

Appendix – A

Table A.1 Literature review of numerical studies performed on hollow bubble columns

Authors and Year	Column Diameter (m)	Geometry	Flow Regimes	Turbulence model	Interfacial Forces			Parameters Investigated	
					Lift	Drag	Turbulence dispersion		
(Deen, Solberg and Hjertager, 2000)	Rectangular (1*0.15*0.15)	2D, 3D	Bubbly	$k - \varepsilon$ model	-	(Ishii and Zuber, 1979) model	-	-	U_L ; α_G ; flow fields; TKE
(Krishna & Van Baten, 2001)	0.1, 0.14, 0.174, 0.19, 0.38, 0.63	2D axisymmetric	Bubbly, Transition, Churn-turbulent	$k - \varepsilon$ model	Constant	Krishna drag model	-	-	U_L ; α_G ; small and large bubble holdups; axial dispersion
(Olmos <i>et al.</i> , 2001)	0.1	2D	Bubbly, Heterogenous	$k - \varepsilon$ model	-	-	Constant ($C_{TD}=0.1$)	-	U_L ; α_G ; d_b ; d_{32}

Authors and Year	Column Diameter (m)	Geometry	Flow Regimes	Turbulence model	Interfacial Forces			Parameters Investigated	
					Lift	Drag	Turbulence dispersion		
(Deen, Solberg and Hjertager, 2001)	Rectangular (1.2*0.2*0.05)	3D	Churn-turbulent	$k - \varepsilon$; $k - \varepsilon$ + BIT; LES; LES + BIT	Constant ($C_L=0.5$)	(Ishii and Zuber, 1979) model	-	-	U_L ; flow fields; TKE
(Buwa & Ranade, 2002)	Rectangular (1.2*0.2*0.05)	3D	Bubbly, Heterogenous	$k - \varepsilon$ model	Constant	(Tsuchiya <i>et al.</i> , 1997) drag model	-	-	U_L ; α_G ; d_b ; d_{32} ; bubble size distribution
(Ekambara and Joshi, 2003)	0.2 and 0.4	3D	Bubbly, Transition, Churn-turbulent	$k - \varepsilon$ model	-	Constant	-	-	U_L ; α_G ; eddy viscosity; axial dispersion coefficients; mixing time
(Dhotre and Joshi, 2004)	0.385	2D	Bubbly, Transition,	$k - \varepsilon$ model	Constant	Constant (Based on	-	-	U_L ; α_G ; heat transfer coefficient

Authors and Year	Column Diameter (m)	Geometry	Flow Regimes	Turbulence model	Interfacial Forces			Parameters Investigated	
					Lift	Drag	Turbulence dispersion		
			Churn-turbulent			average slip velocity)			
(Chen, Sanyal and Dudukovic, 2004)	0.19	2D and 3D	Bubbly, Transition, Churn-turbulent	Modified $k - \varepsilon$ model	-	(Schiller & Naumann, 1933)	-	-	U_L ; α_G ; bubble class holdups; bubble size distribution
(Monahan, Vitankar and Fox, 2005)	0.06, 0.2, 0.4	2D and 3D	Bubbly, Transition	Laminar and $k - \varepsilon$ model	Constant ($C_L=0, 0.375, 0.75$)	(Clift, Grace and Weber, 2005) model	-	-	Flow fields; α_G ; α_L ; slip velocity
(Sanyal <i>et al.</i> , 2005)	0.145	2D	Bubbly, Transition	$k - \varepsilon$ model	Constant	(Schiller & Naumann, 1933)	-	-	α_G ; d_{32} ; bubble class holdups; bubble size distribution

Authors and Year	Column Diameter (m)	Geometry	Flow Regimes	Turbulence model	Interfacial Forces			Parameters Investigated	
					Lift	Drag	Turbulence dispersion		
(Kulkarni and Joshi, 2006)	0.385	2D	Bubbly, Transition, Churn-turbulent	$k - \varepsilon$ model	Constant	Constant (Based on average slip velocity)	-	-	Average circulation velocity; wall heat transfer coefficient
(Zhang, Deen and Kuipers, 2006)	Rectangular (0.45*0.15*0.15) and (0.90*0.15*0.15)	3D	Bubbly	$k - \varepsilon$ model + BIT	Constant ($C_L=0.5, 0.29$)	(Ishii and Zuber, 1979); (Tomiyama, 1998)	Sub-Grid Scale (SGS) model of (Smagorinsky, 1963)	-	$U_L; \alpha_G$; flow fields; μ_L
(Cheung, Yeoh and Tu, 2007)	0.038; 0.058	3D	Bubbly, Transition, Churn-turbulent	$k - \varepsilon$ model; $k - \omega$ model;	(Tomiyama <i>et al.</i> , 2002)	(Ishii and Zuber, 1979) model	(Burns <i>et al.</i> , 2004) ($C_{TD}=1$)	(Antal, Lahey Jr & Flaherty, 1991) model	$U_L; U_G; \alpha_G; d_{32}$; interfacial area concentration

Authors and Year	Column Diameter (m)	Geometry	Flow Regimes	Turbulence model	Interfacial Forces			Parameters Investigated	
					Lift	Drag	Turbulence dispersion		
							($C_{w1}=-0.0064$, $C_{w1}=-0.016$)		
(Bhole et al., 2008)	0.15	3D	Bubbly	$k - \varepsilon$ model +BIT	(Tomiyama <i>et al.</i> , 2002)	(Clift, Grace and Weber, 2005) model	-	-	$U_L ; \alpha_G; d_b; d_{32}$
(Li, Yang and Dai, 2009)	0.4	3D	Transition	$k - \varepsilon$ model +BIT	(Tomiyama <i>et al.</i> , 2002)	(Clift, Grace and Weber, 2005) model	(de Bertodano, 1991)	(Antal, Lahey Jr & Flaherty, 1991) model	$U_L ; \alpha_G; \text{mixing time;}$ ($C_{w1}=-0.0064$, $C_{w2}=-0.016$)

Authors and Year	Column Diameter (m)	Geometry	Flow Regimes	Turbulence model	Interfacial Forces			Parameters Investigated	
					Lift	Drag	Turbulence dispersion		Wall Lubrication
(Ekambara and Dhotre, 2010)	0.15	3D	Bubbly	$k - \varepsilon$; $k - \varepsilon$ RNG; $k - \omega$; RSM & LES	(Tomiyama <i>et al.</i> , 2002) model	(Ishii and Zuber, 1979) model	(de Bertodano, 1991)	(Antal, Lahey Jr & Flaherty, 1991) model ($C_{w1}=-0.01$, $C_{w2}=0.05$)	U_L ; α_G ; flow fields; k ; ε
(Yang <i>et al.</i> , 2011)	0.138	3D	Bubbly, Transition, Churn-turbulent	$k - \varepsilon$ model	-	(Tomiyama, 1998); (White and Corfield, 2006); Dual Bubble Size drag model	-	-	U_L ; α_G ; flow fields
(Silva, d'Ávila and Mori, 2012)	0.162	3D	Bubbly, Transition	$k - \varepsilon$ model; RSM	(Tomiyama <i>et al.</i> , 2002) model	(Grace <i>et al.</i> , 1976; Ishii & Zuber, 1979; Zhang &	(de Bertodano, 1991)	-	U_G ; α_G

Authors and Year	Column Diameter (m)	Geometry	Flow Regimes	Turbulence model	Interfacial Forces			Parameters Investigated	
					Lift	Drag	Turbulence dispersion		Wall Lubrication
						Vanderheyden, 2002)			
(Xing, Wang and Wang, 2013)	0.19	2D	Bubbly, Transition, Churn-turbulent	$k - \varepsilon$ model	-	(Ishii and Zuber, 1979) model	(de Bertodano, 1991)	Constant	$U_L ; \alpha_G$;small and large bubble holdups; BSD; coalescence and breakup rates
(Gupta and Roy, 2013)	Rectangular (1.2*0.2*0.05)	2D	Bubbly	$k - \varepsilon$; $k - \varepsilon$ RNG & RSM	(Auton, 1987); (Magnaudet & Legendre, 1998);	(Schiller & Naumann, 1933); (Tomiya, 1998); (Ishii & Zuber, 1979); (Zhang	-	-	U_L ; flow fields; d_{32}

Authors and Year	Column Diameter (m)	Geometry	Flow Regimes	Turbulence model	Interfacial Forces			Parameters Investigated	
					Lift	Drag	Turbulence dispersion		Wall Lubrication
					(Tomiyama & <i>et al.</i> , 2002)	& Vanderheyden, 2002)			
(Liu and Hinrichsen, 2014)	0.2	2D	Transition; Churn Turbulent	$k - \varepsilon$ model +BIT; RSM + BIT	(Tomiyama <i>et al.</i> , 2002) model; (Behzadi, Issa and Rusche, 2004) model	(Rampure, Kulkarni and Ranade, 2007) model; (Tsuchiya <i>et al.</i> , 1997) model	-	-	$U_L; \alpha_G; k; \varepsilon; U_G d_{32}$

Authors and Year	Column Diameter (m)	Geometry	Flow Regimes	Turbulence model	Interfacial Forces			Parameters Investigated	
					Lift	Drag	Turbulence dispersion		
(Masood, Rauh and Delgado, 2014)	Rectangular (0.45*0.15*0.15)	3D	Bubbly	$k - \varepsilon$; $k - \varepsilon$ RNG; EARSM $k - \varepsilon$; EARSM-BSL	(Tomiyama <i>et al.</i> , 2002) model; Constant ($C_L=0.5$)	(Ishii and Zuber, 1979) model	(de Bertodano, 1991) model; (Burns <i>et al.</i> , 2004) model ($C_{TD}=0.2$)	(Antal, Lahey Jr & Flaherty, 1991) model ($C_{w1}=-0.01$, $C_{w2}=0.05$); (Tomiyama, 1998) model; (Frank <i>et al.</i> , 2008) model ($C_{WC}=10$, $C_{WD}=6.8$, $p=1.7$)	U_L ; α_G ; flow fields; μ_L ; U_G ; k ; ε
(McClure <i>et al.</i> , 2015)	0.39	2D	Bubbly, Transition, Churn-turbulent	$k - \varepsilon + BIT$	-	(Grace, TH and others, 1976) model	(Burns <i>et al.</i> , 2004)	-	Mixing studies, mixing times, dimensionless tracer concentration

Authors and Year	Column Diameter (m)	Geometry	Flow Regimes	Turbulence model	Interfacial Forces			Parameters Investigated	
					Lift	Drag	Turbulence dispersion		Wall Lubrication
(Liang <i>et al.</i> , 2016)	0.138	3D	Bubbly, Transition, Churn-turbulent	$k - \varepsilon$ RNG	-	(Tomiya, 1998); Dual Bubble Size drag model; PBM-customized drag model	-	-	U_L ; α_G ; bubble size distribution;
(Yang, Guo and Wang, 2017)	0.15	2D axisymmetric	Bubbly, Transition, Churn-turbulent	$k - \varepsilon$	Constant	(Wang, Wang and Jin, 2006)	Constant	Constant	α_G ; bubble size distribution
(Saleh <i>et al.</i> , 2018)	0.156	3D	Bubbly	$k - \varepsilon$ +BIT	(Tomiya <i>et al.</i> , 2002) model	(Ishii and Zuber, 1979)	(de Bertodano, 1991)	(Antal, Lahey Jr & Flaherty, 1991) model	U_L ; α_G ; flow fields; U_G

Authors and Year	Column Diameter (m)	Geometry	Flow Regimes	Turbulence model	Interfacial Forces				Parameters Investigated
					Lift	Drag	Turbulence dispersion	Wall Lubrication	
(Cheng <i>et al.</i> , 2018)	0.15	2D axisymmetric	Bubbly	Mixture	(Frank, Shi and Burns, 2004)	(Tomiyama, 1998)	(Burns <i>et al.</i> , 2004)	(Tomiyama, 1998)	$U_L; \varepsilon; \alpha_G; d_b$
(Sarhan, Naser and Brooks, 2018)	0.216	3D	Bubbly, Transition, Churn-turbulent	$k - \varepsilon$	-	(Tomiyama, 1998) model	-	-	$\alpha_G; d_{32}; U_G$
(Gemello <i>et al.</i> , 2018)	0.15, 0.4, 1, 3	3D	Bubbly, Transition, Churn-turbulent	RNG $k - \varepsilon$; $k - \omega$	-	(Tomiyama, 1998) model	(Burns <i>et al.</i> , 2004)	-	$\alpha_G; U_L$; mixing times; turbulent kinematic viscosity

Authors and Year	Column Diameter (m)	Geometry	Flow Regimes	Turbulence model	Interfacial Forces			Parameters Investigated	
					Lift	Drag	Turbulence dispersion		
(Zhang <i>et al.</i> , 2018)	0.15	2D axisymmetric	Churn-turbulent	$k - \varepsilon$ model	(Zhang, 2011)	(Liu Xin; Zhang Yu; Jin Haibo, 2017)	(de Bertodano, 1991)	(Tomiyama, 1998) model	U_L ; α_G ; U_G ; d_b
(Yan <i>et al.</i> , 2019)	0.30	3D	Churn-turbulent	$k - \varepsilon$ model	(Zhang, 2011)	(Schiller & Naumann, 1933); (Xiao, <i>et al.</i> , 2013) model; (Duan <i>et al.</i> , 2011) model; (Buffo <i>et al.</i> , 2016) model; (Roghair <i>et al.</i> , 2011)	(Lahey Jr, De Bertodano and Jones Jr, 1993)	(Tomiyama, 1998) model	α_G ; small and large bubble holdups

Authors and Year	Column Diameter (m)	Geometry	Flow Regimes	Turbulence model	Interfacial Forces			Parameters Investigated	
					Lift	Drag	Turbulence dispersion		
(Schäfer <i>et al.</i> , 2019)	Rectangular (1*0.18*0.04)	3D	Bubbly	Smagorinsky turbulence model	-	(Tomiyama, 1998) model	-	-	Bubble size distribution
(Gholamzadehdevin and Pakzad, 2019)	0.248	3D	Transition	$k - \varepsilon$ model	-	(Schiller & Naumann, 1933)	-	-	α_G ; mixing times; μ
(Shi, J. Yang, <i>et al.</i> , 2020)		3D		$k - \varepsilon$ model+BIT	(Tomiyama <i>et al.</i> , 2002) model	(Grace <i>et al.</i> , 1976) model			α_G ; critical stress; ε ; interfacial area; mass transfer coefficient
(Zhu <i>et al.</i> , 2020)	Rectangular	3D	Bubbly	LES + BIT	Constant; (Tomiyama <i>et al.</i> , 2002) model	Constant; (Schiller & Naumann, 1933); (Ishii & Zuber, 1979)	Sub-Grid Scale (SGS) model of (Smagorinsky, 1963)	-	U_L ; k ; U_G Flow fields;

References

- Antal, S. P., Lahey Jr, R. T. and Flaherty, J. E. (1991) 'Analysis of phase distribution in fully developed laminar bubbly two-phase flow', *International journal of multiphase flow*. Elsevier, 17(5), pp. 635–652.
- Auton, T. R. (1987) 'The lift force on a spherical body in a rotational flow', *Journal of fluid Mechanics*. Cambridge University Press, 183, pp. 199–218.
- Behzadi, A., Issa, R. I. and Rusche, H. (2004) 'Modelling of dispersed bubble and droplet flow at high phase fractions', *Chemical Engineering Science*. Elsevier, 59(4), pp. 759–770.
- de Bertodano, M. (1991) 'Turbulent bubbly flow in a triangular duct', *New York: Rensselaer Polytechnic Institute*.
- Bhole, M. R., Joshi, J. B. and Ramkrishna, D. (2008) 'CFD simulation of bubble columns incorporating population balance modeling', *Chemical Engineering Science*. Elsevier, 63(8), pp. 2267–2282.
- Buffo, A., Vanni, M., Renze, P. and Marchisio, D. L. (2016) 'Empirical drag closure for polydisperse gas–liquid systems in bubbly flow regime: Bubble swarm and micro-scale turbulence', *Chemical Engineering Research and Design*. Elsevier, 113, pp. 284–303.
- Burns, A. D., Frank, T., Hamill, I., Shi, J.-M. and others (2004) 'The Favre averaged drag model for turbulent dispersion in Eulerian multi-phase flows', in *5th international conference on multiphase flow, ICMF*, pp. 1–17.
- Buwa, V. V and Ranade, V. V (2002) 'Dynamics of gas–liquid flow in a rectangular bubble column: experiments and single/multi-group CFD simulations', *Chemical Engineering Science*, 57(22), pp. 4715–4736.
- Chen, P., Sanyal, J. and Dudukovic, M. P. (2004) 'CFD modeling of bubble columns flows: implementation of population balance', *Chemical Engineering Science*, 59(22), pp. 5201–5207.
- Cheng, J., Li, Q., Yang, C., Zhang, Y. and Mao, Z. (2018) 'CFD-PBE simulation of a bubble column in OpenFOAM', *Chinese Journal of Chemical Engineering*, 26(9), pp. 1773–1784.
- Cheung, S. C. P., Yeoh, G. H. and Tu, J. Y. (2007) 'On the numerical study of isothermal vertical bubbly flow using two population balance approaches', *Chemical Engineering Science*. Elsevier, 62(17), pp. 4659–4674.

Clift, R., Grace, J. R. and Weber, M. E. (2005) *Bubbles, drops, and particles*. Courier Corporation.

Deen, N. G., Solberg, T. and Hjertager, B. H. (2000) 'Numerical simulation of the gas-liquid flow in a square cross-sectioned bubble column', in *Proceedings of 14th Int. Congress of Chemical and Process Engineering: CHISA (Praha, Czech Republic, 2000)*.

Deen, N. G., Solberg, T. and Hjertager, B. H. (2001) 'Large eddy simulation of the Gas-Liquid flow in a square cross-sectioned bubble column', *Chemical Engineering Science*, 56(21), pp. 6341–6349.

Dhotre, M. T. and Joshi, J. B. (2004) 'Two-Dimensional CFD Model for the Prediction of Flow Pattern, Pressure Drop and Heat Transfer Coefficient in Bubble Column Reactors', *Chemical Engineering Research and Design*, 82(6), pp. 689–707.

Duan, X. Y., Cheung, S. C. P., Yeoh, G. H., Tu, J. Y., Krepper, E. and Lucas, D. (2011) 'Gas-liquid flows in medium and large vertical pipes', *Chemical engineering science*. Elsevier, 66(5), pp. 872–883.

Ekambara, K. and Dhotre, M. T. (2010) 'CFD simulation of bubble column', *Nuclear Engineering and Design*, 240(5), pp. 963–969.

Ekambara, K. and Joshi, J. B. (2003) 'CFD Simulation of Residence Time Distribution and Mixing in Bubble Column Reactors', *The Canadian Journal of Chemical Engineering*, 81(3-4), pp. 669–676.

Frank, T., Shi, J. and Burns, A. D. (2004) 'Validation of Eulerian multiphase flow models for nuclear safety application', in *Proceeding of the Third International Symposium on Two-Phase Modelling and Experimentation, Pisa, Italy*, pp. 22–25.

Frank, T., Zwart, P. J., Krepper, E., Prasser, H.-M. and Lucas, D. (2008) 'Validation of CFD models for mono- and polydisperse air-water two-phase flows in pipes', *Nuclear Engineering and Design*. Elsevier, 238(3), pp. 647–659.

Gemello, L., Cappello, V., Augier, F., Marchisio, D. and Plais, C. (2018) 'CFD-based scale-up of hydrodynamics and mixing in bubble columns', *Chemical Engineering Research and Design*, 136, pp. 846–858.

Gholamzadehdevin, M. and Pakzad, L. (2019) 'Hydrodynamic characteristics of an activated sludge bubble column through computational fluid dynamics (CFD) and response surface methodology (RSM)', *The Canadian Journal of Chemical Engineering*, 97(4), pp. 967–982.

Grace, J. R., TH, N. and others (1976) 'Shapes and Velocities of Single Drops and Bubbles Moving Freely Through Immiscible Liquids'.

Gupta, A. and Roy, S. (2013) 'Euler--Euler simulation of bubbly flow in a rectangular bubble column: Experimental validation with Radioactive Particle Tracking', *Chemical Engineering Journal*. Elsevier, 225, pp. 818–836.

Ishii, M. and Zuber, N. (1979) 'Drag coefficient and relative velocity in bubbly, droplet or particulate flows', *AIChE Journal*. Wiley Online Library, 25(5), pp. 843–855.

Krishna, R. and Van Baten, J. M. (2001) 'Scaling up Bubble Column Reactors with the Aid of CFD', *Chemical Engineering Research and Design*, 79(3), pp. 283–309.

Kulkarni, A. V and Joshi, J. B. (2006) 'Estimation of Hydrodynamic and Heat Transfer Characteristics of Bubble Column by Analysis of Wall Pressure Measurements and CFD Simulations', *Chemical Engineering Research and Design*, 84(7), pp. 601–609.

Lahey Jr, R. T., De Bertodano, M. L. and Jones Jr, O. C. (1993) 'Phase distribution in complex geometry conduits', *Nuclear Engineering and Design*. Elsevier, 141(1–2), pp. 177–201.

Li, G., Yang, X. and Dai, G. (2009) 'CFD simulation of effects of the configuration of gas distributors on gas--liquid flow and mixing in a bubble column', *Chemical Engineering Science*. Elsevier, 64(24), pp. 5104–5116.

Liang, X.-F., Pan, H., Su, Y.-H. and Luo, Z.-H. (2016) 'CFD-PBM approach with modified drag model for the gas--liquid flow in a bubble column', *Chemical Engineering Research and Design*, 112, pp. 88–102.

Liu Xin; Zhang Yu; Jin Haibo (2017) 'Hydrodynamics simulation of pressurized bubble column based on bubble swarm interphase force models', *CIESC Journal*, 68(11-1946/TQ), pp. 87–96.

Liu, Y. and Hinrichsen, O. (2014) 'Study on CFD–PBM turbulence closures based on $k-\epsilon$ and Reynolds stress models for heterogeneous bubble column flows', *Computers & Fluids*, 105, pp. 91–100.

Magnaudet, J. and Legendre, D. (1998) 'Some aspects of the lift force on a spherical bubble', in *In Fascination of Fluid Dynamics*. Springer, pp. 441–461.

Masood, R. M. A., Rauh, C. and Delgado, A. (2014) 'CFD simulation of bubble column flows: An explicit algebraic Reynolds stress model approach', *International Journal of Multiphase Flow*, 66, pp. 11–25.

McClure, D. D., Aboudha, N., Kavanagh, J. M., Fletcher, D. F. and Barton, G. W. (2015) 'Mixing in bubble column reactors: Experimental study and CFD modeling', *Chemical Engineering Journal*, 264, pp. 291–301.

Monahan, S. M., Vitankar, V. S. and Fox, R. O. (2005) 'CFD predictions for flow-regime transitions in bubble columns', *AIChE journal*. Wiley Online Library, 51(7), pp. 1897–1923.

Olmos, E., Gentric, C., Vial, C., Wild, G. and Midoux, N. (2001) 'Numerical simulation of multiphase flow in bubble column reactors. Influence of bubble coalescence and break-up', *Chemical Engineering Science*, 56(21), pp. 6359–6365.

Rampure, M. R., Kulkarni, A. A. and Ranade, V. V (2007) 'Hydrodynamics of bubble column reactors at high gas velocity: experiments and computational fluid dynamics (CFD) simulations', *Industrial & Engineering Chemistry Research*. ACS Publications, 46(25), pp. 8431–8447.

Roghair, I., Lau, Y. M., Deen, N. G., Slagter, H. M., Baltussen, M. W., Annaland, M. V. S. and Kuipers, J. A. M. (2011) 'On the drag force of bubbles in bubble swarms at intermediate and high Reynolds numbers', *Chemical engineering science*. Elsevier, 66(14), pp. 3204–3211.

Saleh, S. N., Mohammed, A. A., Al-Jubory, F. K. and Barghi, S. (2018) 'CFD assesment of uniform bubbly flow in a bubble column', *Journal of Petroleum Science and Engineering*, 161, pp. 96–107.

Sanyal, J., Marchisio, D. L., Fox, R. O. and Dhanasekharan, K. (2005) 'On the comparison between population balance models for CFD simulation of bubble columns', *Industrial & Engineering Chemistry Research*. ACS Publications, 44(14), pp. 5063–5072.

Sarhan, A. R., Naser, J. and Brooks, G. (2018) 'CFD modeling of bubble column: Influence of physico-chemical properties of the gas/liquid phases properties on bubble formation', *Separation and Purification Technology*, 201, pp. 130–138.

Schäfer, J., Hlawitschka, M. W., Attarakih, M. and Bart, H.-J. (2019) 'Modelling of bubble column hydrodynamics using CFD and SQMOM as a population balance solver', in Kiss, A. A., Zondervan, E., Lakerveld, R., and Özkan, L. (eds) *29th European Symposium on Computer Aided Process Engineering*. Elsevier (Computer Aided Chemical Engineering), pp. 715–720.

Schiller, L. (1933) 'Über die grundlegenden Berechnungen bei der Schwerkraftaufbereitung', *Z. Vereines Deutscher Inge.*, 77, pp. 318–321.

Shi, W., Yang, J., Li, G., Zong, Y. and Yang, X. (2020) 'Computational Fluid Dynamics–Population Balance Modeling of Gas–Liquid Two-Phase Flow in Bubble Column Reactors With an Improved Breakup Kernel Accounting for Bubble Shape Variations', *Heat Transfer Engineering*. Taylor & Francis, 41(15–16), pp. 1414–1430.

Silva, M. K., d'Ávila, M. A. and Mori, M. (2012) 'Study of the interfacial forces and turbulence models in a bubble column', *Computers & Chemical Engineering*. Elsevier, 44, pp. 34–44.

Smagorinsky, J. (1963) 'General circulation experiments with the primitive equations: I. The basic experiment', *Monthly weather review*, 91(3), pp. 99–164.

Tomiyama, A. (1998) 'Struggle with computational bubble dynamics', *Multiphase Science and Technology*, 10(4), pp. 369–405.

Tomiyama, A., Tamai, H., Zun, I. and Hosokawa, S. (2002) 'Transverse migration of single bubbles in simple shear flows', *Chemical Engineering Science*. Elsevier, 57(11), pp. 1849–1858.

Tsuchiya, K., Furumoto, A., Fan, L.-S. and Zhang, J. (1997) 'Suspension viscosity and bubble rise velocity in liquid-solid fluidized beds', *Chemical Engineering Science*. Elsevier, 52(18), pp. 3053–3066.

Wang, T., Wang, J. and Jin, Y. (2006) 'A CFD--PBM coupled model for gas--liquid flows', *AIChE Journal*. Wiley Online Library, 52(1), pp. 125–140.

White, F. M. and Corfield, I. (2006) *Viscous fluid flow*. McGraw-Hill New York.

Xiao, Q., Yang, N. and Li, J. (2013) 'Stability-constrained multi-fluid CFD models for gas-liquid flow in bubble columns', *Chemical Engineering Science*. Elsevier, 100, pp. 279–292.

Xing, C., Wang, T. and Wang, J. (2013) 'Experimental study and numerical simulation with a coupled CFD–PBM model of the effect of liquid viscosity in a bubble column', *Chemical Engineering Science*, 95, pp. 313–322.

Yan, P., Jin, H., He, G., Guo, X., Ma, L., Yang, S. and Zhang, R. (2019) 'CFD simulation of hydrodynamics in a high-pressure bubble column using three optimized drag models of bubble swarm', *Chemical Engineering Science*, 199, pp. 137–155.

Yang, G., Guo, K. and Wang, T. (2017) 'Numerical simulation of the bubble column at elevated pressure with a CFD-PBM coupled model', *Chemical Engineering Science*, 170, pp. 251–262.

- Yang, N., Wu, Z., Chen, J., Wang, Y. and Li, J. (2011) ‘Multi-scale analysis of gas–liquid interaction and CFD simulation of gas–liquid flow in bubble columns’, *Chemical Engineering Science*, 66(14), pp. 3212–3222.
- Zhang, B., Kong, L., Jin, H., He, G., Yang, S. and Guo, X. (2018) ‘CFD simulation of gas–liquid flow in a high-pressure bubble column with a modified population balance model’, *Chinese Journal of Chemical Engineering*, 26(6), pp. 1350–1358.
- Zhang, D., Deen, N. G. and Kuipers, J. A. M. (2006) ‘Numerical simulation of the dynamic flow behavior in a bubble column: a study of closures for turbulence and interface forces’, *Chemical Engineering Science*. Elsevier, 61(23), pp. 7593–7608.
- Zhang, D. Z. and Vanderheyden, W. B. (2002) ‘The effects of mesoscale structures on the disperse two-phase flows and their closures for dilute suspensions’, *International Journal of Multiphase Flow*, 28, pp. 805–822.
- Zhang, Y. (2011) *Hydrodynamics of Turbulent Bubble Column with and without Internals in Well-Developed Flow Region*. Ph. D. Thesis, Zhejiang University, Hangzhou, China, 2011.
- Zhu, S. J., Ooi, A., Manasseh, R. and Skvortsov, A. (2020) ‘Prediction of gas holdup in partially aerated bubble columns using an EE-LES coupled model’, *Chemical Engineering Science*, 217, p. 115492.

Appendix – B

Table B.1 Literature review of numerical studies performed on bubble column with internals

Authors and Year	Column Diameter (m) & U_G (m/s)	Internal Geometry		Interfacial Forces				Parameters Investigated
		(i) Type (ii) No of tubes (N_T) (iii) Tube Diameter (D_T)	Turbulence model	Lift	Drag	Turbulence dispersion	Wall Lubrication	
(Larachi, F. et al., 2006)	$D_c=0.19$, 1.0; $U_G=0.12$	(i) Circular Tube Bundle (ii) $N_T=57, 171$ (iii) $D_T=0.0254$	k- ϵ model + BIT	-	(Morsi and Alexander, 1972)	-	-	U_L ; α_G ; k
(Laborde-Boutet <i>et al.</i> , 2010)	$D_c=0.151$; $U_G=0.343$	(i) U- Tube Bundle (ii) $N_T=2$ bundles (iii) $D_T=0.0267$	RNG k- ϵ model + BIT	-	(Morsi and Alexander, 1972)	-	-	U_L ; α_G ; heat transfer studies

Authors and Year	Column Diameter (m) & U_G (m/s)	Internal Geometry		Interfacial Forces				Parameters Investigated
		(i) Type (ii) No of tubes (N_T) (iii) Tube Diameter (D_T)	Turbulence model	Lift	Drag	Turbulence dispersion	Wall Lubrication	
(Besagni, Guédon and Inzoli, 2016)	$D_c=0.24$; $U_G=0-0.23$	(i) Circular Tube Bundle (ii) $N_T=2$ (iii) $D_T=0.06, 0.075$	k- ω model	(Tomiyama <i>et al.</i> , 2002)	(Tomiyama, 1998)	(Burns <i>et al.</i> , 2004) ($C_{TD}= 1$)	(Antal <i>et al.</i> , 1991) ($C_{w1}= -0.01$, $C_{w2}= 0.05$)	U_L ; α_G ; U_G ; d_{32} ; interfacial area concentration; bubble size distribution
(Guan and Yang, 2017)	$D_c=0.14$; $U_G=0.12$	(i) Circular Tube Bundle (ii) $N_T=16$ (iii) $D_T=0.025$	(Xiao <i>et al.</i> , 2013)	Constant ($C_L= -0.02$)	(Schiller and Naumann, 1933)	(de Bertodano, 1991) ($C_{TD}= 0.3$)	(Antal <i>et al.</i> , 1991) ($C_{w1}= -0.01$, $C_{w2}= 0.05$)	U_L ; α_G ; U_G ; d_{32} ; interfacial area concentration; bubble size distribution
(Bhusare <i>et al.</i> , 2017)	$D_c=0.12$; $U_G=0.014$ – 0.132	(i) Circular Tube Bundle (ii) $N_T=0, 1, 5$	k- ϵ mixture model	Constant ($C_L= -0.08$ to -0.23)	Drift-flux theory	Drift-flux theory	-	U_L ; α_G ; k;

Authors and Year	Column Diameter (m) & U_G (m/s)	Internal Geometry		Interfacial Forces				Parameters Investigated
		(i) Type (ii) No of tubes (N_T) (iii) Tube Diameter (D_T)	Turbulence model	Lift	Drag	Turbulence dispersion	Wall Lubrication	
		(iii) $D_T=0.012$ (at $r/R=0.65$) and $D_T=0.036$ at $r/R=0$)				($C_{TD}= 0.008 - 0.07$)		
(Guo and Chen, 2017)	$D_c=0.14$; $U_G=0.003$, 0.45	(i) Circular Tube Bundle (ii) $N_T=0,8(A)$, 8(B), 31 (iii) $D_T=A:0.0127$, B:0.0254; C: 0.0127	RNG k- ϵ model + BIT	(Tomiya <i>et al.</i> , 2002)	(Ishii and Zuber, 1979)	-	(Frank <i>et al.</i> , 2008) ($C_{wd}= 6.8$, $C_{wc}= 10$, $p=1.7$); (Hosokawa <i>et al.</i> , 2002)	U_L ; α_G ; k; ϵ ; flow fields; bubble size distribution
(Bhusare <i>et al.</i> , 2018)	$D_c=0.12$;	(i) Circular Tube Bundle	k- ϵ mixture model	Constant	Drift-flux theory	Drift-flux theory	-	U_L ; α_G ; eddy diffusivity; axial dispersion

Authors and Year	Column Diameter (m) & U_G (m/s)	Internal Geometry		Interfacial Forces				
		(i) Type (ii) No of tubes (N_T) (iii) Tube Diameter (D_T)	Turbulence model	Lift	Drag	Turbulence dispersion	Wall Lubrication	Parameters Investigated
	$U_G = 0.014, 0.088, 0.221$	(ii) $N_T = 0, 1, 5$ (iii) $D_T = 0.012$ (at $r/R = 0.65$) and $D_T = 0.036$ (at $r/R = 0$)		($C_L = -0.12$ to -0.25)				coefficient; mixing time
(Agahzamin and Pakzad, 2019a)	$D_c = 0.19;$ $U_G = 0.2$	(i) Circular Tube Bundle (ii) $N_T = 48$ (iii) $D_T = 0.0127$	$k-\varepsilon$ model + BIT	(Tomiyama <i>et al.</i> , 2002)	(Schiller and Naumann, 1933)	(Simonin, Viollet and others, 1990)	(Antal <i>et al.</i> , 1991) ($C_{w1} = 0.01, C_{w2} = 0.05$); (Antal <i>et al.</i> , 1991) ($C_{w1} = 0.06 U_s - 0.104, U_s = \text{slip}$)	$U_L; \alpha_G; U_G; k; \varepsilon; d_b;$ bubble size distribution

Authors and Year	Column Diameter (m) & U_G (m/s)	Internal Geometry		Interfacial Forces				Parameters Investigated
		(i) Type (ii) No of tubes (N_T) (iii) Tube Diameter (D_T)	Turbulence model	Lift	Drag	Turbulence dispersion	Wall Lubrication	
							velocity $C_{w2} = 0.147$)	
(Agahzamin and Pakzad, 2019b)	$D_c = 0.19$; $U_G = 0.01, 0.03, 0.1, 0.2$	(i) Circular Tube Bundle (ii) $N_T = 48$ (iii) $D_T = 0.0127$	RSM+BIT	Constant ($C_L = -0.03$)	(Schiller and Naumann, 1933)	(Simonin, Viollet and others, 1990)	(Antal et al., 1991) ($C_{w1} = -0.01$, $C_{w2} = 0.05$)	U_L ; α_G ; U_G ; bubble size distribution; RTD; tracer concentrations

References

- Agahzamin, S. and Pakzad, L. (2019a) 'A comprehensive CFD study on the effect of dense vertical internals on the hydrodynamics and population balance model in bubble columns', *Chemical Engineering Science*, 193, pp. 421–435.
- Agahzamin, S. and Pakzad, L. (2019b) 'CFD investigation of the gas dispersion and liquid mixing in bubble columns with dense vertical internals', *Chemical Engineering Science*, 203, pp. 425–438.
- Antal, S. P., Lahey Jr, R. T. and Flaherty, J. E. (1991) 'Analysis of phase distribution in fully developed laminar bubbly two-phase flow', *International journal of multiphase flow*. Elsevier, 17(5), pp. 635–652.
- de Bertodano, M. (1991) 'Turbulent bubbly flow in a triangular duct', *New York: Rensselaer Polytechnic Institute*.
- Besagni, G., Guédon, G. R. and Inzoli, F. (2016) 'Annular gap bubble column: experimental investigation and computational fluid dynamics modeling', *Journal of Fluids Engineering*. American Society of Mechanical Engineers Digital Collection, 138(1).
- Bhusare, V. H. *et al.* (2017) 'CFD simulations of a bubble column with and without internals by using OpenFOAM', *Chemical Engineering Journal*. Elsevier, 317, pp. 157–174.
- Bhusare, V. H. *et al.* (2018) 'Mixing in a co-current upflow bubble column reactors with and without internals', *The Canadian Journal of Chemical Engineering*. Wiley Online Library, 96(9), pp. 1957–1971.
- Burns, A. D. *et al.* (2004) 'The Favre averaged drag model for turbulent dispersion in Eulerian multi-phase flows', in *5th international conference on multiphase flow, ICMF*, pp. 1–17.
- Frank, T. *et al.* (2008) 'Validation of CFD models for mono- and polydisperse air–water two-phase flows in pipes', *Nuclear Engineering and Design*. Elsevier, 238(3), pp. 647–659.
- Guan, X. and Yang, N. (2017) 'CFD simulation of pilot-scale bubble columns with internals: Influence of interfacial forces', *Chemical Engineering Research and Design*. Elsevier, 126, pp. 109–122.
- Guo, X. and Chen, C. (2017) 'Simulating the impacts of internals on gas–liquid

- hydrodynamics of bubble column', *Chemical Engineering Science*, 174, pp. 311–325. doi:
- Hosokawa, S. *et al.* (2002) 'Lateral migration of single bubbles due to the presence of wall', in *Fluids Engineering Division Summer Meeting*, pp. 855–860.
- Ishii, M. and Zuber, N. (1979) 'Drag coefficient and relative velocity in bubbly, droplet or particulate flows', *AIChE journal*. Wiley Online Library, 25(5), pp. 843–855.
- Laborde-Boutet, C. *et al.* (2010) 'CFD simulations of hydrodynamic/thermal coupling phenomena in a bubble column with internals', *AIChE Journal*, 56(9), pp. 2397–2411.
- Larachi, F. and Desvigne, D. and Donnat, L. and Schweich, D. (2006) 'Simulating the effects of liquid circulation in bubble columns with internals', *Chemical Engineering Science*, 61(13), pp. 4195–4206.
- Morsi, S. A. J. and Alexander, A. J. (1972) 'An investigation of particle trajectories in two-phase flow systems', *Journal of Fluid mechanics*. Cambridge University Press, 55(2), pp. 193–208.
- Schiller, L. (1933) 'Über die grundlegenden Berechnungen bei der Schwerkraftaufbereitung', *Z. Vereines Deutscher Inge.*, 77, pp. 318–321.
- Simonin, C., Viollet, P. L. and others (1990) 'Predictions of an oxygen droplet pulverization in a compressible subsonic coflowing hydrogen flow', *Numerical Methods for Multiphase Flows*. American Society of Mechanical Engineers: Fluids Engineering Division New York, 91(2), pp. 65–82.
- Tomiya, A. (1998) 'Struggle with computational bubble dynamics', *Multiphase Science and Technology*, 10(4), pp. 369–405.
- Tomiya, A. *et al.* (2002) 'Transverse migration of single bubbles in simple shear flows', *Chemical Engineering Science*. Elsevier, 57(11), pp. 1849–1858.

$$\text{Diameter of the inner tube bundle} = 0.0677\text{m}$$

$$\text{Circumference of the inner tube bundle} = \pi * 0.0677 = 0.2127\text{ m}$$

$$\begin{aligned} \text{Total surface area of the inner tube bundle of height } 1.5\text{ m} &= \pi * 0.0677 * 1.5 \\ &= 0.3190\text{ m} \end{aligned}$$

The space between two internals can be considered as rectangles of length 0.0044 m. Then, the area between the tubes can be determined by:

$$\begin{aligned} \text{Area between two internals} &= 15 * \text{Space length} * \text{Height of tubes} \\ &= 15 * 0.0044 * 1.5 = 0.099\text{ m}^2 \end{aligned}$$

Fraction of spaces for the inner internal tube layout

$$\begin{aligned} &= \frac{\text{Area between two internals}}{\text{Total surface area of the inner tube bundle}} = \frac{0.099}{0.3190} \\ &= 0.3103 \end{aligned}$$

Total length covered by perforation holes

$$\begin{aligned} &= \text{Fraction of spaces in the internal tube layout} \\ &\quad * \text{Length of tube bundle} \\ &= 0.3103 * 1.5 = 0.4654\text{ m} \end{aligned}$$

$$\text{Total number of perforations for the inner tube bundle} = \frac{0.4654}{0.0044} = 106$$

Calculation of perforation fractions for 38 tube internal geometry

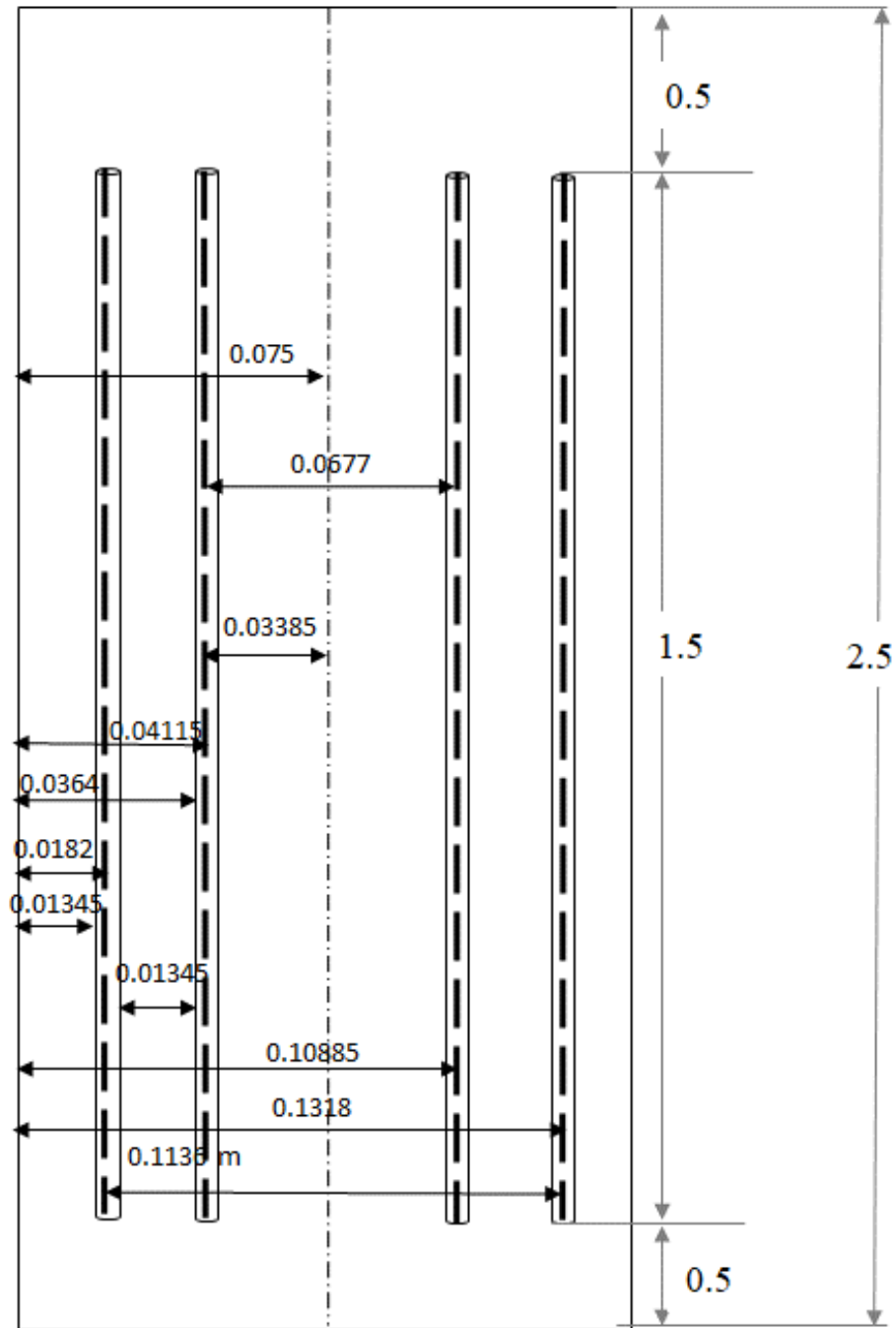


Figure C.2 Two-dimensional representation of 38 tube bundle geometry

For the inner tube bundle, the perforation calculation remains same as the one presented earlier for 15 tube bundle geometry.

$$\text{Diameter of the outer tube bundle} = 0.1132 \text{ m}$$

$$\text{Circumference of the outer tube bundle} = \pi * 0.1132 = 0.3556 \text{ m}$$

$$\begin{aligned} \text{Total surface area of the inner tube bundle of height 1.5 m} &= \pi * D * h \\ &= \pi * 0.1132 * 1.5 = 0.5334 \text{ m} \end{aligned}$$

When 23 tubes are placed in the outer tube bundle, the spacing between them can be calculated as:

$$\frac{\text{Circumference of the outer layout}}{\text{Number of tubes}} - \text{Tube Dia} = \frac{0.3556}{23} - 0.0095 = 0.005961$$

$$\begin{aligned} \text{Area between two internals} &= \text{No of tubes} * \text{Space Length} * \text{Height of Tubes} \\ &= 23 * 0.0059 * 1.5 = 0.204 \end{aligned}$$

Fraction of spaces for the inner internal tube layout

$$\begin{aligned} &= \frac{\text{Area between two internals}}{\text{Total surface area of the inner tube bundle}} = \frac{0.204}{0.5334} \\ &= 0.3816 \end{aligned}$$

Total length covered by perforation holes

$$\begin{aligned} &= \text{Fraction of spaces in the internal tube layout} \\ &* \text{Length of tube bundle} = 0.3816 * 1.5 = 0.5724 \end{aligned}$$

$$\text{Total number of perforations for the outer tube bundle} = \frac{0.5724}{0.0059} = 97$$

Appendix – D

Experimental Evaluation of Overall Gas Holdup

Experimental Methods

Experiments were carried out in the presence of circular tube bundle internals. The air flow rate was controlled by three calibrated sonic nozzles. These experiments were carried out at a static height of 1.4 meters and the range of superficial gas velocity was 0.02 m/s to 0.3 m/s. Tap water was used as a continuous phase and air flow was used as the dispersed phase. Gas was introduced into the column through a six arm sparger with 11.2 cm long arm and holes of the sparger oriented in the downward direction. A visual measurement technique was employed to determine the overall gas holdup values (Equation 1). The variation of dynamic height was captured by using the Canon Powershot SX50 HS camera. The experimental details such as column details, sparger design, and working of gas flow control have been outlined elsewhere (Gandhi et al. 1999; Li and Prakash, 2000; Jhawar and Prakash, 2014; George et al., 2017).

$$\varepsilon_g = \frac{H_{dyn} - H_{st}}{H_{dyn}} \quad (1)$$

Results and Discussion

Overall gas holdup values and its comparison with experimental data has been presented in Figure D-1. At lower velocities, the values of overall gas holdup closely corresponded to other experimental values of Jhawar and Prakash (2014); Kagumba (2013); Guan *et al.* (2015) and Hamed et al. (2010). At higher velocities ($U_G > 0.1$ m/s), our experiments

portrayed a higher gas holdup. In the transition and churn turbulent regime, higher amount of foam is produced near the disengagement region as a result of gas-liquid dispersion. In our visual technique, the foam generated was accounted for which results in higher values of overall gas holdup. The values have been presented after subtracting the height of foam layer.

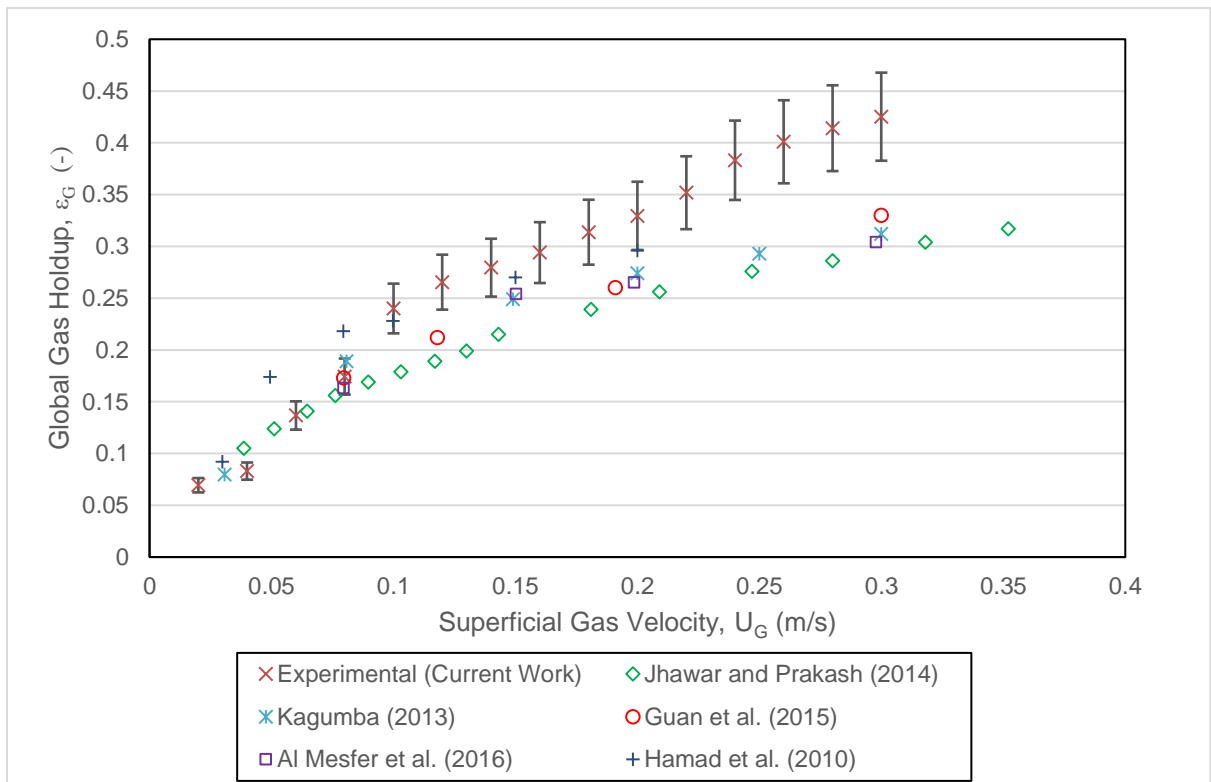


Figure D.1 Comparison of experimental values of gas holdup values with other experimental work

Curriculum Vitae

Name: Glen Cletus Dsouza

Post-secondary Education and Degrees: R. V. College of Engineering
Bangalore, Karnataka, India
2014-2018
Bachelor of Engineering (Chemical Engineering)

Western University
London, Ontario, Canada
2018-Present
Master of Engineering Science (Chemical and Biochemical Engineering)

Honours and Awards: MITACS Internship Grant
October 2020 – Present

Western Engineering Scholarship
2018 – 2020

3 Minute Thesis Research Bridge Competition
Second Place
June 2019

Western Engineering Scholarship for Certificate in Curriculum,
Teaching and Learning in the STEM Disciplines
2019 – 2020

Related Work Experience MITACS Research Intern
Sco-Terra Consulting Group
London, Ontario, Canada
October 2020 – Present

Teaching Assistant
Western University
2018 – 2020

Research Assistant
Western University
2018 – 2020

Conference Proceedings:

DSouza, G. C., Gaurav, T., Zhang, C., Prakash, A., (2019) “CFD Simulation of Bubble Column Reactors in the Presence of Internals”, CFD Society of Canada Conference, The University of Western Ontario, London, June 2-5, pp. 1-13